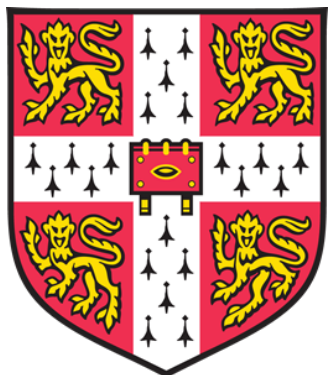


Identification of centrosomal proteomes using COMPACT, a novel tool for purification of centrosomes



Sarah Carden

Cancer Research UK Cambridge Institute
University of Cambridge
Downing College

This dissertation is submitted for the degree of
Doctor of Philosophy

August 2021

“It always seems impossible until it’s done.”

~ Tata Madiba ~

Declaration

This dissertation is the result of my own work and includes nothing which is the outcome of work done in collaboration, except where specifically indicated in the text. I confirm that none of the work in this dissertation is the same as any that I have submitted, or is concurrently being submitted for any degree, diploma, or other qualification, at the University of Cambridge, or any other university.

This dissertation meets the requirements of the Clinical Medicine and Veterinary Medicine Degree Committee and does not exceed 60,000 words.

Sarah Carden

Cambridge, August 2021

Summary

Identification of centrosomal proteomes using COMPACT, a novel tool for purification of centrosomes

Sarah Carden

Centrosomes are small cytoplasmic organelles that play a critical role in multiple cellular processes; from mitotic spindle assembly and cell division, to cell migration, invasion and polarity. The human centrosome consists of two cylindrical structures known as centrioles, decorated at their distal ends by appendage structures, and surrounded by a proteinaceous matrix known as the pericentriolar material. Despite a number of advances in the field, focussing particularly on centrosome structure and assembly in normal and diseased cells, relatively little is known about the spatial and temporal dynamics of centrosome composition, and how this may vary between different cell, tissue, or disease types. Indeed, only a handful of studies have analysed the proteomic composition of the centrosome.

In the first part of this study, I established a novel method for centrosome isolation that was developed in our laboratory. This approach, known as COMPACT (Centrosome Purification by Affinity Capture), involves a single-step affinity purification of centrosomes by a short peptide corresponding to a 33 amino acid C-terminal fragment of the centrosomal protein CCDC61. I have shown that the method is able to isolate centrosomes from a variety of cell types, and that analysis of purified centrosomes using mass spectrometry recovers the majority of known core centrosomal proteins. Importantly, I demonstrated that COMPACT purifies centrosomal components with higher efficiency and specificity than the traditional sucrose sedimentation-based centrosome isolation technique.

In the second part of this study, I performed experiments to gain mechanistic insight into how COMPACT works. I generated cell lines lacking the centrosomal proteins, NIN or CEP128, and showed these proteins (located primarily at the subdistal appendages) to be directly involved in the peptide's ability to purify centrosomes.

In the third part of this study, I performed a comprehensive analysis of the centrosome proteome in a panel of human cell lines, allowing for the identification of tissue-specific as well as differentially expressed centrosomal candidates. In addition to this, a quantitative mass spectrometry-based analysis of centrosome composition in different cell types revealed the absence of distal appendages in the T lymphocyte cell line, Jurkat, a novel and exciting finding.

COMPACT was also shown to be effective at isolating centrosomes from primary tissue, revealing its potential for use as a tool to explore centrosome composition in various centrosome-associated diseases, including microcephaly and cancer.

Finally, by comparing COMPACT across a wide range of cell lines, I was able to identify a number of novel centrosomal candidates, which were independently validated using various techniques. Loss-of-function studies in HEK 293T cells were performed to determine the function of a specific candidate, TRIM27.

This study not only provides a novel method to isolate centrosomes in a spatially and temporally controlled manner, but also an effective tool for the identification of new or previously uncharacterised centrosomal proteins that may have significant roles in centrosome biology.

Acknowledgements

I would like to express my gratitude to the following people:

My supervisors, Dr Fanni Gergely and Professor Jason Carroll, for their encouragement and guidance throughout this project. I am grateful for the opportunity to be a part of the CRUK CI community, this experience has allowed me to grow as a scientist and a person.

Members of the lab, past and present, for creating a pleasant working environment. Special thanks to Julia Tischer for her friendship, interest in my work, endless advice and willingness to help with experiments. Thank you also to Tannia Gracia, Daphne Huberts, Lovorka Stojic, Valentina Quarantotti, Danis Thomas and Bradley Nash, for their enthusiasm and stimulating conversation.

Members of the core facilities at Cancer Research UK Cambridge Institute, particularly Proteomics, Bioinformatics and Light Microscopy. Special thanks to Valar Nila Roamio Franklin, Eva Papachristou and Clive D'Santos for friendly conversation and advice on everything to do with mass spectrometry; Kamal Kishore for his invaluable assistance with quantitative proteomics analysis; Fadwa Joud for help with the confocal microscopes.

Dr Mark van Breugel, Dr Takashi Ochi and Dr Ivan Rosa e Silva for scientific discussion and for providing the HAP1 NIN KO cells.

Cancer Research UK and Cambridge Trust for providing the funding that made completing this PhD possible.

My Cambridge friends, for always being there to offer guidance and support. Special thanks to Ella Brown, Molly Becker, Eloise Kuijer and Carolin Sauer – my rocks, without whom I would not have been able to finish this PhD.

And finally, my wonderful family, for their continuous love, support and encouragement. I particularly want to thank my parents, Kirsty and Kenneth – you have always made it possible for me to follow my dreams, and no real words can describe how grateful I am to you.

Table of contents

Declaration	iv
Summary	vi
Acknowledgements	viii
Table of contents	x
List of figures	xiv
List of tables	xvi
List of abbreviations	xvii
1 Introduction	1
1.1. Overview	1
1.2. Cell cycle	1
1.3. Microtubules	3
1.3.1. Microtubule nucleation and Microtubule Organising Centres	4
1.4. Centrosomes	4
1.4.1. Centrioles	5
1.4.2. Centriolar appendages	7
1.4.3. Pericentriolar material	10
1.5. Centrosome duplication cycle	11
1.5.1. Centriole duplication and elongation	12
1.5.2. Centriole and centrosome maturation	13
1.5.3. Centriole separation	13
1.5.4. Centriole-to-centrosome conversion	14
1.5.5. Centriole disengagement	14
1.5.6. PCM dynamics	15
1.6. Non canonical centriole biogenesis	17
1.7. Cilia	17

1.8. Centriolar satellites	20
1.9. Centrosomes and cilia in disease	20
1.10. Proteomic characterisation of the human centrosome	22
2 Aim of my PhD	24
3 Materials and Methods	25
3.1. Cell culture-based techniques	25
3.1.1. General cell culture	25
3.1.2. Human induced pluripotent stem cell (hiPSC) culture	25
3.1.3. Drug treatments	26
3.1.4. siRNA transfections	27
3.2. Mouse tissue	28
3.2.1. Tissue collection and processing for COMPACT	28
3.3. Cell imaging techniques	29
3.3.1. Immunofluorescence	29
3.3.2. Confocal microscopy	29
3.4. Molecular biology techniques	31
3.4.1. Western blotting	31
3.5. Centrosome Purification by Affinity Capture (COMPACT)	33
3.6. Centrosome purification by sucrose sedimentation	34
3.7. Mass spectrometry: sample preparation	35
3.7.1. “On bead” tryptic digestion of proteins	35
3.7.2. “In solution” tryptic digestion of proteins (sucrose sedimentation samples)	35
3.7.3. Tandem Mass Tag (TMT) quantitative proteomics	35
3.8. Liquid chromatography tandem mass spectrometry (LC-MS/MS)	36
3.8.1. TMT runs	36
3.9. Mass spectrometry: data analysis	37
3.9.1. Data analysis for label-free quantification (LFQ)	37

3.9.2. Data analysis for TMT	37
3.10. Generation of CEP128 knock-out cells by CRISPR/Cas9 genome editing	38
3.10.1. Cloning of gRNA into the px458 vector	38
3.10.2. Transfection and FACS sorting of HEK 293T cells	39
3.10.3. Sequencing of HEK 293T clones	39
3.11. Statistical analysis	40
4 Results I	41
4.1. A novel method for centrosome isolation	41
4.1.1. Centrosome Purification by Affinity Capture (COMPACT)	41
4.2. COMPACT method optimisation and validation	45
4.2.1. Optimisation of the COMPACT protocol in HEK 293T cells	45
4.2.2. Further characterisation and validation of COMPACT in HEK 293T cells	54
4.2.3. A HEK 293T centrosome proteome	67
4.2.4. Investigating how COMPACT purifies centrosomes	73
5 Results II	82
5.1. Using COMPACT to investigate centrosomal proteomes in a panel of cell lines	82
5.2. Investigating the tissue specificity of centrosome composition	90
5.2.1. A non-quantitative comparison of centrosome proteomes in multiple cell lines	90
5.2.2. A quantitative comparison of centrosome composition in U251 and Jurkat cells	93
5.3. COMPACT in primary tissue	103
5.3.1. Investigating the performance of COMPACT in primary mouse tissue	103
6 Results III	111
6.1. Using COMPACT to identify novel centrosomal candidates	111
6.1.1. Investigating the centrosomal role of TRIM27	120
7 Discussion	129
7.1 Optimisation, validation and characterisation of COMPACT in HEK 293T cells	130
7.1.1. Method optimisation and validation of COMPACT	130

7.1.2. Further characterisation of COMPACT	131
7.2. Tissue specificity of centrosome composition	134
7.2.1. A non-quantitative comparison of centrosome proteomes in a panel of cell lines	134
7.2.2. A quantitative comparison of centrosome composition in U251 and Jurkat cells	135
7.2.3. COMPACT in primary tissue	137
7.3. Novel centrosomal candidates	138
8 Conclusion	141
9 References	143
10 Appendices	156

List of figures

Figure 1.1. Centriole and cartwheel architecture	7
Figure 1.2. Assembly and dynamics of centriolar appendages	9
Figure 1.3. PCM organisation during interphase and mitosis	11
Figure 1.4. The centrosome duplication cycle	16
Figure 1.5. Structure of a primary cilium	19
Figure 4.1. CCDC61 peptide sequence alignment	42
Figure 4.2. COMPACT workflow	43
Figure 4.3. Purification of centrosomes by COMPACT	44
Figure 4.4. Optimising cell number for COMPACT in HEK 293T cells	46
Figure 4.5. Comparing COMPACT and BO pulldowns in HEK 293T cells	47
Figure 4.6. Optimising incubation conditions for COMPACT in HEK 293T cells	48
Figure 4.7. Changing bead/peptide proportions for COMPACT in HEK 293T cells	49
Figure 4.8. Adjusting lysis conditions for COMPACT in HEK 293T cells	50
Figure 4.9. Optimising wash buffer conditions for COMPACT in HEK 293T cells	51
Figure 4.10. Comparison between wash buffer conditions for COMPACT in HEK 293T cells	52
Figure 4.11. Ability of unbound fraction to bind fresh beads and peptide	56
Figure 4.12. Immunofluorescence analysis of bound and unbound fractions from COMPACT in HEK 293T cells	57
Figure 4.13. COMPACT efficiency in HEK 293T cells synchronised to different cell cycle stages	58
Figure 4.14. Loss of centrosomes in HEK 293T cells after treatment with the selective PLK4 inhibitor, centrinone	61
Figure 4.15. COMPACT in HEK 293T cells treated with the selective PLK4 inhibitor, centrinone	62
Figure 4.16. COMPACT-MS in HEK 293T cells treated with the selective PLK4 inhibitor, centrinone, compared to the core centrosome dataset	64
Figure 4.17. Purification of centrosomes by sucrose sedimentation in HEK 293T cells	65
Figure 4.18. Comparison of centrosomal proteins isolated using two techniques, COMPACT and sucrose sedimentation	66
Figure 4.19. Comparison of the HEK 293T COMPACT proteome to published centrosome datasets	68
Figure 4.20. Gene Ontology (GO) enrichment analysis on the proteins unique to KE-37	69
Figure 4.21. COMPACT-MS in U251 cells untreated and pre-treated with nocodazole and cytochalasin D, compared to the KE-37 centrosome proteome	70
Figure 4.22. The core HEK 293T centrosome proteome	71
Figure 4.23. Additional markers for HEK 293T COMPACT	72
Figure 4.24. COMPACT in HAP1 WT and NIN KO cells	74
Figure 4.25. Comparison of HAP1 WT and NIN KO centrosome proteomes to the KE-37 centrosome proteome	75

Figure 4.26. Immunofluorescence analysis of centrosomes isolated by COMPACT-IF in HEK 293T cells	76
Figure 4.27. Validation and characterisation of HEK 293T CEP128 KO cells	78
Figure 4.28. COMPACT in HEK 293T WT and CEP128 KO cells	79
Figure 4.29. Immunofluorescence analysis of sDAP and proximal-end centrosomal proteins in HEK 293T WT and CEP128 KO cells	81
Figure 5.1. COMPACT in HEK 293T, U251 and Jurkat cells	83
Figure 5.2. Comparison of COMPACT proteomes to the KE-37 proteome	86
Figure 5.3. Centrosomes and cilia in primary patient-derived glioma cell lines, G166 and G7	87
Figure 5.4. Centrosomes and cilia in the hiPSC line, FSPS13B	88
Figure 5.5. Percentage cilia detected in the cell lines, G166, G7 and FSPS13B	89
Figure 5.6. Comparison of the HEK, U251 and Jurkat COMPACT proteomes	90
Figure 5.7. Experimental workflow for quantitative COMPACT-MS (COMPACT-TMT) performed in U251 and Jurkat cells	94
Figure 5.8. Distribution of data for COMPACT-TMT in U251 and Jurkat cells	95
Figure 5.9. Differential expression plot for COMPACT-TMT in U251 and Jurkat cells	96
Figure 5.10. Comparison of COMPACT-TMT in U251 and Jurkat cells to the published core centrosome dataset	98
Figure 5.11. COMPACT-WB in U251 and Jurkat cells	99
Figure 5.12. Non-quantitative COMPACT-MS from HEK 293T, U251 and Jurkat cells	100
Figure 5.13. DAP and sDAP staining in HEK and Jurkat cells	101
Figure 5.14. COMPACT in mouse liver cells	104
Figure 5.15. Comparison of COMPACT in mouse liver cells to KE-37	105
Figure 5.16. Comparison of COMPACT and BO in mouse liver cells to KE-37	106
Figure 5.17. COMPACT in human hepatocellular carcinoma cells, HepG2	107
Figure 5.18. COMPACT in mouse spleen cells	108
Figure 5.19. Comparison of COMPACT and BO in mouse spleen cells to KE-37	109
Figure 6.1. Workflow for identification and characterisation of novel centrosomal candidates	111
Figure 6.2. Knockdown efficiencies upon siRNA treatment in HEK 293T cells	115
Figure 6.3. COMPACT-IF after siRNA treatment in HEK 293T cells	117
Figure 6.4. EDC4 and TRIM27 staining in centrosomes isolated from HEK 293T cells using COMPACT-IF	118
Figure 6.5. Independent validation of centrosomal candidates by sucrose sedimentation in HEK 293T cells	119
Figure 6.6. TRIM27 functional studies in interphase HEK 293T cells	121
Figure 6.7. TRIM27 functional studies in prometaphase-metaphase HEK 293T cells	123
Figure 6.8. TRIM27 functional studies in anaphase-telophase HEK 293T cells	124
Figure 6.9. Nuclear phenotype in TRIM27-depleted HEK 293T cells	125
Figure 6.10. Loss of centrosomes in HEK 293T cells after treatment with centrinone	126
Figure 6.11. Rescue of TRIM27 depletion phenotype in HEK 293T cells pre-treated with centrinone	127

List of tables

Table 3.1. List of siRNAs used in this thesis	27
Table 3.2. List of all primary antibodies used for immunofluorescence	30
Table 3.3. List of all primary antibodies used for western blotting	32
Table 3.4. CEP128 gRNA cloned into the px458 vector	38
Table 3.5. List of primers used to amplify the CEP128 genomic locus from putative CEP128 knockout clones	39
Table 4.1. Top 20 proteins identified with the highest number of unique peptides in COMPACT-MS in HEK 293T cells	53
Table 5.1. Number of proteins identified using COMPACT in a broad range of cell lines	84
Table 5.2. Tissue specificity of centrosome composition	92
Table 6.1. Table showing a number of novel centrosomal candidates, chosen based on their presence in centrosome proteomes of all cell lines analysed using COMPACT	114

List of abbreviations

AKIP1	A-kinase Interacting Protein 1
AMBIC	Ammonium Bicarbonate
APC	Anaphase Promoting Complex
ARL13B	ADP Ribosylation Factor Like GTPase 13B
AURKA	Aurora Kinase A
BBS	Bardet-Biedl syndrome
BCLAF1	BCL2 Associated Transcription Factor 1
BiоЛD	Proximity-dependent biotin identification
BO	Bead-only
BSA	Bovine Serum Albumin
CA	Centrosome amplification
CCDC61	Coiled-coil Domain Containing 61
CDK	Cyclin-Dependent Kinase
CENPJ	Centromere-associated Protein E/J
CEP	Centrosomal Protein
CETN	Centrin
CNAP1	Centrosomal NEK2-Associated Protein 1
COMPACT	Centrosome Purification by Affinity Capture
CRBN	Cereblon
CRISPR	Clustered Regularly Interspaced Short Palindromic Repeats
CS	Centriolar satellites
Da	Dalton
DAP	Distal appendage
DDB1	Damage Specific DNA Binding Protein 1
DMSO	Dimethyl-Sulfoxide
DNA	Deoxyribonucleic Acid
EDC4	Enhancer of mRNA Decapping 4
EDTA	Ethylenediamine Tetraacetic Acid
EMT	Epithelial-to-Mesenchymal Transition
ExM	Expansion Microscopy
FBS	Fetal Bovine Serum
FGF	Fibroblast Growth Factor
γTuRC	γ-tubulin ring complex
γTuSC	γ-tubulin small complex
GCPs	γ-tubulin complex proteins
GDP	Guanosine Diphosphate

GTP	Guanosine Triphosphate
GGT	G ₁ -G ₂ Tether
GO	Gene Ontology
HGSOC	High-Grade Serous Ovarian Cancer
hiPSC	Human Induced Pluripotent Stem Cell
HPA	Human Protein Atlas
HSET	Kinesin Family Member C1 (KIFC1)
IF	Immunofluorescence
IFT	Intraflagellar transport
JBTS	Joubert syndrome
KIFC3	Kinesin Family Member 3
LC	Liquid Chromatography
M	Mitosis
MAP	Microtubule-Associated Protein
MCPH	Autosomal Recessive Primary Microcephaly
MOPDII	Microcephalic osteodysplastic primordial dwarfism type II
MS	Mass Spectrometry
MT	Microtubule
MTOC	Microtubule Organising Centre
NIN	Ninein
NK	Natural Killer
NOP53	NOP53 Ribosome Biogenesis Factor
OFD	Oro-facio-digital syndrome
PBS	Phosphate Buffered Saline
PCM	Pericentriolar Material
PCM1	Pericentriolar Material 1
PCNT	Pericentrin
PCP	Protein Correlation Profiling
PD	Primordial Dwarfism
PDX	Patient-derived xenograft
pl	Isoelectric point
PI3KC2B	Phosphoinositide 3-kinase Catalytic Subunit Type 2 Beta
PLK1/4	Polo Like Kinase 1/4
RPE-1	Retinal Pigment Epithelial cells
SAS6	Spindle Assembly Abnormal Protein 6 Homolog
SCF	Skp1/Cullin/F-box
SCKL	Seckel syndrome
SD	Standard Deviation
sDAP	Subdistal appendage
SDS	Sodium Dodecyl Sulfate

SILAC	Stable Isotope Labelling by Amino acids in Cell culture
SIM	Structured Illumination Microscopy
siRNA	Small interfering RNA
SPB	Spindle pole body
SPD-5	Spindle Defective 5
SRM	Selected Reaction Monitoring
STORM	Stochastic Optical Reconstruction Microscopy
TBS	Tris-Buffered Saline
TMT	Tandem Mass Tag
TRIM27	Tripartite Motif Containing 27
WB	Western Blot

1 Introduction

1.1. Overview

The centrosome is a small cytoplasmic organelle that plays a critical role in multiple cellular processes due to its organisation of microtubules throughout interphase and mitosis. The centrosome was first described in the late 19th century by scientists, Theodor Boveri and Edouard Van Beneden, who simultaneously and independently discovered these structures while studying mitotic cell division of fertilised nematode embryos (reviewed in Scheer, 2014). It was Boveri's work, however, published a number of decades later, that linked centrosome amplification to aneuploidy and tumour development (Boveri, 1929), establishing a basis for over a century's worth of research into understanding centrosome biology. Despite a number of advances in the field, focussing particularly on centrosome structure and assembly in normal and diseased cells, relatively little is known about the spatial and temporal dynamics of centrosome composition, and how this may vary between different cell, tissue or disease types. Indeed, only a handful of studies have analysed the proteomic composition of the centrosome.

1.2. Cell cycle

The cell cycle is a highly regulated process which ensures the generation of two genetically identical daughter cells from one parental cell. During each cell cycle, cells proceed through a series of precisely timed and highly regulated stages of growth, DNA replication, and division to produce two daughter cells. The eukaryotic cell cycle consists of two major phases: interphase and mitosis. Interphase, which accounts for approximately 95% of the total duration of the human cell cycle, is the phase during which cells grow and DNA is divided. It can be further subdivided into G₁ (Gap phase 1), S-phase, and G₂ (Gap phase 2). During G₁, cells grow and prepare for DNA synthesis. During S-phase, DNA replication results in the formation of two identical sister chromatids per chromosome. In G₂, cells continue to grow and make the final preparations before mitosis (Ono et al., 2004; Schafer, 1998). Mitosis, or M-phase, is the phase during which the duplicated chromosomes are aligned, separated and equally distributed between the two daughter cells, and lasts approximately one hour in most cultured cells. It can be further subdivided into five different phases: prophase, prometaphase, metaphase, anaphase and telophase (and cytokinesis) (reviewed in Walczak et al., 2010).

These phases can be characterised by specific morphological changes to the chromosomes and mitotic spindle. During prophase, chromosomes start to condense and the mitotic spindle begins to form, as microtubules are nucleated from the centrosomes, which are the primary microtubule organising centres (MTOCs) in eukaryotic cells. In prometaphase, the nuclear envelope breaks down and dynamic spindle microtubules start to capture chromosomes at kinetochores; multi-protein complexes assembled at the centromere of each sister chromatid which serve as the attachment sites for spindle microtubules (reviewed in Cleveland et al., 2003). In metaphase, the bipolar spindle apparatus is fully established when chromosomes are aligned at the metaphase plate, an equatorial plane that lies perpendicular to the spindle fibres. Anaphase occurs when the protease separase cleaves the cohesin protein complex (which is responsible for sister chromatid cohesion); this enables sister chromatids to be separated so that they can migrate to opposite poles before being segregated into two daughter cells. Finally, during telophase, the mitotic spindle is broken down and the nuclear envelope is reassembled around each set of separated chromatids, which start to decondense as they are released from the spindle microtubules. This is followed by a process known as cytokinesis, when the cytoplasm is divided by formation of the cleavage furrow, a contractile ring of actin filaments and myosin-II, causing the final separation of the cell into two daughter cells (reviewed in McIntosh, 2016; Pollard, 2010).

The cell cycle is a tightly controlled process regulated by cyclins and cyclin-dependent kinases (CDKs). Through phosphorylation, CDKs, which belong to a family of serine/threonine kinases, signal to the cell that it can progress to the next stage of the cell cycle. Cyclins, which bind to and activate CDKs, undergo a constant cycle of synthesis and degradation during the cell cycle, allowing for the strict regulation of CDK activity (Evans et al., 1983; Malumbres and Barbacid, 2005). During G₁ phase, CDK4 and CDK6 are activated by D-type cyclins (D1, D2 and D3), resulting in the phosphorylation of the retinoblastoma protein (Rb) family and resultant activation of E2F transcription factors. This leads to the activation and transcription of E2F-responsive genes, such as the E-type cyclins (E1 and E2), which triggers S-phase entry (Harbour et al., 1999; Sherr and Roberts, 1999). At the onset of S-phase, CDK2 complexes with A-type cyclins (A1 and A2) in order to activate and maintain DNA synthesis (Coverley et al., 2002). At the G₂/M transition, cyclin A associates with CDK1 in order to initiate prophase. During mitosis, B-type cyclins (B1, B2 and B3) bind to and activate CDK1, and it is the inactivation of CDK1-cyclin B complexes that triggers proper mitotic exit (reviewed in Malumbres and Barbacid, 2005; Otto and Sicinski, 2017; Satyanarayana and Kaldis, 2009). Importantly, CDK1-cyclin A/B complexes, as well as CDK2-cyclin E complexes, are involved in regulation of centrosome duplication (see section 1.5).

In another level of regulation, the activities of CDK-cyclin complexes are controlled by CDK inhibitors, which are categorised into two families; INK4 and Cip/Kip. The INK4 family comprises p16^{INK4a}, p15^{INK4b}, p18^{INK4c}, and p19^{INK4d}, all of which bind to and inhibit CDK4 and CDK6 activity. The Cip/Kip family bind to both cyclins and CDKs, modulating the activity of CDK-cyclin D, E, A and B complexes. Cip/Kip family members include p21^{Cip1}, p27^{Kip1} and p57^{Kip2} (reviewed in Besson et al., 2008; Otto and Sicinski, 2017).

Progression through the cycle is controlled by a number of checkpoints: the G₁-S checkpoint (or restriction point), the DNA damage checkpoint, and the spindle assembly checkpoint. The G₁-S checkpoint determines whether the cell should commit to cell division, by evaluating cell size and energy reserves. At this point, should the cell not be allowed to proceed (such as in the absence of sufficient growth factors), it can reversibly exit the cell cycle and enter a quiescent state, known as G₀-phase. The DNA damage checkpoint is at the G₂/M transition, ensuring that cells that have accumulated errors during DNA replication don't enter mitosis until they have had a chance to repair their DNA. Finally, the spindle assembly checkpoint, which is active during mitosis at the metaphase-anaphase transition, prevents separation of the sister chromatids until all kinetochores are properly attached to the spindle microtubules. As the cell cycle checkpoints facilitate cellular responses to DNA damage and are responsible for the tight regulation of cell proliferation, mutations in genes involved in these pathways can lead to the development of human diseases, including cancer (reviewed Kastan and Bartek, 2004).

1.3. Microtubules

Microtubules (MTs) are a major component of the cell cytoskeleton, playing an essential role in a number of cellular processes including cell motility, cell division and intracellular transport. Individual MTs are composed of α- and β-tubulin heterodimers that are arranged in head-to-tail arrays, which assemble into linear structures known as protofilaments. Mammalian MTs are made up of 13 linearly arranged protofilaments, that assemble to form a 24 nm-wide hollow cylindrical structure (Tilney et al., 1973). Due to the head-to-tail arrangement of tubulin heterodimers, MTs are polarised and thus have two distinct ends: a rapidly growing plus end which is terminated by the β-tubulin subunit, and a slower growing minus end which is terminated by the α -tubulin subunit. In mammalian cells, the MT minus ends are anchored frequently (but not solely) at the centrosome, while the plus ends are free in the cytoplasm (reviewed in Alvarado-Kristensson, 2020; Howard and Hyman, 2003; Petry and Vale, 2015).

MTs are highly dynamic structures; the plus ends can switch between phases of growth (polymerisation) and shrinkage (depolymerisation) by addition and loss of tubulin subunits at their ends, respectively (Mitchison and Kirschner, 1984). This behaviour, termed dynamic instability, is driven by GTP hydrolysis. Importantly, while both α - and β -tubulin monomers have GTP-binding sites, only α -tubulin is able to hydrolyse GTP to GDP during or soon after its incorporation in the MT structure, an action which is essential for MT dynamics (Hyman et al., 1992, 1995). The regulation of MTs occurs through a variety of mechanisms; for example microtubule-associated proteins (MAPs), plus end tracking proteins (+TIPs), and motor proteins such as dynein and kinesin, interact with MTs to regulate MT structure, organisation and dynamics. In addition, MT post-translational modifications, such as detyrosination, polyglutamylation, polyglycylation and acetylation also play a role in MT regulation (reviewed in Janke and Magiera, 2020).

1.3.1. Microtubule nucleation at Microtubule Organising Centres

In most animal cells, MTs are nucleated from the centrosome, which was originally thought to be the sole microtubule organising centre (MTOC). More recently, it has become clear that a range of non-centrosomal MTOCs exist; during mitosis, MTs are nucleated from spindle MTs, kinetochores and in the vicinity of chromatin, while during interphase, MTs are nucleated at the nuclear envelope, Golgi, pre-existing MTs and the plasma membrane (reviewed in Petry and Vale, 2015). The main MT nucleating factors are protein complexes made up of γ -tubulin and γ -tubulin complex proteins (GCPs). Early studies in yeast identified the γ -tubulin small complex (γ -TuSC), consisting of 2 γ -tubulin molecules and one each of GCP2 and GCP3 (Moritz et al., 1998; Oegema et al., 1999). In higher eukaryotes, the components found in γ -TuSC associate with additional subunits (GCP 4, 5 and 6) to form the γ -Tubulin Ring Complex (γ -TuRC), named for its characteristic ring shape observed by cryo-EM (Zheng et al., 1995). Both complexes are able to bind MT minus ends (by the exposed α -tubulin subunit), while the MT plus ends extend into the cytoplasm. Additional factors have been shown to regulate γ -TuRC recruitment to MTOCs, and thereby MT nucleation, including NEDD1, MOZART1, MOZART2A/B, PCNT and CDK5RAP2 (reviewed in Petry and Vale, 2015; Zupa et al., 2021).

1.4. Centrosomes

The centrosome is a non-membranous organelle that serves as the main microtubule organising centre (MTOC) in eukaryotic cells, and is thus important for many critical cellular

processes. In proliferating cells, the centrosome is responsible for microtubule nucleation (*de novo* synthesis); in interphase contributing to cellular processes such as motility, adhesion and polarity, while in mitosis the centrosomes form the poles of the mitotic spindle, thereby facilitating correct mitotic division. In quiescent and differentiated cells, centrosomes are often involved in assembly of motile and immotile cilia and flagella.

The centrosome consists of two cylindrical centrioles surrounded by a multi-layered proteinaceous matrix known as the pericentriolar material (PCM). The centrioles form the core structural component of the centrosome, providing stability, while the PCM is primarily responsible for microtubule anchoring and nucleation (Woodruff et al., 2014), but has additional roles in centriole duplication (Dammermann et al., 2004; Loncarek et al., 2008), cilia formation and disassembly (Moser et al., 2010), DNA damage signalling and protein degradation (D'Angiolella et al., 2010; Griffith et al., 2008). Mutations in a variety of centrosomal genes have been found to be responsible for a number of human diseases, including developmental disorders such as microcephaly, as well as cancer.

1.4.1. Centrioles

Centrioles are cylindrical structures made up microtubules, and are thus polarised along their long axis, with the base known as the proximal end and the tip known as the distal end. In human cells, they are approximately 450 nm long, with an inner and outer width of approximately 130 nm and 250 nm, respectively. Each centrosome comprises two centrioles; a mother and a daughter. The daughter centriole is the youngest of the two, having been assembled in the previous cell cycle, while the older centriole of the pair is called the mother. The mother centriole can be distinguished from the daughter by the presence of distal and subdistal appendages, accessory structures essential for mother centriole docking at the membrane and primary cilia formation, and MT anchoring and centrosome/cilia positioning, respectively (reviewed in Tischer et al., 2021). Perhaps the most striking feature of centrioles is their nine circularly-arranged triplet microtubules, providing them with their typical nine-fold symmetry. In human cells, the proximal part of the centriole is comprised of nine sets of interconnected microtubule triplets, while the distal part is comprised of nine microtubule doublets (Guichard et al., 2013; Li et al., 2012).

The nine-fold symmetry of centrioles is provided by the cartwheel, a structure located in the proximal part of the centriole that resembles the hub and spokes of a wheel. In human cells, the cartwheel is typically ~100 nm high and contains a central hub that is ~22 nm in diameter, from which the nine spokes emanate to connect with the peripheral-most microtubule triplets

through a structure known as the pinhead. Usually appearing as a stacked structure of multiple cartwheels in the centriole lumen of the newly forming centriole (procentriole), the cartwheel appears at the initial stage of daughter centriole assembly and acts as a template to establish its nine-fold symmetry (reviewed in LeGuennec et al., 2021; Vakonakis, 2021). In mammalian cells, cartwheels are present in procentrioles, but disappear at mitosis due to degradation of the protein SAS6 (Strnad et al., 2007). SAS6 is the major component of the cartwheel inner density (lumen of the hub); nine SAS6 homodimers, each comprising a globular head and extended coiled-coil tail, self-assemble (through a hydrophobic interaction between the head domains) into rod-like structures to form the central part of the cartwheel i.e. the spokes (van Breugel et al., 2011, 2014; Kitagawa et al., 2011; Nakazawa et al., 2007). For a detailed illustration showing centrioles and cartwheel structure, see Figure 1.1.

Assembly of the cartwheel initiates formation of a new centriole in most organisms, and thus needs to be tightly regulated in order to maintain proper centriole number in the cell. In human cells, a mechanism of regulation has developed whereby the amount of SAS6 present in the cell is tightly controlled; SAS6 starts to accumulate at the end of G₁-phase and decrease towards the end of mitosis, through APC-mediated proteosomal degradation as well as SCF-mediated ubiquitination (Puklowski et al., 2011; Strnad et al., 2007).

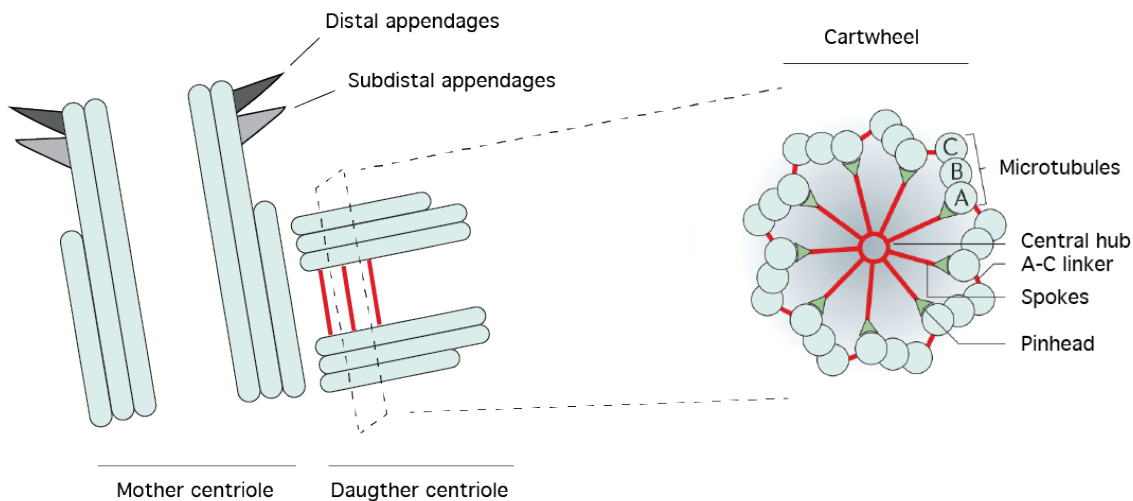


Figure 1.1. Centriole and cartwheel architecture. Schematic representation of a mother and daughter centriole pair. A cross-section of the cartwheel is depicted on the right. The cartwheel is characterised by a central hub, from which nine spokes (SAS6 homodimers) emanate that connect the A-microtubule of the triplets to the pinhead. The nine microtubule triplets (comprised of A-, B-, and C-microtubules) are shown, connected via the A-C linker. Image based on (Gönczy, 2012).

1.4.2. Centriolar appendages

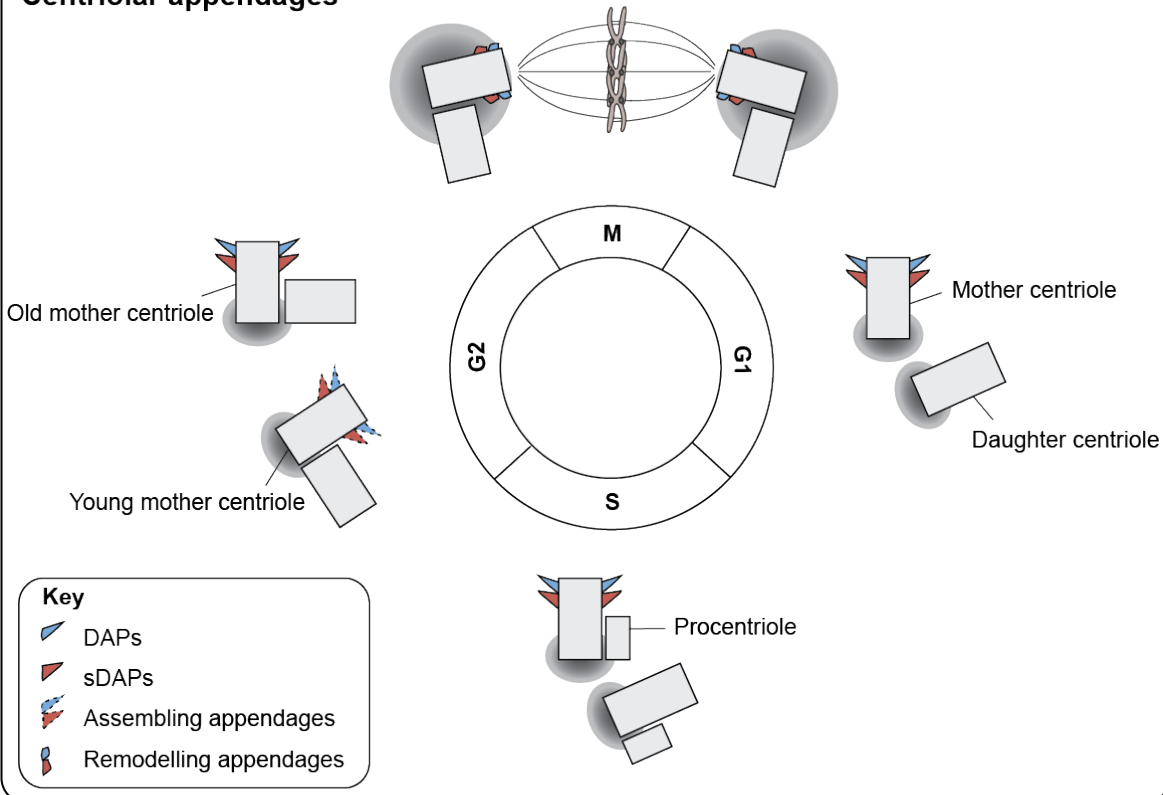
In eukaryotes, mother centrioles are decorated at their distal ends by two types of accessory structures; distal appendages (DAPs) and subdistal appendages (sDAPs), the latter of which are observed only in vertebrates. By forming part of the transition fibres that anchor basal bodies to the ciliary membrane, DAPs are essential for mother centriole docking at the membrane and primary cilia formation, whereas sDAPs are primarily involved in microtubule anchoring and centrosome/cilia positioning (Bornens, 2002; Loncarek and Bettencourt-Dias, 2018; Tanos et al., 2013). While DAPs have been shown to assemble as nine-fold symmetrical structures on the distal centriole wall, the number, distribution and shape of sDAPs on the centriole wall can vary significantly within and across species (Bowler et al., 2019; Uzbekov and Alieva, 2018; Yang et al., 2018).

DAPs and sDAPs are acquired during centriole maturation, a process that begins in G₂, extends through mitosis, and concludes in G₁ of the next cell cycle. This process involves daughter centrioles sequentially incorporating proteins, starting from the centriole wall and extending out towards the centrosome periphery to form the appendage structures, resulting

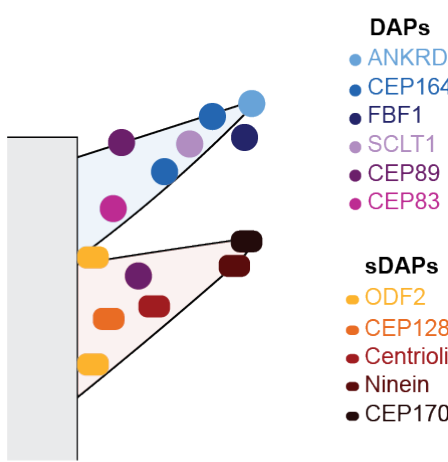
in the conversion of daughter centrioles to young mothers (which will go on to become old mother centrioles in the subsequent cell cycle) (Figure 1.2). Despite a similar temporal pattern, there are important differences in the assembly and dynamics of DAPs and sDAPs (reviewed in Tischer et al., 2021). DAP assembly shows a strict hierarchy; it is initiated in G₂ by the recruitment of C2CD3 and OFD1, followed by CEP83, CEP89 and SCLT1 in early mitosis, and FBF1, CEP164 and ANKRD26 in late mitosis. Recent work found that this process is driven by Talpid3 (or KIAA0586) and C2CD3, which coordinate the removal of daughter centriole-specific proteins, and the subsequent assembly of DAPs (Bowler et al., 2019; Wang et al., 2018). The assembly of sDAPs is initiated by recruitment of ODF2 to the distal part of the centriole wall, followed by CEP128, CCDC68 and CCDC120, which in turn recruit the remaining sDAP proteins. Interestingly, CCDC68, CCDC120 and Ninein (NIN) all function independently to localise CEP170 (Huang et al., 2017; Kashihara et al., 2019; Sullenberger et al., 2020) (Figure 1.2).

In addition to the acquisition of appendages during maturation of daughter centrioles into young mothers, both DAPs and sDAPs undergo transient remodelling during mitosis (Figure 1.2). This process involves the loss of certain appendage proteins from the mother centriole wall in late G₂, which remain largely undetectable until they start to reappear in late mitosis/early G₁. Interestingly, inner appendage proteins (such as ODF2 on sDAPs, and CEP83 and SCLT1 on DAPs) are retained on mother centrioles during remodelling, thereby serving as permanent scaffolds for the recruitment of the more dynamic outer components. It is not entirely clear why appendages need to be remodelled; however, an interesting suggestion is that the process may serve to “reduce the age gap” between the old and young mother centrioles, allowing for better balance in appendage-associated functions (Bowler et al., 2019; Sullenberger et al., 2020).

Centriolar appendages



Protein localisation



Hierarchical assembly

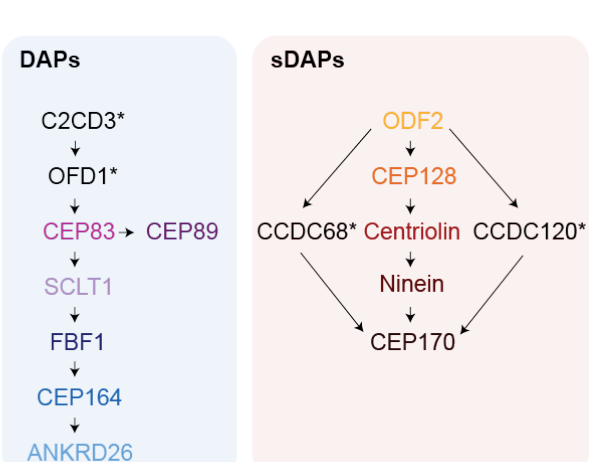


Figure 1.2. Assembly and dynamics of centriolar appendages. Centriolar distal appendages (DAPs) and subdistal appendages (sDAPs) undergo cell cycle-dependent assembly and remodelling (top). DAPs and sDAPs have largely distinct protein composition (bottom left) and assembly pathways (bottom right), however ODF2 and CEP89 have localisations and roles associated with both structures. Asterisks indicate proteins that have not yet been mapped to the DAP or sDAP structures. Note that C2CD3 localises to the centriole lumen, and not the DAP itself. Figure from (Tischer et al., 2021).

1.4.3. Pericentriolar material

The pericentriolar material (PCM), originally described as an amorphous, electron-dense matrix, has more recently emerged as structured, organised and dynamic in nature; it accumulates and expands upon mitotic entry and disassembles upon mitotic exit (reviewed in Mennella et al., 2014; Pimenta-Marques and Bettencourt-Dias, 2020). Due to advances in super-resolution imaging techniques over the past decade, the ordered structure of the PCM is now relatively well understood. During interphase, PCM components are organised as concentric, toroid-like structures surrounding the centrioles (Lawo et al., 2012; Mennella et al., 2012; Sonnen et al., 2012). In particular, by measuring the diameter of PCM toroids in human cells, it has been shown that CEP192, followed by CEP152, form the rings closest to the centriolar wall. Together with CEP152, CEP63 forms a ring around the proximal end of the mother centriole, and these two proteins cooperate to generate a cylindrical self-assembly that is capable of recruiting downstream components (Kim et al., 2019; Lukinavičius et al., 2013; Sir et al., 2011). This complex is followed by layers of CDK5RAP2, NEDD1, and γ -tubulin, which together form the site of MT nucleation and anchoring within interphase centrosomes. Much like the SAS6 spokes of the centriolar cartwheel, PCNT has been found to exist as radial elongations, with its C-terminus docked at the centrioles and its N-terminus extending towards the exterior of the interphase PCM boundary (Lawo et al., 2012; Rale et al., 2018).

During the transition from interphase to mitosis, the PCM expands in size and increases its ability to nucleate microtubules, in a process known as centrosome maturation (see section 1.5.2). In contrast to the organisation of the interphase PCM, the mitotic PCM is not as well-defined, appearing as a cloud of material under sub-diffraction imaging (Mennella et al., 2012). This material is composed primarily of CDK5RAP2, NEDD1 and γ TuRC, and is responsible for initiating MT assembly (reviewed in Tovey and Conduit, 2018). Additional components of the mitotic PCM cloud include the kinases PLK1 and AURKA; the continuous activity of PLK1 is required for maintenance of the mitotic PCM (Mahen et al., 2011). Interestingly, the mitotic PCM has been identified as a scaffold for ubiquitin-proteasome-mediated degradation, with a number of E3 ubiquitin ligase complexes having been shown to localise to the structure, thereby resulting in degradation of a number of cell cycle regulatory proteins, centrosome duplication factors and cell fate determinants (reviewed in Vora and Phillips, 2016). For a detailed illustration of the PCM organisation during interphase and mitosis, see Figure 1.3.

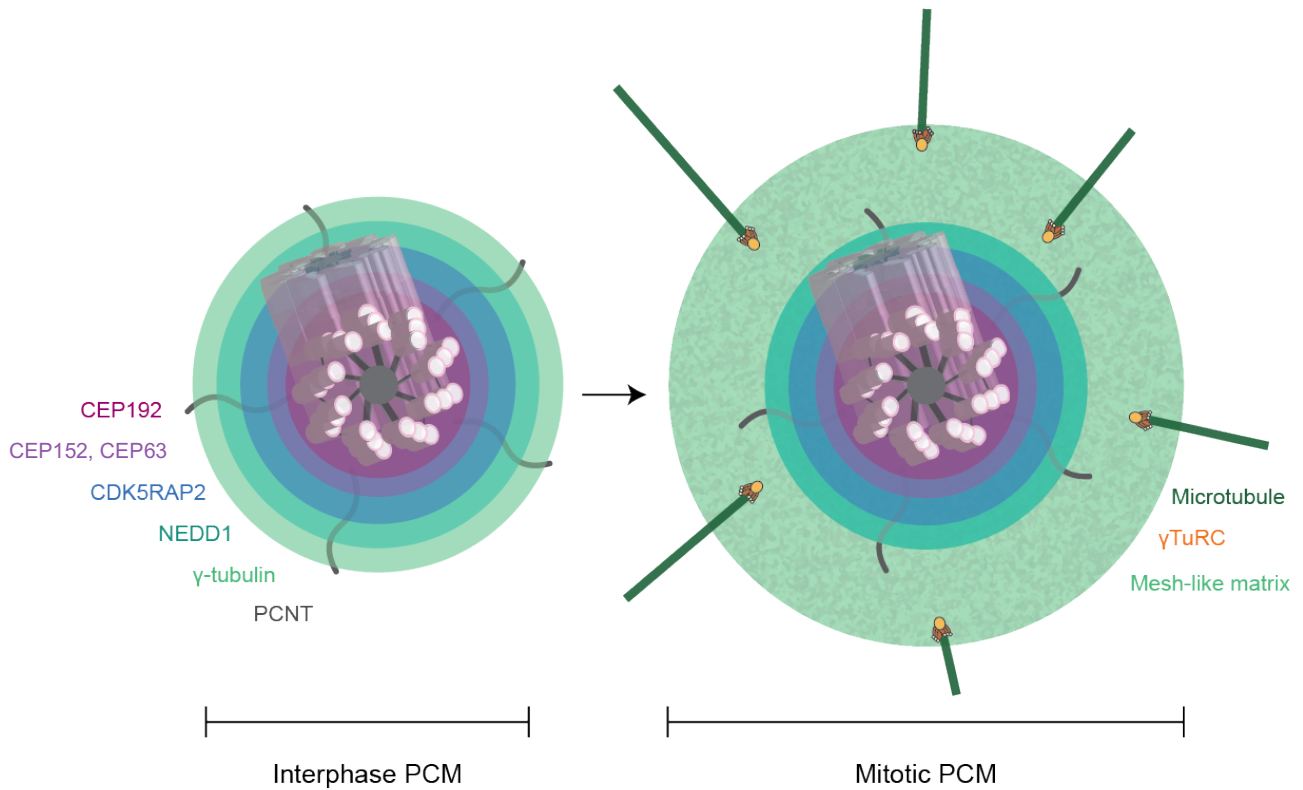


Figure 1.3. PCM organisation during interphase and mitosis. During interphase, the PCM is organised into concentric layers, as shown. During the transition from interphase to mitosis, the PCM expands into a mesh-like matrix comprising many factors critical for the MT nucleation capacity of the centrosome, including CDK5RAP2, NEDD1 and γ TuRC. Image based on (Rale et al., 2018).

1.5. Centrosome duplication cycle

In cycling cells, the centrosome duplicates once per cell cycle, ensuring that each cell contains two centrosomes that are able to organise the bipolar mitotic spindle, allowing for proper cell division to occur. After cell division, each daughter cell inherits one centrosome, which will undergo another round of duplication should the cell continue to divide. The centrosome duplication cycle is made up of a number of different phases, including centriole duplication, elongation, maturation, separation and disengagement (reviewed in Fu et al., 2015; Nigg and Holland, 2018). For a detailed illustration of the centrosome duplication cycle, see Figure 1.4.

1.5.1. Centriole duplication and elongation

Centriole duplication begins at the G₁/S transition of the cell cycle, when new centrioles (procentrioles) begin to assemble at the proximal ends of the pre-existing mother centrioles. This process is highly regulated in order to control for centriole number, and occurs at only one site (the origin of centriole duplication) per centriole (reviewed in Firat-Karalar and Stearns, 2014; Harrison et al., 2011). Interestingly, a number of studies have revealed an overlap in the machinery that regulates the cell cycle and the centrosome duplication cycle (reviewed in Fu et al., 2015; Harrison et al., 2011). Indeed, the G₁-phase CDKs (CDK2 and CDK4) have been revealed to be ‘guardians’ of centrosome dysfunction and genomic integrity, through their phosphorylation of various factors (including Mps1p-like kinase and CP110) to regulate centriole duplication (Chen et al., 2002; Fisk and Winey, 2001).

Three centriole proteins are believed to be the main players involved in defining the location of the origin of centriole duplication; PLK4, STIL and SAS6, which all localise at the site of procentriole assembly at the G₁/S transition (Firat-Karalar and Stearns, 2014; Pelletier et al., 2006). In human cells, the centrosomal scaffold proteins, CEP152, CEP192 and CEP63, cooperate together to ensure the recruitment of PLK4 to the origin of centriole duplication (Brown et al., 2013; Sonnen et al., 2013). Interestingly, overexpression of PLK4 has been shown to cause over-duplication of centrioles in many different cell types and species, confirming the importance of this protein as a ‘limiting initiator’ to the origin of centriole duplication, i.e. the concentration and distribution of PLK4 is known to be critical to limiting duplication to only one site per centriole (Firat-Karalar and Stearns, 2014; Habedanck et al., 2005; Kleylein-Sohn et al., 2007). In early G₁ cells, PLK4 is arranged in a ring-like structure around the mother centriole. In late G₁ and S-phase, however, PLK4 is distributed to a single focus on the mother centriole, and is co-localised with STIL and SAS6, in a process that is known as symmetry breaking (Ohta et al., 2014, 2018). A number of models have recently emerged explaining the mechanisms underlying symmetry breaking in centriole duplication (reviewed in Yamamoto and Kitagawa, 2021). One hypothesis suggests that PLK4 itself breaks its symmetric distribution by its ability to self-organise; inactive and active PLK4 interact with each other to form a single focus of PLK4 on the mother centriole. A second hypothesis suggests that PLK4 forms liquid-like droplets around the mother centriole which have various properties that can induce single focus formation. A third hypothesis suggests that the interaction between PLK4, STIL and phosphatases is what drive symmetry breaking (Leda et al., 2018).

Once the origin of centriole duplication has been defined on the mother centriole, the next step is formation of the cartwheel. During this phase, the newly forming centriole is tightly associated with the pre-existing mother centriole through a proteinaceous linking structure known as the S-phase to M-phase (S-M) linker. This S-M linker keeps the centriole pairs connected until disengagement of the mother and procentriole pair occurs during late mitosis (Nigg and Stearns, 2011). During S- and G₂-phase, microtubules are added to the nine-fold symmetric cartwheel in order to form the microtubule triplets, in a process known as centriole elongation. CPAP (also known as CENPJ or SAS4) is considered to be the master regulator of centriole elongation; it binds to tubulin dimers, allowing for polymerisation at the plus-ends of centriolar MTs, and its overexpression has been shown to result in the formation of abnormally long centrioles (Kohlmaier et al., 2009; Schmidt et al., 2009; Tang et al., 2009). Once the growing centriole has reached an appropriate length, capping on the plus-end of growing microtubules by CP110 is required to prevent further elongation (Kleylein-Sohn et al., 2007; Schmidt et al., 2009).

1.5.2. Centriole and centrosome maturation

After elongation, in a process known as centriole maturation, the mother centrioles acquire distal and subdistal appendages, structures which are essential for microtubule anchoring and ciliation (see section 1.4.2). In parallel, each centrosome starts to enlarge the pericentriolar material (PCM), a proteinaceous matrix in which the two centrioles of each centrosome are embedded. The primary functional role of the PCM is in microtubule nucleation. It is first assembled in interphase as an ordered and compact layer immediately surrounding the centrioles (known as the inner PCM layer), however, at the onset of mitosis, the PCM increases in size as well as microtubule-nucleation capacity, in a process known as centrosome maturation (see section 1.4.3 and Figure 1.2). This process drives spindle formation, orientation and chromosome segregation (Kim and Rhee, 2014; Mennella et al., 2014; Nigg and Stearns, 2014).

1.5.3. Centriole separation

At the onset of mitosis, the two centrosomes need to migrate towards opposite poles of the cell in order to form the bipolar spindle. For this to occur, the two parent centrioles begin to separate by disintegration of the G₁-G₂ tether (GGT), a fibrous structure that links the parental centrioles. The GGT is formed during G₁-phase of the cell cycle, shortly after centriole disengagement, allowing for maintenance of centriole cohesion until mitotic entry (Bornens et al., 1987). Dissolution of the GGT is initiated through a series of phosphorylation events

including the proteins NEK2, CNAP1 (CEP250) and Rootletin (Bahe et al., 2005; Fry et al., 1998a; Mardin et al., 2010). Further separation and movement of the centrosomes to the opposite poles of the nucleus is mediated by microtubule motor proteins, such as the plus-end directed kinesin EG5, which in turn are regulated by the kinases PLK1 and AURKA (Glover et al., 1995; Liu and Ruderman, 2006).

1.5.4. Centriole-to-centrosome conversion

The conversion of centrioles to centrosomes is an important step in which daughter centrioles acquire modifications which allow them to recruit the PCM, and thereby function as the primary MTOC in the cell. This process starts in early mitosis and is mediated by Polo-like Kinase 1 (PLK1), which is involved in dissolution of the cartwheel structure from daughter centrioles (Wang et al., 2011). Another player in this process is the centriole-enriched protein, CEP295, which has been shown to be indispensable for centriole-to-centrosome conversion in both *Drosophila* and human cells (Izquierdo et al., 2014; Saurya et al., 2016). In order for conversion to take place, CEP295 forms a complex with CEP135, CEP152 and CEP192 on the proximal end of daughter centrioles, initiating a PCM protein recruitment cascade on the daughter centriole wall (Fu et al., 2016; Tsuchiya et al., 2016). Recently, the luminal centriolar protein CEP44, as well as its binding partner POC1B, have been shown to be essential components of this conversion pathway (Atorino et al., 2020).

1.5.5. Centriole disengagement

The last step of the centrosome duplication cycle is centriole disengagement, when the S-M linker is dissolved at the onset of anaphase. Interestingly, this step is thought to “license” the centrosome for duplication, as in order for centriole duplication to occur (starting at the next G₁/S transition), centrioles first need to disengage. By keeping the centrioles engaged until late mitosis, centrosome duplication is limited to once per cell cycle (Tsou and Stearns, 2006; Tsou et al., 2009). Concomitant with dissolution of the linker, the PCM is rapidly disassembled at mitotic exit, a process which has been shown to be a driving factor for centriole disengagement in human cells but remains relatively poorly understood (Pimenta-Marques and Bettencourt-Dias, 2020; Seo et al., 2015). Centriole disengagement requires the activity of the mitotic kinase PLK1, which phosphorylates PCNT, thereby priming it for cleavage by separase (Kim et al., 2015). In a recent study, it was shown that CEP57 forms a complex with PCNT that is critical for PCM expansion and centriole engagement; CEP57 depletion causes precocious centriole disengagement and ectopic MTOC activity, resulting in chromosome segregation errors and aneuploidy (Watanabe et al., 2019). Interestingly, the cleavage of

cohesin by separase, in addition to its role in sister chromatid separation at anaphase-onset, is also believed to be involved in centriole disengagement, however the evidence for this is contradictory (reviewed in Fu et al., 2015)

1.5.6. PCM dynamics

Human centrosomes are comprised of up to 300 proteins, including many large coiled-coil domain-containing proteins which are particularly abundant in the PCM. Centrosomes are non-membranous organelles, and this has led to a number of questions as to how these structures assemble. The PCM, specifically, has only recently emerged as a higher-order structure, whose size and composition changes profoundly during the transition from interphase to mitosis (Lawo et al., 2012; Mennella et al., 2012). A number of models of PCM assembly have started to emerge in recent years (reviewed in Lee et al., 2021; Raff, 2019; Rale et al., 2018; Woodruff, 2021). Studies in *Drosophila* revealed that PCM proteins may assemble into micron-scale scaffolds through phospho-regulated multimerisation of centrosomin (Cnn) molecules (Conduit et al., 2014a, 2014b; Feng et al., 2017). A number of recent studies in human cells support this hypothesis, revealing that PCM scaffold proteins, CEP57, CEP63 and CEP152 assemble into a higher-order cylindrical architecture that is capable of recruiting downstream components (Kim et al., 2019; Watanabe et al., 2019; Wei et al., 2020). These proteins all contain multiple coiled-coil domains which provide the physical strength necessary to mediate the protein-protein interactions underlying the PCM scaffold (Lupas and Bassler, 2017). An alternative model suggests that the centrosome may assemble as phase-separated biomolecular condensates; indeed recent work in *C. elegans* has revealed that the key PCM scaffold protein, SPD-5, rapidly assembles *in vitro* into spherical condensates that concentrate tubulin and other PCM proteins that are important for microtubule nucleation (Woodruff et al., 2017; Zwicker et al., 2014). Future work remains to determine the extent to which PCM assembly occurs through high-affinity, well-ordered scaffolds, or liquid-condensate phase transitioning, or perhaps through a combination of both mechanisms; indeed, research from Ahn and colleagues suggests that phase separation of CEP63 and CEP152 is what underlies the formation of the higher-order, supramolecular structure of the PCM (Ahn et al., 2020).

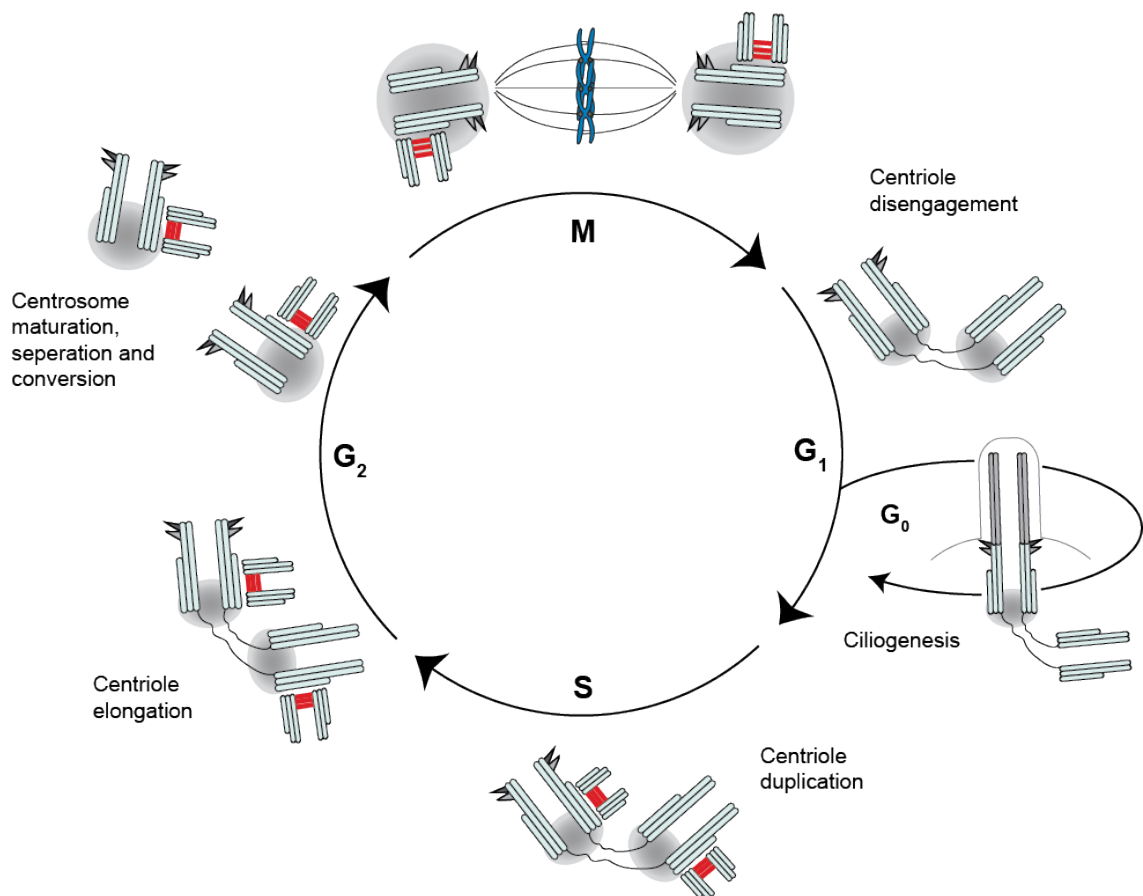


Figure 1.4. The centrosome duplication cycle. The centrosome duplication cycle is divided into a number of different phases, including centriole duplication, elongation, maturation, separation, centriole-to-centrosome conversion and disengagement. Centrosome duplication starts at the G₁/S transition, when procentrioles (cartwheel in red) start to assemble at the proximal ends of the mother centrioles. Duplication is followed by elongation during S and G₂, and maturation at G₂/M (during which the PCM (grey) is expanded). At the start of mitosis, the two centrosomes migrate to opposite poles in order to form the bipolar spindle. At the end of mitosis, the two centrioles disengage and a new centrosome duplication cycle can begin. When cells reversibly exit the cell cycle, the mother centriole serves as a basal body for assembly of the primary cilium (see section 1.7).

1.6. Non canonical centriole biogenesis

Whilst centriole duplication is generally limited to once per cell cycle, ensuring that each daughter cell inherits only one centrosome, in certain cases centriole formation can become uncoupled from the cell cycle and new centrioles can assemble via non-canonical pathways i.e. in the early mouse embryo and multiciliated cells such as in the respiratory tract and brain ependymal (reviewed in Nabais et al., 2017). While in multiciliated cells, it is possible for the mother centriole to template formation of multiple daughter centrioles (forming rosette-like structures), this process is fairly uncommon (Dawe et al., 2007; Loncarek and Khodjakov, 2009). Instead, the vast majority of centrioles in multiciliated cells assemble *de novo* around an electron-dense structure known as the deuterosome, which may or may not be formed using pre-existing centriolar precursors (Nabais et al., 2017; Zhang and Mitchell, 2015). This process is largely regulated by DEUP1 (a parologue of CEP63), CCDC78, as well as many of the proteins that are essential for canonical centriole duplication, including CEP152, PLK4, SAS6 and STIL (Klos Dehring et al., 2013; Zhao et al., 2013). Interestingly, recent research from Mercey and colleagues showed that multiciliated cells lacking deuterosomes are able to self-assemble the correct number of centrioles, revealing that deuterosomes are not essential for non-canonical centriole assembly (Mercey et al., 2019). In addition to this, in a paper published earlier this year, the Bettencourt-Dias lab were able to show that a high concentration of PLK4 is sufficient to trigger *de novo* centriole biogenesis in *Drosophila* egg explants, independent of cell cycle progression and the presence of other centrioles (Nabais et al., 2021). As an interesting supplement to this, researchers also showed that PCM components, γ -tubulin and CEP152 (Asl in *Drosophila*), are also able to promote *de novo* centriole assembly (Nabais et al., 2021).

1.7. Cilia

During the G₀- (quiescent) phase of the cell cycle, or in some differentiated cell types, the mother centriole can mature into a specialised structure called the basal body, which organises a cilium. Cilia can be divided into two main categories; motile or primary (usually immotile) cilia. Motile cilia are usually found in specialised epithelia (such as multi-ciliated epithelium), and are responsible for cell motility. Primary cilia, of which most vertebrate cells will assemble a single primary cilium, act as the signalling “hub” of the cell and are important for cellular sensing and signal transduction. A cilium consists of three main structures: a basal body, a transition zone, and a ciliary axoneme, which is encased by a ciliary membrane (Figure 1.5). The axoneme, which extends from the distal end of the basal body (a structure formed

by the mother centriole and associated PCM proteins), is composed of nine doublet microtubules (MTs), which are converted from the triplet MT structure of the basal body centriole at the region of the transition zone, a macromolecular complex that controls the entrance and exit (gating) of ciliary proteins (reviewed in Anvarian et al., 2019; Buchwalter et al., 2016; Kumar and Reiter, 2021).

The mother centriole templates the primary cilium due to its possession of centriolar appendages, DAPs and sDAPs. DAPs are involved in early ciliogenesis, by mediating docking of the mother centriole to pre-ciliary vesicles in the cytoplasm, and later to the ciliary membrane, steps which mark the conversion of the mother centriole to the basal body (Schmidt et al., 2012; Tanos et al., 2013). sDAPs are dispensable for cilia assembly, but play a role in the spatial control and sensory properties of primary cilia (Mazo et al., 2016). In order for cilia to grow, proteins important for cilium assembly, maintenance and disassembly are transported along the axoneme by a specialised transport system called intraflagellar transport (IFT). IFT complexes, which associate with MT plus-end directed motors (kinesins) and minus-end directed motors (dyneins) are responsible for moving cargoes into the cilium (anterograde transport) and out of the cilium (retrograde transport), respectively (Goetz and Anderson, 2010; Hao and Scholey, 2009). Additionally, it has been shown that centriolar satellites, electron dense granules that surround the centrosome (and the basal body), facilitate cytoplasmic movement of proteins to and from the cilium base (reviewed in Bärenz et al., 2011; Tischer et al., 2021).

Quiescent cells can lose their primary cilia and re-enter the cell cycle in process known as cilium disassembly. Cilium disassembly requires the destabilisation and de-polymerisation of axonemal microtubules, a process that is largely regulated by AURKA and the depolymerising kinesins, KIF2A and KIF24. In an alternative mechanism, cilia can also be removed by severing mechanisms, facilitated by the action of a microtubule-severing enzymes, such as katanin, which separates basal bodies from axonemes prior to mitotic entry (Rasi et al., 2009; reviewed in Sánchez and Dynlacht, 2016).

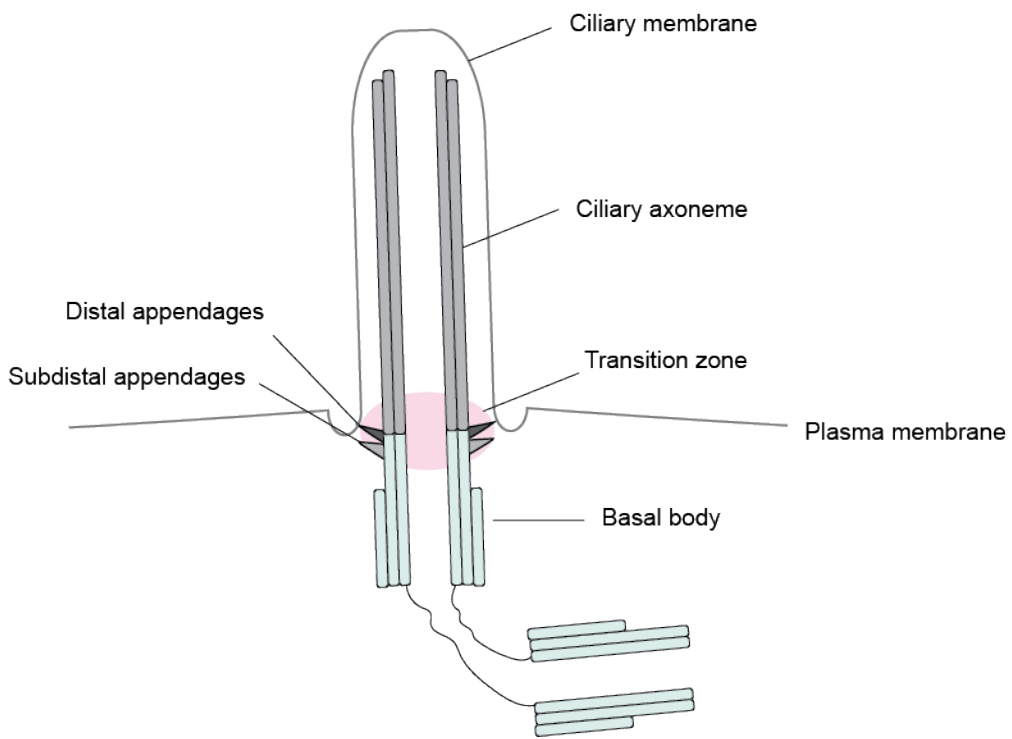


Figure 1.5. Structure of a primary cilium. Each cilium consists of a basal body, a transition zone, and a ciliary axoneme, the latter of which is encased by a ciliary membrane that is continuous with the plasma membrane. DAPs anchor the ciliary membrane to the basal body, as well as helping to recruit ciliary proteins in the transition zone, while sDAPs help to position the cilium in the cell. Image based on (Anvarian et al., 2019; Kumar and Reiter, 2021).

1.8. Centriolar satellites

In vertebrate cells, centrosomes are surrounded by a system of electron-dense granules known as centriolar satellites (CS). These granules were first discovered in cells in 1960, but only recognised and named as CS after the discovery of PCM1 (Bernhard and de Harven, 1960; Dammermann et al., 2004; Kubo et al., 1999). Pericentriolar Material 1 (PCM1) is a large coiled-coil protein that is considered to be the essential scaffolding component of CS; its depletion causes the disappearance of these structures. CS are important regulators of centrosomes (Firat-Karalar et al., 2014a; Kodani et al., 2015) and cilia (Conkar et al., 2017; Gupta et al., 2015; Lee and Stearns, 2013). Despite this knowledge, however, the biogenesis and function(s) of these structures is poorly understood. Until recently, a comprehensive analysis of CS composition was lacking; however, in 2019, two studies independently revealed the proteomic profile of these structures, via sucrose sedimentation and PCM1 affinity purification (Quarantotti et al., 2019), as well as interaction-mapping by performing proximity-dependent biotin identification (BiOID) of 22 known satellite proteins (Gheiratmand et al., 2019). Importantly, both studies revealed a high degree of similarity between CS and centrosome proteome composition, supporting the notion that CS represent cytoplasmic hubs for centrosomal proteins. In addition, CS composition was shown to be largely unaffected by centriole depletion, indicating that CS biogenesis may be independent of the centrosome. Interestingly, by combining proteomic profiling with super-resolution imaging, the Pelletier lab revealed that individual CS can differ in size as well as composition (Gheiratmand et al., 2019). While these results demonstrate an increased understanding of CS composition and behaviour, further studies are required to fully understand the molecular mechanisms of CS assembly and function.

1.9. Centrosomes and cilia in disease

Given the complexity involved in assembly and maintenance of centrosomes and cilia, it is not surprising that mutations in genes involved in these processes give rise to a large number of human diseases; including various developmental disorders, ciliopathies and cancer (reviewed in Goundiam and Basto, 2021).

Due to its role in a number of biological processes, the centrosome is critical during vertebrate development; it has been shown to be involved in cell differentiation as well as cell migration during neurogenesis (reviewed in Tang and Marshall, 2012). Indeed, mutations in centrosomal genes are responsible for the development of a number of rare diseases, including

microcephaly (MCPH), Seckel syndrome (SCKL) and microcephalic osteodysplastic primordial dwarfism type II (MOPDII). All three are autosomal recessive diseases, phenotypically characterised by significantly reduced brain size and intellectual disability, while SCKL and MOPDII patients show overall growth reduction and skeletal dysplasia as well. A number of centrosomal genes have been implicated in these developmental disorders, including core centriole duplication proteins CEP152, PLK4, STIL, SAS6 and CPAP/CENPJ, as well as PCM factors CDK5RAP2, PCNT and NIN (reviewed in Chavali et al., 2014; Marthiens and Basto, 2020).

In addition to various neurodevelopmental disorders, centrosomes have also been implicated in promoting tumourigenesis and the development of cancer. Aberrations in centrosome number, structure and function have been linked to a number of types of cancer. Structural defects occur due to alterations in centriole/PCM size and structure, and usually involve changes in expression of genes controlling centriole structure. A recent study from the Nigg lab showed that dysregulation of ninein-like protein (NLP) induced structural centrosome aberrations that triggered non-cell-autonomous dissemination of metastatic cells from epithelia (Ganier et al., 2018). Numerical defects, including centrosome amplification (CA), are more frequently described in cancer and most commonly arise from dysregulation of the centrosome duplication cycle as well as centriole over-duplication. CA has been shown to lead to the formation of multipolar mitotic spindles, chromosome mis-segregation and chromosome rearrangements (reviewed in Godinho and Pellman, 2014; Goundiam and Basto, 2021). Indeed, a recent study published by Levine and colleagues showed that PLK4 overexpression induced CA and aneuploidy, which was sufficient to induce spontaneous tumourigenesis in mice (Levine et al., 2017). In addition to promoting tumourigenesis, CA can also result in aneuploidy and cell death (due to lethal multipolar divisions). As a mechanism to evade CA, cancer cells have evolved mechanisms to cluster supernumerary centrosomes into a pseudo-bipolar spindle. This process is largely mediated by the MT motor protein, KIFC1/HSET, which is frequently overexpressed in a large number of human cancers. Interestingly, inhibition of HSET has been investigated as a novel anti-cancer therapeutic mechanism (Krämer et al., 2011; Watts et al., 2013). Independently of its role in producing aneuploidy and chromosomal instability (CIN), CA also promotes cell invasion. A recent study by the Godinho lab showed that oxidative stress induced by CA in human mammary cells drives non-cell-autonomous invasion by secretion of pro-inflammatory cytokines (Arnandis et al., 2018).

Centrosomes, in addition to their crucial role in cell division, are essential for the formation of primary cilia (see section 1.7). Mutations in primary cilia-related genes leads to an array of human diseases, collectively termed ciliopathies. Ciliopathies, including Joubert syndrome

(JBTS), Bardet-Biedl syndrome (BBS) and oro-facio-digital (OFD), are characterised by a range of overlapping phenotypes, such as hepatic disease, renal disease, retinal degeneration and brain and skeletal anomalies (reviewed in Reiter and Leroux, 2017; Waters and Beales, 2011).

1.10. Proteomic characterisation of the human centrosome

Mass spectrometry (MS)-based proteomics is a powerful tool for the analysis of complex protein samples, allowing for the study of protein-protein interactions via affinity-based isolation and/or BiOID (proximity-dependent biotin identification), the analysis of protein modifications and conformational changes, as well as mapping of protein composition in subcellular organelles, such as the centrosome. Quantitative MS-based analyses, using labelling strategies including SILAC (Stable Isotope Labelling by Amino acids in Cell culture) and TMT (Tandem Mass Tag), or targeted approaches such as SRM (Selected Reaction Monitoring), have allowed for highly sensitive and reproducible investigation of complex proteomes (reviewed in Aebersold and Mann, 2003; Lindemann et al., 2017; Vidova and Spacil, 2017).

The functional equivalent of the centrosome in budding yeast is called the spindle pole body (SPB). The SPB proteome was elucidated in 1998, when a highly enriched SPB preparation was analysed by MS (Wigge et al., 1998). Using a similar approach, the first proteomic analysis of the human centrosome was reported by Andersen and colleagues (Andersen et al., 2003). Centrosomes were purified through a discontinuous sucrose gradient, using protocols established more than two decades ago (Bornens and Moudjou, 1998), and centrosome composition was analysed by MS-based proteomics. Specifically, centrosome-containing centrifugation fractions were analysed using a quantitative protein correlation profiling (PCP) method, which identified at least 70 genuine centrosomal proteins, validated by *in vivo* localisation studies. A number of years later, using a PCP-SILAC MS-based approach, on centrosomes isolated using the same methodology, Jakobsen and colleagues identified 165 centrosomal proteins, 22 of which were confirmed as novel components. These novel candidates, identified by MS, were validated by a Human Protein Atlas (HPA) antibody-based screen (Jakobsen et al., 2011). The quantitative proteomic methods used in this study allowed for a more comprehensive and accurate coverage of centrosome composition, as well as an insight into the dynamics/turnover of centrosomal proteins. A number of years later, the Nigg lab expanded on this by using targeted proteomics (based on SRM) and EGFP-tagging

of proteins at endogenous loci to determine the absolute amounts of a number of human centriolar and centrosomal proteins (Bauer et al., 2016).

In addition to purification of centrosomes to study protein composition, proximity mapping using the BiOID technique has allowed for the characterisation of protein-protein interactions within centrosomes, cilia and centriolar satellites (CS). In 2015, the Pelletier lab mapped the interaction of 58 known centriole, CS and ciliary transition zone proteins, resulting in the identification of >1700 unique proteins and generating a network of >7000 proximity interactions at the centrosome-cilium interface (Gupta et al., 2015). Subsequently, the CS interactome was mapped using 22 known CS proteins, generating a network of >2000 proximity interactions amongst 660 unique proteins, 40% of which were found to overlap with previous centrosome proteomes (Gheiratmand et al., 2019). A number of studies have utilised BiOID to identify interaction networks of specific subsets of centrosomal proteins, such as those involved in centriole duplication and centriole elongation (Comartin et al., 2013; Firat-Karalar et al., 2014; Liu et al., 2018; Sydor et al., 2018). These are reviewed extensively in (Devi et al., 2021).

2 Aim of my PhD

The primary aim of this project was to establish a novel method for centrosome purification in order to investigate tissue specificity of centrosome composition. To this end, I purified centrosomes from a number of different cell types using the optimised and validated technique, COMPACT (Centrosome Purification by Affinity Capture). These data are presented in Chapters 4 and 5.

A secondary aim of my PhD was to gain mechanistic insight into COMPACT. Using cell lines lacking the centriolar appendage proteins, NIN or CEP128, I investigated the peptide's ability to purify centrosomes. These experiments are outlined in Chapter 4.

Finally, I aimed to use COMPACT as a discovery tool, to identify new centrosomal proteins. To investigate the potential centrosomal roles of candidate proteins, including the E3 ubiquitin-protein ligase TRIM27, I performed functional studies in HEK 293T cells. These data are presented in Chapter 6.

3 Materials and Methods

3.1 Cell culture-based techniques

3.1.1 General cell culture

HEK 293T/17 (HEK 293T) cells were grown in Dulbecco's Modified Eagle's Medium (DMEM) (Gibco) supplemented with 10 % heat-inactivated Fetal Bovine Serum (hi-FBS) (Gibco). U251 cells were grown in DMEM GlutaMAX (Gibco) supplemented with 10 % hi-FBS. Jurkat clone E6-1 (Jurkat) cells were grown in suspension in RPMI-1640 medium (Gibco) supplemented with 10 % hi-FBS (Gibco). Primary patient-derived glioblastoma cell lines, G166 and G7 (kindly donated by Dr Harry Bulstrode, MRC Cambridge Stem Cell Institute), were grown in DMEM/HAMS-F12 (Gibco) supplemented with 0.14 % D-(+)-Glucose solution (10 %; Sigma-Aldrich), 1 X MEM NEAA (100 X; Gibco), 0.01 % Bovine Albumin Fraction V (7.5 %; Gibco), 0.1 mM 2-Mercaptoethanol (50 mM; Gibco), 0.5 X B27 supplement (50 X, serum-free; Gibco) and 0.5 X N2 supplement (100 X; Gibco), on dishes pre-coated with 50 µg/ml Laminin (Cultrex). N1E-115 cells were grown in DMEM High Glucose (Gibco) supplemented with 10 % hi-FBS (Gibco). hTERT RPE-1 (RPE-1) cell lines were grown in DMEM F-12 GlutaMAX (Gibco) supplemented with 10 % hi-FBS (Gibco). HAP1 cells were grown in IMDM-GlutaMAX supplemented with 10 % hi-FBS (Gibco). All cells were cultured at 37 °C in a humidified chamber with 5 % CO₂.

3.1.2 Human induced pluripotent stem cell (hiPSC) culture

The hiPSC line, FSPS13B, was cultured in TesR™-E8™ medium (STEMCELL) in 6-well plates pre-coated with 10 µg/ml Vitronectin XF™ (STEMCELL). Media was exchanged daily and colonies were allowed to grow between 5 and 7 days before passaging.

- Passaging of hiPSCs

For passaging of hiPSCs, cells were washed once with DPBS (Gibco) followed by a 3 minute incubation in 0.5 mM EDTA (Invitrogen). After 3 minutes, when the cells had started to separate and lift from the dish, the EDTA solution was removed and cells were detached/lifted from the dish by pipetting TesR™-E8™ medium (STEMCELL) over the cells using a Gilson™ P1000 pipette. Detached colonies were transferred to a 15 ml falcon tube

using a 5ml pipette and allowed to settle at the bottom of the tube before aspirating the media to remove single cells. The cell pellet was resuspended once in TesRTM-E8TM medium (STEMCELL) and plated into 6-well plates (or larger dishes) pre-coated with Vitronectin XFTM (STEMCELL).

- Freezing hiPSCs

The above-mentioned method was used for passaging of hiPSCs. Once colonies had been detached, cells were collected by centrifugation at 300 g for 3 minutes and the pellet was resuspended in hiPSC freezing media: KnockOutTM Serum Replacement (Gibco) with 10 % DMSO and 10 µM Y-27632 (ROCK inhibitor; STEMCELL). Cells were frozen at -80 °C using a Mr. FrostyTM freezing container (Nalgene) before being placed in liquid nitrogen for long-term storage.

- Thawing hiPSCs

The frozen vial of hiPSCs were partially thawed in a waterbath at 37 °C and transferred carefully into the 15 ml falcon tube containing 1 ml TesRTM-E8TM medium. 9ml TesRTM-E8TM medium with 10 µM Y-27632 (ROCK inhibitor; STEMCELL) was then added dropwise to the cells, before centrifugation at 200 g for 3 minutes to obtain a cell pellet. The pellet was resuspended in 1 ml TesRTM-E8TM medium with 10 µM Y-27632 (ROCK inhibitor, STEMCELL) and added to one well of a 6-well plate pre-coated with Vitronectin XFTM (STEMCELL). Cells were allowed to settle for 24 hours before media was exchanged.

3.1.3 Drug treatments

Before isolation of centrosomes by the sucrose sedimentation-based technique (see Section 4.2.2), HEK 293T cells were treated with 1 µg/ml nocodazole (Sigma-Aldrich) and 1 µg/ml cytochalasin-B (Alfa Aesar) for 1 hour at 37 °C in 5 % CO₂.

For centrinone treatments, HEK 293T cells were treated with 150 nM Centrinone (Tocris) for a period of 8 days, with passaging of cells and fresh drug supplemented every 2-3 days.

For cell cycle synchronisations, HEK 293T cells were treated with 2.5 mM Thymidine (Sigma-Aldrich) for a period of 16-18 hours at 37 °C in 5 % CO₂. After release into fresh media for a

period of 8 hours, cells were either re-treated with 2.5 mM Thymidine or treated with 50 µM Monastrol (Tocris) for 16-18 hours at 37 °C in 5 % CO₂.

3.1.4 siRNA transfections

Cells were seeded the day before transfection, to achieve ~ 40 % confluence on the day of siRNA transfection. The negative control siRNA from Ambion (siRNA ID: 4390084, Silencer Select) was the control siRNA used in all the experiments. Targeting siRNAs (see Table 3.1) were used for functional experiments. The final siRNA final concentration used for all transfections was 50 nM. Transfections were carried out using Lipofectamine RNAiMAX (Invitrogen), according to the manufacturer's instructions. 48 hours after transfection, cells were processed for downstream analysis, such as western blotting, to verify the knock-down efficiency, and immunofluorescence for phenotypic analyses.

Table 3.1. List of siRNAs used in this thesis.

siRNA target	siRNA ID	Sequence (5' – 3')	Company
EDC4	#1; s24265	CAGGUACAGCGCAUCGUUAtt	Ambion, Silencer Select
EDC4	#2; s24266	CCUGUUCUGUGACAACCAUtt	Ambion, Silencer Select
TRIM27	#1; s11960	CAAAAUGUCUAUUCUUGAtt	Ambion, Silencer Select
TRIM27	#2; s11959	GCUGAACUCUUGAGGCCUAtt	Ambion, Silencer Select
DDB1	#1; s3981	GAGAUUGCUCGAGACUUUAtt	Ambion, Silencer Select
DDB1	#2; s3980	CCAUCGAUGAGAUCGCAGAAtt	Ambion, Silencer Select
CRBN	#1; s27634	CAAUUAGAAUCCCUCAAUAtt	Ambion, Silencer Select
CRBN	#2; s27635	GCUGAGACCUUAAUGGACAtt	Ambion, Silencer Select
NOP53	#1; s26871	GAACCAAAGUCCAGAAGAAtt	Ambion, Silencer Select
NOP53	#2; s26873	CUUCGAGACCGGUUCAAGAtt	Ambion, Silencer Select

3.2 Mouse tissue

All animal procedures were performed in accordance with the Animal Welfare and Ethical Body of the CRUK Cambridge Institute (CRUK CI, University of Cambridge), and UK Home Office regulations (in accordance with UK law, Animals Scientific Procedures Act 1986). Mice were housed under specific pathogen-free conditions and cared for in the CRUK CI Biological Resource Unit. Mice used in this study were of the C57BL/6 background.

3.2.1 Tissue collection and processing for COMPACT

Whole livers and spleens were isolated from 10 week old female C57BL/6 mice. Cells were isolated from the liver using a cell strainer (Easystrainer 70 µm, greiner bio-one); liver pieces were passed through the strainer using PBS and the back of a syringe, after which cells were pelleted at 300 g for 5 mins. Supernatant (containing fat) was discarded and pellet was washed with PBS and spun again. The final pellet was resuspended in Buffer P1 (see section 3.5) and lysed for 45 minutes on rollers at 4 °C. Cells were isolated from the spleen by placing the whole spleen in a 15 ml tube containing Buffer P1 and lysed using the TissueRuptor (Qiagen, USA) for approximately 30 seconds, until tissue was broken up. Thereafter, cells were lysed for 45 minutes on rollers at 4 °C.

For COMPACT protocol see section 3.5.

3.3 Cell imaging techniques

3.3.1 Immunofluorescence

Cells were seeded and grown on glass coverslips (VWR) previously washed with 100 % ethanol (Honeywell). Cells were fixed with 100 % ice-cold (-20 °C) methanol for spectroscopy (ACROS Organics) for 5 minutes at - 20 °C. After fixation, cells were permeabilised in PBST (PBS, 0.5 % (v/v) Tween 20 (Promega)), or for centriolar marker staining, in the extraction buffer (0.5 % (v/v) Triton X-100 (ACROS Organics)), 0.05 % (w/v) sodium dodecyl sulfate (SDS) (Sigma-Aldrich) and 0.5 % (v/v) Tween 20 (Promega) in PBS for 5 minutes at room temperature. Thereafter, cells were blocked in 5 % (w/v) Bovine Serum Albumin (BSA) (Sigma-Aldrich) in PBS for 15 minutes at room temperature, or overnight at 4 °C. Coverslips were then transferred into Nunc Delta 4 well plates (Thermo Scientific) for staining, and incubated with primary antibodies diluted in 5 % BSA in PBS according to Table 3.2, for 2 hours at 37 °C. Coverslips were then washed 4 x 5 minutes in PBST before incubation with secondary antibody conjugated to Alexa Flour 488 or 555 (Invitrogen), diluted 1:3000 in 5 % BSA in PBS, for 1 hour at 37 °C in the dark. Coverslips were then washed 3 x 5 minutes in PBST and briefly in PBS, before incubation with 1 µg/ml Hoechst 33258 (Sigma-Aldrich) in PBS, to visualize DNA. Coverslips were then mounted on glass slides (SuperFrost Ultra Plus, Thermo Scientific) using the ProLong Diamond Antifade Mountant (Invitrogen), and dried overnight at room temperature before being stored at 4 °C.

3.3.2 Confocal microscopy

Confocal images of fixed cells were taken using the Confocal White Light Laser (WLL) Leica TCS SP8 Microscope. All the images were acquired as z-stacks (1 µm step size, unless otherwise stated). Images were taken using the HC Plan Apo 100 x/1.40 OIL (CS2) objective and image acquisition was carried out with the Leica Application Suite X (LAS X) software (Leica Microsystems). For higher magnification images of centrosomes on coverslips, an optical zoom of 12 was applied, and single-focal plane images were acquired. These images were then exported to Hyugens Professional (Scientific Volume Imaging), and the Express Deconvolution tool was used for deconvolution of images, with no changes to manufacturers settings. After acquisition, all images acquired were imported into Fiji (version: 2.0.0-rc-59/1.51k) to obtain maximum intensity projections. The images were then converted to RGB and saved as TIFF files.

Table 3.2. List of all primary antibodies used for immunofluorescence.

Antibody	Species	Source and catalogue #	Dilution
ANKRD26	Rabbit	GeneTex; GTX128255	1:500
ARL13B	Rabbit	Proteintech; 17711-1-AP	1:300
CP110	Rabbit	Proteintech; 12780-1-AP	1:250
CEP83	Rabbit	Proteintech; 26013-1-AP	1:300
CEP128	Rabbit	Atlas, HPA001116	1:200
CEP152	Rabbit	Bethyl, A302-479A	1:500
CEP164	Rabbit	Proteintech; 22227-1-AP	1:400
CEP170	Rabbit	Abcam; ab72505	1:200
CETN3	Mouse	Abnova, H000001070-M01	1:300
CNTROB	Mouse	Abnova; H00116840-B01P	1:200
EDC4	Rabbit	Cell Signaling; #2548	1:200
FBF1	Rabbit	Atlas; HPA023677	1:100
NIN	Mouse	Proteintech, 67132-1-Ig	1:300
OFD1	Rabbit	Proteintech; 22851-1-AP	1:300
PCNT	Rabbit	Abcam, ab4448	1:500
SAS6	Mouse	Santa Cruz, sc-81431	1:500
SCLT1	Rabbit	Atlas; HPA036561	1:50
TRIM27	Rabbit	Proteintech, 12205-1-AP	1:200
γ -tubulin	Mouse	Sigma, T6557	1:300

3.4 Molecular biology techniques

3.4.1 Western blotting

- Sample preparation

Cells were lysed in RIPA buffer (50 mM Tris-HCl pH 8.0, 150 mM NaCl, 1 mM EDTA, 1 % (v/v) NP-40, 0.5 % (w/v) Na-deoxycholate, 0.1 % (w/v) SDS), supplemented with protease inhibitor cocktail tablets (Complete EDTA-free, Roche Diagnostics)). After incubating the samples on ice for 45 minutes, cell lysates were centrifuged at 14000 g for 15 minutes at 4 °C. Supernatants (cytoplasmic fraction) were transferred to new 1.5 ml tubes and the pelleted nuclear fractions were discarded. The protein concentration of the extracts was determined using the Direct Detect system (Millipore), after which protein samples were mixed with NuPAGE LDS Sample Buffer (Invitrogen), supplemented with NuPAGE Sample Reducing Agent (Invitrogen), and heated at 80 °C for 10 minutes.

- SDS polyacrylamide gel electrophoresis (SDS-PAGE)

Protein extracts were separated on a Bolt 4-12 % Bis-Tris Plus gel (Invitrogen) in 1 X MOPS buffer (Invitrogen). The PageRuler Plus Prestained Protein Standard (NewEngland Biolabs Inc.) was loaded alongside the proteins as a size reference. The gel was run at 50 V for 30 minutes followed by 150 V for a further 45 minutes, or until the dye front had run off the bottom of the gel.

- Western blotting

Proteins were transferred from the SDS polyacrylamide gel onto nitrocellulose membrane (0.45 µm) using the wet transfer system (TE22 Mighty Small Transfer Tank, Hoefer) in 1 X Transfer Buffer: 20 mM Tris Base, 192 mM glycine and 20 % (v/v) methanol (Honeywell), at 300 mA for 90 minutes at 4 °C. To test the efficiency of the transfer, nitrocellulose membranes were briefly stained with Ponceau S solution (Sigma-Aldrich), after which the stain was removed by incubating the membrane in Tris buffered saline (TBS) for 5-10 minutes at room temperature. The membrane was then blocked in 5 % milk (Marvel) in TBST (TBS, 0.1 % Tween-20) for 1 hour at room temperature on a rocking platform, in order to prevent non-specific binding of the antibody to the membrane. Primary antibodies diluted in 5 % milk in TBST were added to the membrane as in Table 3.3, and incubated

overnight at 4 °C on a rocking platform. Non-specific primary antibody was removed with 3 x 10 minute washes in TBST, with rocking. Horseradish peroxidase (HRP)-conjugated anti-rabbit or anti-mouse secondary antibodies (Dako) diluted in 5 % milk in TBST were added to the membrane and incubated for 1 hour at room temperature with rocking, after which the membrane was washed a further 3 x 10 minutes with TBST. For detection of protein bands, the Pierce ECL Western Blotting Substrate (Thermo Scientific) were mixed and used to cover the nitrocellulose membrane, according to the manufacturer's instructions. The membrane was then transferred into an Amersham Hypercassette Autoradiography Cassette (GE Healthcare Life Sciences) and the chemiluminescent signal was detected using X-ray films (CL-Xposure Film, Thermo Scientific) and the Film Processor MP900E (Colenta).

Table 3.3. List of all primary antibodies used for western blotting.

Antibody	Species	Source and catalogue #	Dilution
α-tubulin	Mouse	Sigma; T9026	1:1000
CP110	Rabbit	Proteintech; 12780-1-AP	1:500
CDK5RAP2	Rabbit	Produced in Gergely lab	1:500
CEP41	Rabbit	Bethyl; A301-798	1:1000
CEP83	Rabbit	Proteintech; 26013-1-AP	1:1000
CEP128	Rabbit	Atlas, HPA001116	1:500
CEP152	Rabbit	Bethyl, A302-479A	1:500
CETN3	Mouse	Abnova, H000001070-M01	1:500
CRBN	Rabbit	Proteintech; 11435-1-AP	1:1000
DDB1	Rabbit	Proteintech; 11380-1-AP	1:1000
EDC4	Rabbit	Cell Signaling; #2548	1:1000
NIN	Mouse	Proteintech, 67132-1-Ig	1:1000
NOP53	Rabbit	Proteintech; 27353-1-AP	1:500
PLK1	Rabbit	Novus; NB100-547	1:500
PCNT	Rabbit	Abcam, ab4448	1:2000
SAS6	Mouse	Santa Cruz, sc-81431	1:500
TRIM27	Rabbit	Proteintech, 12205-1-AP	1:1000
γ-tubulin	Mouse	Sigma, T6557	1:500

3.5 Centrosome Purification by Affinity Capture (COMPACT)

Centrosomes were purified based on a protocol using streptavidin-coated magnetic beads (Dynabeads™ M-280 Streptavidin; Invitrogen) and a biotinylated peptide corresponding to a 33 amino acid fragment of the centrosomal protein, CCDC61 (Biotin-SPSPTGGRALRFDPT AFVKAKERKQREIQMKQQ; Biomatik). Briefly, beads (60 µl per pulldown) were washed three times in TBS-N (TBS with 0.1 % NP-40) and once in Buffer P1 (50 mM Tris HCl pH 8.0, 300 mM NaCl, 0.2 % NP-40, 10 % glycerol, protease inhibitor cocktail (Complete EDTA-free, Roche Diagnostics) and phosphatase inhibitor cocktail (PhosStop; Roche Diagnostics)). Beads were then resuspended in Buffer P1 and peptide (6 µl per pulldown) was added, before being placed on a rotating wheel at 12 rpm for 1.5 hours at 4 °C. Cells (3×10^7 per pulldown) were collected in PBS using a cell scraper, lysed in Buffer P1 for 30 minutes on ice, sonicated briefly (2 x 3 second pulses) with an amplitude of 30 using a 3 mm microtip probe (418-21; Fischer Scientific), and centrifuged at 1800 g for 10 minutes at 4 °C. Supernatants were incubated with the beads plus peptide (pre-washed four times in Buffer P1 before being resuspended in a suitable volume of Buffer P1) on a rotating wheel at 12 rpm for 2 hours at 4 °C. After incubation, the beads were washed four times with Buffer P1. Western blot samples were resuspend in 1 X NuPAGE LDS Sample Buffer (Invitrogen), supplemented with NuPAGE Reducing Agent (Invitrogen) and then boiled at 80 °C for 10 minutes. Thereafter, beads were removed from the sample using a DynaMag™-2 magnet (Invitrogen). For western blotting protocol, see section 3.4.1. For SDS-PAGE, 1.5 % of the total cell lysate and unbound fraction was loaded, whereas bound lane represents 100 % bead-bound protein. Proteins were detected using standard ECL substrate, with exposure times of no longer than 3 minutes. Samples for mass spectrometry were washed twice in 100 mM Ammonium Bicarbonate (AMBIC; Fisher Chemical), before being flash-frozen in dry ice and stored at -80 °C. For mass spectrometry protocol, see sections 3.7 – 3.9. Unless otherwise stated, bead-only (BO) controls (i.e. lysate plus beads without peptide) were run alongside COMPACT samples, and proteins present in these were removed to create a COMPACT-specific protein list. For analysis of purified centrosomes using immunofluorescence, the collected beads were resuspended in Buffer P1 after the final wash, pipetted onto 1.5 mg/ml Poly-L-lysine (Sigma-Aldrich)-coated coverslips (Precision 1.5H, Marienfeld Superior) in a 24-well plate and spun at 2500 g for 10 minutes at 4 °C. For immunofluorescence protocol, see section 3.3.1.

3.6 Centrosome purification by sucrose sedimentation

Centrosomes were purified based on the protocol described by Chavali and Gergely, 2015 . Briefly, HEK 293T cells were treated with 1 µg/ml nocodazole and 1 µg/ml cytochalasin-B for 1 hour, washed in ice-cold PBS, before scraping and centrifugation at 1200 g. The pellet was then resuspended in 25 ml ice-cold TBS, centrifuged at 1200 g for 5 minutes, before being resuspended in 25 ml cold 8 % sucrose-0.1 % TBS. Following centrifugation at 1000 g for 5 minutes at 4 °C, the pellet was lysed in 45 ml Lysis Buffer (1 mM Tris HCl pH 8.0, 0.5 % NP-40, 0.5 mM MgCl₂, 0.1 % β-mercaptoethanol (added fresh before lysis), protease inhibitor cocktail (Complete EDTA-free, Roche Diagnostics) and phosphatase inhibitor cocktail (PhosStop, Roche Diagnostics)). Cells were lysed using a rubber bulb and incubated on ice for 5 minutes. Lysates were cleared by centrifugation at 1800 g for 10 minutes at 4 °C. The supernatant was filtered through a 70 µm cell-strainer cap (BD Falcon), after which 1 M K-PIPES pH 7.2, 1 mM EDTA, and 2250 U DNasel (Sigma-Aldrich) was added to achieve a pH of 6.8, and supernatants were incubated on ice for 15 minutes. Supernatants were pre-fractionated on a 50 % (w/w) sucrose cushion at 11000 rpm for 30 minutes at 4 °C using the SW32 rotor (Beckman Coulter), and then separated on a discontinuous sucrose gradient for 2 hours at 25000 rpm using the SW40 Ti rotor (Beckman Coulter). The discontinuous sucrose gradients were freshly prepared by layering 2 ml 70 % (w/w) sucrose solution, 1.5 ml 50% (w/w) sucrose solution, and 1.5 ml 40% (w/w) sucrose solution on top of each other in Ultra-Clear tubes (14 x 95 mm, Beckman). The sucrose solutions were prepared in 10 mM K-PIPES pH 7.2, 1 mM EDTA, 0.1 % β-mercaptoethanol (freshly added), 0.1 % Triton-X100 (freshly added), protease inhibitor cocktail (Complete EDTA-free, Roche Diagnostics) and phosphatase inhibitor cocktail (PhosStop, Roche Diagnostics)). After centrifugation, 0.5 ml sucrose fractions were collected from the top of the gradient with a p1000 pipette and transferred into separate polycarbonate tubes (11 x 34 mm, Beckman). 800 µl K-PIPES pH 7.2 was added to each collected fraction, and tubes were centrifuged at 35000 rpm for 20 minutes 4 °C using the MLA-130 rotor (Beckman Coulter). Pellets were either resuspended in 10 mM K-PIPES pH 7.2 and prepared for western blotting (see section 3.4.1), or flash-frozen in dry ice and stored at -80 °C for mass spectrometry analysis (see section 3.7 – 3.9).

3.7 Mass spectrometry: sample preparation

Mass spectrometry-based experiments were carried out by the Proteomics Core Facility at the Cancer Research UK Cambridge Institute, who kindly provided the following protocols.

3.7.1 “On bead” tryptic digestion of proteins

Beads were trypsinised with 100 ng of trypsin in 100 mM Ammonium Bicarbonate (AMBIC, Sigma) for overnight at 37 °C, in order to digest the bait and the interacting proteins. After the overnight digest, trypsin was added and digested for another 4 hours at 37 °C. The supernatant was collected and the reaction was stopped with Formic Acid (FA) to a final concentration of 0.5 % (v/v). The peptides were desalted using C18 cartridges (Biochrom). The C18 cartridges were conditioned and equilibrated with 50 % acetonitrile (Fisher Scientific) and 0.1 % FA respectively. The acidified peptides were loaded and the peptide-loaded cartridges were washed 0.1 % FA and eluted with 60 % acetonitrile/0.1 % formic acid. Dried peptides were reconstituted in 0.1 % FA acid, for further LC–MS/MS analysis.

3.7.2 “In solution” tryptic digestion of proteins (sucrose sedimentation samples)

The cell pellets were resuspended in 20 µl lysis buffer containing 100 mM Triethylammonium bicarbonate (TEAB, Sigma), 0.1 % SDS (Sigma) followed by heating at 90 °C for 5 minutes and probe sonication (Active motif). Complete samples were reduced with 2 µl 50 mM tris-2-caraboxymethyl phosphine (TCEP, Sigma) for 1 hour at 60 °C followed by alkylation with 1 µl 200 mM methyl methanethiosulfonate (MMTS, Sigma) for 10 minutes at RT. Protein samples were then digested overnight at 37 °C using trypsin (Thermo Scientific) solution at ratio protein:trypsin ~ 1:30. The next day, protein digest was acidified with FA to a final concentration of 0.5 % (v/v). The peptides were desalted using C18 cartridges (Biochrom) as mentioned above. Dried peptides were reconstituted in 0.1% FA acid, for further LC–MS/MS analysis.

3.7.3 Tandem Mass Tag (TMT) quantitative proteomics

Beads were trypsinised with 100 ng trypsin in 100 mM Ammonium Bicarbonate (AMBIC, Sigma) overnight at 37 °C. After the overnight digest, trypsin was added and digested for a further 4 hours at 37 °C. The supernatant was collected and the reaction stopped with 0.5 % (v/v) FA. The peptides were desalted using C18 cartridges (Biochrom), which were conditioned and equilibrated with 50% acetonitrile (Fisher Scientific) and 0.1 % FA,

respectively. The acidified peptides were loaded and the peptide-loaded cartridges washed 0.1 % FA and eluted with 60 % acetonitrile/0.1 % FA. C18 cleaned peptides were labelled with the TMT-10plex plus reagents (Thermo Scientific) for 1 hour. All the samples were mixed and dried with speed vac concentrator. The TMT-mix samples were fractionated with Reversed-Phase cartridges at high pH (Pierce #84868). Nine fractions were collected using different elution solutions in the range of 5–50 % ACN as per manufacturers protocol. Dried peptides were reconstituted in 0.1% FA, for further LC–MS/MS analysis.

3.8 Liquid chromatography tandem mass spectrometry (LC-MS/MS)

Each dried peptide sample was reconstituted in 25 μ l of 0.1 % (v/v) FA, and 5 μ l injected into the LC column for analysis (for sucrose sedimentation samples, each dried peptide sample was reconstituted in 10 μ l of 0.1 % (v/v) FA, and 10 μ l injected into the LC column for analysis). Peptides were loaded and separated on a reverse-phase trap column (length: 2 cm, inner diameter; 100 μ m) and analytical column (length: 25 cm, inner diameter: 75 μ m), respectively with 5–45 % acetonitrile gradient in 0.1 % FA at 300 nl/min flow rate. In each data collection cycle, one full MS scan (400–1,600 m/z) was acquired in the Orbitrap (60K resolution, automatic gain control (AGC) setting of 3×10^6 and Maximum Injection Time (MIT) of 100 ms). The most abundant ions with a top 10 setting were selected for fragmentation by High-energy Collision induced dissociation (HCD). HCD was performed with a collision energy of 28 %, an AGC setting of 2×10^4 , an isolation window of 2.0 Da, a MIT of 100 ms. Previously analysed precursor ions were dynamically excluded for 30 s.

3.8.1 TMT runs

Peptide fractions were analysed on a Dionex Ultimate 3000 system coupled with the nano-ESI source Fusion Lumos Orbitrap Mass Spectrometer (Thermo Scientific). Peptides were trapped on a 100 μ m ID X 2 cm microcapillary C18 column (5 μ m, 100 A) followed by 2 hour elution using 75 μ m ID X 25 cm C18 RP column (3 μ m, 100 A) with 5–45 % acetonitrile gradient in 0.1 % FA at 300 nl/min flow rate. In each data collection cycle, one full MS scan (380–1,500 m/z) was acquired in the Orbitrap (120K resolution, automatic gain control (AGC) setting of 3×10^5 and Maximum Injection Time (MIT) of 100 ms). The subsequent MS2 was conducted with a top speed approach using a 3 second duration. The most abundant ions were selected for fragmentation by collision induced dissociation (CID). CID was performed with a collision energy of 35 %, an AGC setting of 1×10^4 , an isolation window of 0.7 Da, a MIT of 35 ms. Previously analysed precursor ions were dynamically excluded for 45 seconds. During the

MS3 analyses for TMT quantification, precursor ion selection was based on the previous MS2 scan and isolated using a 2.0 Da m/z window. MS2–MS3 was conducted using sequential precursor selection (SPS) methodology with the top10 settings. HCD was used for MS3, performed using 55 % collision energy and reporter ions were detected using the Orbitrap (50K resolution, an AGC setting of 5×10^4 and MIT of 86 ms).

3.9 Mass spectrometry data analysis

The Proteome Discoverer 1.4 software (Thermo Scientific) was used for the processing of HCD tandem mass spectra. The SequestHT search engine was used and all the spectra searched against the Uniprot Homo sapiens FASTA database (taxon ID 9606). All searches were performed with a static modification of Methylthio at Cysteines (+45.988 Da). Methionine oxidation (+15.9949 Da) and Deamidation on Asparagine and Glutamine (+0.984 Da) were included as dynamic modifications. Mass spectra were searched using precursor ion tolerance 20 ppm and fragment ion tolerance 0.02 Da. For peptide confidence, 1 % FDR was applied and peptides uniquely matched to a protein were used for further analysis.

3.9.1 Data analysis for label-free quantification (LFQ)

The HCD tandem mass spectra were processed with the SequestHT search engine on Proteome Discoverer 2.2 software. The node for SequestHT included the following parameters: Precursor Mass Tolerance 20ppm, Maximum Missed Cleavages sites 2, Fragment Mass Tolerance 0.02Da and Dynamic Modifications were Oxidation of M (+15.995 Da) and Deamidation of N, Q (+0.984 Da). The Minora Feature Detector node was used for label-free quantification and the consensus workflow included the Feature Mapper and the Precursor Ion Quantifier nodes using intensity for the precursor quantification. For peptide confidence, 1 % FDR was applied and peptides uniquely matched to a protein were used for quantification.

3.9.2 Data analysis for TMT

The Proteome Discoverer 2.1 or 2.4 software (Thermo Scientific) was used for the processing of CID tandem mass spectra. The SequestHT search engine was used and all the spectra searched against the Uniprot Homo sapiens FASTA database (taxon ID 9606). All searches were performed using a static modification TMT6plex (+229.163 Da) at any N-terminus and on lysines and Methylthio at Cysteines (+45.988 Da). Methionine oxidation (+15.9949 Da) and

Deamidation on Asparagine and Glutamine (+0.984 Da) were included as dynamic modifications. Mass spectra were searched using precursor ion tolerance 20 ppm and fragment ion tolerance 0.5 Da. Decoy database search was employed to generate high peptide confidence (1 % FDR) and for quantification, information calculated from reporter ion intensities of peptides uniquely matched to a protein were used.

3.10 Generation of CEP128 knock-out cells by CRISPR/Cas9 genome editing

The CRISPR/Cas9 based genome editing technology was used to knock-out CEP128 in HEK 293T cells, following published protocols (Ran et al., 2013). The gRNAs used to target CEP128 were designed online using various tools, including CRISPR Design (www.crispr.mit.edu), CRISPR Search (www.sanger.ac.uk/hgt/wge/find_crisprs), and ChopChop (www.chopchop.cbu.uib.no). Oligonucleotides were designed with overhangs containing the Bbs1 restriction site. The selected gRNAs are listed in Table 3.4.

Table 3.4. CEP128 gRNA cloned into the px458 vector.

gRNA ID	Sense (5' – 3')	Antisense (5' – 3')
CEP128 gRNA_1	GCTGCCAGATCAACGCACAGGG	CCCTGTGCGTTGATCTGGCAGC

3.10.1 Cloning of gRNA into the px458 vector

The oligonucleotide pairs for CEP128 gRNA (sense and antisense) were phosphorylated using the T4 Polynucleotide Kinase (NEB), according to the manufacturer's instructions, and annealed by leaving the tubes in the thermomixer (turned off) for 3 hours. The oligonucleotide duplexes were ligated into the Bbs1 digested pX458 plasmid (#48138, Addgene) previously digested with the Bbs1 restriction enzyme (NEB), using the Quick Ligation Kit (NEB), according to the manufacturer's instructions. The ligated product was transformed into DH5a competent cells, and DNA purified using the GenElute Plasmid Miniprep Kit (Sigma-Aldrich). To verify the correct insertion of the gRNAs into pX458, plasmids were sequenced by Sanger sequencing (using the U6 promoter sequencing primer, 5'-CATGATTCCCTCATATTGCATATAGC-3') through the GATC/Eurofins sequencing service.

3.10.2 Transfection and FACS sorting of HEK 293T cells

HEK 293T cells were seeded the day before transfection, to achieve 40 - 60 % confluency on the day of transfection. FuGENE HD (Promega) was used to transfet the gRNA-Cas9 pX458 vectors, according to the manufacturer's instructions. 24 hours after transfection, GFP-positive cells were single sorted into 96 well plates by FACS, using BD FACSAria IIU (BD Biosciences). Untransfected cells were single sorted as a negative control. Single clones were expanded and screened by western blotting to identify putative CEP128 knock-out clones.

3.10.3 Sequencing of HEK 293T clones

To identify the CRISPR/Cas9-mediated cleavage sites and further characterise the transcript variants, the gRNA-targeted sequences were amplified using gDNA as a template (100 ng, purified using Gentra Puregene Cell Kit) (primers are listed in table 3.5). The blunt-ended PCR products obtained using the Phusion High-fidelity DNA polymerase (New England Biolabs), according to the manufacturer's instructions, were gel extracted using QIAquick Gel Extraction Kit (Qiagen), according to the manufacturer's instructions. PCR products were cloned into the pJET1.2/blunt Cloning vector, using the CloneJET PCR Cloning kit (Thermo Scientific), according to the manufacturer's instructions.

10 single bacterial colonies per gDNA template were analysed by Sanger sequencing using the GATC/Eurofins sequencing service. The primers used for sequencing, pJet1-FP (5'-ACTACTCGATGAGTTTCGG-3') and pJet1-RP (5'-TGAGGTGGTTAGCATAGTTC-3') are both available from GATC/Eurofins.

Table 3.5. List of primers used to amplify the CEP128 genomic locus from putative CEP128 knockout clones.

Primer ID	Sequence (5' – 3')
CEP128_exon1_forward 1	CTGTGTGGCCTTACCTGTG
CEP128_exon1_reverse 1	TTGAGACCCAGTGAGACCAG
CEP128_exon1_forward 2	AGCAGAGACAATGGAGGAGG
CEP128_exon1_reverse 2	GGCAGCCTCTAGAAACCAGA

3.11 Statistical analysis

To summarise data and to perform statistical analysis, GraphPad Prism 9.0 (GraphPad) was used. Unless otherwise stated, the two-tailed unpaired Student's t-test was used, and experiments performed in triplicate were expressed as the mean \pm standard deviation (SD).

4 Results I

4.1. A novel method for centrosome isolation

4.1.1. Centrosome Purification by Affinity Capture (COMPACT)

The current gold-standard for centrosome isolation from human cells involves centrifugation of cell lysates through a discontinuous sucrose gradient, allowing for sedimentation of differently sized particles into separate fractions (Andersen et al., 2003; Bornens and Moudjou, 1998). Due to the nature of this technique, specific fractions contain a number of cellular components that are similar in size, shape and/or density; for example, in addition to centrosomal proteins, Andersen and colleagues found a number of proteins from other cellular compartments, including mitochondria and the nucleus. Additionally, for isolation of a sufficient number of centrosomes to be analysed via MS-based proteomics, up to 3×10^9 cells are required (Andersen et al., 2003; Jakobsen et al., 2011).

A new method for centrosome isolation was identified a number of years ago in our laboratory by Dr Takashi Ochi and Dr Valentina Quarantotti, and further adapted by laboratory members Bradley Nash and myself. This approach, hereafter named COMPACT (Centrosome Purification by Affinity Capture), involves single-step affinity purification of centrosomes by a short peptide corresponding to a 33 amino acid C-terminal fragment of the centrosomal coiled-coil protein, CCDC61 (Figure 4.1). CCDC61 is a parologue of SAS6, which has recently been shown to bind MTs and interact with various centriolar and centriolar satellite proteins (Bärenz et al., 2018; Ochi et al., 2020). Briefly, centrosomes are isolated from cell lysates following incubation with the biotin-labelled peptide that is coupled to streptavidin-coated magnetic beads (Figure 4.2). Initial MS data from COMPACT performed in HEK 293T cells, courtesy of Dr Valentina Quarantotti, suggests that COMPACT is effective in purifying a large number of centrosomal proteins, as approximately 60% of proteins found in the partially validated centrosomal protein list published by Jakobsen and colleagues (Jakobsen et al., 2011) were found in HEK 293T centrosomes by COMPACT-MS (Figure 4.3 A). Additionally, using electron microscopy after COMPACT, Dr Takashi Ochi was able to visualise centriolar structures of the centrosome (Figure 4.3 B) or basal body (Figure 4.3 C).

One of the primary aims of my PhD was to further optimise and validate the COMPACT methodology, in order to use COMPACT as a tool to investigate centrosome proteome composition in a variety of biological contexts.

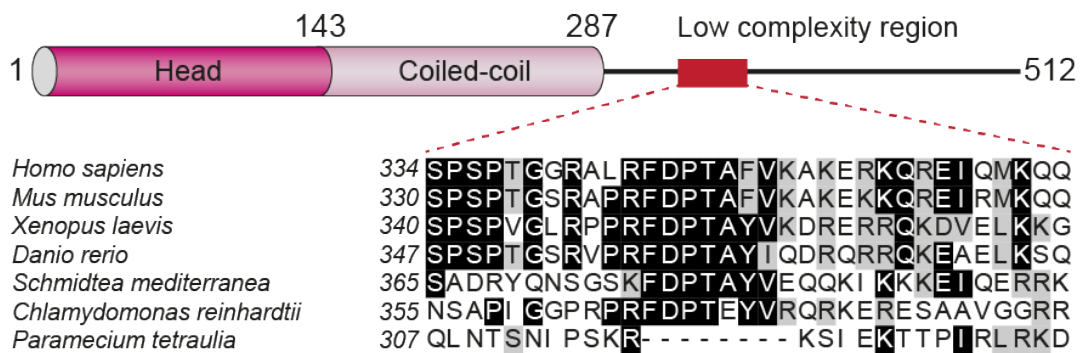


Figure 4.1. CCDC61 peptide sequence alignment. Image shows the full-length CCDC61 protein, with the region from which the peptide originates (highlighted in red) amplified to show amino acid sequence alignment for a number of species. Numbering represents first amino acid position for the peptide sequence in multiple species. Black indicates full conserved regions, grey represents semi-conserved regions. Figure adapted from image provided by Dr Takashi Ochi (The Astbury Centre for Structural Molecular Biology, University of Leeds).

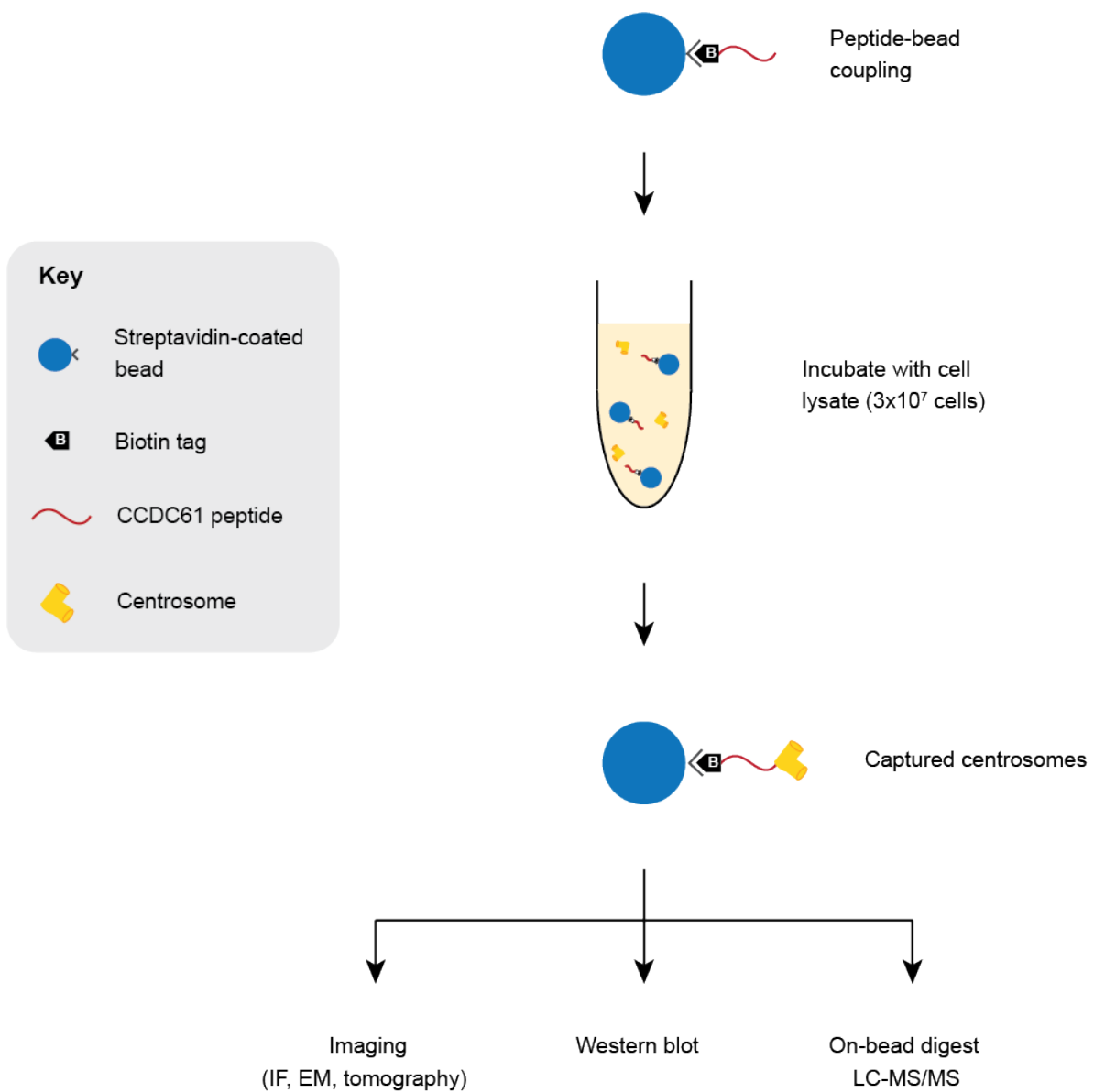


Figure 4.2. COMPACT workflow. Streptavidin-coated magnetic beads coupled to the N-terminally biotinylated CCDC61 peptide (corresponding to amino acids 334 to 367; see Figure 4.1) are incubated with whole cell lysates, allowing for centrosome-bound complexes to form. After washing, beads are collected and bead-bound complexes analysed using various imaging techniques, western blotting and LC-MS/MS.

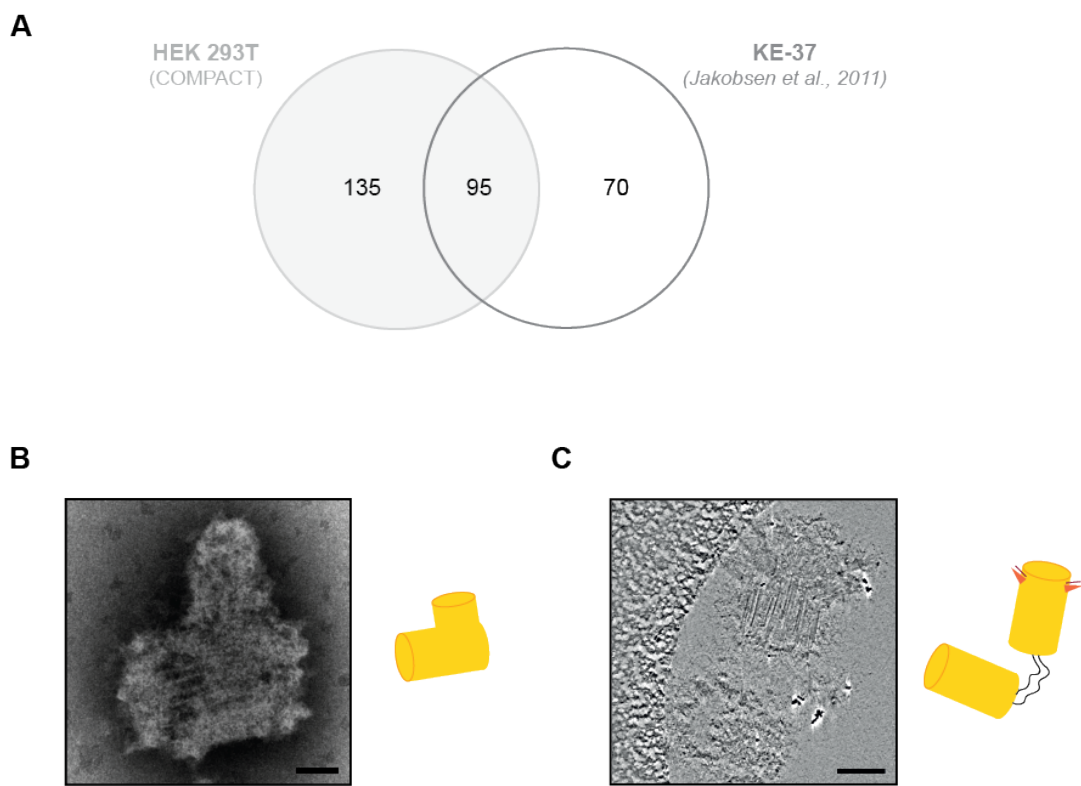


Figure 4.3. Purification of centrosomes by COMPACT. **A:** Venn diagram comparing the total number of proteins identified by COMPACT-MS in HEK 293T cells, compared to the KE-37 centrosome proteome dataset from Jakobsen *et al.*, 2011. HEK 293T COMPACT-MS data courtesy of Dr Valentina Quarantotti. **B:** Negative stain electron microscopy images of a centrosome purified from HEK 293T cells. **C:** Cryo-electron tomographic section of centrioles/basal bodies purified from serum-starved RPE-1 cells. Scale bars, 200nm. Images in B and C courtesy of Dr Takashi Ochi (The Astbury Centre for Structural Molecular Biology, University of Leeds). Cartoon images depict centriole positioning, and presence of structures such as appendages and centriole linker.

4.2. COMPACT method optimisation and validation

4.2.1. Optimisation of the COMPACT protocol in HEK 293T cells

Preliminary data showed that centrosomes could be isolated from human cell lines using the new COMPACT technique (Figure 4.3). A main aim of my PhD was, therefore, to expand on this by further optimising COMPACT to be streamlined, reproducible, easy to perform, and efficient at isolating centrosomes from a broad range of cell lines (using a lower cell number than required by previous methods).

In order to start optimising the COMPACT method, the human embryonic kidney cell line, HEK 293T was chosen as it is easy to grow in culture, and preliminary results had indicated that a large number of centrosomal proteins could be isolated from these cells, identified by COMPACT followed by mass spectrometry; COMPACT-MS (Figure 4.3). One of the main aims for optimising the COMPACT method was to successfully purify centrosomes from significantly fewer cells than used in the traditional centrosome isolation method. As previous COMPACT attempts had not utilised cell counting, but rather cell number estimation based on cell density and number of tissue culture flasks, an experiment was performed in which 1×10^7 , 2×10^7 and 3×10^7 cells were lysed, and western blotting (COMPACT-WB) using primary antibodies against four key centrosomal proteins (PCNT, SAS6, γ -tubulin and CETN3) was used to assess COMPACT efficiency (Figure 4.4). COMPACT was considered suitable for further analysis (i.e. by COMPACT-MS) if the four proteins were visualised in the bound fraction in less than 5 minutes, using a standard ECL western blotting substrate (see section 3.4.1). As a result, 3×10^7 cells (100X fewer than traditionally used, and approximately 3mg/ml of protein) were used for all COMPACT experiments going forward, unless otherwise stated. Importantly, when COMPACT was compared to an experiment performed in exactly the same way but without the addition of the peptide (to identify proteins that bind to the beads in the absence of the peptide i.e. background binding), no centrosomal protein was observed in the bound fraction (Figure 4.5). The apparent shift in band size (bound compared to lysate/unbound) can be explained by the difference in charge between the samples; lysate and unbound samples are diluted in Buffer P1 (containing NaCl), while bound samples are not.

Another attempt at optimisation of COMPACT involved changing the order by which the cell lysate was exposed to the peptide and beads. This experiment was performed in order to determine whether centrosomes are able to bind the peptide alone, or if a pre-formed peptide-bead complex is required for centrosome binding. Figure 4.6 shows that COMPACT was

significantly more efficient when the peptide was incubated with the beads prior to adding the cell lysate (peptide + beads), thus this was the method used going forward (as shown in Figure 4.2 and described in section 3.5). Interestingly, preliminary data from Dr Mark van Breugel (School of Biological and Chemical Sciences, Queen Mary University of London) and Dr Takashi Ochi (The Astbury Centre for Structural Molecular Biology, University of Leeds) revealed that GFP-tagged peptide did not localise to the centrosome (personal communication, data not shown). This observation combined with the above results suggests that a pre-formed peptide-bead complex is required for purification of centrosomes by COMPACT.

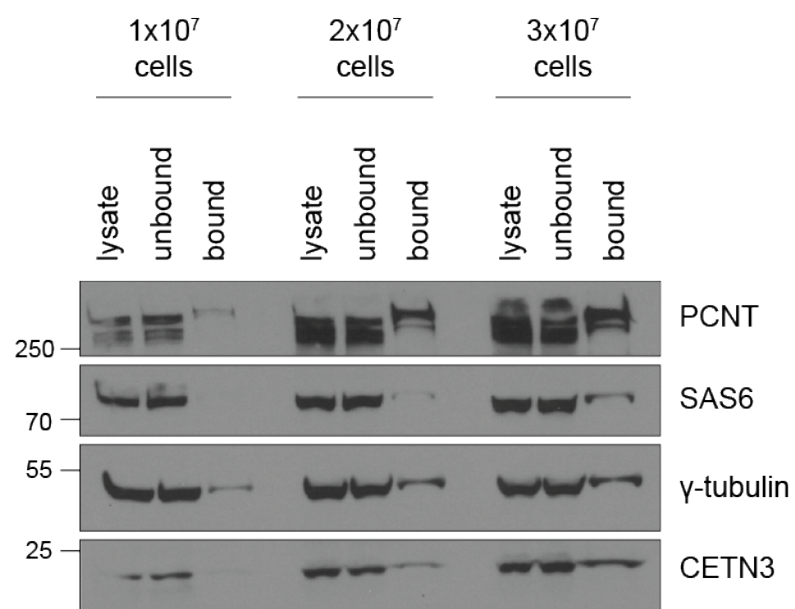


Figure 4.4. Optimising cell number for COMPACT in HEK 293T cells. COMPACT-WB showing centrosome proteins in the bound (bead-bound) fraction, compared to lysate and unbound fractions.

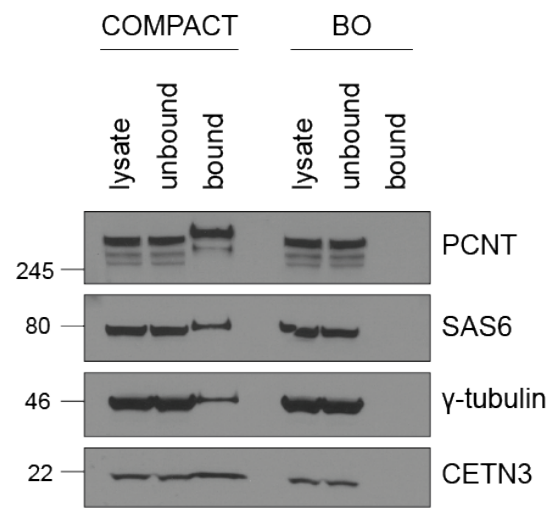


Figure 4.5. Comparing COMPACT and BO pulldowns in HEK 293T cells. COMPACT-WB showing centrosome proteins in the bound (bead-bound) fraction, compared to lysate and unbound fractions, for affinity purifications performed with peptide and beads (COMPACT), or bead-only (BO).

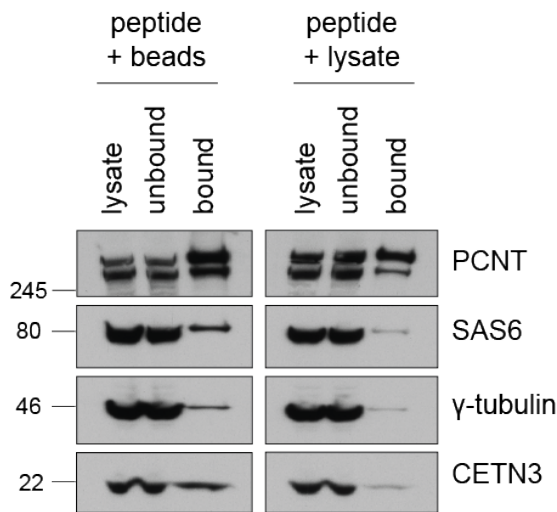


Figure 4.6. Optimising incubation conditions for COMPACT in HEK 293T cells. COMPACT-WB showing centrosome proteins from experiments in which the peptide was incubated with the beads before adding the cell lysate (peptide + beads), or the peptide was incubated with the cell lysate before capturing with the beads (peptide + lysate).

To determine whether I could increase the yield of COMPACT (i.e. saturation of peptide-bound beads with centrosomes), the ratio of beads, or beads and peptide, to lysate was increased. As seen in Figure 4.7, doubling either the volume of beads alone (2x beads) or beads and peptide (2x beads 2x peptide) did not appear to affect the amount of centrosomal protein seen in the bound fraction.

Next, I decided to adjust lysis conditions in order to determine whether there was a more optimal cell lysis method for COMPACT. As seen in Figure 4.8, reducing the number of sonication cycles or using dounce homogenisation as an alternative physical disruption technique did not result in any improvement to COMPACT.

Importantly, while the method works fairly reproducibly, there was a level of variability observed across COMPACT-WB replicates. This is not entirely surprising, as it well known that biological replicates capture random biological variation (Blainey et al., 2014). In addition to this, I noted variations in COMPACT ‘efficiency’ as a result of variability in bead batches (see section 3.5).

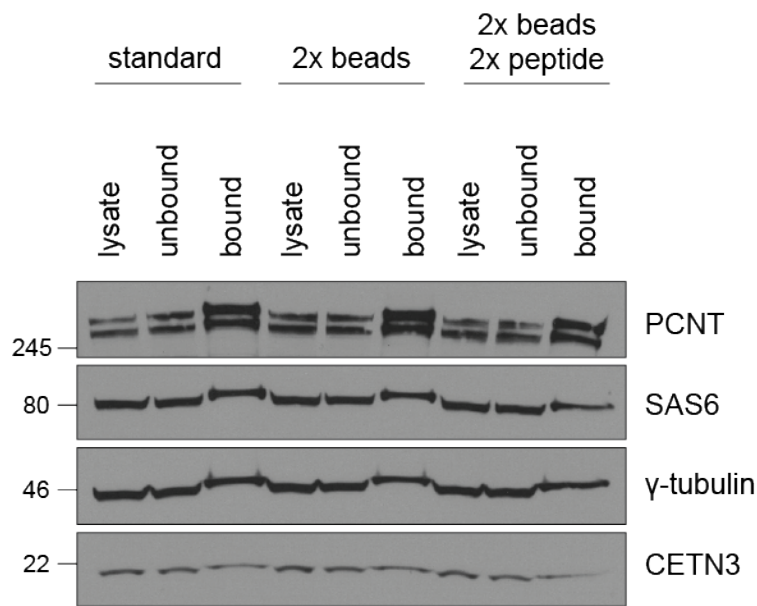


Figure 4.7. Changing bead/peptide proportions for COMPACT in HEK 293T cells. COMPACT-WB showing centrosome proteins in the bound (bead-bound) fraction, compared to lysate and unbound fractions for three conditions: *standard* (standard volume of beads/peptide, see section 3.5); *2x beads* (2x standard volume beads); *2x beads 2x peptide* (2x standard volume beads and peptide).

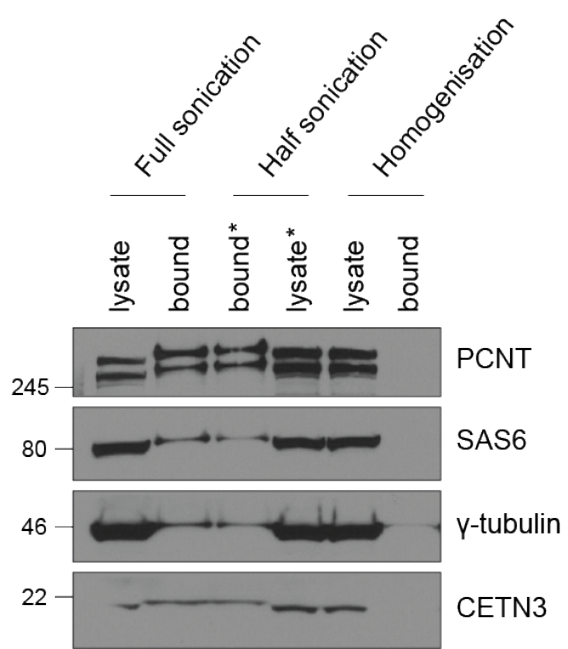
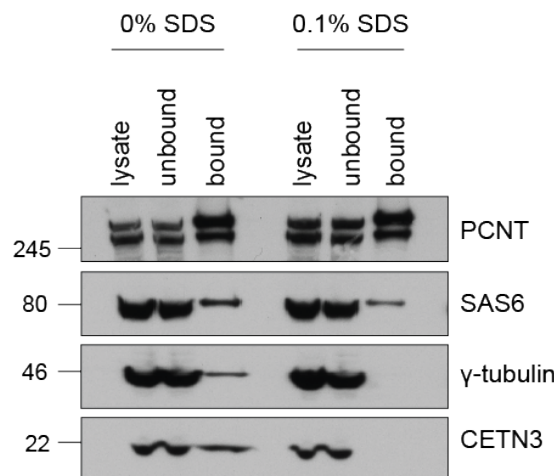


Figure 4.8. Adjusting lysis conditions for COMPACT in HEK 293T cells. COMPACT-WB showing centrosome proteins in the bound (bead-bound) fraction, compared to lysate fractions for three conditions: *full sonication* (standard sonication cycle; see section 3.5); *half sonication* (half sonication cycle); *homogenisation* (dounce homogenisation). * indicates lanes that were accidentally loaded in reverse order.

Finally, preliminary COMPACT-MS data had indicated that there are a number of proteins that non-specifically bind to the beads, even in the absence of peptide. Thus, in an attempt to reduce the number of non-specific bead binding proteins and potentially enrich for certain low abundance centrosomal proteins (that might otherwise be masked by strong-binding non-specific proteins), 0.1% SDS was added to the wash buffer. It is known that the centrosome structure is very stable once the triplet microtubules of the centriole scaffold are assembled, and the main centrosome structure persists even after treatment with various denaturation agents, including potassium iodide and urea (Moritz et al., 1998; Winey and O'Toole, 2014). Figure 4.9 shows that addition of SDS to the COMPACT wash buffer resulted in a reduction/loss of centrosomal proteins SAS6, γ -tubulin and CETN3. Figure 4.10 reveals that a large number of proteins were lost due to the addition of SDS in the wash buffer, including 26 proteins that overlap with the KE-37 centrosome proteome (Jakobsen et al., 2011). These

data indicate that SDS does not appear to add any advantage to the efficiency of the COMPACT method, in terms of increasing the number of centrosomal proteins picked up by the mass spectrometer. In fact, as seen in Table 4.1, addition of 0.1% SDS to the wash buffer was sufficient to result in the loss of various known centrosomal proteins, including CEP83, CEP41, CETN2 and γ -tubulin (otherwise known as TUBG1).

A



B

Centrosome protein	Number of unique peptides			
	0% SDS		0.1% SDS	
	#1	#2	#1	#2
PCNT	110	98	108	96
SAS6	11	14	9	9
γ -tubulin	8	2	0	0
CETN3	4	2	0	0

Figure 4.9. Optimising wash buffer conditions for COMPACT in HEK 293T cells. A: COMPACT-WB showing centrosome proteins in the bound (bead-bound) fraction, compared to lysate and unbound fractions. Bound fraction indicates samples that were washed in Buffer P1 (with or without 0.1% SDS) before collecting the beads. **B:** Table showing number of unique peptides detected via COMPACT-MS, for the four centrosomal proteins probed for using western blot. Two biological replicates (#1 and 2) were analysed per condition, 0% and 0.1% SDS.

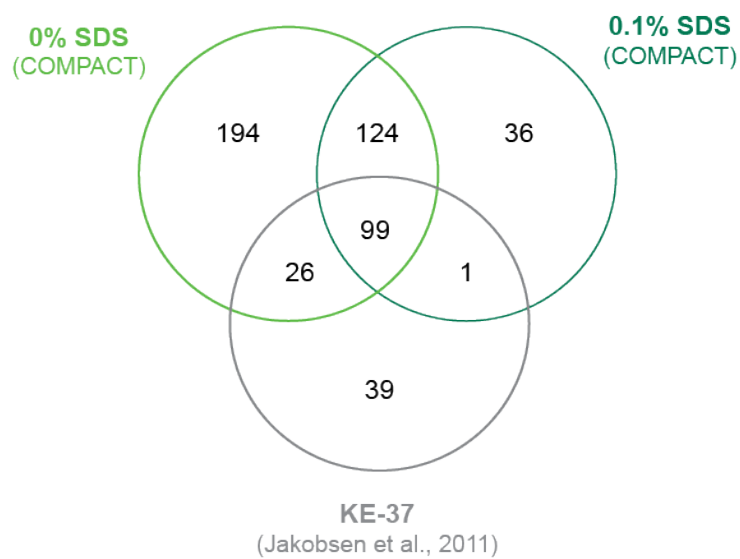


Figure 4.10. Comparison between wash buffer conditions for COMPACT in HEK 293T cells. Venn diagram showing the proteins detected via COMPACT-MS for 0% and 0.1% SDS conditions, compared to the KE-37 centrosome proteome (Jakobsen et al., 2011). Note that bead-only experiments were performed alongside COMPACT and proteins detected in these were removed from the final list of centrosome components.

Table 4.1. Top 20 proteins identified with the highest number of unique peptides (# u.p) in COMPACT-MS in HEK 293T cells.

0% SDS only		0% SDS and 0.1% SDS		0.1% SDS only	
Protein	# u.p	Protein	# u.p (0, 0.1%)	Protein	# u.p
Centrosomal protein 83 (CEP83)	22	Pericentrin (PCNT)	110, 108	Tubulin alpha-1C chain (TUBA1C)	7
Splicing factor 3B subunit 3 (SF3B3)	22	Astrom syndrome protein 1 (ALMS1)	102, 95	Protein JBTS17 (c5orf42)	6
Centrosomal protein 41 (CEP41)	14	Centrosomal protein 250 (CEP250)	87, 87	Ubiquitin-40S ribosomal protein S27a (RPS27A)	4
Nuclear protein MDM1 (MDM1)	14	Centrosomal protein 350 (CEP350)	82, 86	MAP7 domain-containing protein 3 (MAP7D3)	4
Chromodomain-helicase-DNA-binding protein 1 (CHD1)	12	Centriolin (CNTRL)	75, 72	Tubulin beta-4B chain (TUBB4B)	3
Transcription intermediary factor 1-alpha (TRIM24)	11	CDK5 regulatory subunit-associated protein 2 (CDK5RAP2)	60, 58	T-complex protein 1 subunit theta (CCT8)	3
Inner centromere protein (INCENP)	10	Centrosomal protein 128 (CEP128)	57, 55	T-complex protein 1 subunit gamma (CCT3)	3
Trichoplein keratin filament-binding protein (TCHP)	10	Ninein (NIN)	57, 57	General transcription factor II-I (GTF2I)	3
DNA (cytosine-5)-methyltransferase 3A (DNMT3A)	9	Centrosomal protein 135 (CEP135)	53, 52	Alpha-amylase 1 (AMY1A)	2
Centrin-2 (CETN2)	8	Rootletin (CROCC)	51, 20	Telomere-associated protein RIF1 (RIF1)	2
RNA-binding protein 12B (RBM12B)	8	Centrosomal protein 152 (CEP152)	49, 43	Spondin-1 (SPON1)	2
Tubulin gamma-1 chain (TUBG1)	8	Centrosomal protein 290 (CEP290)	49, 44	Zymogen granule protein 16 (ZG16B)	1
60 kDa heat shock protein, mitochondrial (HSPD1)	7	A-kinase anchor protein 9 (AKAP9)	48, 42	CREB-binding protein (CREBBP)	1
60S ribosomal protein L10a (RPL10A)	7	Centrosomal protein 164 (CEP164)	44, 28	Retroviral-like aspartic protease 1 (ASPRV1)	1
Cell division cycle 5-like protein (CDC5L)	7	Ankyrin repeat domain-containing protein 26 (ANKRD26)	43, 40	Nuclear pore complex protein 107 (NUP107)	1
Crooked neck-like protein 1 (CRNL1)	7	Outer dense fibre protein 2 (ODF2)	43, 36	Testis-specific Y-encoded like protein 2 (TSPYL2)	1
Gamma-tubulin complex component 2 (TUBGCP2)	7	Centrosomal protein 295 (CEP295)	41, 39	Dipeptidyl peptidase 4 (DPP4)	1
Nephrocystin-1 (NPHP1)	7	U5 small nuclear ribonucleoprotein 200 kDa (SNRNP200)	40, 6	Ubiquitin-like modifier-activating enzyme 1 (UBA1)	1
Centrosomal protein of 76 kDa (CEP76)	5	Cytoskeleton-associated protein 5 (CKAP5)	38, 32	Tumour suppressor ARF (CDKN2A)	1
Gamma-tubulin complex component 3 (TUBGCP3)	5	Centrosomal protein 192 (CEP192)	37, 41	Coiled-coil domain-containing protein 88B (CCDC88B)	1

4.2.2. Further characterisation and validation of COMPACT in HEK 293T cells

- Further characterisation of COMPACT

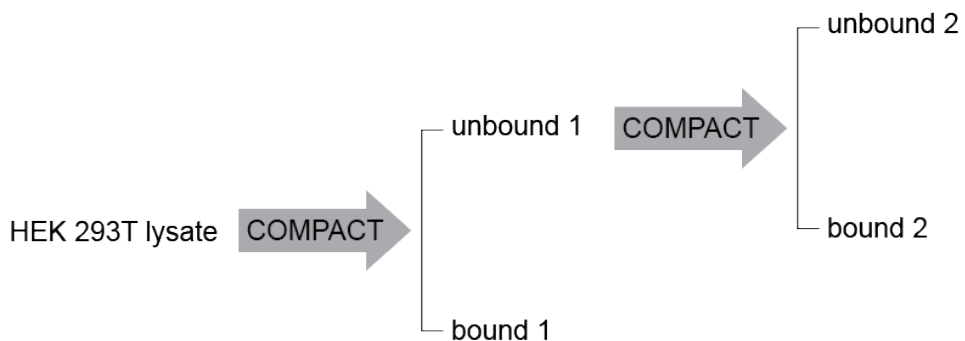
It was apparent from COMPACT-WB experiments that some of the known centrosomal proteins were not binding the peptide-bound beads, and therefore lost in the unbound fraction. In order to confirm whether the centrosomal protein seen in the unbound fractions still had the ability to bind the beads, an experiment was performed in which unbound sample was run over a fresh aliquot of beads and peptide. As seen in Figure 4.11, the majority of centrosomal protein observed in the first unbound fraction remains unbound in the second unbound fraction, and only a very small amount of γ -tubulin protein binds again (bound 2).

It is possible that there are soluble, but not centrosomal, pools of these proteins that are present in the lysate but unable to bind to the peptide. For example, SAS6, γ -tubulin and CETN3 are known to have cytoplasmic protein pools (Bauer et al., 2016). To test this, centrosomes purified form HEK 293T cells using COMPACT were spun onto coverslips and stained for the distal centriole and PCM markers, CETN3 and PCNT, respectively. COMPACT-IF is a useful tool to visualise centrosomes and look specifically for the presence of protein(s) at the centrosome, as a large number of centrosomal proteins have cytoplasmic pools, making their centrosomal localisation difficult to detect using standard whole-cell IF. Figure 4.12 A reveals that PCNT and CETN3-positive foci were detected in both bound and unbound fractions, suggesting that there are centrosomes within a cell lysate that are unable to be captured by the peptide. To explore these structures further, images were captured at a higher magnification and deconvolved using Huygens software in order to visualise bound and unbound structures at a higher resolution. Images obtained for both bound and unbound fractions revealed the expected architecture for human centrosomes; a ring-like pattern for PCM and elongated dot-like pattern for the centrioles (Figure 4.12 B) (Sonnen et al., 2012). These data indicate that the unbound fraction still contains whole centrosomes that seem unable to bind the peptide. A potential reason for this observation could be that a particular centrosomal component needs to be present and/or exposed for the peptide to capture the centrosome, and this component may not always be present or available in the cell lysate. It is equally possible, however, that binding between the centrosome and the peptide is transient with a significant off-rate, meaning that only a proportion of the centrosomes in a given cell lysate will be captured.

To test the first possibility, I sought to determine whether the peptide might preferentially bind centrosomes in a certain cell cycle stage. COMPACT-WB was performed on asynchronous HEK 293T cells as well as cells synchronised using double Thymidine (to achieve a largely S-phase population) and Thymidine plus Monastrol (to achieve a largely mitotic population) (see section 3.1.3 for further detail on synchronisation protocols). The levels of centrosomal proteins CDK5RAP2 (PCM; expands during mitosis), CEP128 (sDAPs, present on mother centrioles), SAS6 (cartwheel; disappears during mitosis) and PLK1 (mitotic kinase) were analysed to assess COMPACT efficiency. Interestingly, there appeared to be more SAS6 at the centrosome of a largely S-phase population of cells, and more PLK1 in the lysate and at the centrosome of a largely mitotic population of cells, which corresponds with what is known of the PLK1 levels during the centrosome duplication cycle (reviewed in Colicino and Hehnly, 2018) and indicates that the synchronisation protocol was effective, albeit not 100% (Figure 4.13). Additionally, while there are some minor changes in COMPACT efficiency, centrosomes do appear to be binding to the peptide-coated beads in all conditions, thus suggesting that the peptide-bead complex does not preferentially bind to centrosomes in a certain cell cycle stage.

From the results shown above it appears that there is a population of centrosomes within a cell lysate that do not bind to the peptide-bound beads. It is not entirely clear why this is the case, as in addition to the experiments performed above, I have also shown that using fewer cells (i.e. a less concentrated protein lysate) resulted in fewer centrosomes binding to the peptide-coated beads (Figure 4.4); therefore, it is not a question of the peptides being oversaturated. Further experimentation is required to identify the mechanism by which COMPACT purifies centrosomes.

A



B

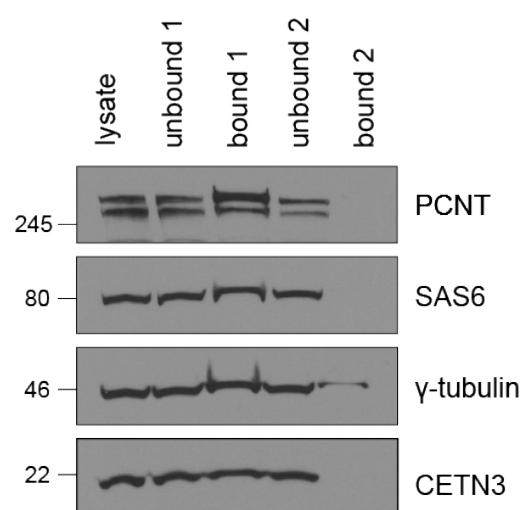


Figure 4.11. Ability of unbound fraction to bind fresh beads and peptide. A: Experimental workflow showing that COMPACT was performed a second time (on unbound fraction 1 using a fresh aliquot of beads and peptide) to produce unbound and bound fractions 2. **B:** COMPACT-WB showing centrosome proteins in the bound (bead-bound) fraction, compared to lysate and unbound fractions.

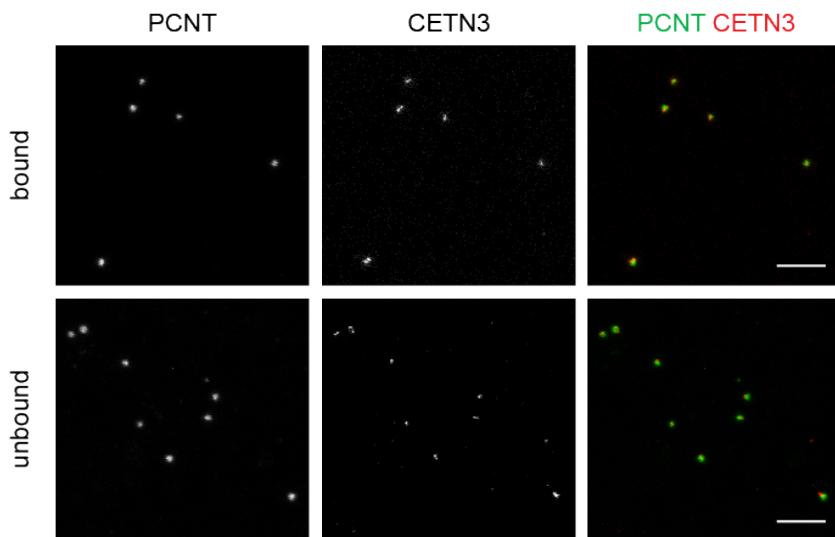
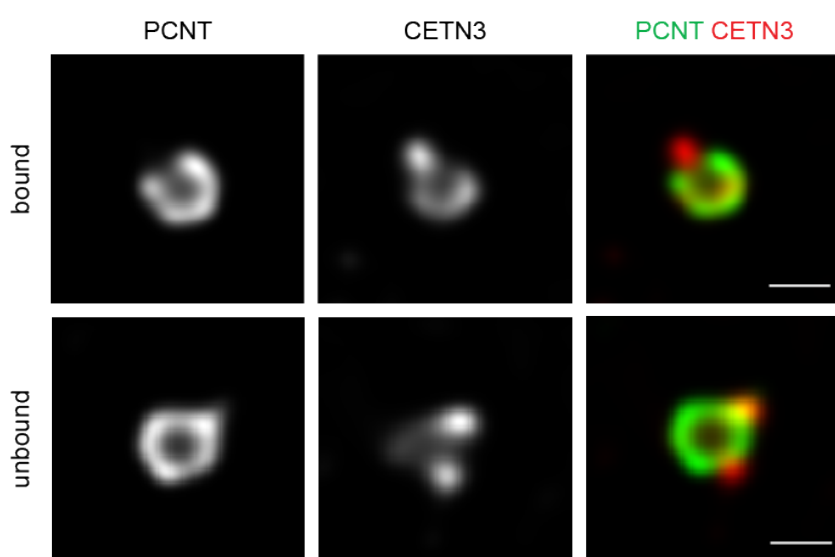
A**B**

Figure 4.12. Immunofluorescence analysis of bound and unbound fractions from COMPACT in HEK 293T cells. **A:** Representative confocal images of bound and unbound fractions from HEK 293T cells, spun onto coverslips and stained with PCNT (green) and CETN3 (red) antibodies. Scale bars, 5 μ m. **B:** Representative deconvolved confocal images (at higher magnification) of bound and unbound centrosomes stained with PCNT (green) and CETN3 (red) antibodies. Scale bars, 500nm.

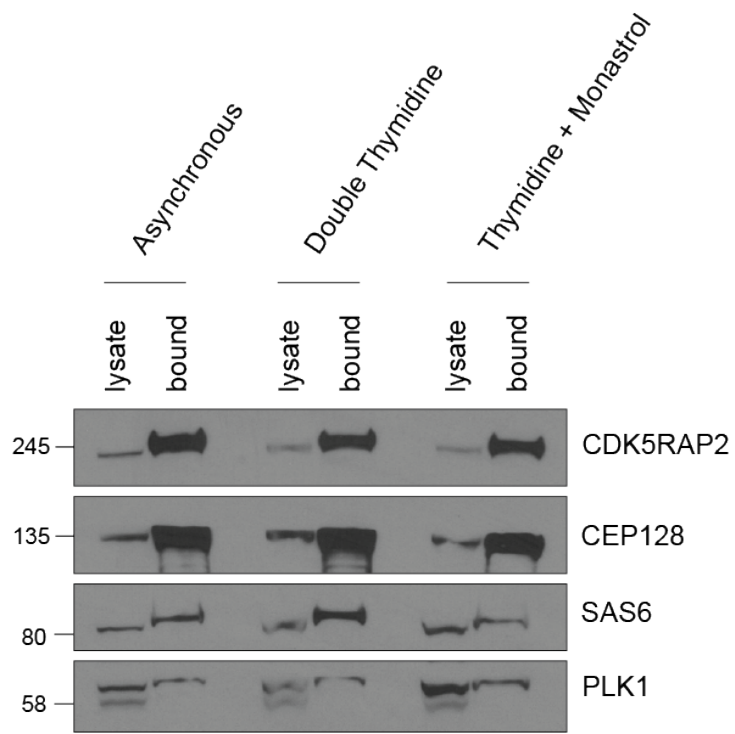


Figure 4.13. COMPACT efficiency in HEK 293T cells synchronised to different cell cycle stages.
 COMPACT-WB showing centrosome proteins in the bound (bead-bound) fraction, compared to lysate fraction for asynchronous, double Thymidine-treated and Thymidine plus Monastrol-treated HEK 293T cells.

- COMPACT in acentrosomal cells

In order to confirm that the peptide is purifying centrosomes (as suggested by the presence of whole centrosomal structures seen via EM and cryo-ET in Figure 4.3, and IF in Figure 4.12) rather than non-centrosomal pools of these proteins, COMPACT was performed on acentrosomal cells. To achieve this, HEK 293T cells were treated with the selective PLK4 inhibitor, centrinone, for a period of 8 days in order to inhibit centriole duplication (Wong et al., 2015). PLK4 inhibition prevents new centriole assembly without disassembling pre-existing centrioles. As expected, continuous treatment of HEK 293T cells with centrinone led to a substantial reduction in foci positive for various centriolar and PCM markers (Figure 4.14). Immunofluorescence analysis revealed that while the vast majority of cells showed absence of SAS6, CEP152 and γ -tubulin staining, ~45% of cells still showed PCNT staining, which may be indicative of PCM remnants or acentrosomal MTOCs (Dzhindzhev et al., 2010; Sir et al., 2013) (Figure 4.14 B).

In order to assess if centrosome loss impairs the ability of COMPACT to purify centrosomes, COMPACT was performed on HEK 293T cells treated with centrinone. COMPACT-WB revealed that only a very small proportion (if any) of various centriolar and centrosomal proteins were observed bound to the peptide (bound fraction), indicating that in the absence of centrosomes, COMPACT was unable to purify these proteins (Figure 4.15). Somewhat surprisingly, γ -tubulin was observed at a proportion similar to what was seen in untreated cells, suggesting that the bound fraction may also contain cytoplasmic pools of this protein, which could be a soluble binding partner of CCDC61 (the protein from which the peptide is derived). It is also possible that the anti- γ -tubulin antibody is cross-reacting with another protein that binds non-specifically, as γ -tubulin was observed to be significantly reduced at the centrosome via immunofluorescence (Figure 4.16).

In addition to COMPACT-WB, COMPACT-MS was performed to analyse the centrosome proteome composition of untreated and centrinone treated HEK 293T cells. Proteins present in at least two out of the three replicates, in untreated (-) and centrinone treated (+) COMPACT samples, were compared to each other, as well as to the core centrosome proteome from Bauer et al., 2016 (Figure 4.16 A). Of the proteins overlapping with the core centrosome dataset, 44 were found exclusively in untreated samples, indicating that COMPACT was unable to capture and pull-down these proteins in the centrinone treated (+) conditions, likely due to the fact that they were lost as a result of centrinone treatment (Figure 4.16 B). The majority of these proteins represent either centriolar proteins (including CP110, SAS6 and

STIL) or PCM proteins (including NEDD1, TUBG1 and various TUBGCPs). 27 proteins were found to be central to all three datasets, indicating proteins that were still present after centrinone treatment, including the known sDAP components ODF2, CEP128, CNTRL, NIN and CEP170 (Figure 4.16 C). Despite the fact that these proteins were detected in centrinone treated (+) samples, they were significantly reduced in almost every case, as indicated by log2FC values ($p < 0.05$) achieved by label-free quantitative analysis of these data (Figure 4.16 C). An exception to this is the protein PLK4, which shows a significant increase/ fold enrichment in the centrinone treated (+) samples. A likely reason for this is that in the absence of its substrate, STIL, PLK4 does not undergo autophosphorylation and subsequent degradation, resulting in its accumulation over multiple cell cycles (Ohta et al., 2014; Yamamoto and Kitagawa, 2019). Indeed, this has been observed before, thereby serving as an important positive control for this experiment (Byrne et al., 2020; Wong et al., 2015). Importantly, no changes in the bead-only (BO) binding proteome were observed upon centrinone treatment, indicating that all observed changes in centrosome proteome composition were as a result of the specific inhibition of PLK4, and thus centriole duplication (Appendix 1). In addition to this, none of the proteins probed for via western blot in Figure 4.15 were observed in the BO proteome after COMPACT-MS (Appendix 2), indicating that the faint bands seen in the BO lanes are likely background signal or as a result of leakage from adjacent bound lanes. It is also possible that unobserved proteins were present in the lysate, but at a level below what was detectable via MS.

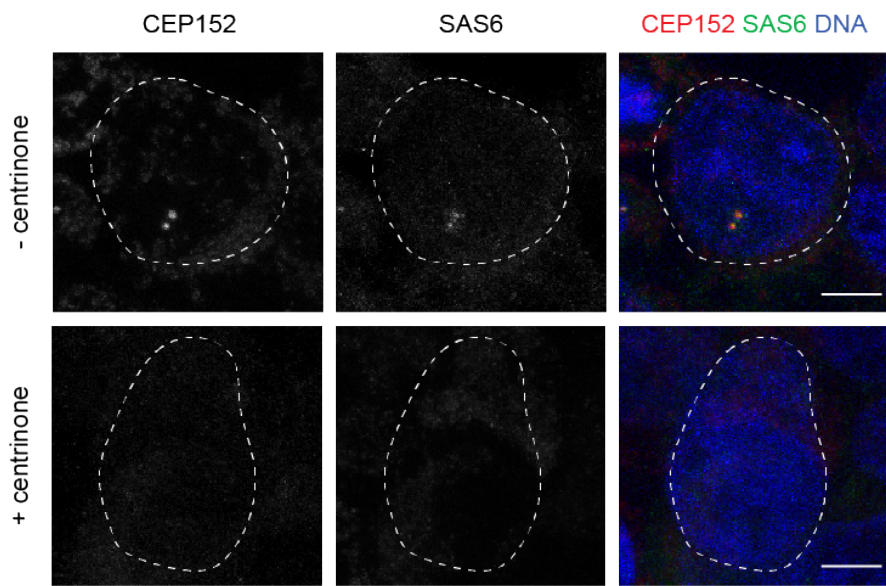
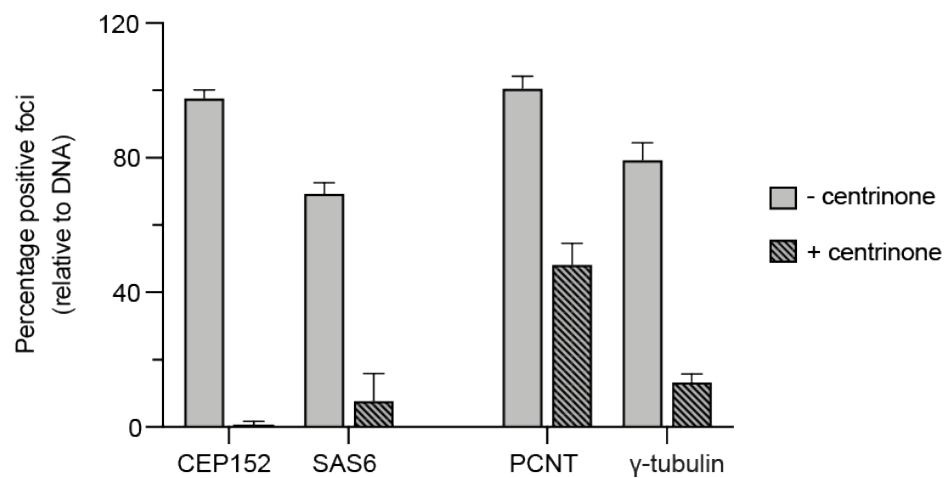
A**B**

Figure 4.14. Loss of centrosomes in HEK 293T cells after treatment with the selective PLK4 inhibitor, centrinone. A: Representative IF images of HEK 293T cells treated for 8 days with centrinone, fixed in MeOH and stained with CEP152 (red) and SAS6 (green) antibodies. DNA was stained with Hoechst. Scale bars, 5 μ m. **B:** Histogram reveals percentage positive foci for centriolar and PCM markers, relative to DNA (number of Hoechst-positive cells). Bar graphs show mean + SD for two independent experiments.

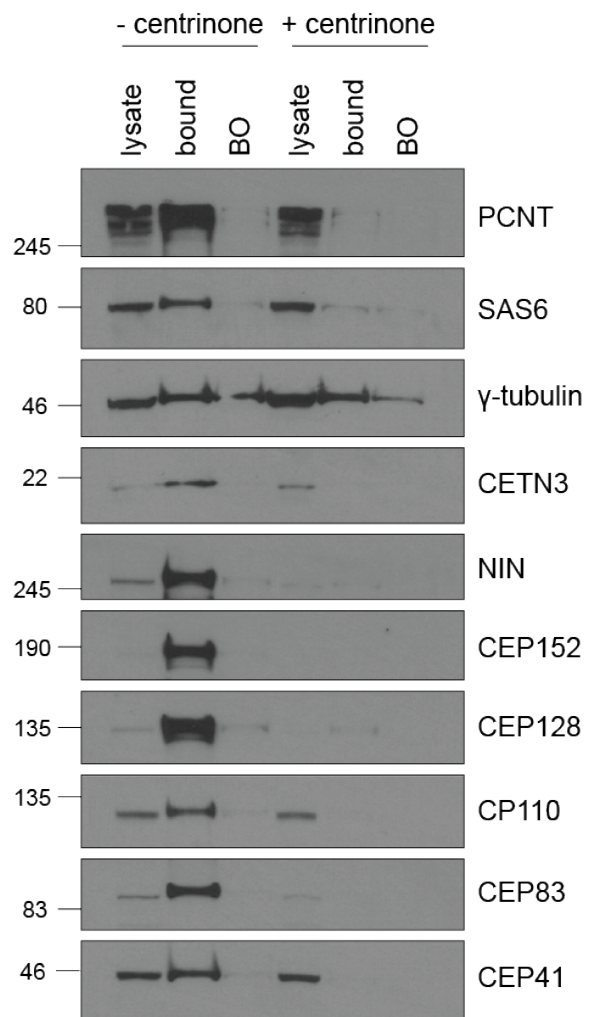
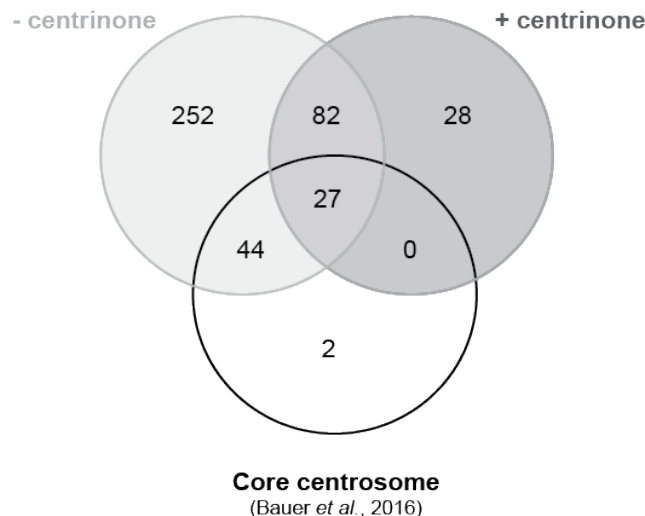


Figure 4.15. COMPACT in HEK 293T cells treated with the selective PLK4 inhibitor, centrinone.
 COMPACT-WB showing centrosome proteins in the lysate, bound (bead-bound) and BO (bead-only) fractions, for cells untreated (- centrinone) and treated with centrinone (+ centrinone) for 8 days.

A**B**

Proteins lost (44)

CEP41	●	SAS6	●	MZT2B	●	SCLT1	●
CEP120	●	POC1A	●	TUBGCP2	●	CEP164	●
CNTROB	●	FAM161A	●	TUBGCP3	●	ODF2L	●
ALMS1	●	STIL	●	NEDD1	●	C2CD3	●
CEP78	●	SSNA1	●	CENPJ	●	LRRC45	●
FOPNL	●	KIAA0586	●	CEP85	●	CEP68	●
SDCCAG8	●	CEP76	●	TUBGCP4	●	CEP131	●
CEP290	●	HYLS1	●	CEP70	●	CEP72	●
CEP97	●	RTTN	●	TUBG1	●	PCM1	●
CP110	●	SFI1	●	TUBGCP5	●	CCDC15	●
CEP295	●	NEK2	●	TUBGCP6	●	CSPP1	●

- Centriole
- PCM
- Appendages

- Linker
- Satellites
- Unknown

C

Proteins remaining (27)

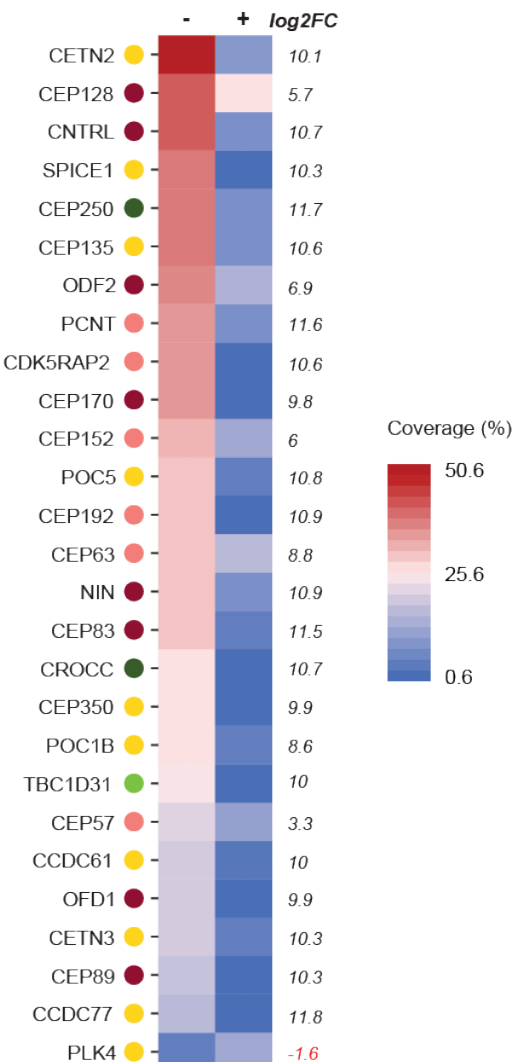


Figure 4.16. COMPACT-MS in HEK 293T cells treated with the selective PLK4 inhibitor, centrinone, compared to the core centrosome dataset. **A:** Venn diagram showing the total number of proteins detected in 2 out of 3 technical replicates for COMPACT in untreated (-) and centrinone treated (+) HEK 293T cells, compared to the core centrosome (Bauer *et al.*, 2016). **B:** Table showing proteins found in HEK 293T untreated (-) and core centrosome but lost in centrinone treated (+) samples. Colours indicate centrosome sub-structure. **C:** Heatmap showing the proteins present in HEK 293T untreated (-) and centrinone treated (+) samples, as well as the core centrosome. Colours indicate centrosome sub-structure. Log2FC values from label-free quantification (untreated to centrinone treated) are shown, $p < 0.05$.

- Comparison to sucrose sedimentation-based centrosome isolation

In order to validate the optimised COMPACT methodology and prove that it is more sensitive and recovers more centrosomal proteins than traditional centrosome isolation via sucrose sedimentation (Andersen *et al.*, 2003; Bornens and Moudjou, 1998), both methods were performed side-by-side, using 5×10^7 HEK 293T cells for each method. Western blotting of fractions collected after sucrose sedimentation revealed the peak centrosomal fraction to be fraction 6, thus this fraction was used for LC-MS/MS analysis (Figure 4.17). As seen in Figure 4.18, while a large number of centrosomal proteins were identified by COMPACT-MS (indicated by an overlap of 134 proteins with the list of 165 centrosomal proteins discovered in the human T cell leukaemia cell line, KE-37 (Jakobsen *et al.*, 2011)), a much smaller number of centrosomal proteins were found via MS after the sucrose sedimentation-based method (indicated by an overlap of 3 proteins with the KE-37 dataset). While western blotting revealed that γ -tubulin and CETN3 were found in the fractions collected after sucrose sedimentation (Figure 4.17), neither were at the abundance required to be detected by the mass spectrometer. Importantly, while neither of these proteins were detectable in the sucrose sedimentation 5×10^7 dataset, when it was performed using 1×10^9 cells instead, both γ -tubulin and CETN3 were identified amongst a total of 87 proteins overlapping with the KE-37 dataset (Figure 4.18). The large number of proteins unique to sucrose sedimentation (1×10^9 cells) can be attributed to the low specificity of this protocol; peak centrosomal fractions contain proteins from a number of cellular components, including mitochondria and the nucleus (Andersen *et al.*, 2003). The relatively small number of proteins observed in the KE-37 dataset was achieved by the authors using protein correlation profiling (PCP) in combination with stable isotope labelling by amino acids in cell culture (SILAC) mass spectrometry (PCP-SILAC MS), which allows for classification of ‘likely’ centrosomal proteins from a list of approximately 2000 proteins detected in the peak centrosomal fractions (Jakobsen *et al.*, 2011). In summary, the

data shown in Figure 4.18 indicates that COMPACT is able to purify centrosomal components with higher efficiency (from fewer cells) and specificity, than the sucrose sedimentation-based method widely used for centrosome enrichment.

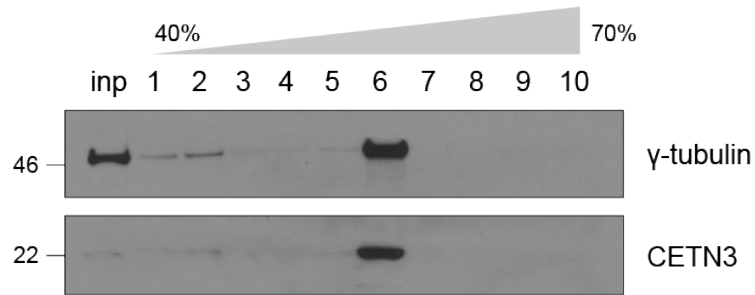


Figure 4.17. Purification of centrosomes by sucrose sedimentation in HEK 293T cells.
Representative western blot showing γ -tubulin and CETN3 sedimentation patterns. Cell lysates were enriched for centrosomes by centrifugation onto a 50% (w/w) sucrose cushion (inp), followed by centrifugation through a discontinuous sucrose gradient of 40-70% (w/w). 1% of the input (inp) and 100% of each sucrose fraction (1-10) were loaded onto the gel.

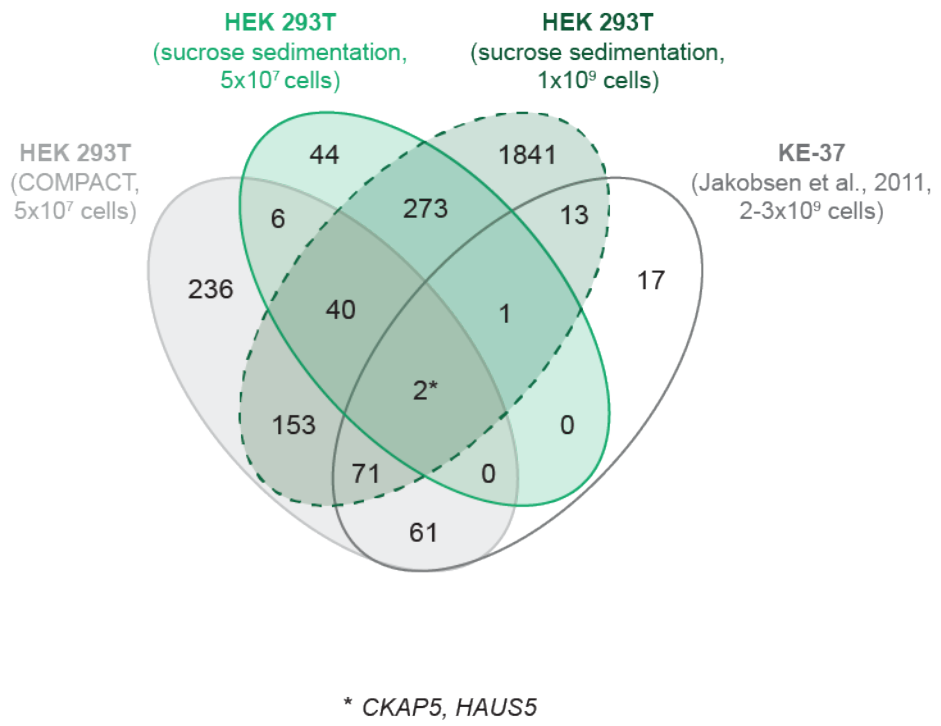


Figure 4.18. Comparison of centrosomal proteins isolated using two techniques, COMPACT and sucrose sedimentation. Venn diagram showing the total number of proteins detected in four different centrosome preparations; HEK 293T COMPACT, HEK 293T sucrose sedimentation (2 different cell numbers), and KE-37 (Jakobsen et al., 2011).

4.2.3. A HEK 293T centrosome proteome

In order to assess reproducibility of the COMPACT method, as well as to create an extensive HEK 293T centrosome proteome, COMPACT-MS was performed a total of six times. The six replicates (three run on the same date [replicates 1-3], three run on different dates [replicates 4-6]) show a large degree of similarity and thereby reproducibility, as indicated by the total number of unique peptides for proteins present in five out of six replicates (Appendix 3).

To assess the efficiency of COMPACT in being able to purify known centrosome components, the proteins found in five out of six HEK 293T COMPACT replicates were compared to a number of published centrosome proteome datasets. In 2011, Jakobsen and colleagues published a partially validated list of 165 centrosomal proteins discovered in the human T cell leukaemia cell line, KE-37 (Jakobsen et al., 2011). A number of years later, Bauer and colleagues published a smaller, but fully validated, list of core centrosomal proteins (Bauer et al., 2016). The results of the comparison are summarised in Figure 4.19, which shows that 76% (125/165) of proteins in the KE-37 dataset, and 97% (71/73) of proteins in the Bauer dataset were discovered by COMPACT in HEK 293T cells. Interestingly, both CEP55 and MZT1 (proteins not found in the HEK 293T centrosome proteome) are found in 3 out of 6 of the COMPACT replicates but only with 1 unique peptide in each instance, indicating that these are likely very lowly abundant or dynamic proteins in HEK 293T cells.

The comparison of the HEK 293T COMPACT proteome (proteins found with at least 1 unique peptide in 5 out of 6 biological replicates) to the KE-37 proteome (Jakobsen et al., 2011) revealed 40 proteins unique to KE-37 (Figure 4.19). When performing gene ontology (GO) enrichment analysis of the proteins unique to the KE-37 proteome, it was revealed that terms relating to microtubule (MT) activity and cytoskeletal protein binding were amongst the most statistically significant GO terms in the “molecular function” category, with various actin-related, dynein and dynein proteins making up a large portion of the list (Figure 4.20). These are dynamic proteins, associated with either MTs or actin, whose presence in the KE-37 proteome may be explained by the use of the MT- and actin-depolymerising agents, nocodazole and cytochalasin D, in the sucrose sedimentation-based centrosome purification methodology (Andersen et al., 2003; Bornens and Moudjou, 1998), which could cause retention of dynamic proteins at the centrosome. To test this further, I treated the U251 human glioblastoma cell line with nocodazole and cytochalasin D prior to performing COMPACT-MS. Interestingly, no increase in dynamic or other proteins was observed (Figure 4.21). In fact, pre-treatment with these agents resulted in the loss of a number of known centrosomal proteins, including the DAP proteins OFD1, CEP83, SCLT1, FBF1, CEP164 and ANKRD26.

It is therefore likely that the presence of the 40 proteins unique to KE-37 (Figure 4.19) can be attributed rather to the differences in the two methods; affinity purification versus sucrose density centrifugation, and/or the differences in centrosome composition between HEK 293T and KE-37 cells.

Comparison of the HEK 293T COMPACT proteome to the KE-37 proteome (Jakobsen et al., 2011) and core centrosome (Bauer et al., 2016), revealed 70 proteins shared by all three datasets (Figure 4.19). When mapping these proteins to the centrosome, it can be seen that there is significant representation of all centrosomal sub-structures, as well as more dynamic proteins and complexes such as kinases and pericentriolar satellites, which together make up the core HEK 293T centrosome proteome (Figure 4.22). In addition to this, all major centriole duplication and assembly factors (Nigg et al., 2014) are represented in the core HEK 293T proteome, further indicating that COMPACT is an effective method for purification of human centrosomes.

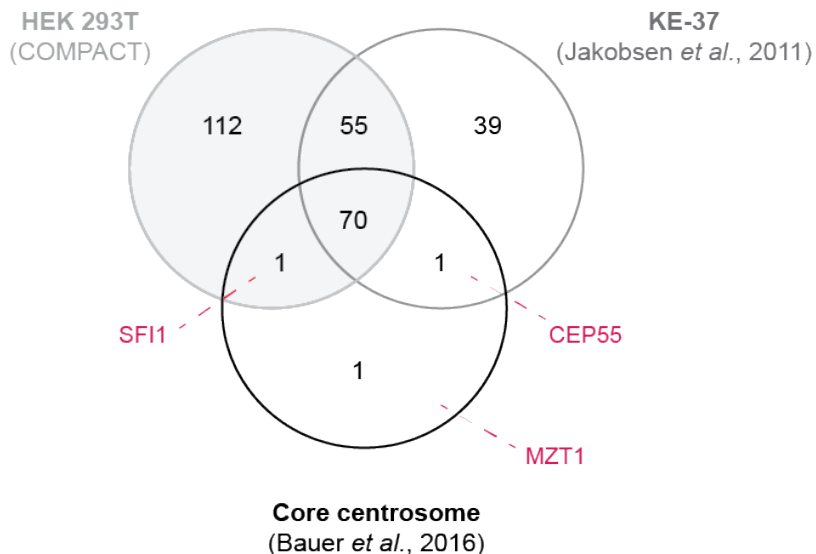


Figure 4.19. Comparison of the HEK 293T COMPACT proteome to published centrosome datasets. Venn diagram showing the total number proteins detected in 5 out of 6 biological replicates for HEK 293T COMPACT, compared to two published centrosome proteomes; KE-37 (Jakobsen et al., 2011) and the core centrosome dataset (Bauer et al., 2016).

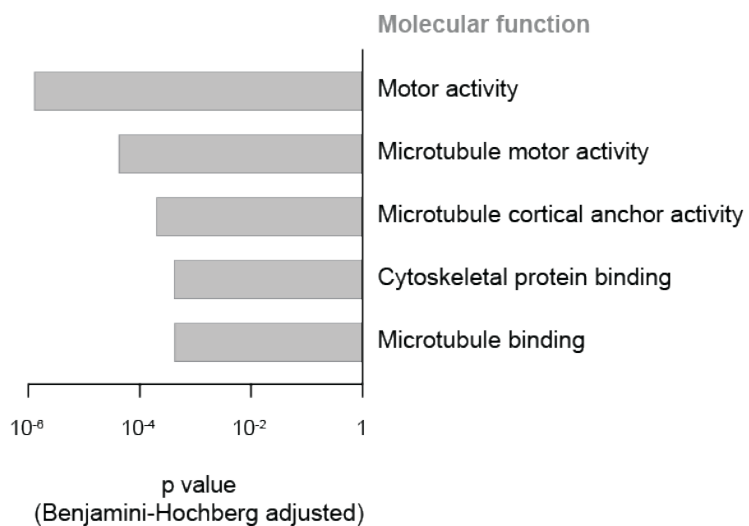


Figure 4.20. Gene Ontology (GO) enrichment analysis on the proteins unique to KE-37. Graph summarising the GO enrichment analysis for 40 proteins identified in KE-37 only (Jakobsen *et al.*, 2011). Terms with the highest significance in the “molecular function” category are reported with their corresponding p values, which were Benjamini-Hochberg adjusted.

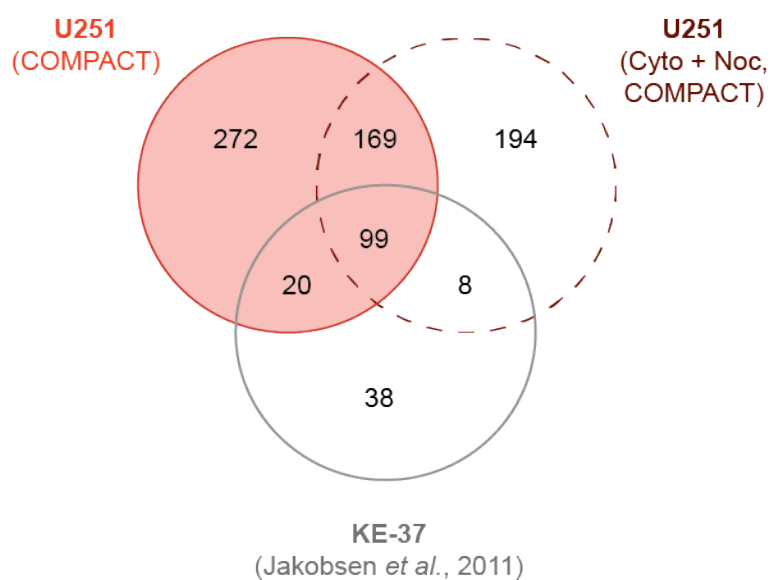


Figure 4.21. COMPACT-MS in U251 cells untreated and pre-treated with nocodazole and cytochalasin D, compared to the KE-37 centrosome proteome. Venn diagram showing the total number proteins detected in 2 biological replicates for U251 COMPACT and U251 Cyto + Noc COMPACT, compared to the published centrosome proteome; KE-37 (Jakobsen *et al.*, 2011). U251 cells were treated with 1 μ g/ml nocodazole and cytochalasin D for 1 hour prior to harvesting and cell lysis.

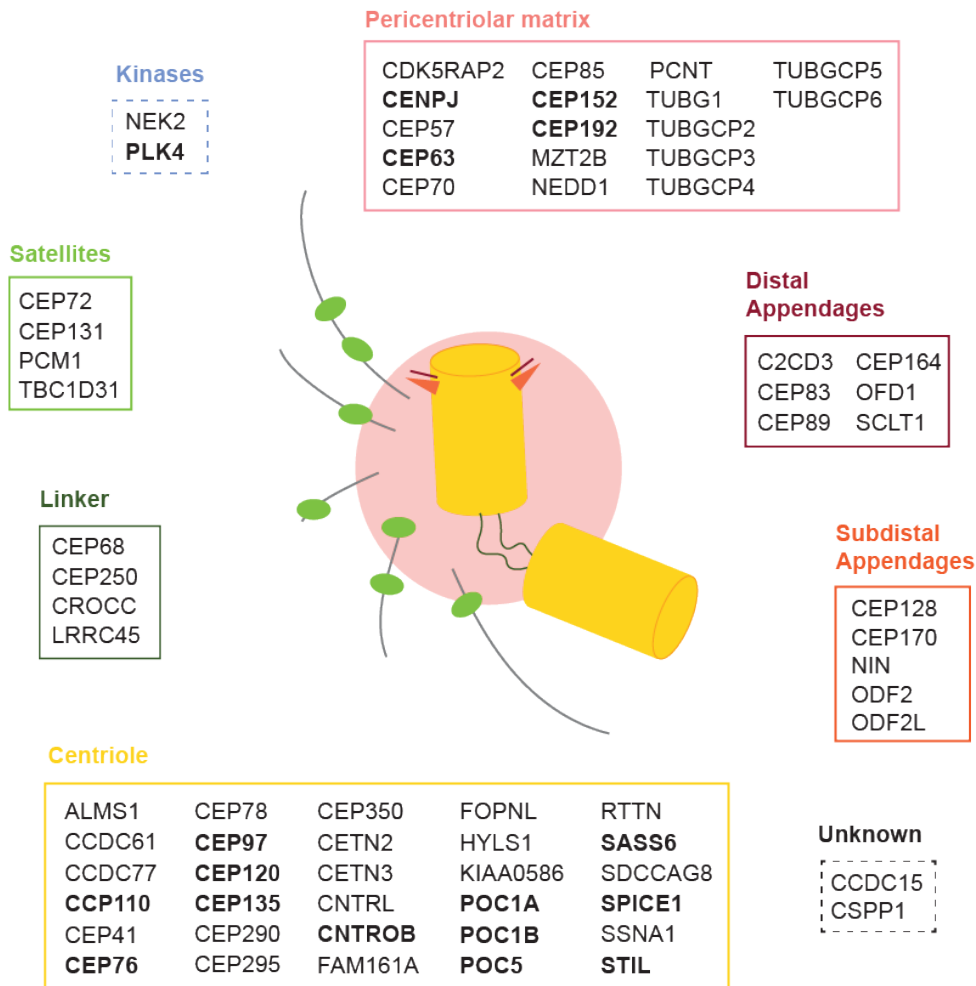


Figure 4.22. The core HEK 293T centrosome proteome. Schematic depicts the 70 centrosome proteins central to HEK COMPACT, KE-37 (Jakobsen *et al.*, 2011) and the core centrosome dataset (Bauer *et al.*, 2016), and their corresponding centrosomal sub-structures. Kinases are indicated separately due to their dynamic nature. Proteins are listed in alphabetical order. *Unknown* indicates proteins that are known to be centrosomal, but no information regarding their sub-structural location is known (Nigg *et al.*, 2014). Bold proteins indicate essential centriole duplication and assembly factors. Note that the schematic depicts a disengaged G1 centrosome.

Supplementary to the core HEK 293T centrosome proteome in Figure 4.22, COMPACT-WB was performed and additional centrosomal markers were detected (Figure 4.23). Interestingly, in contrast to the four centrosomal proteins (PCNT, SAS6, γ -tubulin and CETN3) originally chosen to assess COMPACT efficiency, NIN, CEP152, and CEP128 showed a higher level of enrichment in the bound fraction, compared to lysate. This could suggest that there aren't large cytoplasmic pools of these proteins present (including pools of centrosomal protein at centriolar satellites), and the vast majority of the protein is present at the centrosome and therefore purified by COMPACT.

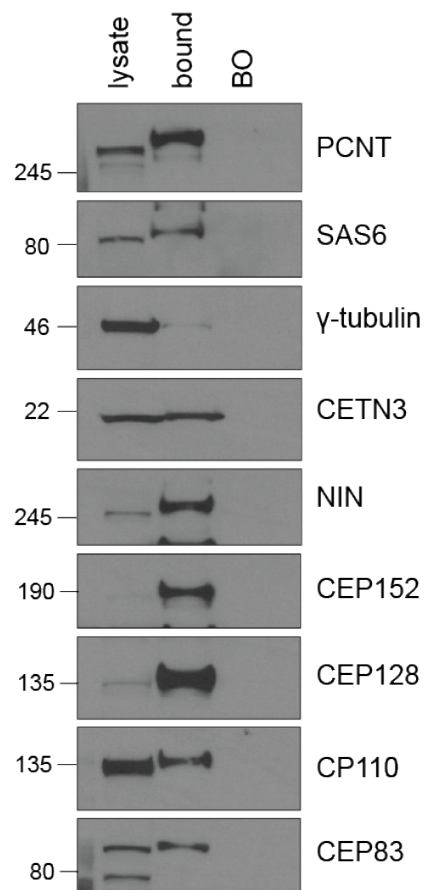


Figure 4.23. Additional markers for HEK 293T COMPACT. COMPACT-WB showing various centrosome proteins form the core HEK 293T centrosome proteome, in the lysate, bound (bead-bound) and BO (bead-only) fractions.

4.2.4. Investigating how COMPACT purifies centrosomes

Previous data have shown that COMPACT is efficient in purifying centrosomes from different cell cycle stages. Thus, I next sought to understand the mechanism by which COMPACT purifies centrosomes (i.e. the centrosomal component(s) required by the peptide-bound beads to capture centrosomes).

Interestingly, Dr Ivan Rosa e Silva, a researcher in the van Breugel lab created a NIN knock-out (KO) line in the near-haploid cell line, HAP1, using the CRISPR/Cas9 technology, and observed in a preliminary experiment that COMPACT failed to purify centrosomes from NIN KO compared to wild-type (WT) HAP1 cells (personal communication with Dr Mark van Breugel and Dr Ivan Rosa e Silva, Queen Mary University of London). We therefore postulated that NIN could be a direct binding partner of the peptide-bead complex, and to confirm this theory I performed COMPACT on HAP1 WT and NIN KO cells (two independent clones created and validated by Dr Ivan Rosa e Silva (see Appendix 4) and kindly donated by Dr Mark van Breugel). I confirmed, using COMPACT-WB, that in comparison to the centrosomal protein that was observed bound to the peptide in WT cells (similarly to what is seen in HEK 293T cells), no centrosomal protein was found in the bound fractions of either of the two NIN KO clones, B4 and B12 (Figure 4.24). To further validate and expand on these observations, COMPACT-MS was performed comparing HAP1 WT to NIN KO (clone B4) cells. As seen in Figure 4.25, none of the known centrosomal proteins from the KE-37 centrosome proteome (Jakobsen *et al.*, 2011) were identified in HAP1 NIN KO COMPACT, despite the fact that a large proportion of known centrosomal proteins were found in HAP1 WT COMPACT. This data indicates that NIN (or a NIN-based structure) is a direct binding partner of the CCDC61-derived peptide-bead complex, as in the absence of NIN, COMPACT fails to purify centrosomes.

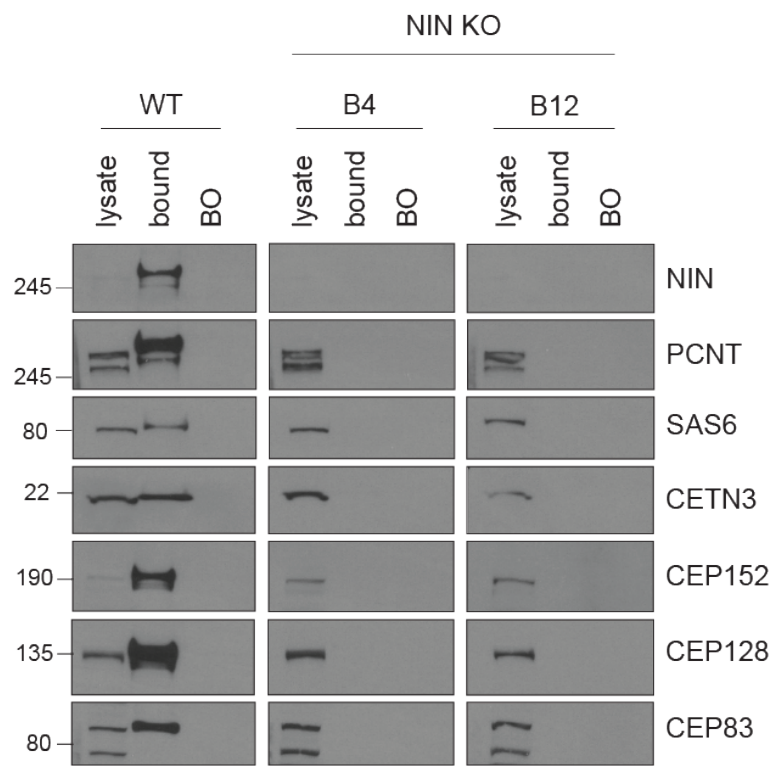


Figure 4.24. COMPACT in HAP1 WT and NIN KO cells. COMPACT-WB showing centrosome proteins in the bound (bead-bound) fraction for HAP1 WT cells, but not for NIN KO clones B4 and B12.

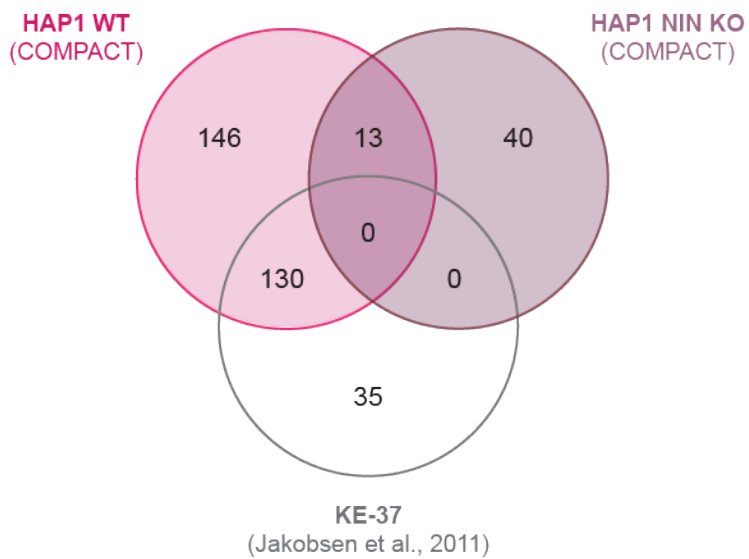


Figure 4.25. Comparison of HAP1 WT and NIN KO centrosome proteomes to the KE-37 centrosome proteome. Venn diagram showing the total number of proteins detected in three replicates each for HAP1 WT and HAP1 NIN KO (clone B4), compared to the KE-37 centrosome proteome (Jakobsen *et al.*, 2011).

Previous studies have shown that there are two pools of NIN that localise to the centrosome, one at the proximal end and the other in the subdistal appendage (sDAP) region (Chong *et al.*, 2020; Sonnen *et al.*, 2012). Therefore, I decided to elucidate which pool of NIN is responsible for COMPACT being able to capture the centrosome. CEP128, a sDAP protein located upstream and involved in the recruitment of NIN to sDAPs (reviewed in Tischer *et al.*, 2021), was previously observed via COMPACT-WB and COMPACT-MS to be very abundant in the bead-bound fraction of HEK 293T cells, and was also one of the proteins that was still observed in the bead-bound fraction after centrinone treatment (Figures 4.15 and 4.16). I therefore postulated that CEP128 may also be involved in the ability of COMPACT to isolate centrosomes. To test this, I first determined whether NIN and CEP128 could be detected at purified centrosomes from HEK 293T cells using COMPACT-IF. In agreement with previous data, NIN localised at the distal and proximal (indicated by colocalisation with CEP250) ends of centrioles, while CEP128 localised exclusively to the distal end of centrioles, just proximally to NIN (Figure 4.26).

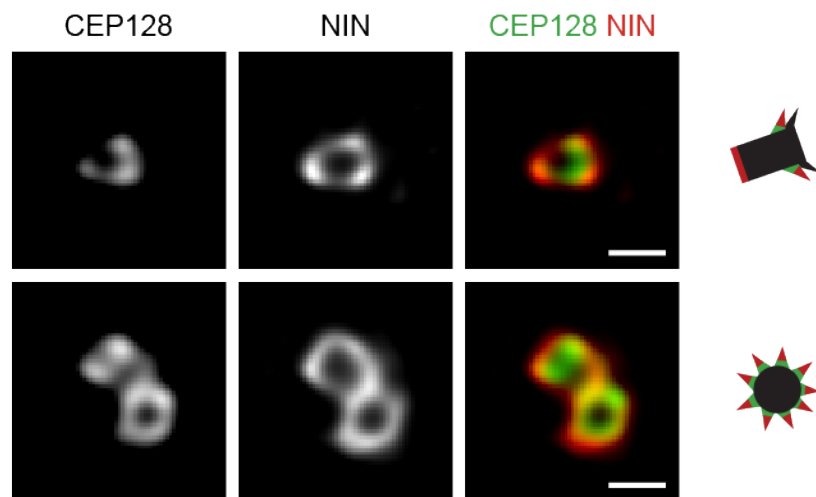
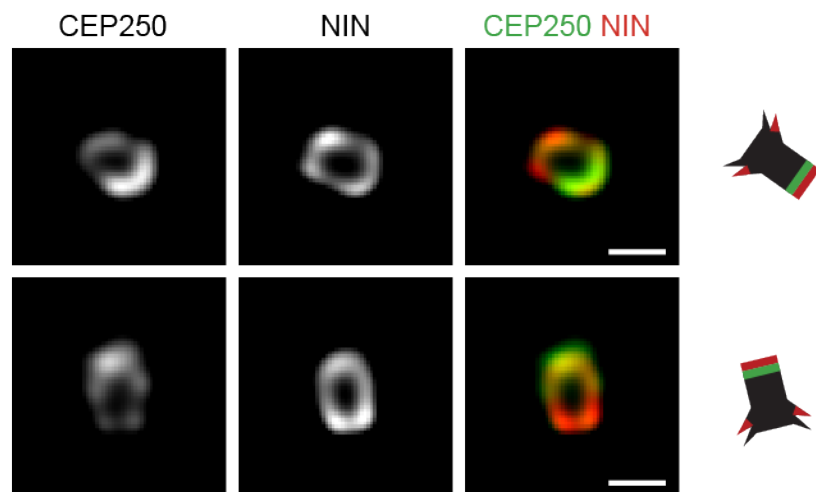
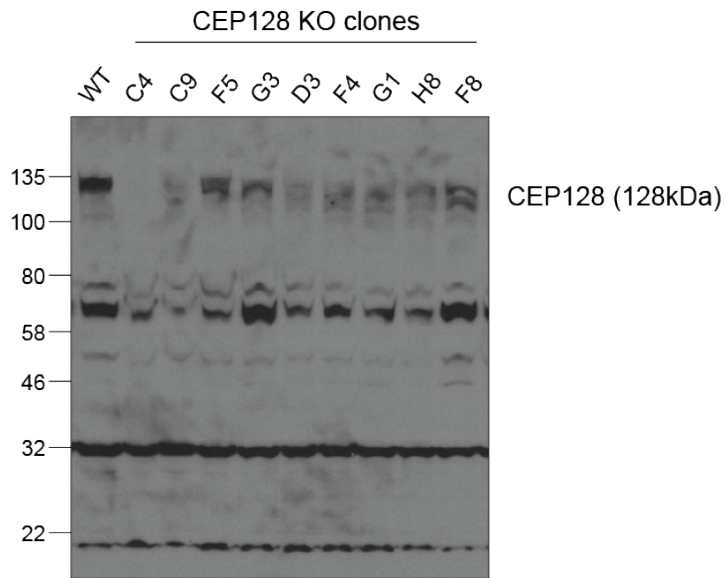
A**B**

Figure 4.26. Immunofluorescence analysis of centrosomes isolated by COMPACT-IF in HEK 293T cells. Representative deconvolved confocal images (at higher magnification) of bound fractions from HEK 293T cells, spun onto coverslips and stained with CEP128 (A; green) or CEP250 (B; green) and NIN (red) antibodies. Scale bars, 500nm. Cartoon images depict centriole positioning and sub-structure staining.

To explore a possible role of CEP128 in the functionality of COMPACT, HEK 293T CEP128 KO cells were created using the CRISPR/Cas9 genome editing technology. Western blot screening of clones revealed loss of CEP128 protein in clones C4 and C9, and this was confirmed by sequencing of genomic DNA, revealing base pair deletions resulting in premature stop codons in both clones (Figure 4.27; further detail on methodology in section 3.10). Based on sequencing results of exon 1, the production of C-terminal truncated proteins cannot be excluded; however, a CEP128 antibody (that recognises the C-terminal region of CEP128) did not detect smaller proteins via western blot (Figure 4.27), suggesting that these clones lack CEP128. COMPACT-WB revealed a marked reduction in selected centrosomal proteins in both CEP128 KO clones when compared to WT (Figure 4.28). It is feasible that the small amounts of centrosomal protein (i.e. PCNT and γ -tubulin) still present in CEP128 KO COMPACT originates from the residual proximal pool of NIN that remains in the absence of CEP128. Indeed, a longer exposure of a separate western blot revealed a weak NIN signal in COMPACT-WB of CEP128 KO cells (Appendix 5). To further test this possibility, HEK 293T WT and CEP128 KO cells were stained with antibodies against NIN, CEP128 and CEP250. Immunofluorescence analysis revealed that while two pools of NIN were visible in WT cells, confirming previous reports (Chong et al., 2020; Sonnen et al., 2012) (see also Figure 4.26), only a single pool of NIN was observed in CEP128 KO cells, and this pool overlapped with the proximal linker protein CEP250 (Figure 4.29 A and B). In addition, CEP128 KO cells revealed a dramatic reduction in NIN signal intensity, which would be expected due to the absence of the NIN at the sDAPs (Figure 4.29 C). These results suggest that while the sDAP pool of NIN, and its upstream partner CEP128, are the main binding partners for the CCDC61 peptide-bead complex, the proximal pool of NIN is still sufficient for COMPACT to purify centrosomes, albeit with a lower efficiency. This may simply be due to smaller amounts of NIN being present at the proximal end, and/or limited accessibility for the peptide to the proximal pool. Further studies will be required to fully understand the molecular mechanism underpinning the peptides ability to bind the centrosome.

A**B**

CEP128 exon 1

↑
ATGGCAGAACATCCAGCGAACATCAGATCACTTCCGCTGTCGTGACCGATTGAGTCCATGGGCTGCC...****

Predicted translational products

WT	MAESSSESDHFRCRDRRLSPWAARSTHRGTRSLPTVEVTEKVNTITSTLQDTSRNLRQVDQMLGRYREYSNG...	(100%)
CEP128 KO C4	MAESSSESDHFRCRDRLSSMGCQINAQGNSKSSYSRSYREGQHYNKYFTGYQSEPATSGPDAWTIPRIQ*	(80%)
	MAESSSESDHFRCRDRLSHGLPDQRTGELEVFLQ*	(20%)
CEP128 KO C9	MAESSSESDHFRCRDRLSHGLPDQRTGELEVFLQ*	(100%)

Figure 4.27. Validation and characterisation of HEK 293T CEP128 KO cells. **A:** Western blot showing CEP128 levels in HEK 293T WT and selected CEP128 KO clones. **B:** Predicted translational products for CEP128 KO clones C4 and C9, compared to WT. For each clone, 10 bacterial colonies were sequenced and the percentage of each translational product is indicated in brackets to the right of each amino acid sequence.

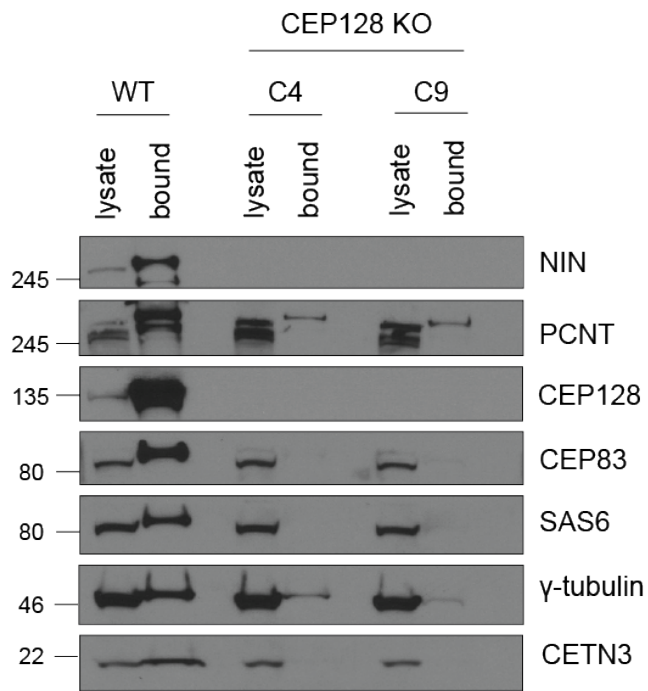
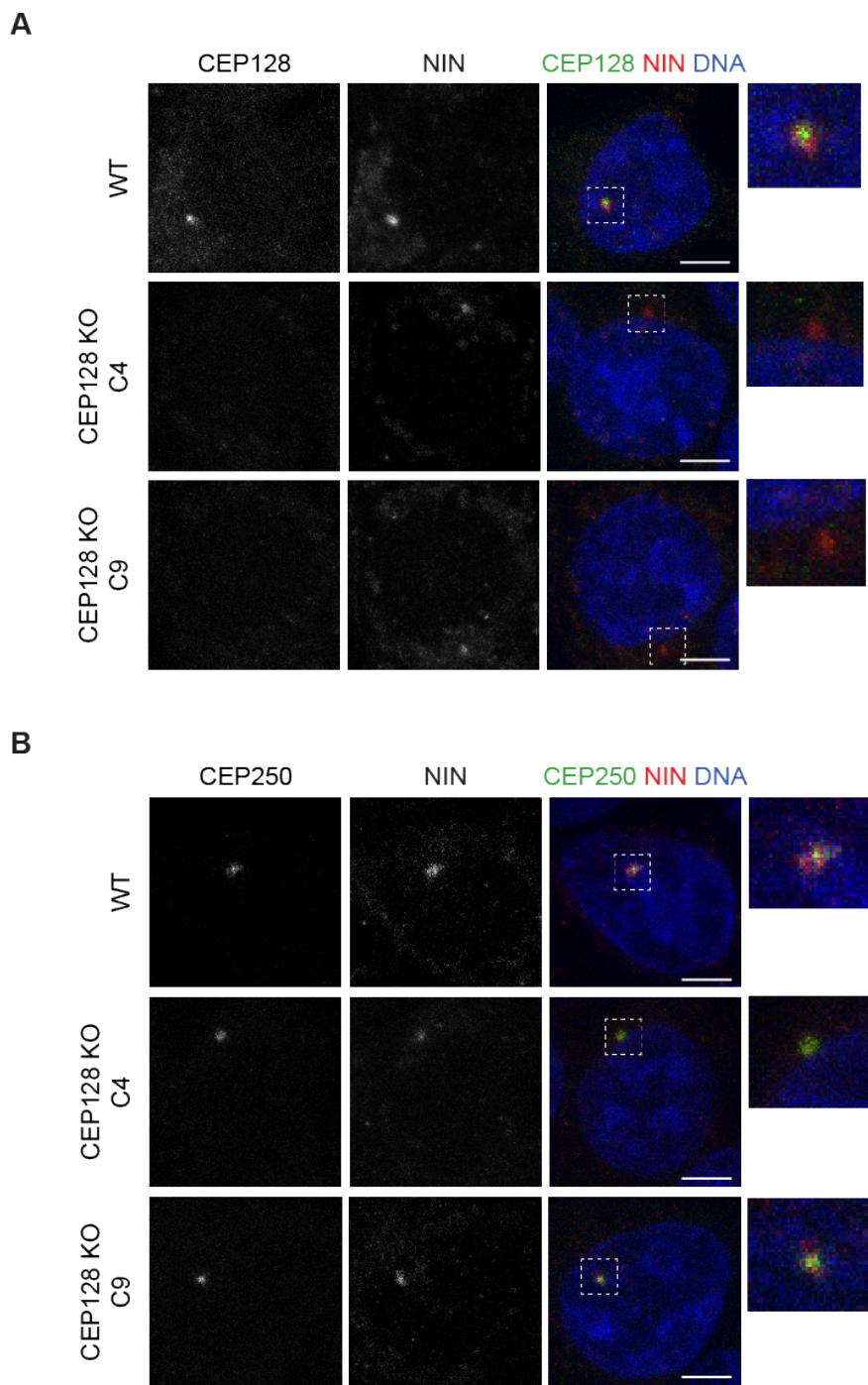


Figure 4.28. COMPACT in HEK 293T WT and CEP128 KO cells. COMPACT-WB showing centrosome proteins in the bound (bead-bound) fraction for HEK 293T WT cells, but minimal/no protein in the CEP128 KO cells C4 and C9.



(Figure continued on next page)

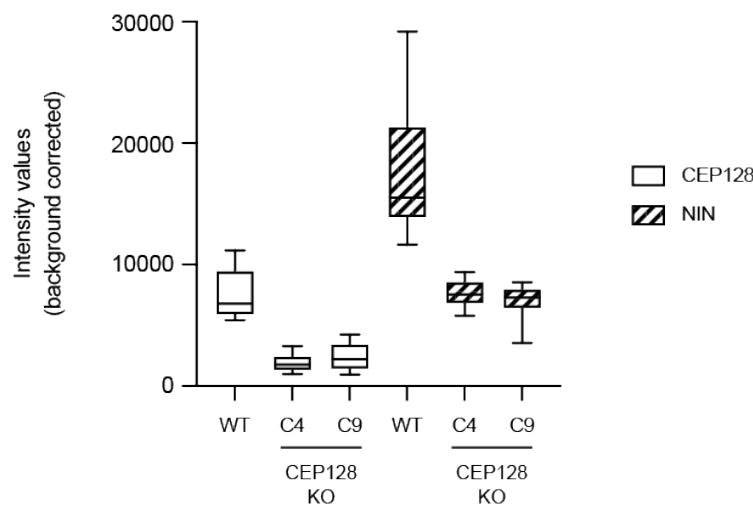
C

Figure 4.29. Immunofluorescence analysis of sDAP and proximal-end centrosomal proteins in HEK 293T WT and CEP128 KO cells. A and B: Representative confocal images of HEK 293T WT and CEP128 KO cells (clones C4 and C9), fixed in MeOH and stained with CEP128 (A; green) or CEP250 (B; green) and NIN (red) antibodies. DNA was stained with Hoechst. Scale bars, 5 μ m. Outlays indicate an enlargement of the region indicated by a white box. **C:** Box plot shows quantification of CEP128 and NIN intensity values (background corrected) in HEK 293T WT and CEP128 KO cells (clones C4 and C9). Whiskers represent 10-90 percentile range.

5 Results II

5.1. Using COMPACT to investigate centrosomal proteomes in a panel of cell lines

Preliminary proteomic data, both from this study and unpublished experiments performed by Bradley Nash, a previous research assistant in the laboratory, suggest that the proteomic composition of the centrosome may in fact differ between specific cell or tissue types. As a result, I performed COMPACT on a panel of cell lines, from different tissues of origin, to investigate whether certain centrosomal proteins may be tissue or cell-type specific. COMPACT proteomes were analysed from a number of transformed/cancer cell lines, including the human embryonic kidney cell line, HEK 293T; the human glioblastoma cell line, U251; the human T cell leukaemia cell line, Jurkat; the primary patient-derived glioma cell lines, G166 and G7 (characterised as mesenchymal and proneural stem cells, respectively); the mouse neuroblastoma cell line, N1E-115; and the human near-haploid cell line, HAP1. Additionally, a COMPACT proteome was acquired for the human induced pluripotent stem cell (hiPSC) line, FSPS13B, as a means to gain insight into centrosome proteome composition of a non-transformed and undifferentiated cell type.

Using COMPACT, centrosomes were isolated from a panel of human cell lines and protein composition was analysed by western blotting (WB) and mass spectrometry (MS). Additionally, for cell lines in which centrosomes have not been studied before, such as the primary patient-derived glioma cell lines, G166 and G7, and the human induced pluripotent stem cell line, FSPS13B, immunofluorescence (IF) analyses were conducted.

Figure 5.1 shows representative COMPACT-WBs performed in three different transformed cell lines, HEK 293T, U251 and Jurkat. Interestingly, subtle differences in protein abundance (of the four centrosomal markers PCNT, SAS6, γ -tubulin and CETN3), could already be observed at the level of western blot, when comparing bound (bead-bound) to lysate fractions, in the three different cell lines. Table 5.1 summarises data from all cell lines in which COMPACT-MS was performed, including number of replicates and total number of proteins in the bead-bound fraction. Bead-only (BO) binding proteins were removed from each protein list in order to create COMPACT-specific proteomes, and the protein lists of all replicates within a single cell line were combined to create a list of proteins that were present in one or more of the replicates with at least one unique peptide. Protein lists (all replicates within a particular cell line, except for HEK 293T and HAP1) were combined due to the fact that not all replicates

were performed or run on the mass spectrometer at the same time. Due to the fact that there were a large number of replicates for HEK 293T and HAP1, I was able to use more stringent filtering, and thus only proteins present in at least 3 out of 6, or 2 out of 4 of the replicates, respectively, were included in Table 5.1. Proteins identified via COMPACT-MS were compared to the published KE-37 centrosome proteome (Jakobsen et al., 2011). As seen in Figure 5.2, the number of proteins found to be overlapping between COMPACT and KE-37, in all of the cell lines analysed, was very similar (~80%), indicating a likely similarity in the proteins found in both datasets, across all cell lines; a potential ‘core’ centrosome proteome that is present in all cell and tissue types, including essential centriole duplication and assembly factors such as CEP192, CEP152 and SAS6. Despite the substantial overlap with known centrosomal proteins, there were also a large number of proteins identified in each cell line that were absent from the KE-37 centrosome proteome, and some of these may represent tissue-specific centrosomal candidates.

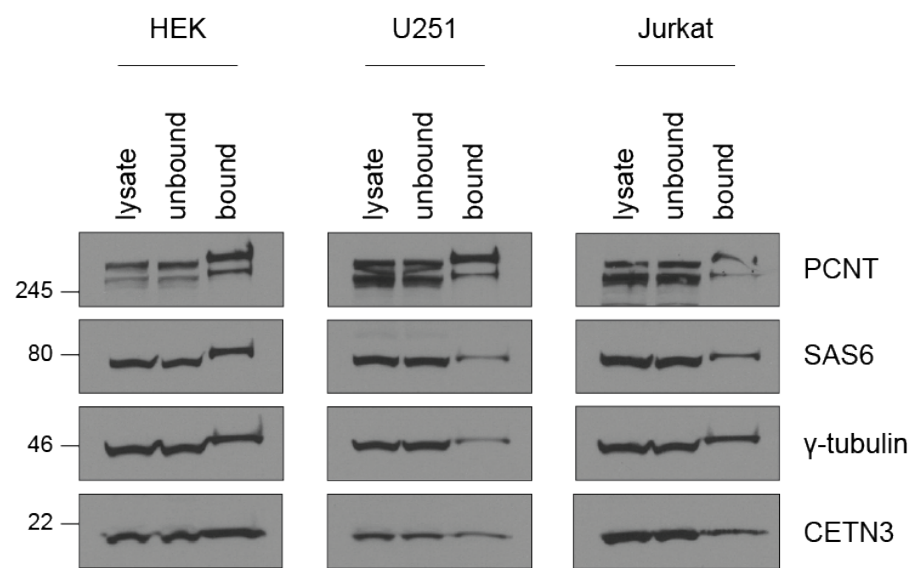


Figure 5.1. COMPACT in HEK 293T, U251 and Jurkat cells. COMPACT-WB showing centrosome proteins in the bound (bead-bound) fraction, compared to lysate and unbound fractions, for HEK 293T, U251 and Jurkat cells. COMPACT-WB samples of different cell lines were not loaded on the same gel, but exposure times for were kept similar for all three cell lines.

Table 5.1. Number of proteins identified using COMPACT in a broad range of cell lines. For HEK 293T and HAP1, proteins present in at least 3 out of 6, or 2 out of 4 of the replicates are indicated, respectively. For the remaining cell lines, proteins present in at least 1 replicate are shown.

Cell line	Replicates	Total no. of proteins
HEK 293T	6	394
U251	3	649
Jurkat	3	501
G166	2	1906
G7	2	1117
N1E-115	2	548
HAP1	4	373
FSPS13B	1	1026



Figure 5.2. Comparison of COMPACT proteomes to the KE-37 proteome. Venn diagrams showing the total number of proteins detected in the bead-bound fractions of a panel of human cell lines analysed via COMPACT-MS, compared to KE-37 centrosome proteome (Jakobsen *et al.*, 2011).

The primary patient-derived glioma cell lines, G166 and G7, as well as the hiPSC line, FSPS13B, showed a much larger number of proteins present in the COMPACT proteome that do not overlap with KE-37 (Figure 5.2). As stem cells, it might be expected that these cell lines express a larger number of proteins than those that have committed to their lineage, such as HEK 293T cells. While many of these additional proteins could represent non-specific binders (and validation experiments would need to be conducted to indicate otherwise), it is possible that the presence of many of these proteins could be attributed to the fact that the centrosome may act as a scaffold for the accumulation of proteins and signalling molecules important for various differentiation processes (reviewed in Arquint *et al.*, 2014). Figures 5.3 and 5.4 show PCM (indicated by PCNT staining) and distal centriole (indicated by CETN3) staining in patient-derived glioma and hiPSC lines, respectively. In addition to this, when these cells were stained with the cilium-specific antibody ARL13B, the G7 and FSPS13B cell lines revealed that 20-30% of ciliated cells (Figure 5.5), despite the presence of growth factors in the culture medium. This could lead to changes in centrosome proteome composition, particularly in the transition zone and basal body-associated PCM. Indeed, the Pelletier group has shown, using BioID, that the proximity interaction landscape changes dramatically during ciliogenesis (Gupta *et al.*, 2015), and recent studies by the Dammermann and Feldman groups revealed in *C.elegans* sensory neurons that the PCM persists at the ciliary base and continues to recruit proteins important for scaffolding and MT nucleation (Garbrecht *et al.*, 2021; Magescas *et al.*, 2021).

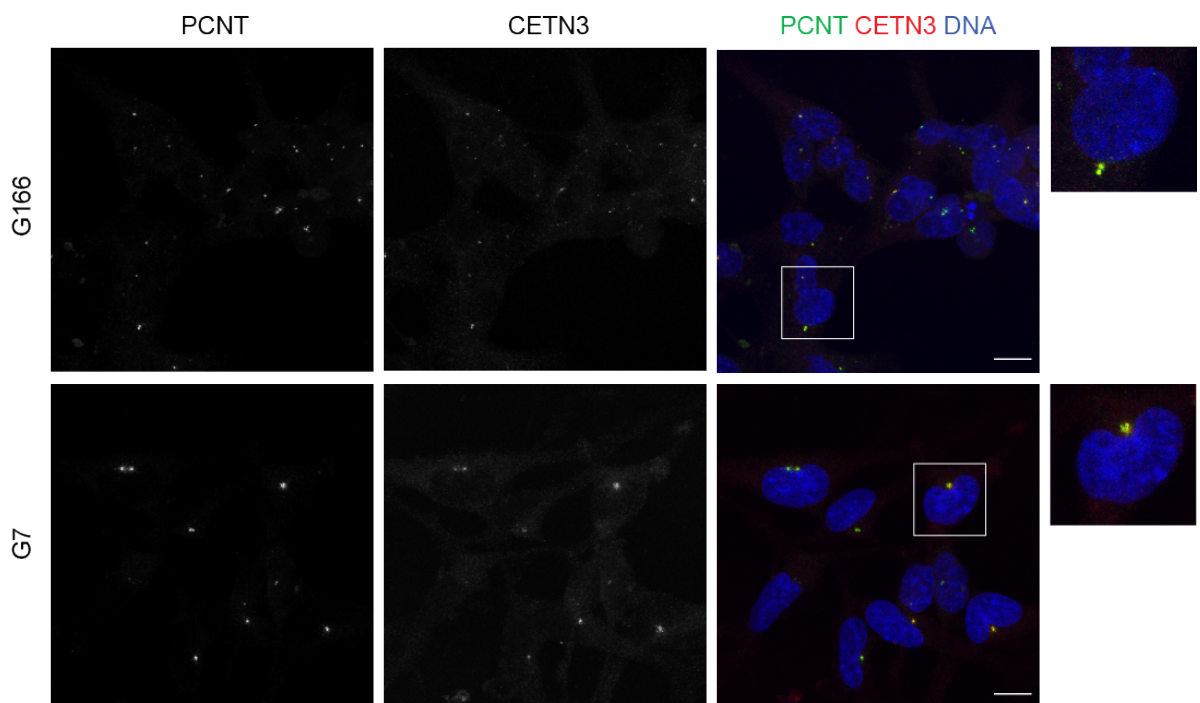
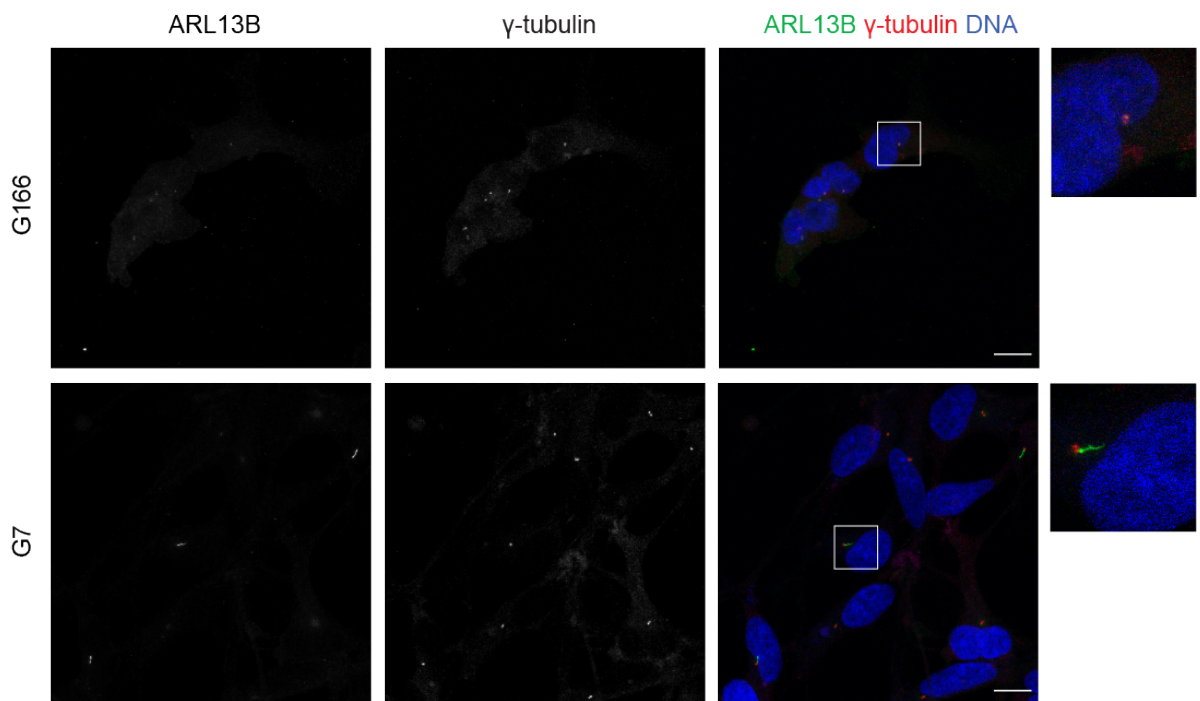
A**B**

Figure 5.3. Centrosomes and cilia in primary patient-derived glioma cell lines, G166 and G7.
Representative immunofluorescence images of G166 and G7 cells stained with PCNT (green) and CETN3 (red) antibodies (A) or ARL13B (green) and γ -tubulin (red) antibodies (B). Scale bars, 15 μ m. Outlays indicate an enlargement of region indicated by white box.

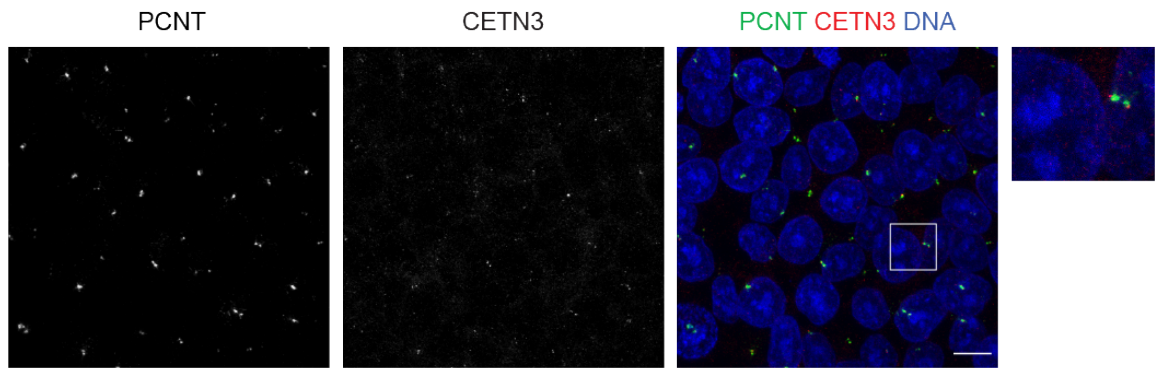
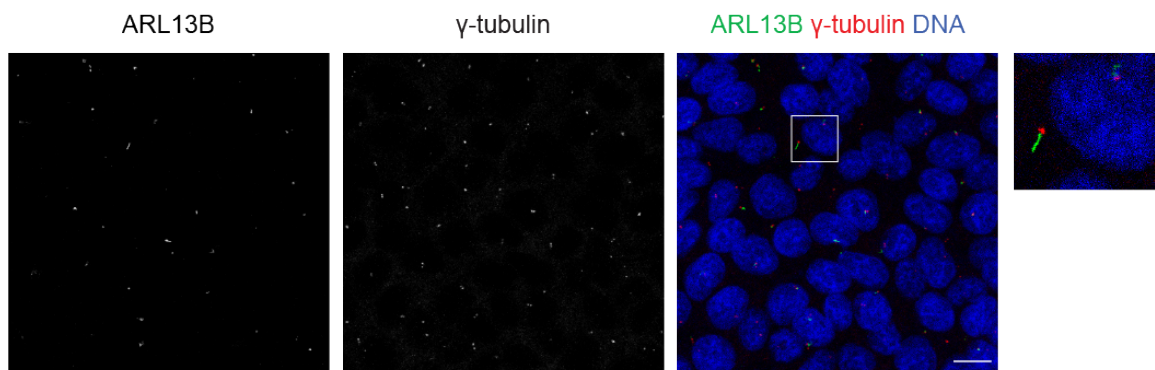
A**B**

Figure 5.4. Centrosomes and cilia in the hiPSC line, FSPS13B. Representative immunofluorescence images of FSPS13B cells stained with PCNT (green) and CETN3 (red) antibodies (A), or ARL13B (green) and γ -tubulin (red) antibodies (B). Scale bars, 15 μ m. Outlays indicate an enlargement of region indicated by white box.

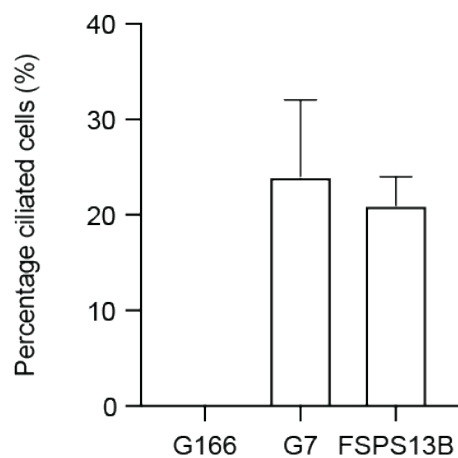


Figure 5.5. Percentage cilia detected in the cell lines, G166, G7 and FSPPS13B. Bar graph showing quantification of the number of cilia observed in G166, G7 and FSPPS13B cells. Results shown represent mean + SD over five fields of view for experiments performed at least two independent times.

5.2. Investigating the tissue specificity of centrosome composition

5.2.1. A non-quantitative comparison of centrosome proteomes in multiple cell lines

Results from performing COMPACT-MS in a large panel of cell lines revealed that while a number of proteins overlapped with the KE-37 centrosome proteome, likely representing a ‘core’ centrosome proteome that is present in all cell and tissue types, there were also a large number of proteins that were unique to a specific cell line (Figure 5.2). When comparing COMPACT-MS data from three cell lines that differ in tissue-type; HEK 293T (embryonic kidney), U251 (glioblastoma) and Jurkat (T lymphocyte), it was observed that while a large number of proteins were overlapping between two or all three cell lines (many of these being highly conserved centriolar and PCM components), there was also a large number of proteins that were unique to each cell line, and these could represent tissue-specific centrosomal candidates (Figure 5.6).

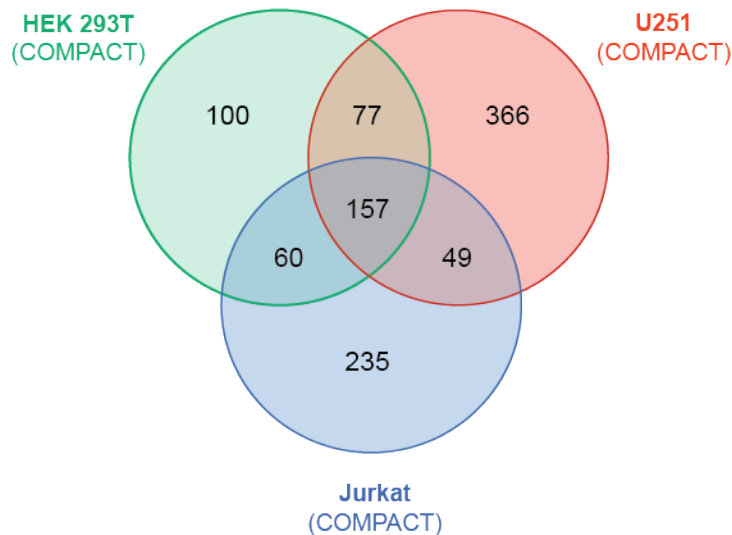


Figure 5.6. Comparison of the HEK, U251 and Jurkat COMPACT proteomes. Venn diagram showing the total number proteins detected via COMPACT-MS in HEK 293T, U251 and Jurkat cell lines. For HEK 293T COMPACT, proteins present in at least 3 out of 6 of the replicates were included. For U251 and Jurkat COMPACT, proteins present in at least 1 out of 3 replicates were included.

To gain an initial understanding of the diversity of centrosome composition across different cell and tissue types, a tissue-specificity table was created from the centrosome proteomes represented in Table 5.1 (Table 5.2 and Appendix 6). Table 5.2 shows a number of representative proteins for novel centrosomal candidates (including proteins found to be ubiquitously expressed and those that appear to be cell type specific), as well as cell type specific candidates that are already known centrosomal components. For example, CCDC88B represents both a novel centrosomal and cell type specific candidate; it is found specifically at the centrosome in Jurkat cells, which makes sense given its role in T cell maturation and lytic granule transport (Ham et al., 2015). Novel centrosomal candidates will be investigated further in Chapter 6. In terms of known centrosomal proteins, interestingly, the distal appendage (DAP) proteins ANKRD26 and CEP164 are both found to be absent in Jurkat centrosomes specifically (see section 5.2.2 for further details). Due to the fact that not all experimental replicates for each cell line analysed in Figure 5.2 were performed or run on the mass spectrometer at the same time, there is limited scope for quantitative data analysis, and thus only preliminary conclusions can be drawn at this stage. Further candidate validation and/or quantitative MS analysis will be needed to compare protein abundance across samples.

Table 5.2. Tissue specificity of centrosome composition. Presence (✓) or absence (grey) of representative proteins discovered by COMPACT-MS in a panel of cell lines. Data obtained from Figure 5.2, and full tissue specificity table in Appendix 6.

		HEK 293T	U251	Jurkat	G166	G7	N1E-115	HAP1	FSPS13B	Centrosomal interactions (BioGRID)	Function
Ubiquitous (novel candidates)	CCDC171	✓	✓	✓	✓	✓		✓	✓	-	unknown
	COPA	✓	✓	✓	✓	✓	✓	✓	✓	TUBG1, CEP128	COPI, trafficking
	EDC4	✓	✓	✓	✓	✓	✓	✓	✓	-	mRNA decapping
	TRIM27	✓	✓	✓	✓	✓	✓	✓	✓	CEP162, NEDD1	E3 ubiquitin ligase
	CRBN	✓	✓	✓	✓	✓	✓	✓	✓	-	E3 ubiquitin ligase
Cell type specific (novel candidates)	CCDC88B			✓						-	lytic granule transport
	CCDC138	✓		✓				✓	✓	PCM1, CEP162	unknown
	KIAA1328	✓			✓	✓		✓	✓	PCM1, OFD1	unknown
Cell type specific (known)	ANKRD26	✓	✓		✓	✓	✓	✓	✓	OFD1, CEP164	primary cilia assembly
	CEP164	✓	✓		✓	✓	✓	✓	✓	CEP89, ANKRD26	primary cilia assembly
	ASPM				✓	✓				CEP78	spindle pole dynamics

5.2.2. A quantitative comparison of centrosome composition in U251 and Jurkat cells

Preliminary data suggested that centrosome composition varies across different cell and tissue types (Figure 5.6 and Appendix 6). Thus, in order to be able to study tissue specificity in a quantitative manner, tandem mass tag (TMT) MS was utilised, due to its multiplexing capabilities (allowing for the labelling of up to 11 samples in one experiment). Briefly, samples were digested with trypsin and peptides labelled with a set of isobaric mass tags, which have the same nominal mass, but upon fragmentation yield reporter ions of differing mass. The relative ratio of reporter ions measured on the mass spectrometer represents the relative abundance of tagged peptides, thereby allowing for protein quantification (Thompson et al., 2003).

Using 11-plex TMT, a proof of principle experiment was designed, in which two cell lines differing in tissue type, morphology (flat vs. round) and behaviour (adherent vs. non-adherent) were chosen; U251 and Jurkat, respectively. For each cell line, five COMPACT replicates, five BO replicates and one reference (COMPACT with a 1:1 mix of each cell line, allowing for comparison across TMT experiments (Rauniyar and Yates, 2014)) were analysed (Figure 5.7 and Appendix 7). This design allowed for a significantly powered experiment, with each condition represented by five biological (different passage) replicates. Technical variation was also introduced due to the fact that samples had to be collected over two consecutive days due to time constraints in tissue culture. Despite this, however, Figure 5.8 shows that COMPACT replicates correlate highly with each other, but not with BO replicates, for both U251 and Jurkat cells.

For quantitative analysis, proteins were considered to be COMPACT-specific if they were found to be significantly enriched above the BO binders ($p < 0.05$). These proteins, from each cell line, were then compared to each other in order to identify proteins differentially expressed (or localised) in U251 compared to Jurkat centrosomes. For this analysis, 1844 peptides (corresponding to 232 proteins) in U251 samples, and 2567 peptides (corresponding to 259 proteins) in Jurkat samples were compared, revealing a total of 73 differentially expressed proteins (Figure 5.9). Importantly, a few of the proteins from Figure 5.9 were chosen at random and whole cell expression levels analysed via western blotting. These data revealed that the differences in centrosomal protein expression observed via COMPACT-TMT were not necessarily due to changes in whole cell protein expression, but rather as a result of differential localisation to or interaction at the centrosome (Appendix 8).

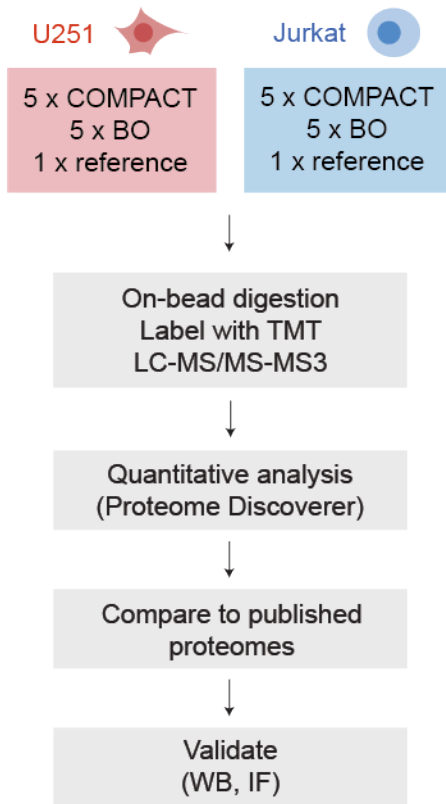


Figure 5.7. Experimental workflow for quantitative COMPACT-MS (COMPACT-TMT) performed in U251 and Jurkat cells. For both U251 (red) and Jurkat (blue) cells, five COMPACT replicates, five bead-only (BO) replicates, and one reference were digested using trypsin, peptides were labelled with TMT labels, and separated and analysed using LC-MS/MS-MS3. Reference samples represent a 1:1 mix of each cell line, upon which COMPACT was performed. Quantitative analysis was performed using the Proteome Discoverer software, and the resulting COMPACT proteomes were compared and validated.

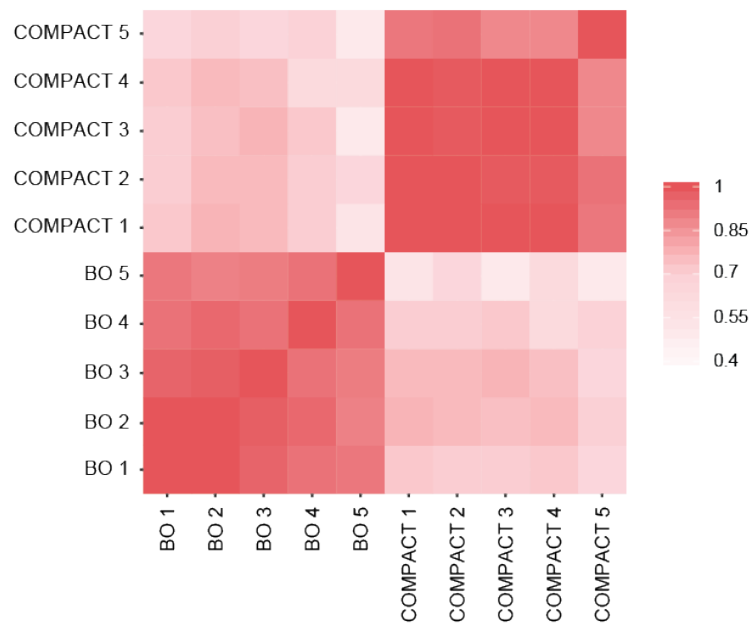
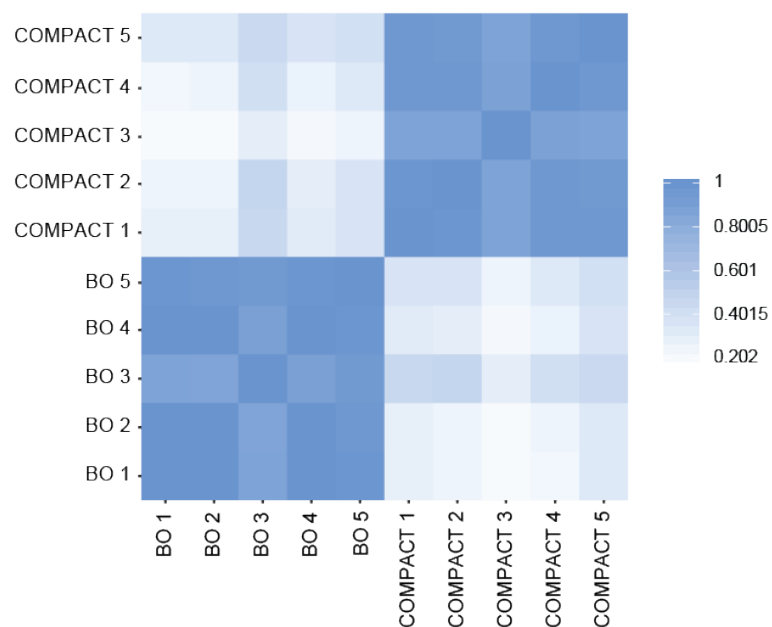
A**B**

Figure 5.8. Distribution of data for COMPACT-TMT in U251 and Jurkat cells. Correlation plots for COMPACT and BO replicates for U251 (A) and Jurkat (B) cells. Pearson correlation values were computed based on raw protein intensities for each replicate.

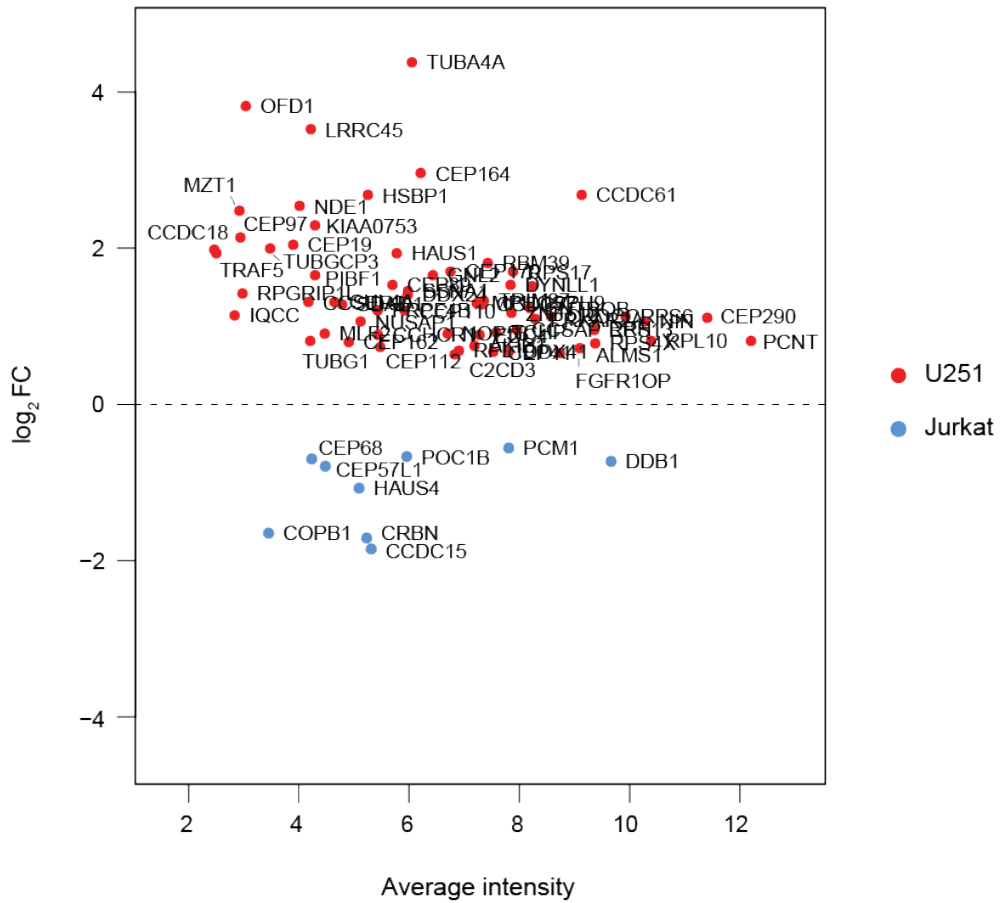
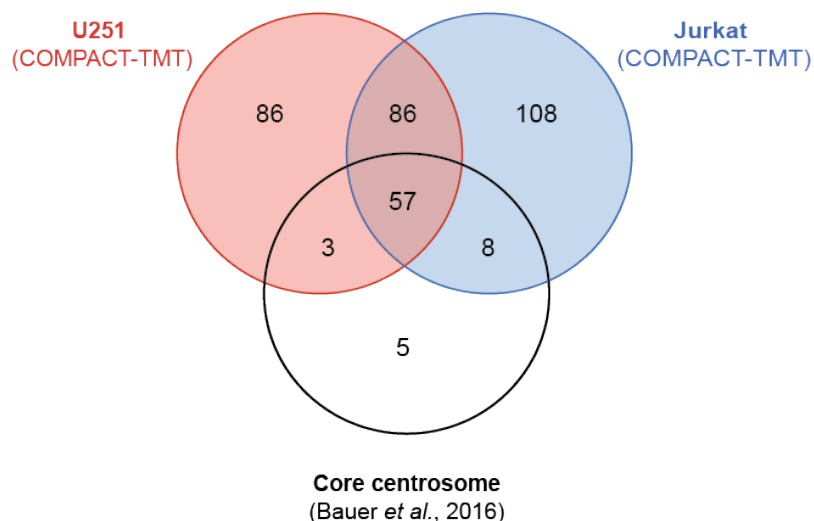


Figure 5.9. Differential expression plot for COMPACT-TMT in U251 and Jurkat cells. Graph shows average intensity plotted against log2FC (fold change) for proteins present in both U251 and Jurkat COMPACT (for each cell line, peptide-specific or peptide-enriched binders were first identified, and cell lines were compared to each other thereafter). Red dots correspond to proteins significantly enriched in U251, blue dots correspond to proteins significantly enriched in Jurkat. Proteins that are common to both cell lines, but not enriched, are not shown. $p < 0.05$.

Next, the U251 and Jurkat COMPACT-TMT datasets were compared to the core centrosome protein dataset (Bauer *et al.*, 2016). For this analysis, all proteins found to be significantly enriched above BO binders ($p < 0.05$) in each cell line were compared (Figure 5.10). When looking specifically at the core centrosome components and where they fall within the U251 and Jurkat COMPACT-TMT datasets, I observed a number of proteins that were common between both cell lines, some that were enriched in one or the other, and others that were unique to one or the other (Figure 5.10 and Figure 5.11). Indeed, while many of the proteins essential to centriole duplication and assembly were present in both cell lines (including SAS6, CEP152, CEP192 and CEP63), a number of proteins showed enrichment in U251 (including OFD1 and CEP164) or Jurkat (including CEP68 and PCM1), or were only observed in U251 (including CEP83 and SCLT1) or Jurkat (including NEDD1 and NEK2). Interestingly, Jurkat cells have a faster doubling time than U251 cells (Cellosaurus, Swiss Institute of Bioinformatics), meaning that they likely have a proportionally shorter G₁ phase compared to the slower cycling U251 cells (G₁-phase is the most variable in length of the cell cycle stages (Chao *et al.*, 2019)). As a result, one could expect to find an over-representation of duplicating and maturing (S- and G₂-phase) centrosomes in Jurkat cells, and thus an enrichment in proteins involved in this process, such as STIL and the mitotic PCM expansion factors NEDD1, NEK2 and CEP68. In contrast, one could expect an over-representation of G₁ centrosomes in U251 cells, as these would represent a larger portion of the total cell cycle length. In this case, one could expect an enrichment in mature centriole and appendage proteins, such as OFD1, NIN and SCLT1.

A**B****Core centrosome components**

CEP128	CEP70	CNTRL	SSNA1	FOPNL	NEK2
POC1A	KIAA0586	CEP63	TUBGCP2	SCLT1	TUBGCP4
CEP131	CEP350	FAM161A	CCDC77	CCDC15	SFI1
CETN2	SAS6	OFD1	CNTROB	CEP85	TUBGCP6
ODF2	CEP57	LRRC45	CCP110	CEP55	TUBGCP5
CETN3	TBC1D31	CEP164	CROCC	CEP68	MZT2B
CEP120	CENPJ	CCDC61	NIN	POC1B	CEP76
POC5	CSPP1	MZT1	TUBG1	PCM1	PLK4
CEP78	SPICE1	CEP97	PCNT	STIL	
CEP250	CEP295	TUBGCP3	ALMS1	HYLS1	
CEP192	CDK5RAP2	CEP170	CEP41	CEP72	
SDCCAG8	CEP152	CEP89	C2CD3	NEDD1	
RTTN	CEP135	CEP290	CEP83	ODF2L	

- Common, not enriched
- Enriched in U251
- Only in U251
- Enriched in Jurkat
- Only in Jurkat
- Absent in both

Figure 5.10. Comparison of COMPACT-TMT in U251 and Jurkat cells to the published core centrosome dataset. A: Venn diagram showing the total number proteins significantly enriched in U251 COMPACT-TMT and Jurkat COMPACT-TMT, compared to the core centrosome (Bauer et al., 2016). p < 0.05. **B:** Table showing all core centrosomal proteins (Bauer et al., 2016), and where they fall within the U251 and Jurkat TMT datasets. Proteins are arranged in descending order according to Log2FC values.

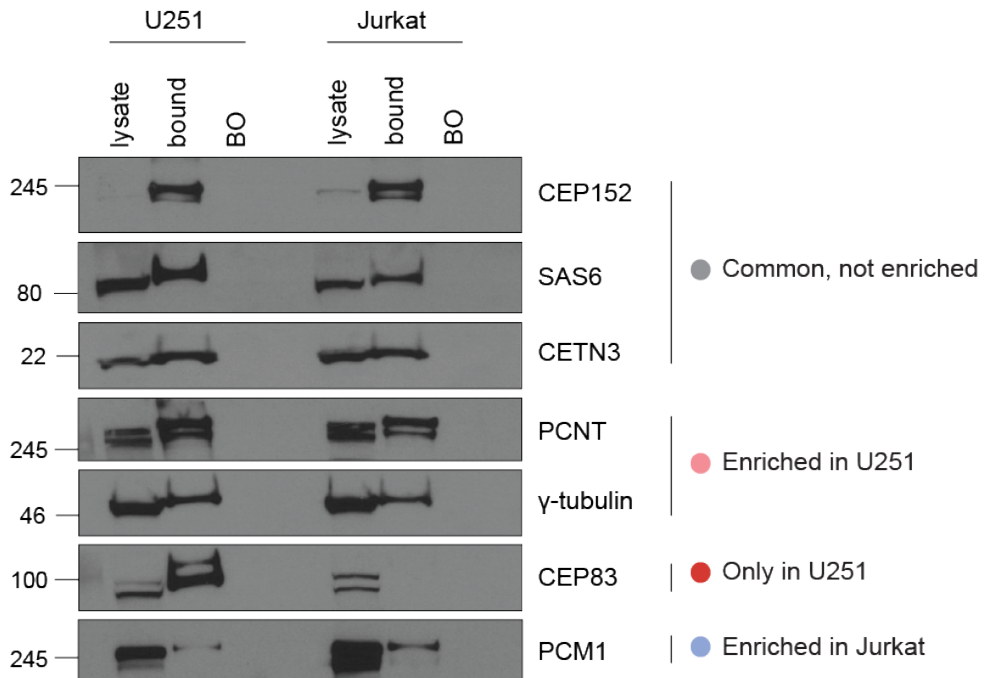


Figure 5.11. COMPACT-WB in U251 and Jurkat cells. COMPACT-WB showing centrosome proteins in the bound (bead-bound) fraction, compared to lysate fraction, for U251 and Jurkat COMPACT.

Remarkably, it is apparent from the COMPACT-TMT data that the distal appendage (DAP) proteins, specifically, were either missing or significantly down-regulated in Jurkat compared to U251 cells. This trend was confirmed by additional COMPACT-WB experiments (see CEP83 in Figure 5.11), as well as by re-analysing the non-quantitative data from COMPACT-MS performed in HEK 293T, U251 and Jurkat cell lines (Figure 5.12). These results revealed that several DAP proteins (OFD1, CEP83, SCLT1, FBF1, CEP164 and ANKRD26) were absent in Jurkat centrosomes when compared to HEK 293T and U251 centrosomes. To independently confirm the absence, centrosomal localisation of various DAP proteins was compared in HEK 293T and Jurkat cells, using immunofluorescence (Figure 5.13 A). Quantification of the staining for a number of DAP markers revealed significantly lower centrosomal levels of these proteins in Jurkat compared to HEK 293T cells (Figure 5.13 B).

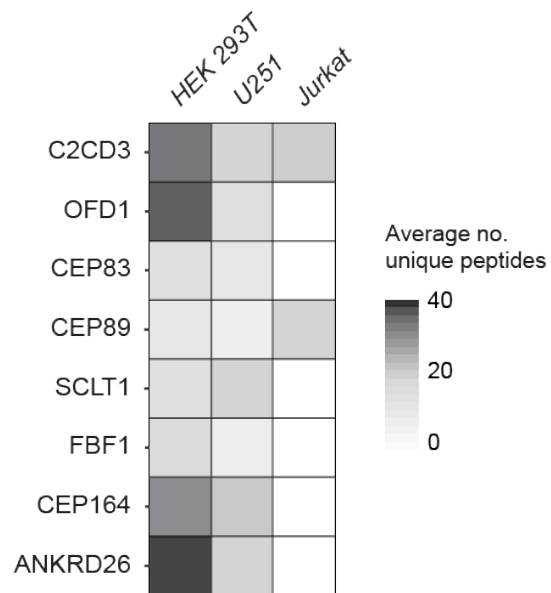


Figure 5.12. Non-quantitative COMPACT-MS from HEK 293T, U251 and Jurkat cells. Heat map showing average number of unique peptides for known DAP proteins (arranged according to hierarchical assembly of components) found in 3-4 replicates of COMPACT-MS performed in HEK 293T, U251 and Jurkat cells. See also Appendix 6.

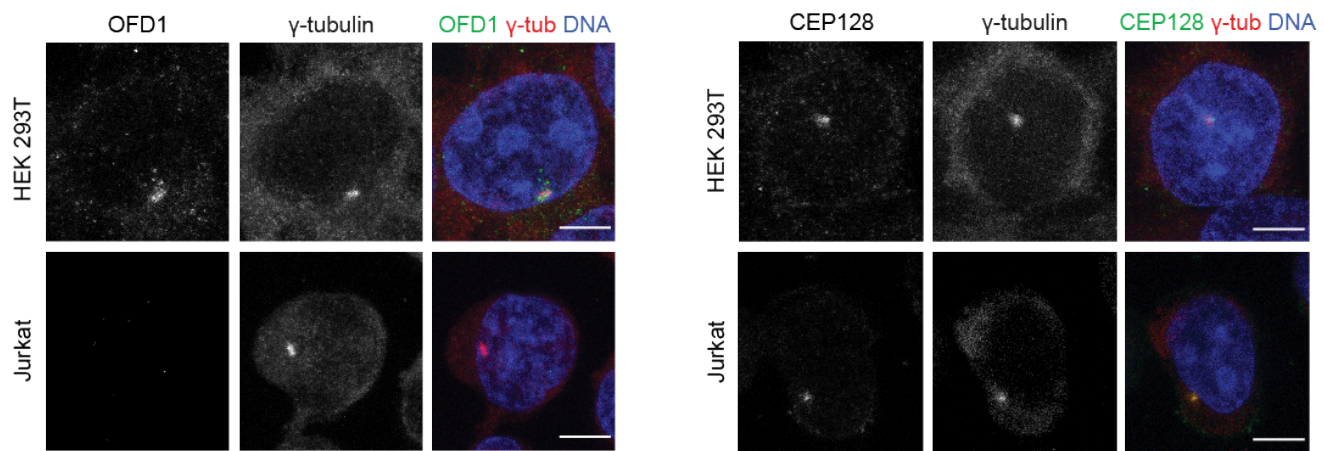
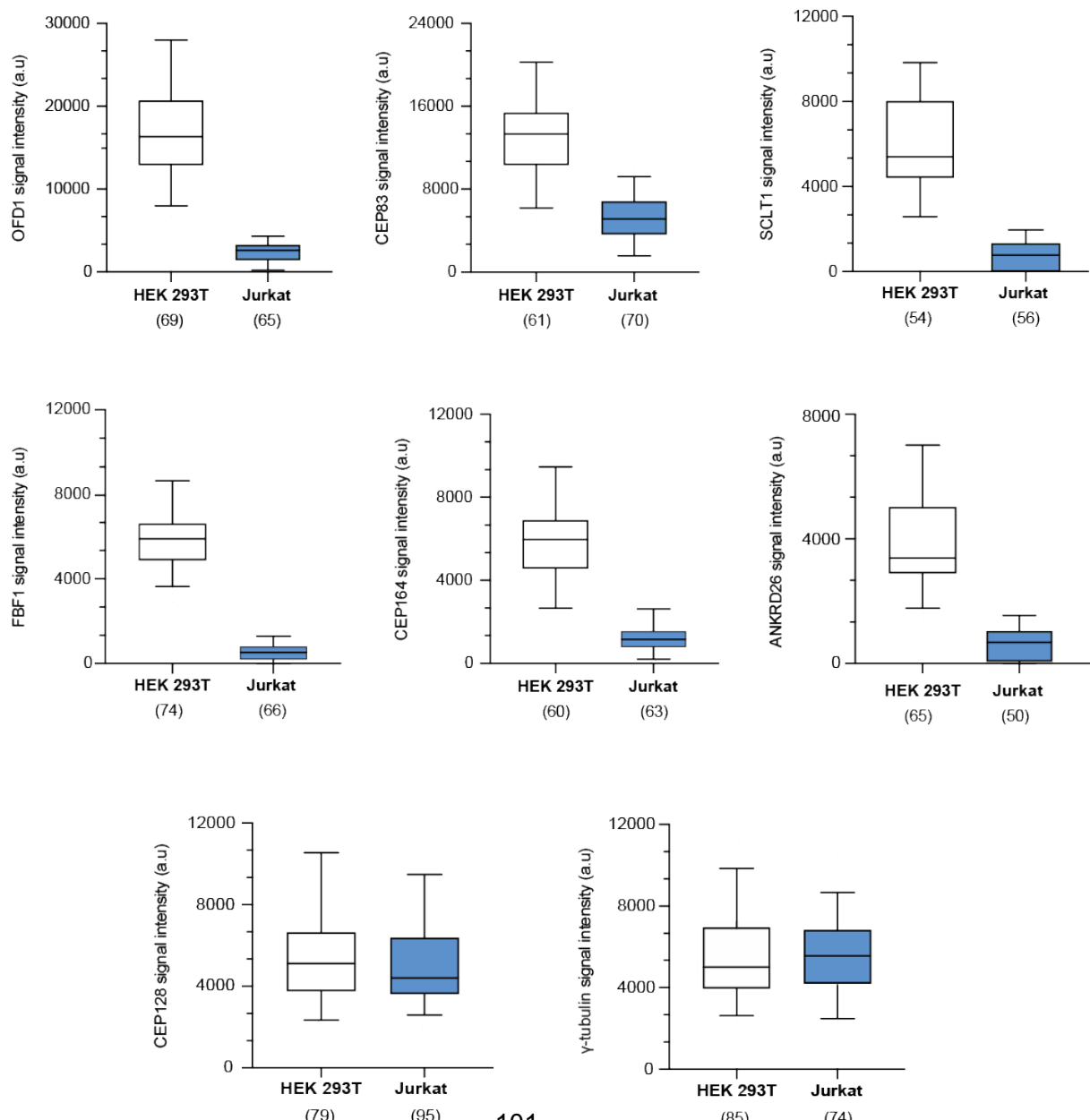
A**B**

Figure 5.13. DAP and sDAP staining in HEK and Jurkat cells. **A:** Representative immunofluorescence images of HEK 293T and Jurkat cells, fixed in MeOH and stained with OFD1 or CEP128 (green) and γ -tubulin (red) antibodies. DNA was stained with Hoescht. Scale bars, 15 μ m. **B:** Box plots showing the signal intensity (background corrected) for DAP proteins in HEK 293T and Jurkat cells. CEP128 and γ -tubulin, which do not localise to DAPs, were used as negative controls. Numbers in brackets represent the number of centrosomes that were quantified. Results shown represent data from experiments performed three independent times. Whiskers represent 10-90 percentile range.

In summary, I have shown that DAP structures (or at least those comprising the traditional DAP proteins, see section 1.4.2) may be tissue-specific rather than ubiquitous, a new and interesting finding. Further studies will be required to explore this in more detail. The above results have demonstrated that COMPACT-TMT can be used to elucidate quantitative differences in centrosome composition across cell types; therefore, having established an effective pipeline for the quantitative analysis of centrosome composition using COMPACT-TMT, it would be interesting to expand on this to include a number of non-transformed cell types.

5.3. COMPACT in primary tissue

5.3.1. Investigating the performance of COMPACT in primary mouse tissue

- COMPACT in mouse liver cells

Due to the success of COMPACT in a panel of cell lines, I decided to expand the use of COMPACT into primary tissue. Results from the mouse neuroblastoma cell line, N1E-115 (Table 5.1 and Figure 5.2), indicated that the COMPACT technique could be extended beyond its use in human cells, to be used in mouse cells as well. As a result, I chose the mouse liver to test the functionality of COMPACT in primary tissue, due to its size and relative homogeneity; hepatocytes constitute at least 70% of the total liver cell population (Ding et al., 2016). Whole livers from 10-week old female C57BL/6 mice were used, due to lower fat content in the organs of younger mice, and the fact that the protein content (after lysis) was roughly similar to what was used for COMPACT in cells. COMPACT-WB indicated that centrosomal proteins were being recovered in the bound fraction (Figure 5.14), and thus samples were submitted for MS analysis. COMPACT-MS results revealed a number of known centrosomal proteins, as indicated by an overlap with the KE-37 dataset (Jakobsen et al., 2011), but not the enrichment that was expected based on the results from COMPACT performed in cells lines (Figure 5.15 A, refer to Figure 5.2 for comparison). In fact, a large number of known centrosomal proteins were completely absent in liver COMPACT, including CEP350, CEP290, NIN and CEP192 (Figure 5.15 B). On closer observation, I noticed that the majority of proteins found in liver COMPACT were also found in the BO samples, including those centrosomal proteins found to be overlapping with KE-37 (Figure 5.16 A). This was also observed when samples were analysed by western blot using the standard centrosomal markers PCNT, γ -tubulin and CETN3 (Figure 5.16 B). The most abundant proteins identified in liver COMPACT (according to number of unique peptides as well as protein coverage) were intermediate filament proteins, scaffold/linker proteins, and proteins found within desmosomes (i.e. plectin, spectrins, desmoplakin, and various keratins). It is possible that these proteins are present in large quantities in the liver cells and interfere with COMPACT, by potentially masking/blocking the efficiency of the peptide-bound beads to capture centrosomes. Interestingly, when COMPACT was tested in a human liver cell line, the hepatocellular carcinoma line, HepG2, the same trend was observed, indicating that COMPACT is unable to efficiently purify centrosomes from all liver cells, not just primary cells from mouse tissue (Figure 5.17).

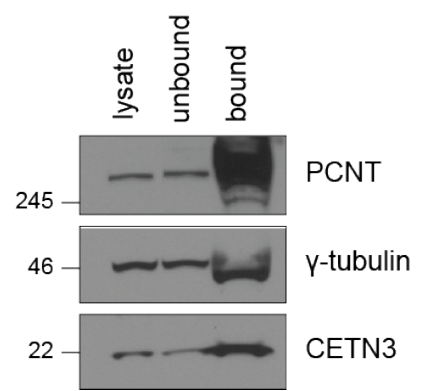
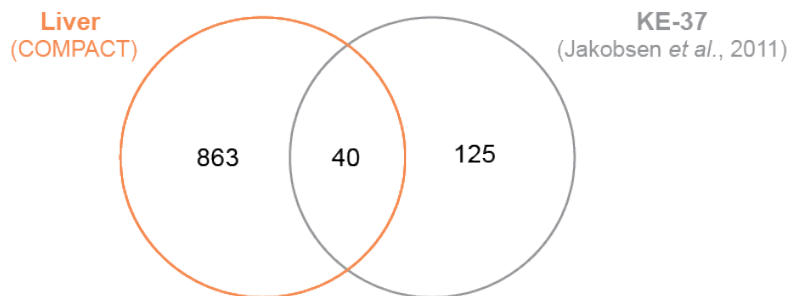


Figure 5.14. COMPACT in mouse liver cells. COMPACT-WB showing centrosome proteins in the bound (bead-bound) fraction, compared to lysate and unbound fractions, for COMPACT in freshly-isolated mouse liver cells.

A**B**

Liver only		Liver and KE-37		KE-37 only	
PLEC	192	PCNT	14	CEP350	-
SPTAN1	130	DYNC1H1	13	CEP290	-
EPPK1	127	CEP135	10	NIN	-
DSP	117	CEP250	10	CEP57	-
SPTBN1	82	ODF2	8	CCP110	-
MYH9	80	CNTROB	7	CEP76	-
KRT18	53	CSNK1A1	6	CEP97	-
KRT8	53	AKAP9	6	CEP41	-
MACF1	45	CEP152	6	PCM1	-
TLN1	39	PDE4DIP	6	CEP192	-

Figure 5.15. Comparison of COMPACT in mouse liver cells to KE-37. A: Venn diagram showing the total number of proteins common to three biological replicates for liver COMPACT, compared to the KE-37 centrosome proteome (Jakobsen et al., 2011). Note that bead-only binding proteins were not removed from liver COMPACT. **B:** Table showing the top 10 proteins detected in liver only, liver and KE-37, and KE-37 only and their corresponding number of unique peptides from COMPACT-MS in the liver (average of 3 replicates).

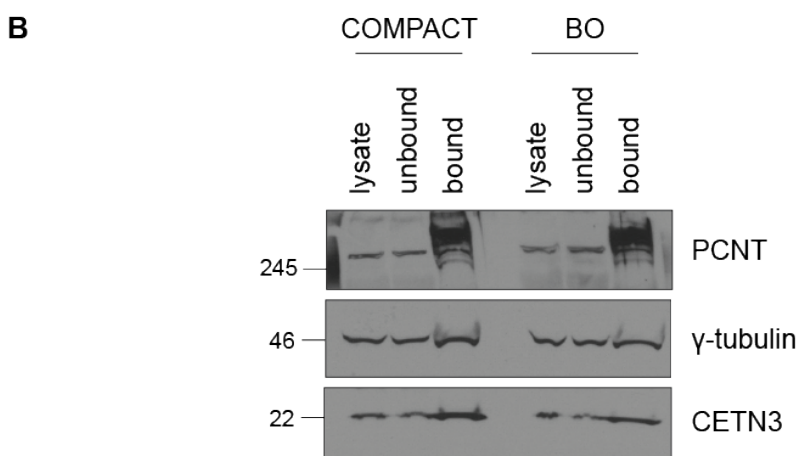
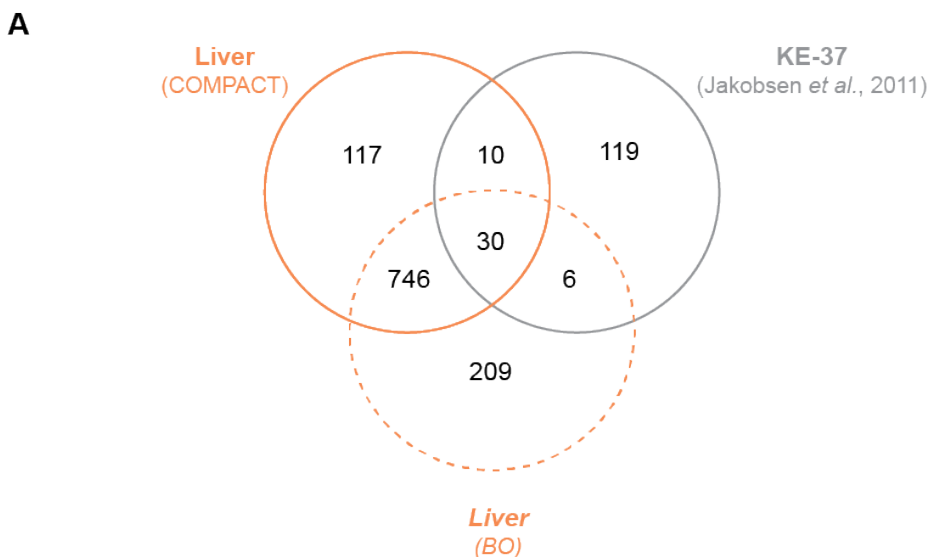


Figure 5.16. Comparison of COMPACT and BO in mouse liver cells to KE-37. **A:** Venn diagram showing the total number proteins common to three biological replicates for liver COMPACT (bead-only binding proteins not removed), and two biological replicates for BO, compared to the KE-37 centrosome proteome (Jakobsen et al., 2011). **B:** Western blot showing centrosome proteins in the bound (bead-bound) fraction, compared to lysate and unbound fractions, for COMPACT and BO in freshly-isolated mouse liver cells.

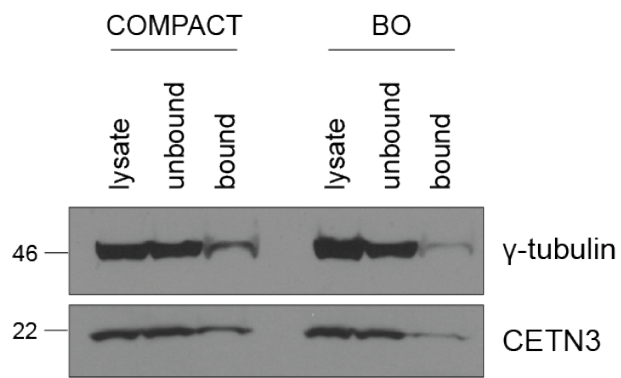


Figure 5.17. COMPACT in human hepatocellular carcinoma cells, HepG2. COMPACT-WB showing centrosome proteins in the bound (bead-bound) fraction, compared to lysate and unbound fractions, for COMPACT in HepG2 cells.

- COMPACT in mouse spleen cells

Due to the success of COMPACT in Jurkat (T lymphocyte) cells, I next decided to investigate the performance of COMPACT in cells freshly isolated from mouse spleen; T lymphocytes comprise up to 35% of the mouse spleen (Mouse Phenome Database, The Jackson Laboratory). Initial experiments indicated that the cell strainer method (see section 3.2) was not able to recover sufficient protein for COMPACT, and thus rotor-stator homogenisation, using the TissueRuptor (Qiagen, USA) was utilised (Figure 5.18). COMPACT-MS revealed that 52% (86/165) of centrosomal proteins in KE-37 dataset (Jakobsen et al., 2011) overlapped with the mouse spleen (Figure 5.19 A). Additionally, a much smaller number of proteins were found to be overlapping with the BO proteome (178 proteins), compared to what was seen in the liver (746 proteins), and none of these proteins were known centrosomal proteins according to a comparison with the KE-37 proteome (Figure 5.19 A). Proteins found exclusively in the spleen represent potential tissue-specific centrosomal candidates (Figure 5.19 B and Appendix 9).

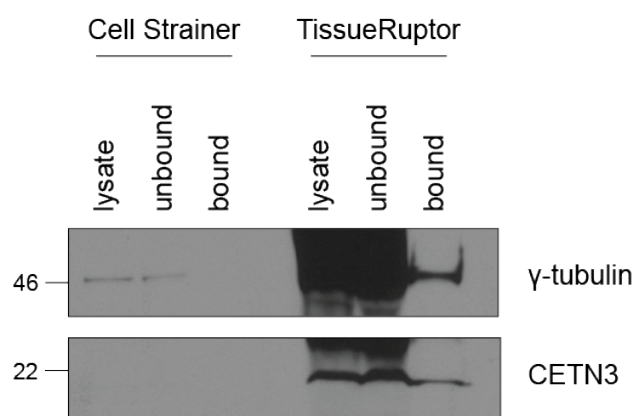
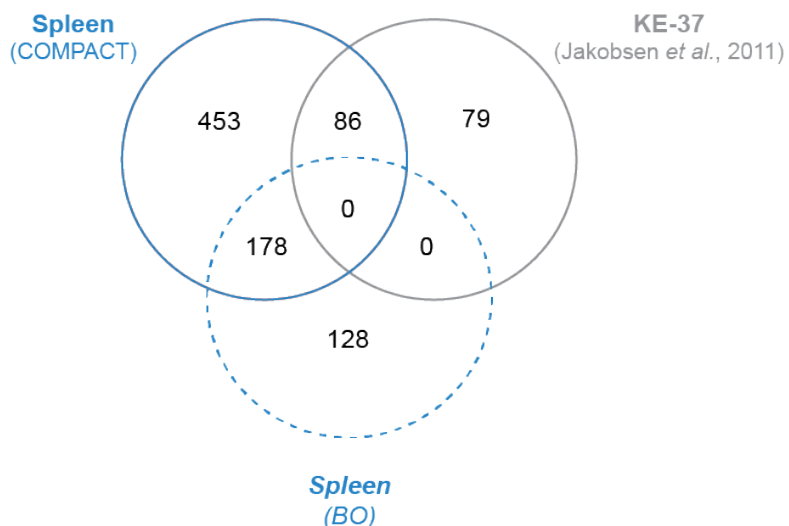


Figure 5.18. COMPACT in mouse spleen cells. COMPACT-WB showing centrosome proteins in the bound (bead-bound) fraction, compared to lysate and unbound fractions, for COMPACT performed in cells freshly isolated from whole mouse spleens. Cells were isolated using a cell strainer or TissueRuptor (for more details see section 3.2).

A**B**

	Spleen only	Spleen and KE-37	KE-37 only
SPTA1	69	PCNT	52
TAF1	36	CNTRL	CEP290
SPTB	26	CEP250	CEP76
FN1	24	AKAP9	47
MYH11	24	CROCC	CEP192
COPA	24	CEP350	CSPP1
SPTAN1	21	CEP135	CEP131
SYNM	20	NIN	HAUS6
COPB2	18	CEP128	LRRC45
TAF2	18	CDK5RAP2	ACTR1A
			DCTN4

Figure 5.19. Comparison of COMPACT and BO in mouse spleen cells to KE-37. A: Venn diagram showing the total number proteins common to two biological replicates for spleen COMPACT (bead-only binding proteins not removed), and one BO, compared to the KE-37 centrosome proteome (Jakobsen et al., 2011). B: Table showing the top 10 proteins detected in spleen only, spleen and KE-37, and KE-37 only and their corresponding number of unique peptides from COMPACT-MS performed in the spleen (average of 2 replicates). Bead-only binding peptides were removed for final analysis.

In summary, I have shown that COMPACT can be used to determine centrosome composition in primary cells, particularly cells isolated from the mouse spleen. This is a novel and exciting finding, as the sucrose sedimentation-based technique requires a large number of cells that are not feasible to collect from primary tissue. In addition, COMPACT-MS performed on freshly isolated mouse spleen cells revealed a number of potential tissue-specific candidates, and further experimentation is required for their validation and functional characterisation.

6 Results III

6.1. Using COMPACT to identify novel centrosomal candidates

Upon creating the tissue-specificity table in section 5.2.1 (Table 5.2 and Appendix 6), as well as analysing the COMPACT-TMT data from U251 and Jurkat cells, I identified a number of novel centrosomal candidate proteins. The pipeline used to identify and validate candidates is summarised in Figure 6.1. Candidates were chosen based on their absence from the centrosome and cilium database (CCDB), a high-quality reference list of 1554 proteins with previous evidence for centrosome or cilium association (Gupta et al., 2015), but presence in most, if not all, of the cell lines in which COMPACT-MS was performed.

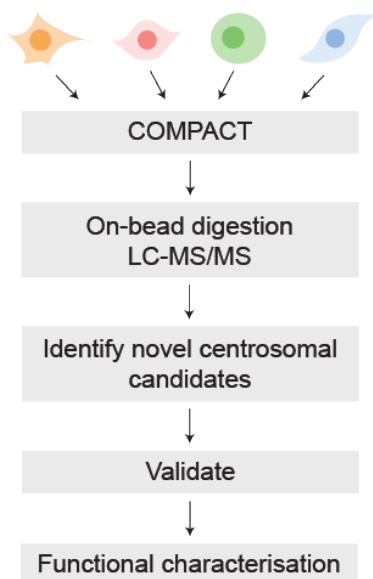


Figure 6.1. Workflow for identification and characterisation of novel centrosomal candidates. COMPACT-MS was performed on a panel of cell lines (see section 5.2.1), and novel centrosomal candidates were identified based on their absence from the centrosome and cilium database; CCDB (Gupta et al., 2015), but presence in most, if not all, of the cell lines in which COMPACT-MS was performed.

A number of centrosomal candidates were selected for further analysis and validation based on the following criteria: first, I queried the protein's function using the online database GeneCards (GeneCards.org). Next, I performed extensive literature searches to reveal whether the candidate protein had ever been found to be associated with the centrosome or known centrosomal proteins. Finally, I used the SAINT (www.saint-apms.sourceforge.net/) and/or BioGRID (www.thebiogrid.org) computational tools to identify potential interactions between candidates and known centrosomal proteins. The SAINT software was developed to assign confidence scores to protein-protein interactions based on quantitative proteomics data from affinity purification (AP)-MS experiments (Choi et al., 2011), while BioGRID is a regularly curated online repository containing information on protein interactions, chemical interactions, as well as post-translational modifications.

The candidates I chose to analyse further in this study were: EDC4, TRIM27, AKIP1, DDB1, CRBN, NOP53 and CCDC171. EDC4 (Enhancer of mRNA decapping 4) is an mRNA decapping protein commonly found in P-bodies. Interestingly, centrosomes and P-bodies have been shown to share components (reviewed in Johnson and Malicki, 2019). The SAINT tool revealed a high confidence interaction for EDC4 with SAS6. TRIM27 (Tripartite Motif Containing 27) is an E3 ubiquitin-protein ligase that mediates the ubiquitination of PIK3C2B and inhibits its activity. A number of studies have suggested that the centrosome acts as a scaffold for ubiquitin-proteosome-mediated degradation (reviewed in Vora and Phillips, 2016), and SAINT scores reveal a number of potential interactions with TRIM27 at the basal body-centrosome complex. AKIP1 (A-Kinase Interacting Protein 1) is a transcriptional activator of the NF κ B signalling cascade, and centrosomes have been postulated to act as signalling hubs in a number of studies (reviewed in Arquint et al., 2014). BioGRID reveals centriolar proteins POC1A and POC5 as interactors of AKIP1. DDB1 (Damage Specific DNA Binding Protein 1) and CRBN (Cereblon) are components of a cullin-RING ubiquitin-protein ligase complex that mediates ubiquitination and degradation of multiple protein targets. A recent paper showed that an E3 ubiquitin ligase complex at the centrosome, consisting of DDB1, mediates the ubiquitination of CP110 (Hossain et al., 2017). Additionally, there is evidence of a number of cullin-RING complexes being involved in centrosome duplication (reviewed in Jang et al., 2020). NOP53 (NOP53 Ribosome Biogenesis Factor) regulates the activation of p53 in response to ribosome biogenesis perturbations, DNA damage and other stress conditions. This study (see Appendix 6) and others have shown the presence of p53 at the centrosome (Ciciarello et al., 2001; Contadini et al., 2019). CCDC171 (Coiled-coil Domain Containing 171) has an unknown function, but coiled-coil domain-containing proteins (including CEP57, CEP63 and CEP152; see section 1.5.6) have long been known as centrosomal scaffolds important for recruitment of other proteins.

Validation of centrosomal candidates was performed first by identifying suitable antibodies and verifying their specificity by RNAi. Thereafter, centrosomal localisation of candidates was independently investigated using immunofluorescence; whole cell staining and COMPACT-IF in order to identify centrosomal sub-structure. All candidate validation experiments were performed in HEK 293T cells. Results are summarised in Table 6.1, and exemplary data for various candidates can be seen in Figures 6.2 - 6.4.

Figure 6.2 shows that siRNAs used to target EDC4, TRIM27, DDB1, CRBN and NOP53 show a marked reduction in protein levels after 48 hours transfection. Neither of the siRNAs selected for CCDC171 (Figure 6.2) showed protein depletion, while I was unable to find a suitable antibody for AKIP1 (data not shown). As a result, AKIP1 and CCDC171 were excluded from further analysis. Next, I performed COMPACT-IF on cells transfected with candidate-targeting siRNA for 48 hours. Results in Figure 6.3 show that the centrosomal signals of EDC4 and TRIM27 were absent after siRNA-mediated protein depletion, however no reduction in signal intensity at the centrosome was observed for candidates DDB1, CRBN, and NOP53. This could indicate that for these candidates the antibody staining at the centrosome was non-specific, or that the siRNA treatment failed to deplete the centrosomal pools of these proteins within the 48 hour transfection period, if at all.

Images captured on the confocal microscope and deconvolved using Huygens software (see section 3.3.2) of EDC4 and TRIM27 specifically, revealed centrosomal localisation patterns of the two candidates. EDC4 appeared to cap centrioles at both proximal and distal ends, while TRIM27 appeared as a ring-like structure indicative of the PCM (Figure 6.4).

Table 6.1. Table showing a number of novel centrosomal candidates, chosen based on their presence in centrosome proteomes of all cell lines analysed using COMPACT-MS.

Protein	Known protein function (GeneCards.org)	Antibody (specificity by RNAi, WB)	Validation		Sub-structure (COMPACT-IF)
			IF	COMPACT-IF	
EDC4	mRNA decapping	X		X	Centriole, capping
TRIM27	E3 ubiquitin-protein ligase	X		X	PCM
AKIP1	Transcriptional activator, NF κ B pathway				
DDB1	E3 ubiquitin-protein ligase complex component	X	X	X	Weak, PCM
CRBN	E3 ubiquitin-protein ligase complex component	X	X	X	Weak, PCM
NOP53	Ribosome biogenesis, p53 regulator	X	X	X	Weak, proximal centriole
CCDC171	Unknown				

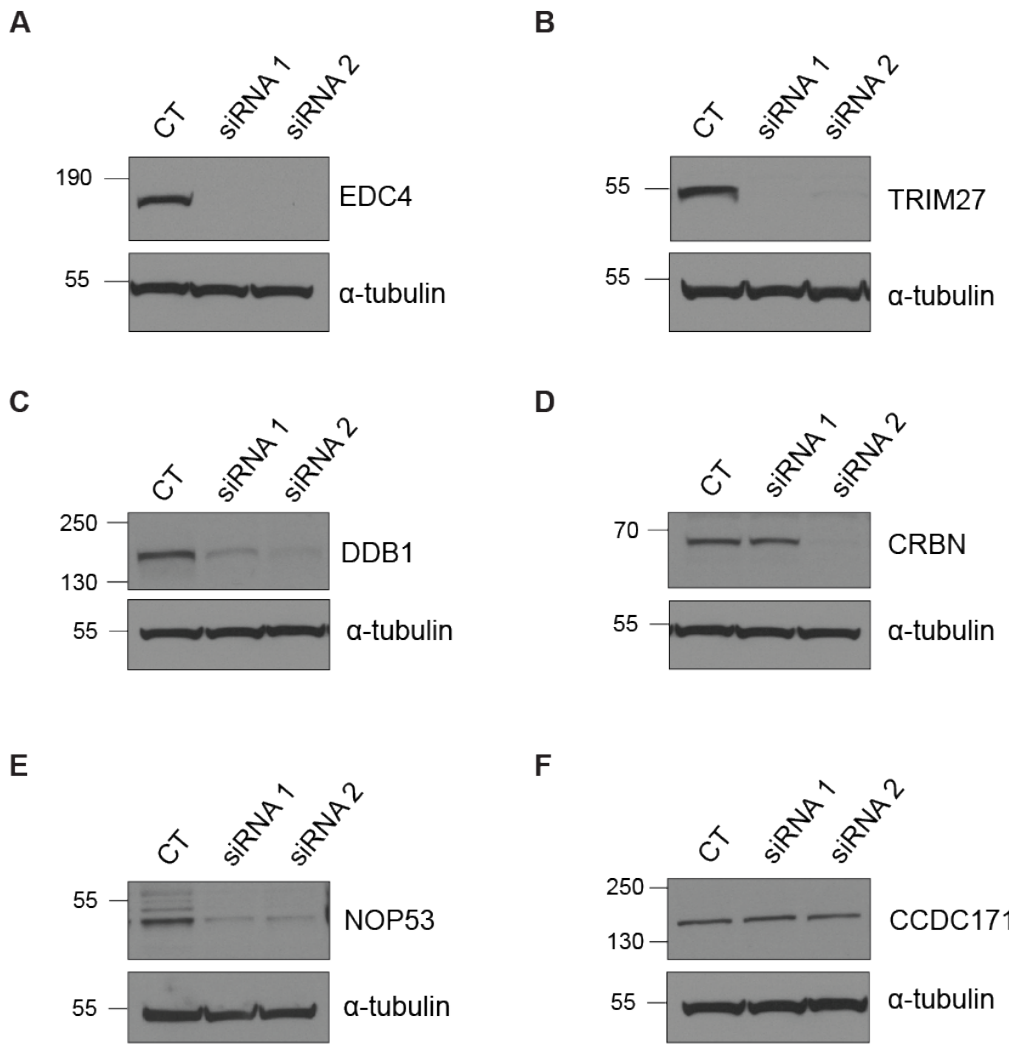


Figure 6.2. Knockdown efficiencies upon siRNA treatment in HEK 293T cells. Western blots showing EDC4 (A), TRIM27 (B), DDB1 (C), CCRN (D), NOP53 (E) and CCDC171 (F) levels in HEK 293T cells transfected with control (CT) and two different targeting siRNAs for 48 hours. α-tubulin was used as a loading control.

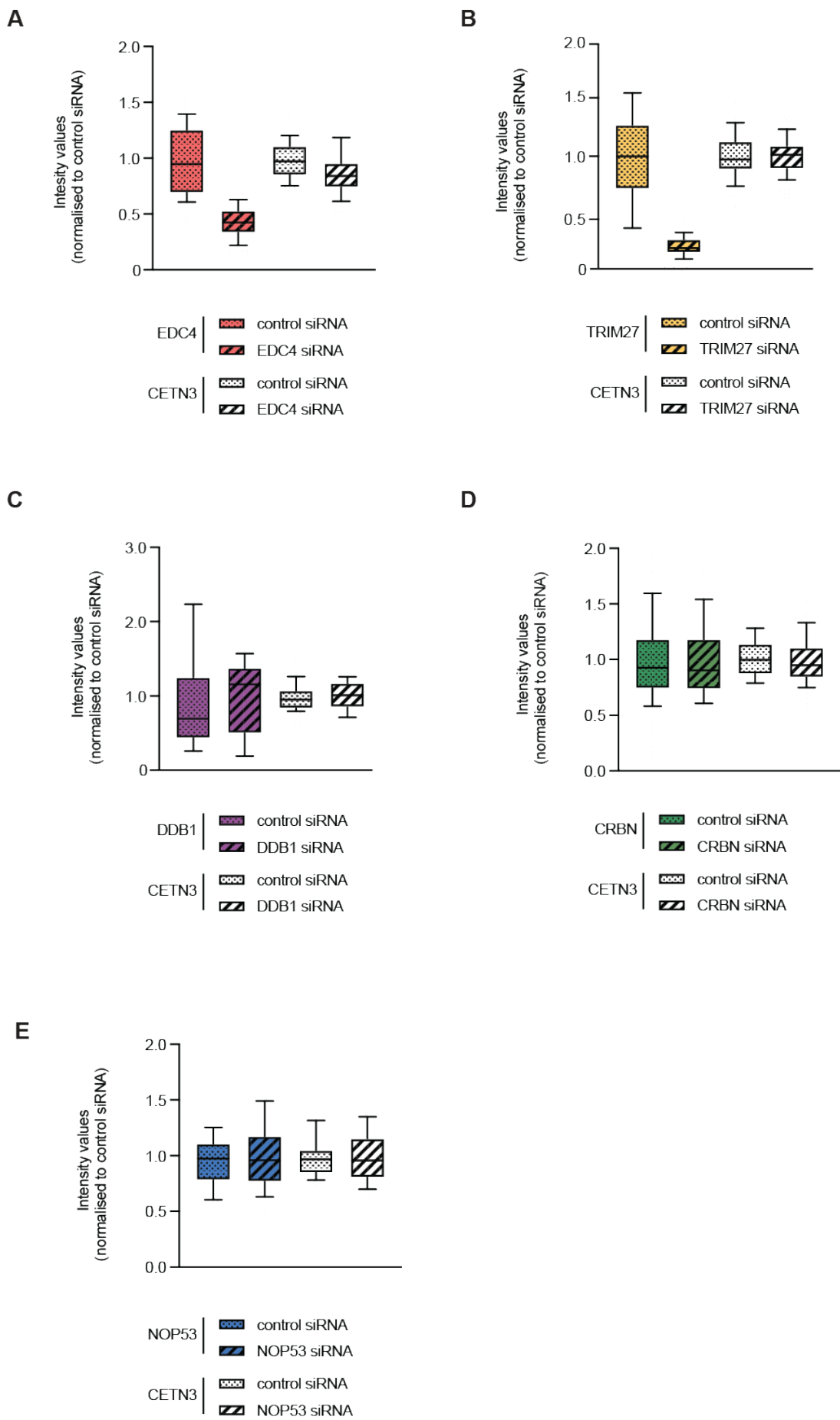


Figure 6.3. COMPACT-IF after siRNA treatment in HEK 293T cells. Box plots showing the centrosomal signal intensities of novel candidates. HEK 293T cells were transfected with candidate-specific siRNA for 48 hours, after which centrosomes isolated by COMPACT were spun onto coverslips and stained with candidate-specific antibodies EDC4 (A), TRIM27 (B), DDB1 (C), CRBN (D) and NOP53 (E). The distal centriole marker, CETN3, was used as a negative control. 100-200 centrosomes were analysed per candidate (and control) siRNA, for experiments performed two independent times. Whiskers represent 10-90 percentile range.

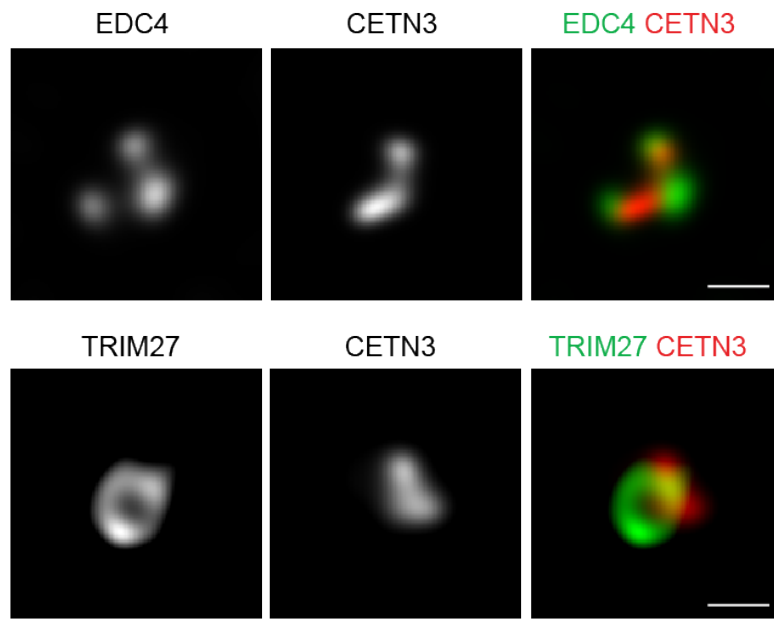


Figure 6.4. EDC4 and TRIM27 staining in centrosomes isolated from HEK 293T cells using COMPACT-IF. Representative deconvolved confocal images of centrosomes isolated from HEK 293T cells by COMPACT, spun onto coverslips and stained with novel candidates, EDC4 or TRIM27 (green) and CETN3 (red) antibodies. Scale bars, 5 μ m.

In order to independently validate centrosomal localisation of novel candidates, I performed the sucrose-sedimentation-based centrosome isolation method (Bornens and Moudjou, 1998), followed by western blotting to confirm the presence of novel candidates in centrosome-enriched fractions. Interestingly, I observed a wider sedimentation pattern than I had seen previously (Figure 6.5 compared to Figure 4.17). Due to the fact that sucrose density was created using w/v measurements for this experiment (instead of w/w), the sucrose cushion and sucrose density gradient were of a lower percentage than they should have been (measured post-experiment using a refractometer). Despite this, all novel candidates showed the same sedimentation pattern as known centrosomal proteins, with fractions 6 and 7 indicating the peak centrosomal fractions. α -tubulin and GAPDH, which should not co-sediment with centrosomes, do not show the same pattern.

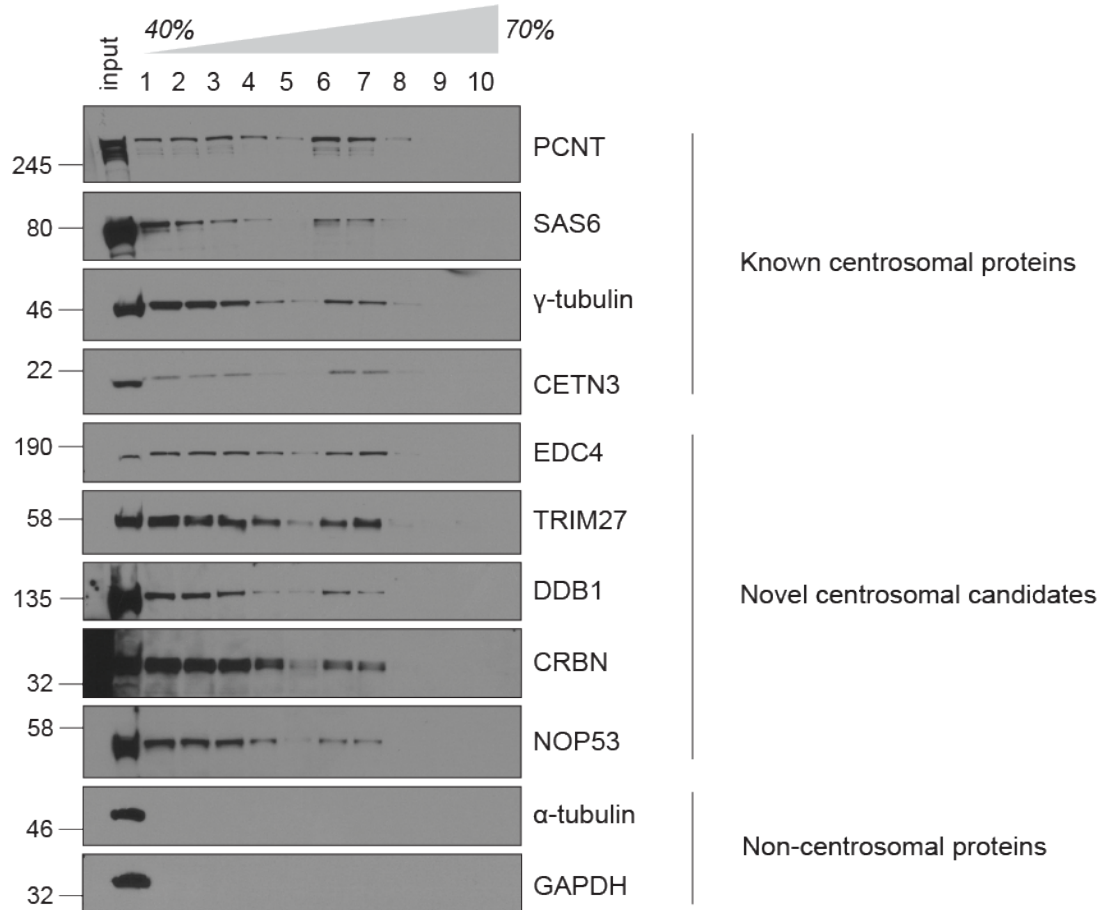


Figure 6.5. Independent validation of centrosomal candidates by sucrose sedimentation in HEK 293T cells. Representative western blot showing sedimentation patterns of novel centrosomal candidates, alongside known centrosomal proteins PCNT, SAS6, γ -tubulin and CETN3. α -tubulin and GAPDH were used as negative controls. Cell lysates (from approximately 1×10^9 cells) were enriched for centrosomes by centrifugation onto a 50% (w/v) sucrose cushion (input), followed by centrifugation through a discontinuous sucrose gradient of 40-70% (w/v). 0.5% of the input and 10% of each sucrose fraction (1-10) were loaded onto the gel.

In summary, I have shown that COMPACT can be used as a tool for the identification of novel centrosomal proteins. Future work in the lab aims to explore centrosomal candidates (those discussed above as well as others; Table 5.2 and Appendix 6), and their putative roles in centrosome biology.

6.1.1. *Investigating the centrosomal role of TRIM27*

TRIM27 is a E3 ubiquitin-protein ligase that mediates the ubiquitination of PIK3C2B, leading to a decrease in its enzymatic activity (Cai et al., 2011). Interestingly, the centrosome is known to function as a signalling centre and scaffold for proteasomal mediated degradation, and many PI3K pathway components have, in fact, been shown to be associated with the centrosome (Arquint et al., 2014; Cai et al., 2011; Vanhaesebroeck et al., 2019). As a result, I decided to investigate the potential role for TRIM27 at the centrosome by performing loss-of-function studies in HEK 293T cells.

Based on the observation that a 48-hour transfection of TRIM27-targeting siRNA was able to deplete a large proportion of the whole cell and centrosomal protein (Figure 6.2 and Figure 6.3, respectively), the same conditions were used to assess the biological phenotypes associated with TRIM27 depletion. Using two independent siRNAs, potential centrosomal phenotypes were investigated in interphase and mitotic cells using immunofluorescence, by staining for the PCM marker, γ -tubulin, and the centriole marker, CETN3, and counting positive foci per cell. As seen in Figure 6.6, very few interphase cells with abnormal numbers of γ -tubulin foci (>2) were observed. When looking specifically at mitotic (prometaphase-metaphase) cells, approximately 30% showed centrosomal abnormalities, i.e. an increased number of γ -tubulin- and CETN3-positive foci (Figure 6.7). Figure 6.8 shows that this trend is similar when looking at anaphase-telophase cells. Interestingly, when DNA content (i.e. number of mononucleated versus binucleated cells) was quantified, almost no binucleated interphase cells were observed in either condition, indicating that the increased number of centrosomes observed as a result of TRIM27 depletion is unlikely due to a failure of cytokinesis (Figure 6.9).

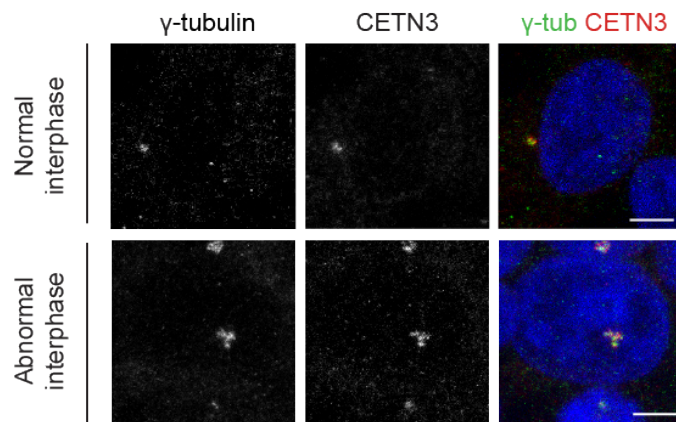
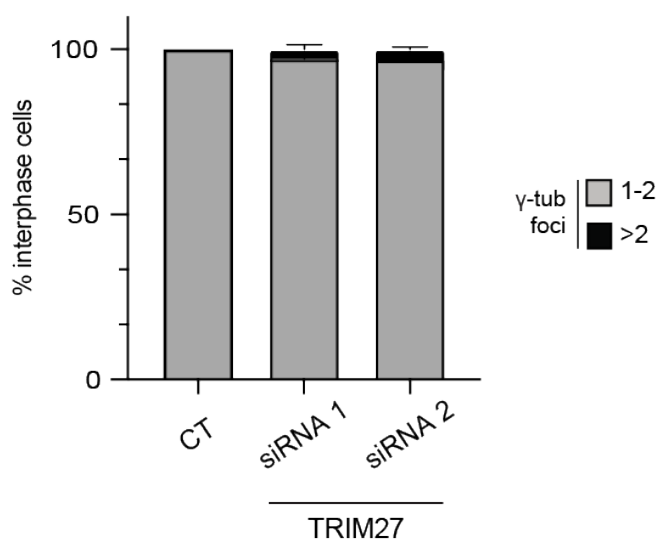
A**B**

Figure 6.6. TRIM27 functional studies in interphase HEK 293T cells **A:** Representative immunofluorescence images of TRIM27 siRNA-transfected HEK 293T cells stained with γ -tubulin (green) and CETN3 (red) antibodies. DNA was stained with Hoescht (blue). Scale bars, 15 μ m. **B:** Bar graph showing the percentage of interphase cells with 1-2 or >2 γ -tubulin foci. HEK 293T cells transfected with control (CT) or TRIM27 siRNA for a period of 48 hours were compared. 100-200 cells per condition were scored. Data represents mean + SD from three independent experiments.

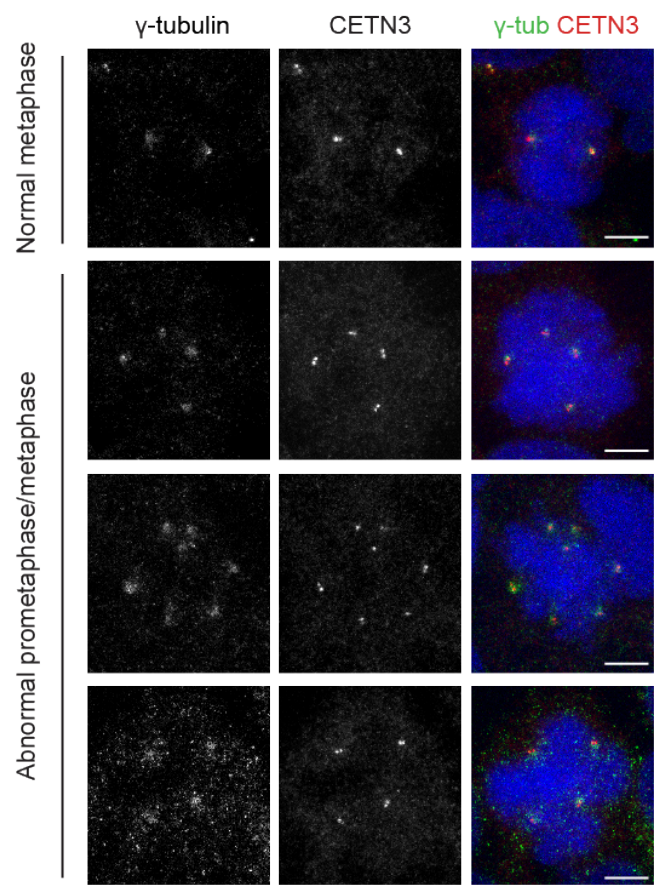
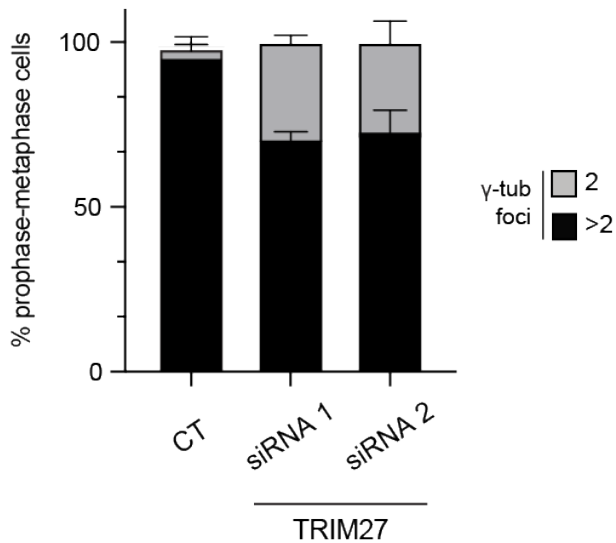
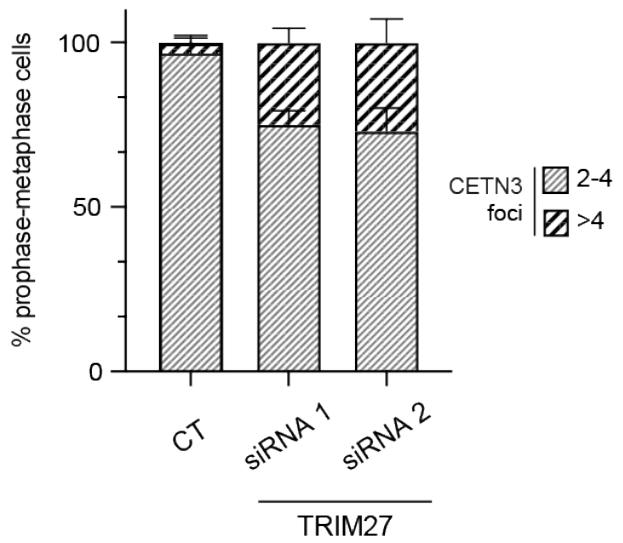
A**B****C**

Figure 6.7. TRIM27 functional studies in prometaphase-metaphase HEK 293T cells **A:** Representative immunofluorescence images of TRIM27 siRNA-transfected HEK 293T cells stained with γ -tubulin (green) and CETN3 (red) antibodies. DNA was stained with Hoescht (blue). Scale bars, 15 μ m. **B and C:** Bar graphs showing the percentage of mitotic cells with 2 or >2 γ -tubulin foci (B) or 2-4 or >4 CETN3 foci (C). HEK 293T cells transfected with control (CT) or TRIM27 siRNA for a period of 48 hours were compared. 50-100 mitotic cells per condition were scored. Data represents mean + SD from three independent experiments.

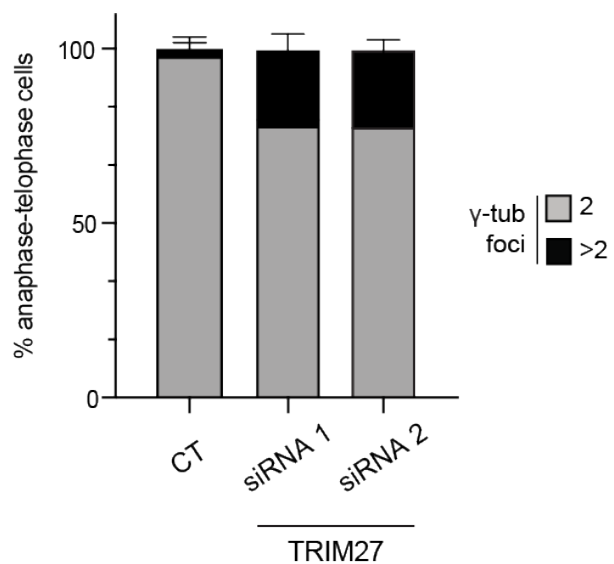


Figure 6.8. TRIM27 functional studies in anaphase-telophase HEK 293T cells. Bar graph showing the percentage of mitotic cells with 2 or >2 γ -tubulin foci. HEK 293T cells transfected with control (CT) or TRIM27 siRNA for a period of 48 hours were compared. 30-50 mitotic cells were per condition were scored. Data represents mean + SD from three independent experiments.

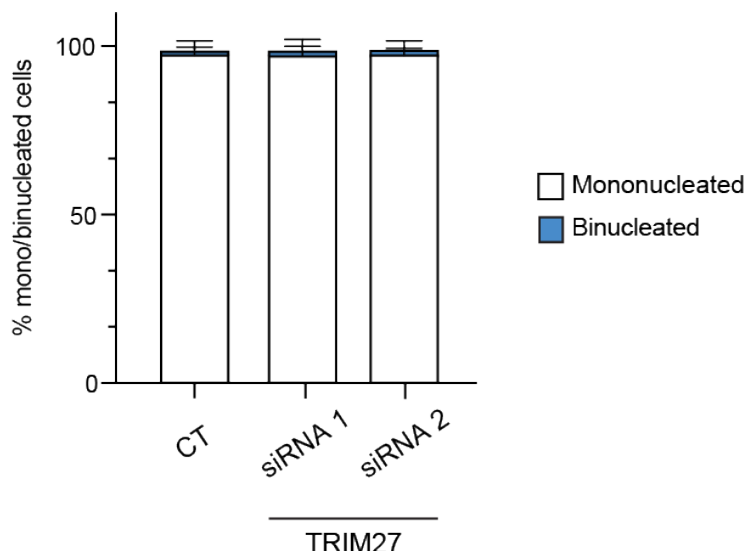


Figure 6.9. Nuclear phenotype in TRIM27-depleted HEK 293T cells. Bar graph showing the percentage of interphase cells with 1 (mononucleated) or 2 (binucleated) nuclei, determined using Hoescht staining. HEK 293T cells transfected with control (CT) or TRIM27 siRNA for a period of 48 hours were compared. 100-200 cells per condition were scored. Data represents mean + SD from three independent experiments.

Next, in order to determine whether the increase in number of mitotic cells with extra centrosomes upon TRIM27 depletion is centriole-dependent, HEK 293T cells were treated with centrinone for a period of 8 days prior to 48-hour siRNA transfection (in the presence of centrinone). Figure 6.10 shows that a large proportion of centrosomal protein (indicated by CETN3 and γ -tubulin staining) is absent in control cells after 8 days, confirming that centrinone treatment results in centrosome loss. All conditions were analysed for the presence of extra centrosomes, and while approximately 30% of untreated (-centrinone) mitotic cells transfected with TRIM27 siRNA were found to contain extra centrosomes (similar to what was observed in Figures 6.7 and 6.8), only 10-12% of mitotic cells pre-treated with centrinone (+centrinone) displayed extra centrosomes (Figure 6.11). Interestingly, the cells with mitotic abnormalities (such as multipolar spindles as seen via DNA morphology and α -tubulin staining) appeared to be those that still contained extra centrosomes, despite centrinone treatment (see exemplary cell in Figure 6.11 A, panel 3). Cells that showed a normal mitotic phenotype (i.e. bipolar spindle and/or properly aligned metaphase plate) were those that contained only one or zero visible centrosomes (see exemplary cell in Figure 6.11 A, panel 2). These data indicate that the TRIM27 depletion phenotype is centrosome dependent, as only cells with intact

centrosomes (indicated by PCNT staining) displayed abnormalities upon centrinone treatment.

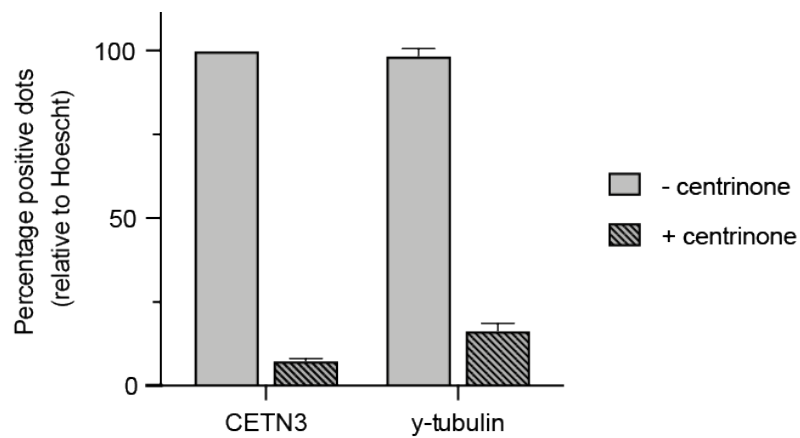


Figure 6.10. Loss of centrosomes in HEK 293T cells after treatment with centrinone. HEK 293T cells treated for 8 days with centrinone. Histogram reveals percentage positive foci for centriolar and PCM markers, CETN3 and γ -tubulin, relative to DNA (number of Hoechst-positive cells). 100-200 cells per condition were scored. Data shown represents the mean + SD for experiments performed three independent times.

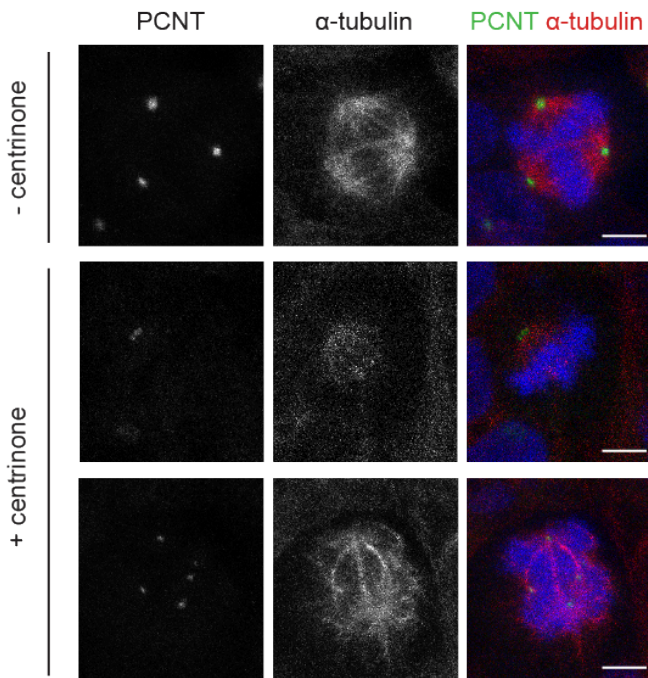
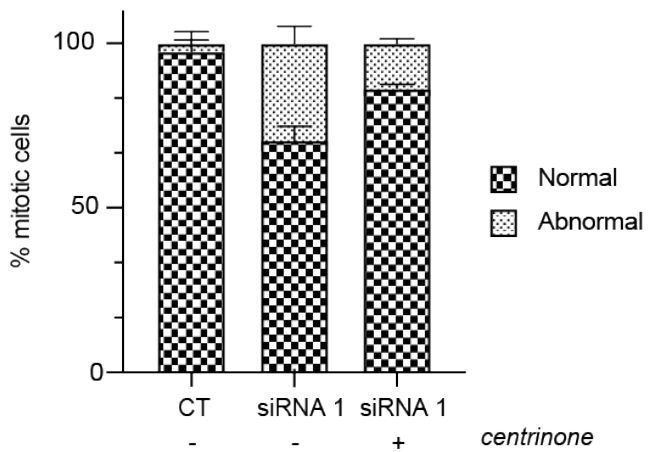
A**B**

Figure 6.11. Rescue of TRIM27 depletion phenotype in HEK 293T cells pre-treated with centrinone. **A:** Representative immunofluorescence images of TRIM27 siRNA-transfected HEK 293T cells, untreated (-) or treated with centrinone (+) for a period of 8 days prior to transfection with control (CT) or TRIM27-targeting siRNA. Formaldehyde-fixed cells were stained with PCNT (green) and α -tubulin (red) antibodies. DNA was stained with Hoescht (blue). Scale bars, 15 μ m. **B:** Bar graph showing the percentage of normal (identified by the presence of a metaphase plate and/or bipolar spindle) and abnormal (identified by the presence of multipolar spindles) mitotic cells in untreated (-) and centrinone treated (+) HEK 293T cells transfected with control or TRIM27 siRNA 1 for a period of 48 hours. Data shown represents the mean + SD for experiments performed three independent times.

In summary, depletion of TRIM27 using two independent siRNAs resulted in an increase in the number of mitotic cells with extra centrosomes. The cause for this, however, remains largely unclear, as neither metaphase failure (i.e. inability to proceed to anaphase) or cytokinetic failure appeared to be responsible (Figure 6.8 and 6.9, respectively). Moreover, I did not detect evidence of abnormal centrosome duplication; mitotic cells displayed centriole pairs and no rosette-like configurations (i.e. when mother centrioles are surrounded by multiple daughters). In addition, I observed very few/no supernumerary centrioles in interphase, which may have indicated *de novo* centriole assembly. Further experiments are required to fully elucidate the role of TRIM27 at the centrosome. To this end, TRIM27 knock-out cell lines have been generated in our lab using the CRISPR/Cas9 technology (Dr Elisa Vitiello, Department of Biochemistry, University of Oxford), and functional experiments are ongoing.

7 Discussion

While the field of centrosome biology has been fairly well-studied to date, with advances in genome editing, high-resolution microscopy, proteomics and structural biology having allowed for a more detailed understanding of centrosome assembly, function, and role(s) in human disease, relatively little is known about centrosome composition and how it varies between different organisms, cell types and diseases. A number of studies have focussed on the impact of centrosomal defects in the development of human diseases, such as cancer, with a focus on particular proteins such as HSET (Chavali et al., 2016; Rhys et al., 2018; Watts et al., 2013) and PLK4 (Levine et al., 2017; reviewed in Zhang et al., 2021). Additionally, many studies have investigated centrosome biogenesis and the role of certain centrosome components in this process. Only a handful of studies, however, have looked specifically at the proteomic composition of the human centrosome (Andersen et al., 2003; Bauer et al., 2016; Jakobsen et al., 2011), and none of these have studied, in any detail, centrosome composition across different cell, tissue or disease types.

The overall goal of my PhD was to establish a novel method for centrosome isolation identified in our laboratory, known as COMPACT (Centrosome Purification by Affinity Capture). In this thesis, I have demonstrated that COMPACT purifies centrosomes with higher efficiency and specificity than the sucrose sedimentation-based centrosome isolation method. In addition, results revealed that COMPACT can be used to study centrosome composition across multiple different cell types, during dynamic biological processes, as well as in situations when cell number may be limited (i.e. primary cells or tissue). Furthermore, I have shown that COMPACT can be used as a discovery tool, for the identification of new centrosomal components.

In this section, I will discuss the different aspects of this project, from optimisation of the COMPACT methodology, through to identification and validation of novel candidates, identifying experimental caveats as well as areas for potential future work.

7.1. Optimisation, validation and characterisation of COMPACT in HEK 293T cells

7.1.1. Method optimisation and validation of COMPACT

Due to their size and number, centrosome composition has been traditionally challenging to study. Appearing as little more than ‘dots’ using standard fluorescence microscopy, these organelles have also proven difficult to purify due to the fact that they make up a very small proportion of the total cell lysate, lack delineating membranes, and are frequently associated with the nuclear membrane (Andersen et al., 2003). As a result, despite the fact that Bornens and colleagues published a protocol for the purification of human centrosomes by sucrose density centrifugation more than three decades ago, (Bornens et al., 1987), the first human centrosome proteome was published only 15 years later (Andersen et al., 2003). In this study, 73 centrosomal proteins were identified amongst a large background of non-specific proteins. A number of years later, researchers in the Andersen group were able to expand this list to 165 centrosomal proteins, aided by the use of SILAC to increase the confidence of identifying novel candidates (by comparison to an internal standard) (Jakobsen et al., 2011). Despite the relative success of this methodology in these and other studies (Bauer et al., 2016), a number of caveats exist. Specifically, the technique itself is time-consuming and requires a large amount of starting material, making it difficult to analyse anything but static centrosome composition in easy-to-grow cell types. In addition, the large number of non-specific proteins that co-sediment in the peak centrosomal fractions make identifying new centrosomal proteins a challenge.

A novel method for centrosome isolation (now known as COMPACT) was discovered in our laboratory shortly before the start of my PhD. Upon arrival, I set out to optimise the technique by testing a number of variables including cell number, lysis conditions and buffer composition. In summary, I found that COMPACT was able to effectively purify centrosomes from as few as 3×10^7 cells, 100 X fewer than traditionally required, using a lysis protocol that involved sonication and low-speed centrifugation. Using cell lines and primary tissue, I found that strong physical disruption methods were required for efficient recovery of centrosomes, most likely due to dissociation, and thus recovery, of the centrosome from the nuclear membrane.

One of the main aims of the first part of my PhD was to prove that COMPACT is an effective tool for the isolation of centrosomes from a variety of cell types, preferably with higher efficiency and specificity than the traditional centrosome isolation technique (sucrose sedimentation). Comparing both methods, I found that COMPACT identified a much larger number of known centrosomal proteins compared to the sucrose sedimentation-based

technique (81% and 2%, respectively, when compared to the KE-37 dataset (Jakobsen et al., 2011)). Even when the traditional method was performed using 20 X more cells, a cell number that is much closer to those used in previous studies (Andersen et al., 2003; Bornens and Moudjou, 1998), only 60% of known centrosomal proteins were identified. In addition to the fact that the sucrose sedimentation-based technique results in the isolation of a large number of non-centrosomal proteins (Figure 4.18; Andersen et al., 2003; Jakobsen et al., 2011), the methodology is also time-consuming (involving multiple rounds of ultracentrifugation) and requires a large number of cells. In contrast, COMPACT is much simpler and faster to perform, and requires 100 X fewer cells (3×10^7 vs. 3×10^9 cells). As a result, I believe that COMPACT provides a new and improved method for isolating centrosomes, with a potential for studying changes in centrosome composition during dynamic biological process, such as ciliogenesis and epithelial-to-mesenchymal transition, as well as isolating centrosomes from primary cells or tissue.

7.1.2. Further characterisation of COMPACT

Early COMPACT experiments revealed that a significant portion of centrosomal protein was not binding to the peptide-coated beads, and therefore lost in the unbound fraction. This raised a number of questions as to why some centrosomal protein remains unbound. It was apparent from the beginning of my PhD that cell number scaled with COMPACT efficiency (i.e. more cells lead to more protein in the bound fraction; Figure 4.4). Somewhat surprisingly, however, this also lead to a parallel scaling of the unbound fraction, meaning that this fraction does not arise due to the peptide-bound beads being over-saturated. This conclusion was supported by Figure 4.7, which shows that increasing the volume of peptide and/or beads did not affect the amount of centrosomal protein observed in the bound or unbound fractions. As a result, I set out to try and understand why a significant portion of centrosomal protein within the lysate was remaining unbound. COMPACT-IF revealed that the unbound fraction contained whole centrosomes rather than soluble centrosomal proteins, as initially hypothesised (Figure 4.12). These data suggested a number of possibilities for the presence of unbound centrosomes, one being that binding between the peptide and centrosomes is transient, and only a proportion of centrosomes in a cell lysate are captured at any given moment. Another possibility is that a particular centrosome component may need to be present and/or exposed for the peptide to capture the centrosome, and this particular component may not always be present or available in the cell lysate. Interesting future experiments could involve using western blotting and mass spectrometry to further characterise the unbound fraction, comparing centrosomal proteins to those found in the bound fraction.

Further to the above, experiments performed in cells lacking centrosomal proteins NIN or CEP128 revealed that the ability of COMPACT to purify centrosomes is based on the presence of these proteins. NIN and CEP128 are components of the sDAP structures on centrioles, the latter being required for recruitment of the former (reviewed in Tischer et al., 2021). A number of studies have shown that DAP and sDAP components are remodelled during mitosis; NIN specifically was shown to completely disappear from HeLa cell centrosomes in metaphase and anaphase, reappearing in telophase (Chen et al., 2003; reviewed in Tischer et al., 2021). This raises the possibility that there may be a pool of mitotic centrosomes that are unable to be captured by the peptide due to the fact that NIN is not present, and this would need to be further investigated with careful synchronisation experiments. Importantly, daughter centrioles in G₁ and S phase do not have appendages (see section 1.4.2), but it is likely that the peptide would still capture them due to their connection to mother centrioles via the GGT.

Interestingly, I showed in Figure 4.6 that the peptide-bead complex is required for efficient purification of centrosomes by COMPACT. For this experiment, the peptide plus lysate (second column) was incubated with beads for 45 minutes, in comparison to the peptide plus beads (first column) which were incubated with the lysate for 2 hours and 15 minutes. Thus, while I can't exclude the possibility that the peptide was able to bind centrosomes before the addition of the beads (Figure 4.6, column 2), it is more likely that that the centrosomal proteins observed were as a result of centrosomes binding to the peptide-bead complexes formed after addition of the beads. In line with this, collaborators of ours showed that GFP-tagged peptide did not localise to the centrosome (personal communication, data not shown). As a result, I believe that the ability of COMPACT to purify centrosomes is not based solely on the sequence of the peptide, but also on charge and/or secondary structure (or the structure that is formed when the peptide binds to the beads). A previous study using centrosomes purified from early *Drosophila* embryos showed that the organelles are negatively charged in buffers with a pH greater than 3.1 (Hormeño et al., 2009). Interestingly, the biotinylated CCDC61 peptide is positively charged, with a theoretical pI (isoelectric point) of 11.46 (www.novoprolabs.com/tools). Therefore, in a Tris-HCl buffer (~pH 8.0) these structures would be attracted due to charge complementarity. Interestingly, preliminary experiments showed that COMPACT was unsuccessful when alternative (smaller) beads (Dynabeads MyOne, Thermo Scientific) were used (personal communication with Dr Mark van Bruegel and Dr Takashi Ochi, data not shown), indicating that the structure formed when the peptide is bound to the beads used specifically in this study (Dynabeads M-280, Thermo Scientific) adds to the efficiency of COMPACT.

In an attempt to prove that COMPACT purifies intact centrosomes rather than soluble centrosomal proteins, I performed COMPACT-MS in HEK 293T cells treated for a period of 8 days with centrinone. Centrinone is a selective PLK4 inhibitor that causes centrosome loss by inhibiting centriole assembly without disassembling pre-existing centrioles (Wong et al., 2015). As a result, if COMPACT purifies centrosomes, rather than non-centrosomal pools of centrosomal proteins, one would expect to see a significant reduction in and/or absence of centrosomal proteins discovered by MS. Indeed, Figure 4.16 shows a significant reduction in the COMPACT proteome when cells were pre-treated with centrinone (137 proteins vs. 405 proteins observed in untreated cells). When the proteins discovered in both conditions were compared to the core centrosome dataset (Bauer et al., 2016), it was found that 60% (44/73) of the core centrosomal proteins were not detected in cells pre-treated with centrinone (i.e. lost upon centrinone treatment), while 37% (27/73) were still detected in cells pre-treated with centrinone, albeit at a significantly reduced level compared to untreated cells (Figure 4.16). Interestingly, a large proportion of the proteins lost as a result of centrinone treatment are centriolar proteins (including SAS6, STIL, CEP120, CNTROB and CP110), many of which have been shown to interact (inferred by proximity) via BioID experiments (Gupta et al., 2015). In addition, a large number of outer PCM proteins (including NEDD1, γ -tubulin (TUBG1) and various TUBGCPs) are also lost. This could indicate that the centrosomal proteins more readily disrupted upon centrinone treatment are those that form protein-protein interactions at the centriole, or the more dynamic outer structure of the PCM. Alternatively, those that remain could be more protected due to their higher order structure (including the inner PCM and appendages (reviewed in Lee et al., 2021; Tischer et al., 2021)), and/or by the fact that they assemble as phase-separated condensates, such as CEP63 and CEP152 (Ahn et al., 2020) and PCNT (Jiang et al., 2021). These results reveal COMPACT as an exciting new tool for in-depth investigations into centrosome assembly, due to the fact that centrosome composition can be explored in multiple biological/chemical scenarios. For instance, an interesting experiment would involve treating cells and/or centrosomes with 1,6-hexanediol (hex), a liquid-liquid phase separation disruptor. Preliminary results from a single experiment that I performed uncovered a number of differences (when comparing hex-treated to untreated centrosomes isolated by COMPACT, data not shown), but further optimisation and validation is required.

Surprisingly, γ -tubulin (TUBG1) was never observed with many unique peptides via COMPACT-MS, despite the fact that γ -tubulin molecules are known to be particularly abundant at the centrosome (Bauer et al., 2016). It is possible that the amount of γ -tubulin isolated is dependent on cell cycle (hence centrosome cycle) stage, with interphase centrosomes containing less γ -tubulin than mitotic centrosomes. Alternatively, or additionally, the salt in the

COMPACT wash buffer (300mM NaCl) may deplete centrosomal γ -tubulin; indeed, treatment of purified mitotic centrosomes with high salt concentrations has been shown to strip centrosomes of γ -tubulin as well as a number of other proteins (Moritz et al., 1998). It is possible that an alternative buffer composition would allow for purification of centrosomes with intact γ -tubulin, and this would need to be explored further.

7.2. Tissue specificity of centrosome composition

7.2.1. A non-quantitative comparison of centrosome proteomes in a panel of cell lines

While various studies have suggested that centrosome composition may differ between cell and tissue types, none have compared centrosome composition across a range of cell lines. In 2016, the Nigg lab used targeted proteomics (selected reaction monitoring; SRM) to measure the absolute and relative abundance of a select number of centrosomal proteins in whole cell lysates of five different cell lines. While this study provided some information as to the changes in centrosome composition between cell types, it was limited to only nine proteins and based on *a priori* assumptions of protein abundance (Bauer et al., 2016). I have shown in this study that COMPACT presents itself as a valuable tool for the purification of centrosomes from a panel of cell lines. I have purified and analysed centrosomes from a number of transformed/cancer cell lines (representing a range of different cell types). Results revealed that while a large number of proteins in each cell line overlapped with the KE-37 centrosome proteome (Jakobsen et al., 2011), a significant number of proteins were unique to each cell line and some of these may represent tissue-specific centrosomal candidates (Figure 5.2).

Interestingly, the primary patient-derived glioma cell lines, G166 and G7, as well as the hiPSC line, FSPS13B, showed a much larger number of proteins present in the COMPACT proteome that did not overlap with KE-37 (Figure 5.2). As stem cells, it might be expected that these cell lines express a larger number of proteins than those that have committed to their lineage, such as HEK 293T cells. It is also possible that the presence of many of these proteins could be attributed to the fact that centrosomes may act as scaffolds for the accumulation of proteins and signalling molecules important for various differentiation processes (reviewed in Arquint et al., 2014). Indeed, a recent study showed that the protein C3G, an important regulator of cell proliferation and differentiation, is localised to the centrosome in undifferentiated myocytes but is lost during differentiation to skeletal muscle myotubes (Nayak and Radha, 2020). The function of the centrosome during differentiation remains largely unstudied, and COMPACT

presents an exciting new tool for this as it allows for the purification of centrosomes during dynamic processes.

A tissue specificity table was created using all the centrosome proteome data gathered via COMPACT-MS (Table 5.2 and Appendix 6). While only preliminary conclusions can be drawn from this data, due to the fact that experiments were performed and run on the mass spectrometer at different times, a number of interesting observations can be made. CCDC88B is a coiled-coil domain containing protein that acts as a positive regulator of T cell maturation and inflammatory function, and has also been shown to play a role in MTOC polarisation (Ham et al., 2015). Using COMPACT, I identified CCDC88B in Jurkat cells only, raising the possibility that it may be a centrosomal component that is specific to T cells. Another centrosomal candidate, AKNA, which I found in all cell lines via COMPACT-MS (Appendix 6), was recently shown in an independent study to localise to the centrosome (Camargo Ortega et al., 2019). In addition, a pan-cancer study investigating centrosome amplification (CA) gene expression signatures identified COPA as a putative promoter of CA (De Almeida et al., 2019), which supports the fact that it was identified in the COMPACT proteome of all cell lines analysed (Appendix 6). These data indicate that COMPACT can be used to investigate the tissue specificity of centrosome composition, and could be particularly powerful if combined with quantitative MS.

7.2.2 A quantitative comparison of centrosome composition in U251 and Jurkat cells

In order to be able to study the tissue specificity of centrosome composition in a quantitative manner, TMT-MS was used. TMT was chosen over SILAC due to the fact that SILAC requires cells to be grown in specific media allowing for the incorporation of stable isotope-labelled amino acids, and options for multiplexing are limited. In contrast, TMT labels are incorporated upon sample digestion, eliminating the need for any changes in cell culture, and they currently provide a higher multiplexing capability; just last year a new set of TMT reagents were released allowing for the quantitative comparison of up to 16 samples (TMTpro; Li et al., 2020). At the time of experimental design only 11-plex TMT was available, and thus together with the proteomics core facility, I designed the quantitative COMPACT experiment outlined in Figure 5.7. To create a highly powered experiment, we decided to use five biological replicates each for COMPACT and BO, for the two cell lines U251 and Jurkat. This meant that even if there was an error (experimental or technical) with one of the samples, the experiment would still provide valuable data. Due to the fact that 11 samples could be analysed per experiment, the final TMT label was assigned to a reference sample, a 1:1 mix of COMPACT performed in

each cell line. Reference samples are commonly used for comparison of multiple isobaric labelling experiments (Rauniyar and Yates, 2014).

One of the ideas going into this experiment was that I might achieve increased sensitivity or protein coverage, but this was not necessarily the case as various proteins that had been observed via non-quantitative COMPACT-MS (such PLK4 and TUBGCP5/6; Figure 5.10) were not detected in this instance. A caveat for this experimental design is that comparison of two experiments using reference samples could result in the compression of data, as a peptide needs to be present in all samples to be assigned a quantitative value. As a result, an improved experimental design, since the advent of TMTpro allowing for quantification of up to 16 samples, would be to compare all conditions in one experiment, forgoing the need for a reference sample.

Regardless of the above caveat, COMPACT-TMT in U251 and Jurkat cells provided some high quality and valuable data. Firstly, COMPACT-specific peptides were identified in each cell line by determining which peptides were significantly enriched above BO. Thereafter, these peptides were compared to reference sample peptides and then to each other, in order to identify proteins that were differentially expressed in U251 compared to Jurkat centrosomes. For this analysis, 1844 peptides (corresponding to 232 proteins) in U251 samples, and 2567 peptides (corresponding to 259 proteins) in Jurkat samples were compared, revealing a total of 73 differentially expressed proteins (Figure 5.9). As far as I am aware, this is the first study that has shown extensive differential expression data for centrosomal proteins in two different cell lines.

Figures 5.9 and 5.10 show proteins that are differentially present in U251 compared to Jurkat centrosomes. Importantly, the changes observed at the centrosome via COMPACT aren't necessarily due to whole cell protein expression, but rather changes in centrosomal localisation or interaction of various proteins (Appendix 8). The most interesting observation made as a result of this experiment was the fact that various DAP components appeared to be significantly downregulated or even absent in Jurkat compared to U251 centrosomes. These observations were further validated by non-quantitative COMPACT-MS as well as IF experiments (Figures 5.12 and 5.13). In a recent publication by Viol and colleagues, NEK2 was found to be responsible for displacing DAPs from mitotic centrosomes, and overexpression of NEK2 was shown to be able to prematurely dissociate DAPs from interphase centrosomes (Viol et al., 2020). As seen in Figure 5.10, NEK2 was found exclusively in Jurkat cells (importantly, NEK2 was observed in U251 cells via COMPACT-MS in other experiments, however with a much lower number of unique peptides compared to

Jurkat). Thus, it is possible that the enrichment of NEK2 in Jurkat cells is the reason for the loss of DAP proteins OFD1, CEP83, SCLT1, FBF1, CEP164 and ANKRD26 (note that CEP83 is required for the recruitment of downstream DAP proteins such as SCLT1 and CEP164, but CEP89 is not (Tanos et al., 2013; Viol et al., 2020)). It is, however, also feasible that the higher NEK2 levels observed in Jurkat centrosomes arise simply due the proportionately shorter G₁-phase of these cells; NEK2 kinase regulates centrosome separation in late G₂ phase (Fry et al., 1998b).

Perhaps the most significant role for DAP proteins is the docking of the centrosome at the membrane during ciliogenesis (Tanos et al., 2013). While lymphocytes don't appear to form a primary cilium, a very similar process has been observed in cytotoxic T lymphocytes (CTLs), whereby centrosomes dock at the site of the immunological synapse (IS), allowing for the delivery and secretion of lytic granules (Stinchcombe et al., 2006). Research from the Griffiths lab suggests that the mother centriole may preferentially dock and attach to the membrane via its DAPs (Stinchcombe et al., 2015). These studies were performed in CD8+ T cells (CTLs), while Jurkat cells are CD4+ T cells (helper T cells), so it is possible that while DAPs may be essential for the function of CTLs, they may not be required for helper T cells. Indeed, research has shown that centrosome polarisation and docking doesn't appear to be required for IS formation and cytokine release by CD4+ T cells (Chemin et al., 2012). The data provided in this study offers, to the best of my knowledge, the first set of evidence that DAPs may be tissue-specific rather than ubiquitous structures.

7.2.3 COMPACT in primary tissue

One of the major caveats of the sucrose-sedimentation based methodology is that it requires billions of cells, limiting the use of the technique to cells that are easy to culture/expand to the volumes required. This means that the technique cannot be used to study centrosome composition in primary cell lines or tissue. Due to the success of COMPACT in a panel of cell lines, and the fact that it was able to effectively purify centrosomes from 100 X fewer cells than traditionally required, I decided to expand the use of COMPACT into primary tissue, specifically mouse liver and spleen. Surprisingly, coverage of centrosomal proteins via COMPACT-MS was very low in cells isolated from the liver, and a number of centrosomal proteins were also found to be non-specifically binding the beads (i.e in BO samples) (Figure 5.15 and 5.16). I believe that in certain cell or tissue types, such as the liver (i.e. hepatocytes), the cytoskeletal protein network, comprising large proteins including plectin, desmoplakin and various keratins (see Figure 5.15 B), interferes with the ability of COMPACT to purify centrosomes, due to the fact that centrosomes may be embedded within these structures.

Current research in our lab is aimed at improving COMPACT in these cell lines, by altering buffer composition and/or lysis conditions.

In contrast to the mouse liver, COMPACT performed more efficiently in cells freshly isolated from the mouse spleen, with no known centrosomal proteins found in the BO samples. A number of interesting observations can be made when analysing the proteins specific to the spleen (after removal of BO), which represent potential tissue-specific centrosomal candidates (Figure 5.19 B). For instance, the protein kinase SYK (spleen tyrosine kinase) was detected in mouse spleen centrosomes, but not in any of the cell lines analysed in section 5.2.1. Interestingly, a large number of TAF proteins, components of the TFIID basal transcription factor complex and TATA box binding proteins, are found exclusively in the spleen centrosome proteome, including TAFs 1-12. TAF15 was found in Jurkat cells when scanning the COMPACT-MS data from section 5.2.1. It is possible that the centrosome acts as a scaffold to recruit/compartmentalise these factors (before their use and/or localisation to other parts of the cell) specifically in lymphoid cells, however this data is only preliminary and further experimentation and validation would be required to confirm this.

The ability of COMPACT to isolate centrosomes from primary tissue raises an exciting possibility for its use as a tool to study the changes in centrosome composition during disease progression and/or treatment. A recent unpublished study by the Basto group showed that high levels of centrosome amplification (CA) in patient-derived xenograft (PDX) models of epithelial ovarian cancer positively impacts the response to chemotherapy, while low levels of CA do not (Morretton et al., 2019). In this instance, a tool like COMPACT could be useful to study potential dynamics in centrosome composition during this process i.e. to understand changes in centrosome composition during CA, and/or to investigate the centrosome-specific response to chemotherapy. For example, tumours with high and low levels of CA from PDX models of high grade serous ovarian cancer (HGSOC) could be collected, and COMPACT-TMT performed to quantitatively compare the centrosome proteomes in both conditions.

7.3 Novel centrosomal candidates

In addition to using COMPACT to study changes in centrosome composition across different cell types and/or biological processes, it can also be used as a tool to discover new centrosomal candidates. To identify candidate centrosomal proteins in this study, I generated a pipeline which included classifying COMPACT-identified proteins as candidates based on their absence from the CCDB (Gupta et al., 2015) but presence in most, if not all, of the cell

lines in which COMPACT-MS was performed (Figure 6.1). A number of interesting candidates were identified, including EDC4, TRIM27, DDB1, CCRN and NOP53. I was able to validate antibodies that showed a strong and specific centrosomal signal via WB and COMPACT-IF, for EDC4 (mRNA decapping protein found predominantly in P-bodies) and TRIM27 (E3 ubiquitin-protein ligase). Excitingly, deconvolved confocal immunofluorescence images provided high-resolution data revealing centrosomal sub-structure, information which could only previously be obtained using super-resolution microscopy techniques such as Structured Illumination Microscopy (SIM) and Stochastic Optical Reconstruction Microscopy (STORM) (Bowler et al., 2019; Sonnen et al., 2012; Yang et al., 2018), or Expansion Microscopy (ExM) (Gambarotto et al., 2019; Sahabandu et al., 2019). ExM allows for visualisation of macromolecular ultrastructures (such as centrioles) using optical microscopy, but expansion of samples can be variable, meaning that centrosomes may be unevenly or disproportionately expanded (Büttner et al., 2021; Chen et al., 2015). COMPACT, therefore, offers an alternative methodology for the analysis of centrosome structure, allowing for visualisation of centrosomes in their native form (without expansion) using standard fluorescence microscopy.

COMPACT-IF revealed that EDC4 is present at the proximal and distal ends of centrioles, and might act as a potential capping structure (Figure 6.4). This is interesting and unusual, as centriolar capping proteins are usually observed at either the distal or proximal ends of centrioles, but not both. For instance, CP110 is observed at the distal ends of centrioles, capping them after elongation, while CEP250 (or C-NAP1) is observed at the proximal ends, acting as an anchor for the proteinaceous linker that connects centrioles after disengagement. Further research will be required to uncover the role for EDC4 at the centrosome. In contrast to EDC4, TRIM27 appeared as a ring via COMPACT-IF, indicative of the PCM (Figure 6.4). Importantly, the PCM has been identified as a scaffold for ubiquitin-proteasome-mediated degradation, with a number of E3 ubiquitin ligase complexes having been shown to localise to the structure (reviewed in Vora and Phillips, 2016).

TRIM27 is a E3 ubiquitin-protein ligase that mediates the ubiquitination of PIK3C2B, leading to a decrease in its enzymatic activity (Cai et al., 2011). Interestingly, the centrosome acts as a scaffold for signalling molecules and a centre for proteasomal mediated degradation, and many PI3K pathway components have been shown to be associated with the centrosome (Arquint et al., 2014; Cai et al., 2011; Vanhaesebroeck et al., 2019). As a result, I hypothesised that TRIM27's role in ubiquitination of PIK3C2B is centrosome-dependent, and that dysregulation of this process can drive chromosomal instability. Indeed, aberrant PI3K activity has been shown to have negative effects on mitotic progression and cytokinesis, and recent

data have implicated PI3K activation in centrosome amplification (Berenjeno et al., 2017; reviewed in Vanhaesebroeck et al., 2019).

Using two independent siRNAs, I observed an approximate 30% increase in centrosome number in mitotic cells (Figure 6.7 and 6.8), and showed that this phenotype was centriole-dependent by performing rescue experiments in cells depleted of centrosomes (Figure 6.11). As mentioned in section 1.6, centrioles can assemble non-canonically via *de novo* duplication or as rosette-like structures, for which multiple daughter centrioles assemble around a mother. Detailed analysis of the structures formed upon TRIM27 depletion (i.e. staining for mother- and daughter-specific centriole markers) will be important to determine the nature of these extra centrosomes, but preliminary results revealed no evidence for centriolar rosettes. Centrosome amplification (CA), a feature observed in many different cancer cells, can arise a number of ways, including due to failure in cell division, dysregulation of the centrosome duplication cycle, or *de novo* centriole biogenesis. It is apparent from the results shown in Figures 6.8 and 6.9 that the increase in centrosome number that I observed upon TRIM27 depletion is not as a result of metaphase or cytokinesis failure. Despite this observation, it remains unclear how the increase in mitotic cells with extra centrosomes arises, and further experimentation will be required to fully elucidate the role of TRIM27 at the centrosome. Indeed, phenotypic studies using CRISPR/Cas9 knockouts of TRIM27 (and a number of other candidate proteins) are currently underway, and interesting future experiments could involve investigating PI3K pathway activation (as well as centrosomal localisation of PI3K components and substrates) in these cells. Interestingly, in addition to their role in the ubiquitination process, TRIM proteins have also been shown to have non-degradatory roles; including MT association, mitotic regulation and coordination of centrosome duplication (reviewed in Venuto and Merla, 2019). It is possible that the role of TRIM27 at the centrosome is entirely independent of its ubiquitin-protein ligase activity, and this would need to be explored further.

8 Conclusion

The overall goal of my PhD was to establish a novel method for centrosome isolation identified in our laboratory, known as COMPACT (Centrosome Purification by Affinity Capture). Only a handful of studies have ever investigated the proteomic composition of the human centrosome, and none have been able to study the tissue specificity of centrosome composition in any detail. As a result, one of the primary aims of my PhD was to show that COMPACT can be used to determine the spatial and temporal dynamics of centrosome composition.

In the first part of my PhD, I performed a number of experiments to optimise and validate COMPACT. I showed that the method is able to isolate centrosomes from a variety of cell types, and that analysis of purified centrosomes using mass spectrometry recovers the majority of known core centrosomal proteins. Importantly, I demonstrated that COMPACT purifies centrosomal components with higher efficiency and specificity than the sucrose sedimentation-based centrosome isolation technique. Using cell lines lacking the centriolar appendage proteins, NIN or CEP128, I was able to show that these proteins are directly involved in the ability of COMPACT to purify centrosomes.

In the second part of my PhD, I performed a comprehensive analysis of the centrosome proteome in different cell lines and tissue. These results revealed that COMPACT can be used to study centrosome composition across multiple cell types, during dynamic biological processes, as well as in situations when samples may be limited (i.e. primary cells or tissue). In addition to this, quantitative mass spectrometry-based analysis of centrosome composition in different cell types revealed the absence of DAPs in the T lymphocyte cell line, Jurkat. This finding is, to the best of my knowledge, the first set of evidence revealing that DAPs may be tissue-specific rather than ubiquitous structures.

In the third part of my PhD, I showed that COMPACT can be used as a discovery tool to identify novel centrosomal components. I selected a number of candidate proteins and validated their centrosomal localisation using various independent techniques. Finally, I performed loss-of-function studies in HEK 293T cells and showed that depletion of TRIM27, an E3 ubiquitin-protein ligase, resulted in an increase in centrosome number in mitosis. Further analysis is required to fully elucidate the role of TRIM27 at the centrosome.

In conclusion, COMPACT presents itself as an exciting new tool for studying centrosome composition in a spatially and temporally controlled manner, with the potential for in-depth analyses of processes involved in centrosome duplication, as well as the role of the centrosome in various dynamic biological processes. In addition, work carried out during my PhD has shown that COMPACT can be used for the identification of novel or previously uncharacterised centrosomal proteins that may have significant roles in centrosome biology.

9 References

- Aebersold, R., and Mann, M. (2003). Mass spectrometry-based proteomics. *Nature* 422, 198–207.
- Ahn, J. H., Park, J.E., Meng, L., Zhang, L., Kim, T.S., Kruhlak, M.J., Kim, B.Y., and Lee, K.S. (2020). Phase separation of the Cep63•Cep152 complex underlies the formation of dynamic supramolecular self-assemblies at human centrosomes. *Cell Cycle* 19, 3437–3457.
- De Almeida, B.P., Vieira, A.F., Paredes, J., Bettencourt-Dias, M., and Barbosa-Morais, N.L. (2019). Pan-cancer association of a centrosome amplification gene expression signature with genomic alterations and clinical outcome. *PLoS Comput. Biol.* 15, e1006832.
- Alvarado-Kristensson, M. (2020). Choreography of the centrosome. *Heliyon* 6, e03238.
- Andersen, J.S., Wilkinson, C.J., Mayor, T., Mortensen, P., Nigg, E.A., and Mann, M. (2003). Proteomic characterization of the human centrosome by protein correlation profiling. *Nature* 426, 570–574.
- Anvarian, Z., Mykytyn, K., Mukhopadhyay, S., Pedersen, L.B., and Christensen, S.T. (2019). Cellular signalling by primary cilia in development, organ function and disease. *Nat. Rev. Nephrol.* 15, 199–219.
- Arnandis, T., Monteiro, P., Adams, S.D., Bridgeman, V.L., Rajeeve, V., Gadaleta, E., Marzec, J., Chelala, C., Malanchi, I., Cutillas, P.R., et al. (2018). Oxidative Stress in Cells with Extra Centrosomes Drives Non-Cell-Autonomous Invasion. *Dev. Cell* 47, 409–424.
- Arquint, C., Gabryjonczyk, A.-M., and Nigg, E.A. (2014). Centrosomes as signalling centres. *Philos. Trans. R. Soc. B Biol. Sci.* 369, 20130464.
- Atorino, E.S., Hata, S., Funaya, C., Neuner, A., and Schiebel, E. (2020). CEP44 ensures the formation of bona fide centriole wall, a requirement for the centriole-to-centrosome conversion. *Nat. Commun.* 11.
- Bahe, S., Stierhof, Y.D., Wilkinson, C.J., Leiss, F., and Nigg, E.A. (2005). Rootletin forms centriole-associated filaments and functions in centrosome cohesion. *J. Cell Biol.* 171, 27–33.
- Bärenz, F., Mayilo, D., and Gruss, O.J. (2011). Centriolar satellites: Busy orbits around the centrosome. *Eur. J. Cell Biol.* 90, 983–989.
- Bärenz, F., Kschonsak, Y.T., Meyer, A., Jafarpour, A., Lorenz, H., and Hoffmann, I. (2018). Ccdc61 controls centrosomal localization of Cep170 and is required for spindle assembly and symmetry. *Mol. Biol. Cell* 29, 3105–3118.
- Bauer, M., Cubizolles, F., Schmidt, A., and Nigg, E.A. (2016). Quantitative analysis of human centrosome architecture by targeted proteomics and fluorescence imaging. *EMBO J.* 35, 2152–2166.
- Berenjeno, I.M., Piñeiro, R., Castillo, S.D., Pearce, W., McGranahan, N., Dewhurst, S.M., Meniel, V., Birkbak, N.J., Lau, E., Sansregret, L., et al. (2017). Oncogenic PIK3CA induces centrosome amplification and tolerance to genome doubling. *Nat. Commun.* 8.
- Bernhard, W., and de Harven, E. (1960). L'ultrastructure du centriole et d'autres éléments de l'appareil achromatique. *Fourth Int. Conf. Electron Microsc.* Springer.
- Besson, A., Dowdy, S.F., and Roberts, J.M. (2008). CDK Inhibitors: Cell Cycle Regulators and Beyond. *Dev. Cell* 14, 159–169.
- Blainey, P., Krzywinski, M., and Altman, N. (2014). Replication. Quality is often more important than quantity. *Nat. Methods* 11, 879–880.

- Bornens, M. (2002). Centrosome composition and microtubule anchoring mechanisms. *Curr. Opin. Cell Biol.* 14, 25–34.
- Bornens, M., and Moudjou, M. (1998). Studying the Composition and Function of Centrosomes in Vertebrates. *Methods Cell Biol.* 61, 13–34.
- Bornens, M., Paintrand, M., Berges, J., Marty, M., and Karsenti, E. (1987). Structural and chemical characterization of isolated centrosomes. *Cell Motil. Cytoskeleton* 8, 238–249.
- Boveri, T. (1929). The origin of malignant tumours. *J. Cell Sci.* 121.
- Bowler, M., Kong, D., Sun, S., Nanjundappa, R., Evans, L., Farmer, V., Holland, A., Mahjoub, M.R., Sui, H., and Loncarek, J. (2019). High-resolution characterization of centriole distal appendage morphology and dynamics by correlative STORM and electron microscopy. *Nat. Commun.* 10.
- van Breugel, M., Hirano, M., Andreeva, A., Yanagisawa, H.A., Yamaguchi, S., Nakazawa, Y., Morgner, N., Petrovich, M., Ebong, I.O., Robinson, C. V., et al. (2011). Structures of SAS-6 suggest its organization in centrioles. *Science* (80-.). 331, 1196–1199.
- van Breugel, M., Wilcken, R., McLaughlin, S.H., Rutherford, T.J., and Johnson, C.M. (2014). Structure of the SAS-6 cartwheel hub from Leishmania major. *Elife* 3, e01812.
- Brown, N.J., Marjanović, M., Lüders, J., Stracker, T.H., and Costanzo, V. (2013). Cep63 and Cep152 Cooperate to Ensure Centriole Duplication. *PLoS One* 8, e69986.
- Buchwalter, R.A., Chen, J. V., Zheng, Y., and Megraw, T.L. (2016). Centrosome in Cell Division, Development and Disease. In ELS, John Wiley & Sons, Ltd.
- Büttner, M., Lagerholm, C.B., Waithe, D., Galiani, S., Schliebs, W., Erdmann, R., Eggeling, C., and Reglinski, K. (2021). Challenges of Using Expansion Microscopy for Super-resolved Imaging of Cellular Organelles. *ChemBioChem* 22, 686–693.
- Byrne, D.P., Clarke, C.J., Brownridge, P.J., Kalyuzhnny, A., Perkins, S., Campbell, A., Mason, D., Jones, A.R., Eyers, P.A., and Eyers, C.E. (2020). Use of the Polo-like kinase 4 (PLK4) inhibitor centrinone to investigate intracellular signalling networks using SILAC-based phosphoproteomics. *Biochem. J.* 477, 2451–2475.
- Cai, X., Srivastava, S., Sun, Y., Li, Z., Wu, H., Zuvela-Jelaska, L., Li, J., Salamon, R.S., Backer, J.M., and Skolnik, E.Y. (2011). Tripartite motif containing protein 27 negatively regulates CD4 T cells by ubiquitinating and inhibiting the class II PI3K-C2 . *Proc. Natl. Acad. Sci.* 108, 20072–20077.
- Camargo Ortega, G., Falk, S., Johansson, P.A., Peyre, E., Broix, L., Sahu, S.K., Hirst, W., Schlichthaerle, T., De Juan Romero, C., Draganova, K., et al. (2019). The centrosome protein AKNA regulates neurogenesis via microtubule organization. *Nature* 567, 113–117.
- Chao, H.X., Fakhreddin, R.I., Shimerov, H.K., Kedziora, K.M., Kumar, R.J., Perez, J., Limas, J.C., Grant, G.D., Cook, J.G., Gupta, G.P., et al. (2019). Evidence that the human cell cycle is a series of uncoupled, memoryless phases. *Mol. Syst. Biol.* 15, e8604.
- Chavali, P.L., Pütz, M., and Gergely, F. (2014). Small organelle, big responsibility: the role of centrosomes in development and disease. *Philos. Trans. R. Soc. B Biol. Sci.* 369, 20130468.
- Chavali, P.L., Chandrasekaran, G., Barr, A.R., Tátrai, P., Taylor, C., Papachristou, E.K., Woods, C.G., Chavali, S., and Gergely, F. (2016). A CEP215-HSET complex links centrosomes with spindle poles and drives centrosome clustering in cancer. *Nat. Commun.* 7.
- Chemin, K., Bohineust, A., Dogniaux, S., Tourret, M., Guégan, S., Miro, F., and Hivroz, C. (2012). Cytokine Secretion by CD4 + T Cells at the Immunological Synapse Requires Cdc42-Dependent Local Actin Remodeling but Not Microtubule Organizing Center Polarity . *J. Immunol.* 189, 2159–2168.

- Chen, C.H., Howng, S.L., Cheng, T.S., Chou, M.H., Huang, C.Y., and Hong, Y.R. (2003). Molecular characterization of human ninein protein: Two distinct subdomains required for centrosomal targeting and regulating signals in cell cycle. *Biochem. Biophys. Res. Commun.* 308, 975–983.
- Chen, F., Tillberg, P.W., and Boyden, E.S. (2015). Expansion microscopy. *Science*. 347, 543–548.
- Chen, Z., Indjeian, V.B., McManus, M., Wang, L., and Dynlacht, B.D. (2002). CP110, a cell cycle-dependent CDK substrate, regulates centrosome duplication in human cells. *Dev. Cell* 3, 339–350.
- Choi, H., Larsen, B., Lin, Z.Y., Breitkreutz, A., Mellacheruvu, D., Fermin, D., Qin, Z.S., Tyers, M., Gingras, A.C., and Nesvizhskii, A.I. (2011). SAINT: Probabilistic scoring of affinity purification-mass spectrometry data. *Nat. Methods* 8, 70–73.
- Chong, W.M., Wang, W.-J., Lo, C.-H., Chiu, T.-Y., Chang, T.-J., Liu, Y.-P., Tanos, B., Mazo, G., Tsou, M.-F.B., Jane, W.-N., et al. (2020). Super-resolution microscopy reveals coupling between mammalian centriole subdistal appendages and distal appendages. *Elife* 9, e53580.
- Ciciarello, M., Mangiacasale, R., Casenghi, M., Limongi, M.Z., D'Angelo, M., Soddu, S., Lavia, P., and Cundari, E. (2001). p53 Displacement from Centrosomes and p53-mediated G1 Arrest following Transient Inhibition of the Mitotic Spindle. *J. Biol. Chem.* 276, 19205–19213.
- Cleveland, D.W., Mao, Y., and Sullivan, K.F. (2003). Centromeres and kinetochores: From epigenetics to mitotic checkpoint signaling. *Cell* 112, 407–421.
- Colicino, E.G., and Hehnly, H. (2018). Regulating a key mitotic regulator, polo-like kinase 1 (PLK1). *Cytoskeleton* 75, 481–494.
- Comartin, D., Gupta, G.D., Fussner, E., Coyaud, É., Hasegan, M., Archinti, M., Cheung, S.W.T., Pinchev, D., Lawo, S., Raught, B., et al. (2013). CEP120 and SPICE1 cooperate with CPAP in centriole elongation. *Curr. Biol.* 23, 1360–1366.
- Conduit, P.T., Richens, J.H., Wainman, A., Holder, J., Vicente, C.C., Pratt, M.B., Dix, C.I., Novak, Z.A., Dobbie, I.M., Schermelleh, L., et al. (2014a). A molecular mechanism of mitotic centrosome assembly in Drosophila. *Elife* 3, 1–23.
- Conduit, P.T., Feng, Z., Richens, J.H., Baumbach, J., Wainman, A., Bakshi, S.D., Dobbelaere, J., Johnson, S., Lea, S.M., and Raff, J.W. (2014b). The centrosome-specific phosphorylation of Cnn by Polo/Plk1 drives Cnn scaffold assembly and centrosome maturation. *Dev. Cell* 28, 659–669.
- Conkar, D., Culfa, E., Odabasi, E., Rauniyar, N., Yates, J.R., and Firat-Karalar, E.N. (2017). The centriolar satellite protein CCDC66 interacts with CEP290 and functions in cilium formation and trafficking. *J. Cell Sci.* 130, 1450–1462.
- Contadini, C., Monteonofrio, L., Virdia, I., Prodosmo, A., Valente, D., Chessa, L., Musio, A., Fava, L.L., Rinaldo, C., Rocco, G. Di, et al. (2019). p53 mitotic centrosome localization preserves centrosome integrity and works as sensor for the mitotic surveillance pathway. *Cell Death Dis.* 10.
- Coverley, D., Laman, H., and Laskey, R.A. (2002). Distinct roles for cyclins E and A during DNA replication complex assembly and activation. *Nat. Cell Biol.* 4, 523–528.
- D'Angioletta, V., Donato, V., Vijayakumar, S., Saraf, A., Florens, L., Washburn, M.P., Dynlacht, B., and Pagano, M. (2010). SCF(Cyclin F) controls centrosome homeostasis and mitotic fidelity through CP110 degradation. *Nature* 466, 138–142.
- Dammermann, A., Müller-Reichert, T., Pelletier, L., Habermann, B., Desai, A., and Oegema, K. (2004). Centriole Assembly Requires Both Centriolar and Pericentriolar Material Proteins. *Dev. Cell* 7, 815–829.
- Dawe, H.R., Farr, H., and Gull, K. (2007). Centriole/basal body morphogenesis and migration during ciliogenesis in animal cells. *J. Cell Sci.* 120, 7–15.

- Devi, R., Pelletier, L., and Prosser, S.L. (2021). Charting the complex composite nature of centrosomes, primary cilia and centriolar satellites. *Curr. Opin. Struct. Biol.* 66, 32–40.
- Dhruti, P., Shyamala, M., Sandrine, P., Pierre, G., and Vincent, E.G. (2018). STIL balancing primary microcephaly and cancer. *Cell Death Dis.* 9.
- Ding, C., Li, Y., Guo, F., Jiang, Y., Ying, W., Li, D., Yang, D., Xia, X., Liu, W., Zhao, Y., et al. (2016). A cell-type-resolved liver proteome. *Mol. Cell. Proteomics* 15, 3190–3202.
- Dzhindzhev, N.S., Yu, Q.D., Weiskopf, K., Tzolovsky, G., Cunha-Ferreira, I., Riparbelli, M., Rodrigues-Martins, A., Bettencourt-Dias, M., Callaini, G., and Glover, D.M. (2010). Asterless is a scaffold for the onset of centriole assembly. *Nature* 467, 714–718.
- Evans, T., Rosenthal, E.T., Youngblom, J., Distel, D., and Hunt, T. (1983). Cyclin: A protein specified by maternal mRNA in sea urchin eggs that is destroyed at each cleavage division. *Cell* 33, 389–396.
- Feng, Z., Caballe, A., Wainman, A., Johnson, S., Haensele, A.F.M., Cottee, M.A., Conduit, P.T., Lea, S.M., and Raff, J.W. (2017). Structural Basis for Mitotic Centrosome Assembly in Flies. *Cell* 169, 1078–1089.
- Firat-Karalar, E.N., and Stearns, T. (2014). The centriole duplication cycle. *Philos. Trans. R. Soc. B Biol. Sci.* 369, 20130460.
- Firat-Karalar, E.N., Rauniyar, N., Yates, J.R., and Stearns, T. (2014). Proximity interactions among centrosome components identify regulators of centriole duplication. *Curr. Biol.* 24, 664–670.
- Fisk, H.A., and Winey, M. (2001). The mouse Mps1p-like kinase regulates centrosome duplication. *Cell* 106, 95–104.
- Firat-Karalar, E.N., and Stearns, T. (2014). The centriole duplication cycle. *Philos. Trans. R. Soc. B Biol. Sci.* 369, 20130460.
- Fry, A.M., Mayor, T., Meraldi, P., Stierhof, Y.D., Tanaka, K., and Nigg, E.A. (1998a). C-Nap1, a novel centrosomal coiled-coil protein and candidate substrate of the cell cycle-regulated protein kinase Nek2. *J. Cell Biol.* 141, 1563–1574.
- Fry, A.M., Meraldi, P., and Nigg, E.A. (1998b). A centrosomal function for the human Nek2 protein kinase, a member of the NIMA family of cell cycle regulators. *EMBO J.* 17, 470–481.
- Fu, J., Hagan, I.M., and Glover, D.M. (2015). The centrosome and its duplication cycle. *Cold Spring Harb. Perspect. Biol.* 5, a015800.
- Fu, J., Lipinszki, Z., Rangone, H., Min, M., Mykura, C., Chao-Chu, J., Schneider, S., Dzhindzhev, N.S., Gottardo, M., Riparbelli, M.G., et al. (2016). Conserved molecular interactions in centriole-to-centrosome conversion. *Nat. Cell Biol.* 18, 87–99.
- Gambarotto, D., Zwettler, F.U., Guennec, M. Le, and Fortun, D. (2019). Imaging cellular ultrastructures using expansion microscopy (U-ExM). *Nat. Methods* 16, 71–74.
- Ganem, N.J., Godinho, S.A., and Pellman, D. (2009). A mechanism linking extra centrosomes to chromosomal instability. *Nature* 460, 278–282.
- Ganier, O., Schnerch, D., Oertle, P., Lim, R.Y., Plodinec, M., and Nigg, E.A. (2018). Structural centrosome aberrations promote non-cell-autonomous invasiveness. *EMBO J.* 37, e98576.
- Garbrecht, J., Laos, T., Holzer, E., Dillinger, M., and Dammermann, A. (2021). An acentriolar centrosome at the *C. elegans* ciliary base. *Curr. Biol.* 31, 2418–2428.

Gheiratmand, L., Coyaud, E., Gupta, G.D., Laurent, E.M., Hasegan, M., Prosser, S.L., Gonçalves, J., Raught, B., and Pelletier, L. (2019). Spatial and proteomic profiling reveals centrosome-independent features of centriolar satellites. *EMBO J.* 38, e101109.

Glover, D.M., Leibowitz, M.H., McLean, D.A., and Parry, H. (1995). Mutations in aurora prevent centrosome separation leading to the formation of monopolar spindles. *Cell* 81, 95–105.

Godinho, S.A., and Pellman, D. (2014). Causes and consequences of centrosome abnormalities in cancer. *Philos. Trans. R. Soc. B Biol. Sci.* 369, 20130467.

Goetz, S.C., and Anderson, K. V (2010). The Primary Cilium: A Signaling Center During Vertebrate Development. *Nat. Rev. Genet.* 11, 331–344.

Gönczy, P. (2012). Towards a molecular architecture of centriole assembly. *Nat. Rev. Mol. Cell Biol.* 13, 425–435.

Goundiam, O., and Basto, R. (2021). Centrosomes in disease: how the same music can sound so different? *Curr. Opin. Struct. Biol.* 66, 74–82.

Griffith, E., Walker, S., Martin, C.-A., Vagnarelli, P., Stiff, T., Vernay, B., Sanna, N. Al, Saggar, A., Hamel, B., Earnshaw, W.C., et al. (2008). Mutations in pericentrin cause Seckel syndrome with defective ATR-dependent DNA damage signaling. *Nat. Genet.* 40, 232–236.

Guichard, P., Hachet, V., Majubu, N., Neves, A., Demurtas, D., Olieric, N., Fluckiger, I., Yamada, A., Kihara, K., Nishida, Y., et al. (2013). Native Architecture of the Centriole Proximal Region Reveals Features Underlying Its 9-Fold Radial Symmetry. *Curr. Biol.* 23, 1620–1628.

Gupta, G.D., Coyaud, É., Gonçalves, J., Mojarrad, B.A., Liu, Y., Wu, Q., Gheiratmand, L., Comartin, D., Tkach, J.M., Cheung, S.W.T., et al. (2015). A Dynamic Protein Interaction Landscape of the Human Centrosome-Cilium Interface. *Cell* 163, 1484–1499.

Habedanck, R., Stierhof, Y.-D., Wilkinson, C.J., and Nigg, E.A. (2005). The Polo kinase Plk4 functions in centriole duplication. *Nat. Cell Biol.* 7, 1140–1146.

Ham, H., Huynh, W., Schoon, R.A., Vale, R.D., and Billadeau, D.D. (2015). HkRP3 Is a Microtubule-Binding Protein Regulating Lytic Granule Clustering and NK Cell Killing. *J. Immunol.* 194, 3984–3996. Hao, L., and Scholey, J.M. (2009). Intraflagellar transport at a glance. *J. Cell Sci.* 122, 889–892.

Harbour, J.W., Luo, R.X., Dei Santi, A., Postigo, A.A., and Dean, D.C. (1999). Cdk phosphorylation triggers sequential intramolecular interactions that progressively block Rb functions as cells move through G1. *Cell* 98, 859–869.

Harrison, M.K., Adon, A.M., and Saavedra, H.I. (2011). The G1 phase Cdks regulate the centrosome cycle and mediate oncogene-dependent centrosome amplification. *Cell Div.* 6.

Hormeño, S., Ibarra, B., Chichón, F.J., Habermann, K., Lange, B.M.H., Valpuesta, J.M., Carrascosa, J.L., and Arias-Gonzalez, J.R. (2009). Single centrosome manipulation reveals its electric charge and associated dynamic structure. *Biophys. J.* 97, 1022–1030.

Hossain, D., Esfehani, Y.J., Das, A., and Tsang, W.Y. (2017). Cep78 controls centrosome homeostasis by inhibiting EDD-DYRK2-DDB1 VprBP. *EMBO Rep.* 18, 632–644.

Howard, J., and Hyman, A.A. (2003). Dynamics and mechanics of the microtubule plus end. *Nature* 422, 753–758.

Huang, N., Xia, Y., Zhang, D., Wang, S., Bao, Y., He, R., Teng, J., and Chen, J. (2017). Hierarchical assembly of centriole subdistal appendages via centrosome binding proteins CCDC120 and CCDC68. *Nat. Commun.* 8.

Hyman, A.A., Salser, S., Drechsel, D.N., Unwin, N., and Mitchison, T.J. (1992). Role of GTP Hydrolysis in Microtubule Dynamics: Information from a Slowly Hydrolyzable Analogue, GMPCPP. *Mol. Biol. Cell* 12, 1155–1167.

Hyman, A.A., Chrétien, D., Arnal, I., and Wade, R.H. (1995). Structural Changes Accompanying GTP Hydrolysis in Microtubules: Information from a Slowly Hydrolyzable Analogue Guanylyl-(alpha,beta)-Methylene-Diphosphonate. *J. Cell Biol.* 128, 117–125.

Izquierdo, D., Wang, W.-J., Uryu, K., and Tsou, M.F.B. (2014). Stabilization of cartwheel-less centrioles for duplication requires CEP295-mediated centriole to centrosome conversion. *Cell Rep.* 8, 957–965.

Jakobsen, L., Vanselow, K., Skogs, M., Toyoda, Y., Lundberg, E., Poser, I., Falkenby, L.G., Bennetzen, M., Westendorf, J., Nigg, E.A., et al. (2011). Novel asymmetrically localizing components of human centrosomes identified by complementary proteomics methods. *EMBO J.* 30, 1520–1535.

Jang, S.M., Redon, C.E., Thakur, B.L., Bahta, M.K., and Aladjem, M.I. (2020). Regulation of cell cycle drivers by Cullin-RING ubiquitin ligases. *Exp. Mol. Med.* 52, 1637–1651.

Janke, C., and Magiera, M.M. (2020). The tubulin code and its role in controlling microtubule properties and functions. *Nat. Rev. Mol. Cell Biol.* 21, 307–326.

Jiang, X., Ho, D.B.T., Mahe, K., Mia, J., Sepulveda, G., Antkowiak, M., Jiang, L., Yamada, S., and Jao, L.-E. (2021). Condensation of pericentrin proteins in human cells illuminates phase separation in centrosome assembly. *J. Cell Sci.* 134, jcs258897.

Johnson, C.A., and Malicki, J.J. (2019). Perspective The Nuclear Arsenal of Cilia. *Dev. Cell* 49, 161–170.

Kashihara, H., Chiba, S., Kanno, S. ichiro, Suzuki, K., Yano, T., and Tsukita, S. (2019). Cep128 associates with Odf2 to form the subdistal appendage of the centriole. *Genes to Cells* 24, 231–243.

Kastan, M.B., and Bartek, J. (2004). Cell-cycle checkpoints and cancer. *Nature* 432, 316–323.

Kim, S., and Rhee, K. (2014). Importance of the CEP215-pericentrin interaction for centrosome maturation during mitosis. *PLoS One* 9.

Kim, J., Lee, K., and Rhee, K. (2015). PLK1 regulation of PCNT cleavage ensures fidelity of centriole separation during mitotic exit. *Nat. Commun.* 6.

Kim, T.S., Zhang, L., Il Ahn, J., Meng, L., Chen, Y., Lee, E., Bang, J.K., Lim, J.M., Ghirlando, R., Fan, L., et al. (2019). Molecular architecture of a cylindrical self-assembly at human centrosomes. *Nat. Commun.* 10.

Kitagawa, D., Vakonakis, I., Olieric, N., Hilbert, M., Keller, D., Olieric, V., Bortfeld, M., Erat, M.C., Flückiger, I., Gönczy, P., et al. (2011). Structural basis of the 9-fold symmetry of centrioles. *Cell* 144, 364–375.

Kleylein-Sohn, J., Westendorf, J., Le Clech, M., Habedanck, R., Stierhof, Y.D., and Nigg, E.A. (2007). Plk4-Induced Centriole Biogenesis in Human Cells. *Dev. Cell* 13, 190–202.

Klos Dehring, D.A., Vladar, E.K., Werner, M.E., Mitchell, J.W., Hwang, P., and Mitchell, B.J. (2013). Deuterosome-Mediated Centriole Biogenesis. *Dev. Cell* 27, 103–112.

Kodani, A., Yu, T.W., Johnson, J.R., Jayaraman, D., Johnson, T.L., Al-Gazali, L., Sztriha, L., Partlow, J.N., Kim, H., Krup, A.L., et al. (2015). Centriolar satellites assemble centrosomal microcephaly proteins to recruit CDK2 and promote centriole duplication. *Elife* 4, e07519.

Kohlmaier, G., Lončarek, J., Meng, X., McEwen, B.F., Spektor, A., Dynlacht, B.D., Khodjakov, A., and Gönczy, P. (2009). Overly long centrioles and defective cell division upon excess of the SAS-4-related protein CPAP. *Curr. Biol.* 19, 1012–1018.

- Krämer, A., Maier, B., and Bartek, J. (2011). Centrosome clustering and chromosomal (in)stability: A matter of life and death. *Mol. Oncol.* 5, 324–335.
- Kubo, A., Sasaki, H., Yuba-Kubo, A., Tsukita, S., and Shiina, N. (1999). Centriolar satellites: Molecular characterization, ATP-dependent movement toward centrioles and possible involvement in ciliogenesis. *J. Cell Biol.* 147, 969–979.
- Kumar, D., and Reiter, J. (2021). How the centriole builds its cilium: of mothers, daughters, and the acquisition of appendages. *Curr. Opin. Struct. Biol.* 66, 41–48.
- Lawo, S., Hasegan, M., Gupta, G.D., and Pelletier, L. (2012). Subdiffraction imaging of centrosomes reveals higher-order organizational features of pericentriolar material. *Nat. Cell Biol.* 14, 1148–1158.
- Leda, M., Holland, A.J., and Goryachev, A.B. (2018). Autoamplification and Competition Drive Symmetry Breaking: Initiation of Centriole Duplication by the PLK4-STIL Network. *IScience* 8, 222–235.
- Lee, J.Y., and Stearns, T. (2013). FOP Is a Centriolar Satellite Protein Involved in Ciliogenesis. *PLoS One* 8, e58589.
- Lee, K.S., Park, J.E., Ahn, J. il, and Zeng, Y. (2021). Constructing PCM with architecturally distinct higher-order assemblies. *Curr. Opin. Struct. Biol.* 66, 66–73.
- LeGuennec, M., Klena, N., Aeschlimann, G., Hamel, V., and Guichard, P. (2021). Overview of the centriole architecture. *Curr. Opin. Struct. Biol.* 66, 58–65.
- Levine, M.S., Bakker, B., Boeckx, B., Moyett, J., Lu, J., Vitre, B., Spierings, D.C., Lansdorp, P.M., Cleveland, D.W., Lambrechts, D., et al. (2017). Centrosome Amplification Is Sufficient to Promote Spontaneous Tumorigenesis in Mammals. *Dev. Cell* 40, 313–322.
- Li, J., Van Vranken, J.G., Pontano Vaites, L., Schweppe, D.K., Huttlin, E.L., Etienne, C., Nandhikonda, P., Viner, R., Robitaille, A.M., Thompson, A.H., et al. (2020). TMTpro reagents: a set of isobaric labeling mass tags enables simultaneous proteome-wide measurements across 16 samples. *Nat. Methods* 17, 399–404.
- Li, S., Fernandez, J.J., Marshall, W.F., and Agard, D.A. (2012). Three-dimensional structure of basal body triplet revealed by electron cryo-tomography. *EMBO J.* 31, 552–562.
- Lindemann, C., Thomanek, N., Hundt, F., Lerari, T., Meyer, H.E., Wolters, D., and Marcus, K. (2017). Strategies in relative and absolute quantitative mass spectrometry based proteomics. *Biol. Chem.* 398, 687–699.
- Liu, Q., and Ruderman, J. V (2006). Aurora A, mitotic entry, and spindle bipolarity. *Proc. Natl. Acad. Sci.* 103, 5811–5816.
- Liu, Y., Gupta, G.D., Barnabas, D.D., Agircan, F.G., Mehmood, S., Wu, D., Coyaud, E., Johnson, C.M., McLaughlin, S.H., Andreeva, A., et al. (2018). Direct binding of CEP85 to STIL ensures robust PLK4 activation and efficient centriole assembly. *Nat. Commun.* 9.
- Loncarek, J., and Bettencourt-Dias, M. (2018). Building the right centriole for each cell type. *J. Cell Biol.* 217, 823–835.
- Loncarek, J., and Khodjakov, A. (2009). Ab ovo or de novo? Mechanisms of centriole duplication. *Mol. Cells* 27, 135–142.
- Loncarek, J., Hergert, P., Magidson, V., and Khodjakov, A. (2008). Control of daughter centriole formation by the pericentriolar material. *Nat. Cell Biol.* 10, 322–328.
- Lukinavičius, G., Lavogina, D., Orpinell, M., Umezawa, K., Reymond, L., Garin, N., Gönczy, P., and Johnsson, K. (2013). Selective chemical crosslinking reveals a Cep57-Cep63-Cep152 centrosomal complex. *Curr. Biol.* 23, 265–270.

- Lupas, A.N., and Bassler, J. (2017). Coiled Coils – A Model System for the 21st Century. *Trends Biochem. Sci.* 42, 130–140.
- Magescas, J., Eskinazi, S., Tran, M. V., and Feldman, J.L. (2021). Centriole-less pericentriolar material serves as a microtubule organizing center at the base of *C. elegans* sensory cilia. *Curr. Biol.* 31, 2410–2417.
- Mahen, R., Jeyasekharan, A.D., Barry, N.P., and Venkitaraman, A.R. (2011). Continuous polo-like kinase 1 activity regulates diffusion to maintain centrosome self-organization during mitosis. *PNAS* 108, 9310–9315.
- Malumbres, M., and Barbacid, M. (2005). Mammalian cyclin-dependent kinases. *Trends Biochem. Sci.* 30, 630–641.
- Mardin, B.R., Lange, C., Baxter, J.E., Hardy, T., Scholz, S.R., Fry, A.M., and Schiebel, E. (2010). Components of the Hippo pathway cooperate with Nek2 kinase to regulate centrosome disjunction. *Nat. Cell Biol.* 12, 1166–1176.
- Marthiens, V., and Basto, R. (2020). Centrosomes: The good and the bad for brain development. *Biol. Cell* 112, 153–172.
- Mazo, G., Soplop, N., Wang, W.J., Uryu, K., and Tsou, M.F.B. (2016). Spatial Control of Primary Ciliogenesis by Subdistal Appendages Alters Sensation-Associated Properties of Cilia. *Dev. Cell* 39, 424–437.
- Mcintosh, J.R. (2016). Mitosis. *Cold Spring Harb. Perspect. Biol.* 8, a023218.
- Mennella, V., Keszthelyi, B., McDonald, K.L., Chhun, B., Kan, F., Rogers, G.C., Huang, B., and Agard, D.A. (2012). Subdiffraction-resolution fluorescence microscopy reveals a domain of the centrosome critical for pericentriolar material organization. *Nat. Cell Biol.* 14, 1159–1168.
- Mennella, V., Agard, D.A., Huang, B., and Pelletier, L. (2014). Amorphous no more: subdiffraction view of the pericentriolar material architecture. *Trends Cell Biol.* 24, 188–197.
- Mercey, O., Levine, M.S., LoMastro, G.M., Rostaing, P., Brotslaw, E., Gomez, V., Kumar, A., Spassky, N., Mitchell, B.J., Meunier, A., et al. (2019). Massive centriole production can occur in the absence of deuterosomes in multiciliated cells. *Nat. Cell Biol.* 21, 1544–1552.
- Mitchison, T., and Kirschner, M. (1984). Dynamic instability of microtubule growth. *Nature* 312, 237–242.
- Moritz, M., Zheng, Y., Alberts, B.M., and Oegema, K. (1998). Recruitment of the γ-tubulin ring complex to *Drosophila* salt-stripped centrosome scaffolds. *J. Cell Biol.* 142, 775–786.
- Morretton, J.-P., Herbette, A., Cosson, C., Mboup, B., Latouche, A., Gestraud, P., Popova, T., Stern, M.-H., Nemati, F., Decaudin, D., et al. (2019). Centrosome amplification favours survival and impairs ovarian cancer progression. *bioRxiv*. doi: 10.1101/623983.
- Moser, J.J., Fritzler, M.J., Ou, Y., and Rattner, J.B. (2010). The PCM–basal body/primary cilium coalition. *Semin. Cell Dev. Biol.* 21, 148–155.
- Nabais, C., Pereira, S.G., and Bettencourt-Dias, M. (2017). Noncanonical Biogenesis of Centrioles and Basal Bodies. *Cold Spring Harb. Symp. Quant. Biol.* 82, 123–135.
- Nabais, C., Pessoa, D., de-Carvalho, J., van Zanten, T., Duarte, P., Mayor, S., Carneiro, J., Telley, I.A., and Bettencourt-Dias, M. (2021). Plk4 triggers autonomous de novo centriole biogenesis and maturation. *J. Cell Biol.* 220.
- Nakazawa, Y., Hiraki, M., Kamiya, R., and Hirono, M. (2007). SAS-6 is a Cartwheel Protein that Establishes the 9-Fold Symmetry of the Centriole. *Curr. Biol.* 17, 2169–2174.

- Nayak, S.C., and Radha, V. (2020). C3G localizes to the mother centriole in a cenexin-dependent manner and regulates centrosome duplication and primary cilium length. *J. Cell Sci.* 133.
- Nigg, E.A., and Holland, A.J. (2018). Once and only once: Mechanisms of centriole duplication and their deregulation in diseases. *Nat. Rev. Mol. Cell Biol.* 19, 297–312.
- Nigg, E.A., and Stearns, T. (2011). The centrosome cycle: Centriole biogenesis, duplication and inherent asymmetries. *Nat. Cell Biol.* 13, 1154–1160.
- Nigg, S., and Stearns, T. (2014). The centrosome cycle: Centriole biogenesis, duplication and inherent asymmetries. *Nat. Cell Biol.* 13, 1154–1160.
- Nigg, E.A., Čajánek, L., and Arquint, C. (2014). The centrosome duplication cycle in health and disease. *FEBS Lett.* 588, 2366–2372.
- Ochi, T., Quarantotti, V., Lin, H., Jullien, J., Rosa e Silva, I., Boselli, F., Barnabas, D.D., Johnson, C.M., McLaughlin, S.H., Freund, S.M.V., et al. (2020). CCDC61/VFL3 Is a Paralog of SAS6 and Promotes Ciliary Functions. *Structure* 28, 674–689.
- Oegema, K., Wiese, C., Martin, O.C., Milligan, R.A., Iwamatsu, A., Mitchison, T.J., and Zheng, Y. (1999). Characterization of two related *Drosophila* γ -tubulin complexes that differ in their ability to nucleate microtubules. *J. Cell Biol.* 144, 721–733.
- Ohta, M., Ashikawa, T., Nozaki, Y., Kozuka-Hata, H., Goto, H., Inagaki, M., Oyama, M., and Kitagawa, D. (2014). Direct interaction of Plk4 with STIL ensures formation of a single procenitrode per parental centriole. *Nat. Commun.* 5, 5267.
- Ohta, M., Watanabe, K., Ashikawa, T., Nozaki, Y., Yoshioka, S., Kimura, A., and Kitagawa, D. (2018). Bimodal Binding of STIL to Plk4 Controls Proper Centriole Copy Number. *Cell Rep.* 23, 3160–3169.
- Ono, T., Fang, Y., Spector, D.L., and Hirano, T. (2004). Spatial and Temporal Regulation of Condensins I and II in Mitotic Chromosome Assembly in Human Cells. *Mol. Biol. Cell* 15, 3296–3308.
- Otto, T., and Sicinski, P. (2017). Cell cycle proteins as promising targets in cancer therapy. *Nat. Rev. Cancer* 17, 93–115.
- Park, J.E., Zhang, L., Bang, J.K., Andresson, T., DiMaio, F., and Lee, K.S. (2019). Phase separation of Polo-like kinase 4 by autoactivation and clustering drives centriole biogenesis. *Nat. Commun.* 10.
- Pelletier, L., O'Toole, E., Schwager, A., Hyman, A.A., and Müller-Reichert, T. (2006). Centriole assembly in *Caenorhabditis elegans*. *Nature* 444, 619–623.
- Petry, S., and Vale, R.D. (2015). Microtubule nucleation at the centrosome and beyond. *Nat. Cell Biol.* 17, 1089–1093.
- Pimenta-Marques, A., and Bettencourt-Dias, M. (2020). Pericentriolar material. *Curr. Biol.* 30, R677–R697.
- Pollard, T.D. (2010). Mechanics of cytokinesis in eukaryotes. *Curr. Opin. Cell Biol.* 22, 50–56.
- Puklowski, A., Homsi, Y., Keller, D., May, M., Chauhan, S., Kossatz, U., Grünwald, V., Kubicka, S., Pich, A., Manns, M.P., et al. (2011). The SCF–FBXW5 E3-ubiquitin ligase is regulated by PLK4 and targets HsSAS-6 to control centrosome duplication. *Nat. Cell Biol.* 13, 1004–1009.
- Quarantotti, V., Chen, J., Tischer, J., Tejedo, C.G., Papachristou, E.K., Santos, C.S.D., Kilmartin, J. V, Miller, M.L., and Gergely, F. (2019). Centriolar satellites are acentriolar assemblies of centrosomal proteins. *EMBO J.* 38, e101082.
- Raff, J.W. (2019). Phase Separation and the Centrosome : A Fait Accompli? *Trends Cell Biol.* 29, 612–622.

- Rale, M.J., Kadzik, R.S., and Petry, S. (2018). Phase Transitioning the Centrosome into a Microtubule Nucleator. *Biochemistry* 57, 30–37.
- Ran, F.A., Hsu, P.D., Wright, J., Agarwala, V., Scott, D.A., and Zhang, F. (2013). Genome engineering using the CRISPR-Cas9 system. *Nat. Protoc.* 8, 2281–2308.
- Rasi, M.Q., Parker, J.D.K., Feldman, J.L., Marshall, W.F., and Quarmby, L.M. (2009). Katanin Knockdown Supports a Role for Microtubule Severing in Release of Basal Bodies before Mitosis in Chlamydomonas. *Mol. Biol. Cell* 20, 379–388.
- Rauniyar, N., and Yates, J.R. (2014). Isobaric Labeling-Based Relative Quantification in Shotgun Proteomics. *J. Proteome Res.* 13, 5293–5309.
- Reiter, J.F., and Leroux, M.R. (2017). Genes and molecular pathways underpinning ciliopathies. *Nat. Rev. Mol. Cell Biol.* 18, 533–547.
- Rhys, A.D., Monteiro, P., Smith, C., Vaghela, M., Arnandis, T., Kato, T., Leitinger, B., Sahai, E., McAinsh, A., Charras, G., et al. (2018). Loss of E-cadherin provides tolerance to centrosome amplification in epithelial cancer cells. *J. Cell Biol.* 217, 195–209.
- Sahabandu, N., Kong, D., Magidson, V., Nanjundappa, R., Sullenberger, C., Mahjoub, M., and Loncarek, J. (2019). Expansion microscopy for the analysis of centrioles and cilia. *J. Microsc.* 0, 1–15.
- Sánchez, I., and Dynlacht, B.D. (2016). Cilium assembly and disassembly. *Nat. Cell Biol.* 18, 711–717.
- Satyanarayana, A., and Kaldis, P. (2009). Mammalian cell-cycle regulation: Several cdks, numerous cyclins and diverse compensatory mechanisms. *Oncogene* 28, 2925–2939.
- Saurya, S., Roque, H., Novak, Z.A., Wainman, A., Aydogan, M.G., Volanakis, A., Sieber, B., Pinto, D.M.S., and Raff, J.W. (2016). *Drosophila* Ana1 is required for centrosome assembly and centriole elongation. *J. Cell Sci.* 129, 2514–2525.
- Schafer, K.A. (1998). The Cell Cycle: A Review. *Vet. Pathol.* 35, 461–478.
- Scheer, U. (2014). Historical roots of centrosome research: discovery of Boveri's microscope slides in Würzburg. *Philos. Trans. R. Soc. B Biol. Sci.* 369, 20130469.
- Schmidt, K.N., Kuhns, S., Neuner, A., Hub, B., Zentgraf, H., and Pereira, G. (2012). Cep164 mediates vesicular docking to the mother centriole during early steps of ciliogenesis. *J. Cell Biol.* 199, 1083–1101.
- Schmidt, T.I., Kleylein-Sohn, J., Westendorf, J., Le Clech, M., Lavoie, S.B., Stierhof, Y.-D., and Nigg, E.A. (2009). Control of Centriole Length by CPAP and CP110. *Curr. Biol.* 19, 1005–1011.
- Seo, M.Y., Jang, W., and Rhee, K. (2015). Integrity of the pericentriolar material is essential for maintaining centriole association during M phase. *PLoS One* 10, e0138905.
- Sherr, C.J., and Roberts, J.M. (1999). CDK inhibitors: Positive and negative regulators of G1-phase progression. *Genes Dev.* 13, 1501–1512.
- Sir, J.H., Barr, A.R., Nicholas, A.K., Carvalho, O.P., Sossick, A., Reichelt, S., Santos, C.D., Woods, C.G., and Gergely, F. (2011). A Primary Microcephaly Protein Complex forms a ring around parental centrioles. *Nat. Genet.* 43, 1147–1153.
- Sir, J.H., Pütz, M., Daly, O., Morrison, C.G., Dunning, M., Kilmartin, J. V., and Gergely, F. (2013). Loss of centrioles causes chromosomal instability in vertebrate somatic cells. *J. Cell Biol.* 203, 747–756.
- Sonnen, K.F., Schermelleh, L., Leonhardt, H., and Nigg, E.A. (2012). 3D-structured illumination microscopy provides novel insight into architecture of human centrosomes. *Biol. Open* 1, 965–976.

- Sonnen, K.F., Gabryjonczyk, A.-M., Anselm, E., Stierhof, Y.-D., and Nigg, E.A. (2013). Human Cep192 and Cep152 cooperate in Plk4 recruitment and centriole duplication. *J. Cell Sci.* 126, 3223–3233.
- Stinchcombe, J.C., Majorovits, E., Bossi, G., Fuller, S., and Griffiths, G.M. (2006). Centrosome polarization delivers secretory granules to the immunological synapse. *Nature* 443, 462–465.
- Stinchcombe, J.C., Randzavola, L.O., Angus, K.L., Mantell, J.M., Verkade, P., and Griffiths, G.M. (2015). Mother Centriole Distal Appendages Mediate Centrosome Docking at the Immunological Synapse and Reveal Mechanistic Parallels with Ciliogenesis. *Curr. Biol.* 25, 3239–3244.
- Strnad, P., Leidel, S., Vinogradova, T., Euteneuer, U., Khodjakov, A., and Gönczy, P. (2007). Regulated HsSAS-6 levels ensure formation of a single procentriole per centriole during the centrosome duplication cycle. *Dev. Cell* 13, 203–213.
- Sullenberger, C., Vasquez-limeta, A., Kong, D., and Loncarek, J. (2020). With Age Comes Maturity: Biochemical and Structural Transformation of a Human Centriole in the Making. *Cells* 9.
- Sydar, A.M., Coyaud, E., Rovelli, C., Laurent, E., Liu, H., Raught, B., and Mennella, V. (2018). PPP1R35 is a novel centrosomal protein that regulates centriole length in concert with the microcephaly protein RTTN. *Elife* 7, e37846.
- Tang, N., and Marshall, W.F. (2012). Centrosome positioning in vertebrate development. *J. Cell Sci.* 125, 4951–4961.
- Tang, C.J.C., Fu, R.H., Wu, K.S., Hsu, W. Bin, and Tang, T.K. (2009). CPAP is a cell-cycle regulated protein that controls centriole length. *Nat. Cell Biol.* 11, 825–831.
- Tanios, B.E., Yang, H.J., Soni, R., Wang, W.J., Macaluso, F.P., Asara, J.M., and Tsou, M.F.B. (2013). Centriole distal appendages promote membrane docking, leading to cilia initiation. *Genes Dev.* 27, 163–168.
- Thompson, A., Schäfer, J., Kuhn, K., Kienle, S., Schwarz, J., Schmidt, G., Neumann, T., and Hamon, C. (2003). Tandem mass tags: A novel quantification strategy for comparative analysis of complex protein mixtures by MS/MS. *Anal. Chem.* 75, 1895–1904.
- Tilney, L.G., Bryan, J., Bush, D.J., Fujiwara, K., Mooseker, M.S., Murphy, D.B., and Snyder, D.H. (1973). Microtubules: Evidence for 13 protofilaments. *J. Cell Biol.* 59, 267–275.
- Tischer, J., Carden, S., and Gergely, F. (2021). Accessorizing the centrosome: new insights into centriolar appendages and satellites. *Curr. Opin. Struct. Biol.* 66, 148–155.
- Tovey, C.A., and Conduit, P.T. (2018). Microtubule nucleation by γ -tubulin complexes and beyond. *Essays Biochem.* 62, 765–780.
- Tsou, M.F.B., and Stearns, T. (2006). Mechanism limiting centrosome duplication to once per cell cycle. *Nature* 442, 947–951.
- Tsou, M.F.B., Wang, W., Yule, K.A., Uryu, K., and Jallepalli, P. V (2009). Polo kinase and separase regulate the mitotic licensing of centriole duplication in human cells. *Dev. Cell* 17, 344–354.
- Tsuchiya, Y., Yoshioka, S., Gupta, A., Watanabe, K., and Kitagawa, D. (2016). Cep295 is a conserved scaffold protein required for generation of a bona fide mother centriole. *Nat. Commun.* 7.
- Uzbekov, R., and Alieva, I. (2018). Who are you, subdistal appendages of centriole? *R. Soc. Open Sci.* 8, 180062.
- Vakonakis, I. (2021). The centriolar cartwheel structure: symmetric, stacked, and polarized. *Curr. Opin. Struct. Biol.* 66, 1–7.

- Vanhaesebroeck, B., Bilanges, B., Madsen, R.R., Dale, K.L., Lau, E., and Vladimirou, E. (2019). Perspective: Potential impact and therapeutic implications of oncogenic PI3K activation on chromosomal instability. *Biomolecules* 9, 331–349.
- Venuto, S., and Merla, G. (2019). E3 Ubiquitin Ligase TRIM Proteins, Cell Cycle and Mitosis. *Cells* 8.
- Vidova, V., and Spacil, Z. (2017). A review on mass spectrometry-based quantitative proteomics: Targeted and data independent acquisition. *Anal. Chim. Acta* 964, 7–23.
- Viol, L., Hata, S., Pastor-peidro, A., Neuner, A., Murke, F., Wuchter, P., Ho, A.D., and Giebel, B. (2020). Nek2 kinase displaces distal appendages from the mother centriole prior to mitosis. *J. Cell Biol.* 219, e201907136.
- Vora, S.M., and Phillips, B.T. (2016). The benefits of local depletion: The centrosome as a scaffold for ubiquitin-proteasome-mediated degradation. *Cell Cycle* 15, 2124–2134.
- Walczak, C.E., Cai, S., and Khodjakov, A. (2010). Mechanisms of chromosome behaviour during mitosis. *Nat. Rev. Mol. Cell Biol.* 11, 91–102.
- Wang, L., Failler, M., Fu, W., and Dynlacht, B.D. (2018). A distal centriolar protein network controls organelle maturation and asymmetry. *Nat. Commun.* 9.
- Wang, W.J., Soni, R.K., Uryu, K., and Tsou, M.F.B. (2011). The conversion of centrioles to centrosomes: Essential coupling of duplication with segregation. *J. Cell Biol.* 193, 727–739.
- Watanabe, K., Takao, D., Ito, K.K., Takahashi, M., and Kitagawa, D. (2019). The Cep57-pericentrin module organizes PCM expansion and centriole engagement. *Nat. Commun.* 10.
- Waters, A.M., and Beales, P.L. (2011). Ciliopathies: An expanding disease spectrum. *Pediatr. Nephrol.* 26, 1039–1056.
- Watts, C.A., Richards, F.M., Bender, A., Bond, P.J., Korb, O., Kern, O., Riddick, M., Owen, P., Myers, R.M., Raff, J., et al. (2013). Design, synthesis, and biological evaluation of an allosteric inhibitor of HSET that targets cancer cells with supernumerary centrosomes. *Chem. Biol.* 20, 1399–1410.
- Wei, Z., Kim, T.-S., Ahn, J. Il, Meng, L., Chen, Y., R, E.K., Ku, B., Zhou, M., Kim, S.J., Bang, J.K., et al. (2020). Requirement of the Cep57-Cep63 Interaction for Proper Cep152 Recruitment and Centriole Duplication. *Mol. Cell. Biol.* 40, e00535-19.
- Wigge, P.A., Jensen, O.N., Holmes, S., Souès, S., Mann, M., Kilmartin, J. V, Riley, D.J., Chen, P., and Cell, W.L.M. (1998). Analysis of the *Saccharomyces* Spindle Pole by Matrix-assisted Laser Desorption/Ionization (MALDI) Mass Spectrometry. *J. Cell Biol.* 141, 967–977.
- Winey, M., and O'Toole, E. (2014). Centriole structure. *Philos. Trans. R. Soc. B Biol. Sci.* 369, 20130457.
- Wong, Y.L., Anzola, J. V., Davis, R.L., Yoon, M., Motamedi, A., Kroll, A., Seo, C.P., Hsia, J.E., Kim, S.K., Mitchell, J.W., et al. (2015). Reversible centriole depletion with an inhibitor of Polo-like kinase 4. *Science* (80-.). 348, 1155–1160.
- Woodruff, J.B. (2021). The material state of centrosomes: lattice, liquid, or gel? *Curr. Opin. Struct. Biol.* 66, 139–147.
- Woodruff, J.B., Wueseke, O., and Hyman, A.A. (2014). Pericentriolar material structure and dynamics. *Philos. Trans. R. Soc. B Biol. Sci.* 369, 20130459.
- Woodruff, J.B., Ferreira Gomes, B., Widlund, P.O., Mahamid, J., Honigmann, A., and Hyman, A.A. (2017). The Centrosome Is a Selective Condensate that Nucleates Microtubules by Concentrating Tubulin. *Cell* 169, 1066–1077.

Yamamoto, S., and Kitagawa, D. (2019). Self-organization of Plk4 regulates symmetry breaking in centriole duplication. *Nat. Commun.* 10.

Yamamoto, S., and Kitagawa, D. (2021). Emerging insights into symmetry breaking in centriole duplication: updated view on centriole duplication theory. *Curr. Opin. Struct. Biol.* 66, 8–14.

Yang, T.T., Chong, W.M., Wang, W.J., Mazo, G., Tanos, B., Chen, Z., Tran, T.M.N., Chen, Y., De, Weng, R.R., Huang, C.E., et al. (2018). Super-resolution architecture of mammalian centriole distal appendages reveals distinct blade and matrix functional components. *Nat. Commun.* 9.

Zhang, S., and Mitchell, B.J. (2015). Centriole biogenesis and function in multiciliated cells. *Methods Cell Biol.* 129, 103–127.

Zhang, X., Wei, C., Liang, H., and Han, L. (2021). Polo-Like Kinase 4's Critical Role in Cancer Development and Strategies for Plk4-Targeted Therapy. *Front. Oncol.* 11, 587554.

Zhao, H., Zhu, L., Zhu, Y., Cao, J., Li, S., Huang, Q., Xu, T., Huang, X., Yan, X., and Zhu, X. (2013). The Cep63 parologue Deup1 enables massive de novo centriole biogenesis for vertebrate multiciliogenesis. *Nat. Cell Biol.* 15, 1434–1444.

Zheng, Y., Wong, M.L., Alberts, B., and Mitchison, T. (1995). Nucleation of microtubule assembly by a γ -tubulin-containing ring complex. *Nature* 378, 578–583.

Zupa, E., Liu, P., Würtz, M., Schiebel, E., and Pfeffer, S. (2021). The structure of the γ -TuRC: a 25-years-old molecular puzzle. *Curr. Opin. Struct. Biol.* 66, 15–21.

Zwicker, D., Decker, M., Jaensch, S., Hyman, A.A., and Jülicher, F. (2014). Centrosomes are autocatalytic droplets of pericentriolar material organized by centrioles. *Proc. Natl. Acad. Sci.* 111, E2636–E2645.

10 Appendices

Appendix 1 - Number of unique peptides for the top 30 bead-only binding proteins found via COMPACT-MS in HEK 293T cells untreated (-) and treated (+) with centrinone.

	- centrinone		+ centrinone	
	<i>BO rep 1</i>	<i>BO rep 2</i>	<i>BO rep 1</i>	<i>BO rep 2</i>
ACACA	91	94	88	100
ACACB	53	55	51	56
PC	47	51	48	48
PCCA	32	30	31	28
MCCC1	29	27	27	26
MCCC2	27	27	26	27
KRT2	20	18	19	17
PCCB	19	19	20	19
KRT10	19	19	24	18
KRT1	19	22	27	18
VIM	18	25	26	27
KRT9	17	32	30	23
TUFM	12	10	10	13
DDX41	12	16	10	11
LMNB1	11	15	16	11
TUBA1B	11	10	12	11
HLCS	9	10	10	13
ACTB	7	4	6	6
HNRNPU	7	11	12	7
DDX17	6	8	10	6
ECH1	6	7	6	7
RPS3	6	5	3	3
RBM14	6	9	9	8
KRT5	6	9	11	7
TRAP1	6	4	6	8
TCOF1	6	7	10	9
CCT6A	6	8	6	7
ALB	6	7	8	8
ECI2	5	2	2	2
RPS4X	5	6	2	3

Appendix 2 - Average number of unique peptides for a select number of centrosomal proteins found via COMPACT-MS in HEK 293T cells untreated (-) and treated (+) with centrinone.

	- centrinone		+ centrinone	
	<i>Bound</i>	<i>BO</i>	<i>Bound</i>	<i>BO</i>
PCNT	98	-	20	-
SAS6	13	-	-	-
TUBG1	4	-	-	-
CETN3	2	-	-	-
NIN	49	-	12	-
CEP152	45	-	17	-
CEP128	47	-	24	-
CP110	14	-	-	-
CEP83	16	-	3	-
CEP41	9	-	-	-

Appendix 3 - COMPACT replicates performed in HEK 293T cells (three technical [reps 1-3], three biological [reps 4-6]). Proteins present in five out of six replicates are shown. Number of unique peptides are indicated for each experiment, and sorted from high to low according to colour (red – green).

Protein	Number of unique peptides					
	rep 1	rep 2	rep 3	rep 4	rep 5	rep 6
PCNT	104	91	98	104	110	115
ALMS1	86	75	79	82	102	102
AKAP9	86	73	68	47	48	70
CNTRL	78	79	81	70	75	92
CEP250	74	76	72	71	87	89
CEP350	62	58	61	76	82	84
CEP192	56	53	57	56	37	68
CEP290	53	45	44	56	49	65
NIN	52	45	50	53	57	57
CDK5RAP2	51	46	48	48	60	53
CROCC	49	43	48	36	51	38
CEP128	48	44	50	46	57	56
CEP135	46	40	41	45	53	49
ANKRD26	46	35	40	44	43	55
CEP152	44	39	51	49	49	52
CEP295	41	36	34	41	41	47
CKAP5	41	42	38	37	38	52
C2CD3	33	29	30	33	34	48
AKNA	32	27	35	24	20	34
CEP164	30	33	31	34	44	44
CEP170	29	25	29	28	27	31
ODF2	28	29	28	28	43	37
CEP120	27	22	24	25	25	35
SPICE1	27	25	21	27	21	26
CEP162	22	16	16	26	27	28
HSPA5	21	21	20	17	12	19
PIBF1	20	20	22	26	21	29
FBF1	20	15	16	13	20	27
CNTROB	19	17	21	23	22	30
CEP63	19	17	21	22	20	20
HERC2	19	15	10	11	4	20
CEP112	18	21	17	25	25	26
CCDC171	18	19	21	24	22	29
TBC1D31	18	16	22	17	22	26
CENPJ	18	15	22	25	20	27
CCHCR1	18	12	12	18	18	25
HSPA8	18	18	16	15	18	21
OFD1	18	13	14	20	16	19
CP110	18	13	12	17	12	18
CEP83	17	13	19	22	22	21
MPHOSPH9	17	16	18	23	13	26
KIAA0753	17	10	15	13	13	16
HSPA9	17	17	15	8	8	12

SCLT1	16	16	16	19	18	22
STIL	16	12	12	19	13	18
LRRC45	16	11	14	16	9	13
CEP89	15	11	8	14	8	22
HAUS6	15	14	14	18	7	24
TUBGCP2	15	13	11	11	7	24
CEP170B	15	13	12	4	6	16
CCDC18	15	15	13	30	4	21
EDC4	14	15	11	18	19	25
MDM1	14	14	13	14	14	16
SAS6	14	11	14	16	11	24
RTTN	14	9	13	15	10	28
TUBGCP3	14	12	12	9	5	17
DDB1	13	12	9	14	29	21
CEP95	13	11	12	15	20	18
CEP78	13	13	12	14	18	19
CEP97	13	13	13	10	10	12
HSPA1B	13	14	14	12	0	18
CCDC15	13	11	12	18	9	17
NPHP4	12	12	14	15	21	24
CEP68	12	9	12	7	14	11
POC5	12	12	12	15	14	15
FGFR1OP	12	13	13	14	13	13
SDCCAG8	12	13	12	13	8	16
FTSJ3	12	13	8	10	16	0
CCSER2	12	8	8	8	7	12
HAUS5	12	12	12	11	5	13
CEP131	12	6	5	6	3	15
CEP41	11	6	9	10	14	12
CCDC14	11	9	11	18	12	13
CNTLN	11	11	11	23	12	19
KIAA0586	11	9	10	14	11	22
CSPP1	11	10	8	11	10	10
ODF2L	10	6	12	15	15	19
NEK2	10	9	7	9	13	9
CEP85	10	4	7	8	11	9
CCDC61	10	9	8	8	10	12
WRAP73	10	7	6	7	7	8
CCDC102A	10	7	9	6	2	11
CPLANE1	10	6	9	19	2	33
PCM1	10	6	7	5	1	5
WDR90	10	6	8	10	1	11
RPGRIP1L	9	11	12	18	23	31
CEP57	9	10	13	11	15	13
TRIM27	9	6	8	7	13	13
DZIP1	9	9	9	10	11	16
TCHP	9	8	13	14	10	11
CEP85L	9	8	12	7	8	11
PRKAR2A	9	8	9	5	8	9
FAM161A	9	7	8	8	6	9

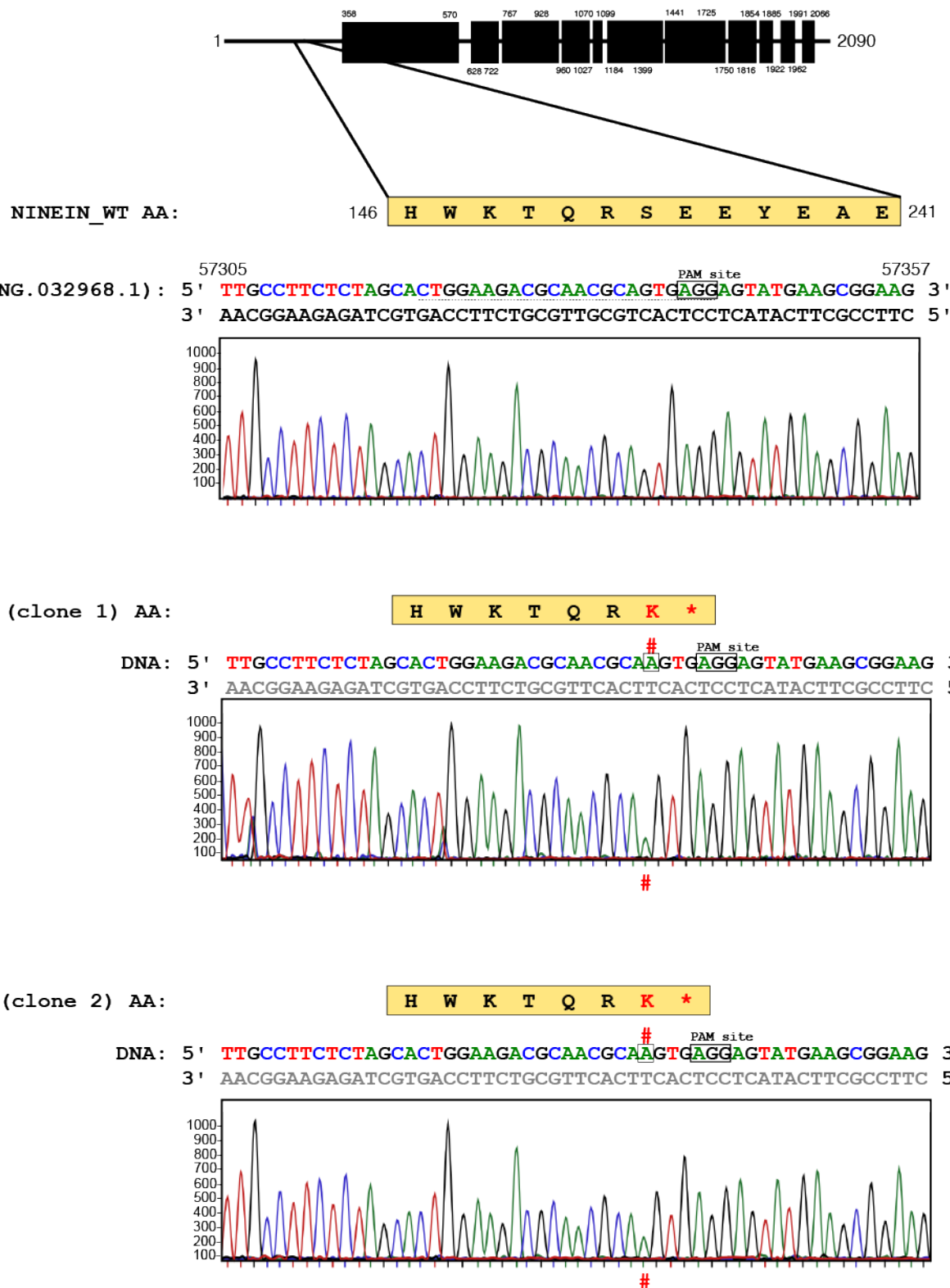
KIZ	9	6	5	10	5	11
HAUS1	9	9	3	11	3	9
BICD2	9	5	5	5	2	10
FAM92A	8	9	8	6	7	11
NEDD1	8	6	6	10	6	12
CCDC138	8	8	8	8	5	11
HAUS3	8	7	5	13	5	14
IQCB1	8	7	6	8	5	11
POC1B	7	7	7	10	11	11
CEP57L1	7	8	6	8	10	7
SPATA18	7	3	4	4	0	9
KIF7	7	4	7	5	0	4
RPS9	7	8	8	5	9	7
CCDC77	7	6	6	7	8	7
CP	7	7	6	6	8	6
NDE1	7	7	5	10	5	7
IFFO1	7	3	5	5	4	5
HAUS8	7	6	6	4	3	8
KIF2A	7	9	10	7	2	12
DZIP1L	6	7	10	8	10	12
PPP2R3C	6	7	6	11	9	15
HAUS4	6	8	6	8	8	11
RBM39	6	6	1	0	3	4
CETN2	6	6	7	7	8	7
NPHP1	6	4	5	6	7	13
NME7	6	4	6	6	5	7
SFI1	6	2	6	5	5	15
IRAK1BP1	6	3	3	8	5	7
SLAIN1	6	7	7	6	4	9
CCDC57	6	3	5	9	4	9
NOP53	5	4	5	5	8	6
POC1A	5	6	5	5	8	9
RPS13	5	4	3	4	7	4
CEP72	5	3	3	6	7	7
COPE	5	3	2	5	7	6
CEP19	5	4	6	6	5	8
TUBGCP4	5	6	3	5	0	8
CEP76	5	5	5	4	5	9
KIAA1328	5	7	7	9	5	10
YWHAE	5	5	5	5	2	9
CLASP2	5	4	5	8	2	7
SLAIN2	5	7	6	6	1	8
WDR47	5	4	6	8	1	9
CEP70	4	7	6	7	10	8
PLK1	4	4	3	4	9	7
NEK1	4	3	1	3	0	4
CEP44	4	9	8	6	8	7
CBY1	4	4	6	5	7	7
MIIP	4	5	4	7	7	6
HSPD1	4	5	3	8	7	11

WDPCP	4	2	1	4	0	6
MAP9	4	2	6	11	7	7
FOPNL	4	2	2	3	6	6
CCSAP	4	3	5	5	6	7
CRBN	4	3	2	3	5	4
TP53	4	5	5	7	4	5
HAUS2	4	4	5	2	4	5
TUBGCP5	4	1	1	1	0	6
ARRB2	4	5	4	8	4	8
HSBP1	4	4	4	4	4	4
PLK4	4	3	4	8	3	6
PPP1R35	4	3	3	4	3	4
INTU	4	1	4	7	3	10
IQCC	4	4	2	5	3	6
KIF2C	4	5	1	3	2	1
NDEL1	4	3	3	5	1	1
TUBGCP6	4	3	3	3	1	5
NOL6	3	8	3	4	12	1
TUBG1	3	6	2	6	8	12
NPM1	3	5	4	4	5	6
DCP1A	3	2	1	5	0	2
RRP12	3	7	1	9	8	0
RPS14	3	3	4	4	5	3
MLF2	3	2	2	3	4	5
SPATA24	3	2	2	2	0	1
TRIM37	3	1	1	1	4	4
HYLS1	3	1	2	3	4	6
MZT2B	3	3	1	1	2	3
CFAP410	3	2	2	3	0	2
C3orf14	3	2	1	4	2	4
YWHAQ	3	2	2	4	1	5
NUSAP1	2	4	2	5	0	4
PARP1	2	13	4	18	18	12
NUP214	2	15	3	3	10	1
AKIP1	2	4	5	6	6	6
DCTN2	2	2	2	1	0	3
AHI1	2	2	2	2	6	15
CLASP1	2	2	3	11	5	2
LRRCC1	2	1	2	8	4	6
CETN3	2	2	2	2	4	6
KCNAB2	2	2	1	2	0	4
PRKACA	2	1	2	0	3	5
UBC	2	4	3	4	4	4
TUBB3	2	2	3	0	1	4
SKP1	2	3	1	4	3	3
PROSER3	2	1	2	3	2	4
HAUS7	2	3	3	3	2	5
IFFO2	2	3	1	3	2	6
EFCAB11	2	1	2	2	0	3
DNAJC10	2	4	1	4	1	5

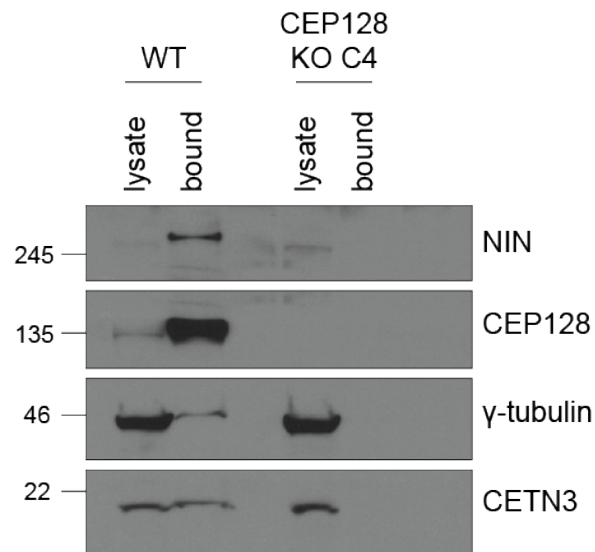
	2	1	2	2	1	2
CCDC34	2	1	2	2	1	2
NEURL4	1	2	0	1	1	2
PPP2CB	2	2	3	2	1	1
BICD1	1	1	1	2	0	2
SNRNP200	1	24	8	19	40	2
CAMSAP3	1	1	1	2	0	2
FUZ	1	1	1	2	0	7
BTRC	1	0	3	2	1	1
ARF4	1	1	1	0	1	1
NUP62	1	4	1	0	2	2
RUVBL2	1	4	3	3	7	2
WDR62	1	1	1	1	0	2
IMMT	1	11	2	2	2	0
PPP2R3B	1	0	2	3	1	5
AURKA	1	2	1	6	5	6
RPL35	1	2	1	1	4	2
PPP1CC	1	1	1	3	3	1
DYNLL1	1	1	2	2	2	2
RPS19	1	0	1	2	2	2
TUBB4A	1	0	1	1	2	1
TUBB4B	1	3	1	1	0	1
RUVBL1	1	6	0	2	4	2
TCP1	1	1	0	2	1	4
SSNA1	1	1	2	2	2	2
FBXW11	1	4	0	1	2	5
GAS8	1	1	2	1	0	2
KIAA1549	1	0	1	1	2	4
KPNA2	1	8	5	3	9	0
FAM83H	1	2	1	5	2	3
HSP90AA1	1	5	3	3	2	8
B9D2	1	1	1	0	2	3
SPOUT1	1	2	1	1	2	0
CKAP2	1	2	2	1	0	1
NUMA1	0	27	3	17	21	2
NUP93	0	17	1	7	3	1
KPNB1	0	13	1	4	6	5
SF3B3	0	11	9	14	22	2
H2AFY	0	8	6	8	10	2
PPAN	0	5	3	4	4	1
RPL27	0	3	1	2	6	2
SRSF7	0	3	1	1	3	1
RPL12	0	2	1	2	2	1
TTLL4	0	1	2	7	5	3
TUBAL3	0	1	1	1	1	1
CC2D2A	1	1	2	1	1	13

238 proteins

Appendix 4 – Characterisation of HAP1 WT and NIN KO (clone B4) cells by sequencing of the genomic DNA. Experiments performed by (and image courtesy of) Dr Ivan Rosa e Silva, School of Biological and Chemical Sciences, Queen Mary University of London.



Appendix 5 – COMPACT-WB showing centrosome proteins in the bound (bead-bound) fraction for HEK 293T WT cells, but no protein in the CEP128 KO cells, clone C4.



Appendix 6 – Tissue specificity table for centrosome proteins (top 500, according to average no. of unique peptides [indicated] discovered by COMPACT-MS performed in a panel of cell lines. CCDB, Centrosome and Cilium Database (Gupta et al., 2015).

All proteins	In CCDB?	HEK 293T	U251	Jurkat	G166	G7	N1E115	HAP1	FSPS13B
<i>PCNT</i>	Yes	91	110	118	62	72	107	86	52
<i>ALMS1</i>	Yes	75	72	107	57	58	52	95	51
<i>AKAP9</i>	Yes	73	41	101	43	60	33	121	13
<i>CNTRL</i>	Yes	79	70	95	33	38	77	95	52
<i>CEP250</i>	Yes	76	74	87	59	64	66	108	79
<i>CEP350</i>	Yes	58	60	85	45	50	40	84	36
<i>CEP192</i>	Yes	53	35	55	29	28	-	67	32
<i>CEP290</i>	Yes	45	28	59	18	17	11	54	18
<i>NIN</i>	Yes	45	44	56	37	42	44	62	38
<i>CDK5RAP2</i>	Yes	46	53	59	29	35	64	57	31
<i>CROCC</i>	Yes	43	36	29	25	48	35	73	42
<i>CEP128</i>	Yes	44	68	48	33	31	46	54	50
<i>ANKRD26</i>	Yes	35	11	-	25	15	45	47	32
<i>CEP135</i>	Yes	40	30	59	30	31	47	61	30
<i>CEP152</i>	Yes	39	46	56	26	-	59	44	22
<i>CEP295</i>	Yes	36	20	50	11	17	40	36	18
<i>CKAP5</i>	Yes	42	8	42	19	15	17	41	18
<i>C2CD3</i>	Yes	29	13	41	12	13	24	47	11
<i>AKNA</i>		27	35	38	13	14	28	37	22
<i>CEP164</i>	Yes	33	18	-	13	13	37	32	23
<i>CEP170</i>	Yes	25	14	12	24	30	31	28	19
<i>ODF2</i>	Yes	29	25	36	26	23	29	34	17
<i>COPA</i>		22	23	41	17	-	28	16	25

SPICE1	Yes	25	8	24	22	14	28	25	14
CEP120	Yes	22	22	28	18	15	40	31	13
CEP162	Yes	16	11	24	9	10	21	28	4
HSPA5	Yes	21	14	19	20	-	18	-	24
PIBF1	Yes	20	11	-	17	18	-	30	13
FBF1	Yes	15	6	-	9	6	7	13	6
CEP63	Yes	17	17	22	10	12	29	17	12
HERC2		15	-	10	6	7	2	42	2
CNTROB	Yes	17	10	25	14	10	33	30	14
OFD1	Yes	13	6	-	7	13	29	21	7
CCDC171		19	5	27	1	7	-	12	5
CENPJ		15	14	26	10	7	18	20	10
TBC1D31	Yes	16	17	23	11	16	25	25	11
CEP112	Yes	21	9	12	13	17	-	15	7
CP110	Yes	13	10	19	5	1	11	19	2
CCHCR1	Yes	12	7	21	2	3	7	22	5
HSPA8	Yes	18	10	18	18	-	18	-	21
MPHOSPH9	Yes	16	14	22	7	11	1	27	1
KIAA0753	Yes	10	11	13	6	5	19	14	8
CEP83	Yes	13	10	-	9	7	21	19	15
HSPA9	Yes	17	7	11	19	-	16	-	24
LRRC45	Yes	11	6	-	6	5	7	17	13
STIL	Yes	12	1	19	2	1	4	15	3
SCLT1	Yes	16	4	-	14	8	14	16	15
CEP170B		13	5	-	6	1	-	20	9
CCDC18	Yes	15	1	1	1	2	9	23	-
CEP89	Yes	11	7	22	7	7	9	22	12

HAUS6	Yes	14	7	18	7	8	-	23	5
TUBGCP2	Yes	13	13	23	4	3	27	20	6
COPB2		18	17	32	12	-	17	10	9
EDC4		15	9	27	5	9	18	23	7
SAS6	Yes	11	2	18	3	-	6	14	5
RTTN	Yes	9	1	18	2	4	7	24	2
TUBGCP3	Yes	12	7	20	3	6	29	16	5
MDM1	Yes	14	15	23	18	16	29	16	8
DDB1		12	-	30	-	-	-	-	11
CEP97	Yes	13	5	12	3	3	5	19	1
CCDC15	Yes	11	2	20	9	6	10	21	4
CEP78	Yes	13	5	16	7	8	10	18	2
HSPA1B	Yes	14	1	-	-	-	-	-	-
CEP95		11	9	22	3	4	13	16	10
NPHP4	Yes	12	-	2	2	6	2	2	6
CEP68	Yes	9	6	7	5	7	5	16	6
FGFR1OP	Yes	13	11	13	8	10	9	-	6
POC5	Yes	12	7	16	8	9	17	15	11
HAUS5		12	7	17	9	5	11	18	9
FTSJ3	Yes	13	5	3	16	-	3	-	12
SDCCAG8	Yes	13	2	-	4	5	12	16	5
CEP131	Yes	6	1	1	1	1	2	8	1
CCSER2	Yes	8	10	11	5	5	1	11	2
CCDC14	Yes	9	11	4	9	10	19	17	5
KIAA0586	Yes	9	2	14	1	4	-	24	8
CSPP1	Yes	10	3	15	1	1	-	19	2
CEP41	Yes	6	9	14	7	6	11	12	7

<i>CNTLN</i>	Yes	11	-	-	11	18	-	27	2
<i>ODF2L</i>	Yes	6	-	8	1	-	4	8	4
<i>NEK2</i>	Yes	9	2	10	1	4	2	13	7
<i>PCM1</i>	Yes	6	6	27	9	9	18	26	11
<i>CCDC102A</i>	Yes	7	1	1	1	4	-	5	-
<i>CCDC61</i>	Yes	9	6	7	8	-	2	9	10
<i>WDR90</i>		6	1	-	1	-	20	18	-
<i>WRAP73</i>	Yes	7	1	11	6	4	9	13	3
<i>CPLANE1</i>		6	-	-	-	-	2	-	-
<i>CEP85</i>	Yes	4	-	10	2	-	4	4	5
<i>CEP85L</i>	Yes	8	-	14	-	-	-	6	11
<i>DZIP1</i>	Yes	9	1	-	4	9	1	4	4
<i>RPGRIPI1L</i>	Yes	11	1	2	3	10	4	1	4
<i>HAUS1</i>	Yes	9	5	12	4	3	6	12	5
<i>PRKAR2A</i>	Yes	8	12	10	9	7	5	12	3
<i>KIZ</i>		6	-	-	1	-	1	7	5
<i>TCHP</i>	Yes	8	8	14	8	8	7	16	4
<i>FAM161A</i>	Yes	7	1	6	6	3	-	6	3
<i>CEP57</i>	Yes	10	14	16	10	9	18	11	4
<i>BICD2</i>	Yes	5	1	4	3	1	-	4	-
<i>NEDD1</i>	Yes	6	7	9	3	4	13	12	5
<i>CCDC138</i>		8	-	2	-	3	-	4	2
<i>HAUS3</i>	Yes	7	4	11	8	3	7	20	4
<i>FAM92A</i>		9	4	-	3	4	8	7	6
<i>IQCB1</i>	Yes	7	1	5	2	-	-	9	2
<i>NDE1</i>	Yes	7	9	7	7	7	3	9	4
<i>CCDC77</i>	Yes	6	7	8	1	4	11	7	5

<i>KIF2A</i>	Yes	9	3	9	3	3	1	13	4
<i>SPATA18</i>		3	-	-	-	-	-	-	-
<i>KIF7</i>	Yes	4	-	-	-	-	-	2	-
<i>POC1B</i>	Yes	7	6	13	5	7	9	12	2
<i>RPS9</i>	Yes	8	8	8	9	-	8	-	12
<i>CP</i>	Yes	7	5	6	5	-	2	-	5
<i>CEP57L1</i>	Yes	8	6	10	7	8	10	9	8
<i>HAUS8</i>	Yes	6	5	6	4	2	1	9	4
<i>IFFO1</i>		3	1	5	3	1	-	3	-
<i>PPP2R3C</i>	Yes	7	2	9	3	2	1	18	2
<i>NPHP1</i>	Yes	4	-	-	-	4	-	-	2
<i>NME7</i>	Yes	4	6	10	4	7	7	9	3
<i>SLAIN1</i>	Yes	7	2	4	2	2	2	7	3
<i>RBM39</i>	Yes	6	1	5	3	-	3	-	4
<i>HAUS4</i>	Yes	8	3	11	9	4	7	13	3
<i>SFI1</i>		2	4	16	1	1	4	13	-
<i>DZIP1L</i>	Yes	7	1	-	4	3	14	11	2
<i>IRAK1BP1</i>	Yes	3	1	1	3	4	4	7	3
<i>CETN2</i>	Yes	6	7	8	5	5	8	7	6
<i>CCDC57</i>	Yes	3	3	-	-	-	2	-	-
<i>NOP53</i>		4	2	-	-	-	1	5	-
<i>CEP19</i>	Yes	4	3	5	1	3	5	6	1
<i>POC1A</i>	Yes	6	7	6	4	3	10	5	4
<i>SLAIN2</i>	Yes	7	3	7	1	1	2	6	3
<i>RPS13</i>	Yes	4	2	3	6	-	-	-	6
<i>WDR47</i>		4	1	6	-	1	-	8	-
<i>ZC3H12B</i>		2	-	-	-	-	-	-	-

<i>YWHAE</i>	Yes	5	2	1	4	-	3	3	3
<i>TUBGCP4</i>	Yes	6	2	8	-	1	4	8	2
<i>CEP76</i>	Yes	5	2	4	-	3	3	9	1
<i>CEP72</i>	Yes	3	1	7	-	3	1	7	2
<i>KIAA1328</i>		7	-	-	1	2	-	6	1
<i>COPE</i>		3	6	11	1	3	3	2	-
<i>COPB1</i>		1	-	6	-	-	1	-	3
<i>CLASP2</i>		4	1	6	2	1	4	8	2
<i>TP53</i>	Yes	5	-	-	-	1	-	-	-
<i>PLK1</i>	Yes	4	1	9	2	2	5	8	6
<i>PLK4</i>	Yes	3	1	3	2	-	7	7	-
<i>NEK1</i>	Yes	3	-	5	1	-	-	7	-
<i>NDEL1</i>	Yes	3	1	3	-	-	-	3	-
<i>CEP70</i>	Yes	7	3	11	5	5	16	11	4
<i>CALM2</i>	Yes	4	-	-	-	-	-	-	-
<i>CBY1</i>	Yes	4	4	-	3	4	6	3	3
<i>FOPNL</i>	Yes	2	5	2	4	3	3	-	4
<i>WDPCP</i>	Yes	2	-	-	-	-	-	-	-
<i>HAUS2</i>	Yes	4	2	8	2	1	4	6	1
<i>MIIP</i>	Yes	5	3	5	3	2	5	4	4
<i>KIF2C</i>		5	-	-	-	1	1	11	3
<i>PPP1R35</i>		3	1	5	1	-	-	5	1
<i>TTF1</i>		3	-	1	7	1	-	1	-
<i>ARRB2</i>	Yes	5	1	6	1	-	2	5	-
<i>HSPD1</i>	Yes	5	3	5	16	-	10	-	9
<i>TUBGCP5</i>	Yes	1	-	3	-	-	7	5	-
<i>TUBGCP6</i>	Yes	3	3	5	1	1	14	8	1

CCSAP	Yes	3	8	7	4	3	4	6	3
CRBN		3	2	8	1	4	8	2	2
CEP44	Yes	9	1	7	3	4	8	9	3
INTU	Yes	1	-	-	-	1	-	-	1
IQCC		4	-	5	1	2	2	4	3
MAP9		2	3	4	-	1	4	10	-
LUZP1		2	-	-	3	-	-	10	3
HSBP1		4	3	4	3	2	2	4	2
LUC7L		2	-	1	1	-	1	-	2
NPM1	Yes	5	-	-	5	-	3	-	6
NOL6	Yes	8	2	2	6	-	-	-	8
MZT2B	Yes	3	2	3	1	1	-	2	1
C3orf14		2	1	-	-	-	-	-	-
DCP1A		2	-	2	-	1	-	6	-
GAN		1	-	-	-	-	-	-	-
RRP12	Yes	7	1	3	16	-	-	-	9
MRPL47	Yes	2	-	1	3	1	-	2	-
KIF5B		4	-	-	-	-	1	4	-
MLF2		2	2	4	-	-	1	5	1
KIF22		6	-	6	4	2	-	-	-
TRIM37		1	-	-	-	-	-	1	1
SPATA24		2	-	2	-	-	-	3	-
RPS14	Yes	3	2	4	6	-	2	-	5
TUBB2B	Yes	1	-	2	2	-	-	-	2
TUBG1	Yes	6	9	14	2	1	20	14	1
PPP2R1A		3	1	5	-	-	-	-	1
YWHAQ	Yes	2	-	3	4	-	3	-	2

<i>CFAP410</i>		2	-	-	-	-	-	1	3	-
<i>HYLS1</i>	Yes	1	-	3	1	1	6	4	2	
<i>ARCN1</i>		2	-	-	6	1	1	-	2	
<i>MAP7D2</i>		2	-	-	-	-	1	-	-	
<i>NUP214</i>	Yes	15	6	2	16	-	1	-	16	
<i>NUSAP1</i>		4	3	12	-	-	1	3	1	
<i>LRRCC1</i>	Yes	1	-	7	1	-	2	16	1	
<i>PARP1</i>	Yes	13	7	-	16	-	5	-	12	
<i>FLNA</i>	Yes	4	15	2	45	-	-	-	19	
<i>DNAJC10</i>		4	1	-	1	1	-	1	-	
<i>DCTN2</i>	Yes	2	-	-	1	-	-	1	1	
<i>DDX10</i>		10	1	1	-	3	1	-	14	
<i>RPS19BP1</i>		2	-	1	-	1	1	-	-	
<i>CETN3</i>	Yes	2	3	4	2	3	6	6	1	
<i>CCDC34</i>	Yes	1	5	4	1	1	1	4	3	
<i>FMR1</i>		2	-	3	1	1	1	2	-	
<i>CACTIN</i>		1	1	1	2	-	7	-	1	
<i>SKP1</i>	Yes	3	1	5	3	-	-	-	-	
<i>PROSER3</i>		1	1	2	1	-	3	4	-	
<i>TRMO</i>		2	-	2	-	-	-	1	-	
<i>KCNAB2</i>		2	-	1	-	-	-	2	-	
<i>PRKACA</i>	Yes	1	4	5	2	1	4	5	-	
<i>KPRP</i>		1	-	-	3	-	-	-	-	
<i>PPP2CB</i>	Yes	2	-	3	3	-	1	4	-	
<i>RPL34</i>		2	-	1	-	-	-	-	3	
<i>TUBB6</i>		2	-	-	4	1	-	-	1	
<i>TCTN1</i>	Yes	-	-	-	-	-	-	-	-	

<i>TUBB3</i>	Yes	2	1	1	-	-	6	-	1
<i>TFAM</i>		2	-	1	5	-	-	-	4
<i>UBC</i>	Yes	4	3	3	4	-	-	-	-
<i>SSX2IP</i>	Yes	1	-	1	1	-	-	4	-
<i>AKIP1</i>		4	1	6	4	2	1	5	3
<i>AHI1</i>	Yes	2	-	-	-	-	-	-	1
<i>AATF</i>	Yes	7	-	5	8	-	1	-	9
<i>CLASP1</i>	Yes	2	2	1	1	1	8	11	3
<i>EFCAB11</i>		1	-	2	1	-	1	-	-
<i>CTBP2</i>		2	-	-	1	1	-	1	3
<i>EPB41L5</i>		3	-	1	-	-	-	-	-
<i>HAUS7</i>	Yes	3	1	6	2	3	2	5	3
<i>IFFO2</i>	Yes	3	-	-	-	-	-	4	-
<i>GFPT1</i>		2	-	1	4	-	2	-	2
<i>COPG1</i>		3	3	1	8	3	-	-	3
<i>PDIA6</i>		1	3	-	1	1	-	2	3
<i>MKS1</i>	Yes	1	-	-	-	-	-	-	-
<i>NPTX2</i>		1	-	-	-	-	-	-	-
<i>NOL7</i>		3	-	-	-	-	-	-	5
<i>PCBP1</i>		1	1	1	-	-	-	-	3
<i>MAP7D3</i>	Yes	1	-	-	1	-	-	5	-
<i>MYH9</i>		10	-	-	-	-	-	-	-
<i>NEURL4</i>		2	-	-	-	-	-	5	1
<i>DYNLL1</i>	Yes	1	1	1	1	-	2	2	2
<i>DHX8</i>		5	-	-	5	1	-	-	1
<i>FLNB</i>		2	-	7	4	-	-	-	5
<i>DDX54</i>		3	-	-	-	-	-	-	3

<i>BICD1</i>	Yes	1	1	1	1	1	-	7	-
<i>CCDC112</i>		-	-	-	-	-	-	1	-
<i>CDC14A</i>	Yes	-	-	-	-	-	3	5	-
<i>CPLANE2</i>		-	-	-	-	-	-	-	-
<i>CC2D2A</i>	Yes	1	-	-	-	1	-	-	-
<i>CAMSAP3</i>		1	-	-	-	-	-	4	-
<i>CEP170P1</i>		1	-	-	1	1	-	1	-
<i>BOLA2</i>		-	-	1	2	-	-	1	2
<i>FUZ</i>	Yes	1	-	-	-	-	-	-	-
<i>BTRC</i>		-	-	2	-	-	-	2	-
<i>ARF4</i>	Yes	1	-	1	3	-	1	-	1
<i>RPL36A</i>		1	1	2	-	-	-	-	1
<i>TWNK</i>		-	1	-	-	-	-	-	-
<i>POLR3H</i>	Yes	-	-	2	-	-	1	1	1
<i>PFN1</i>		3	1	-	-	-	-	-	-
<i>NUP62</i>	Yes	4	-	2	3	-	-	-	2
<i>SLIT2</i>		1	-	-	-	-	1	-	-
<i>U2AF1</i>		1	-	-	-	-	-	-	-
<i>SNRNP200</i>	Yes	24	6	-	46	-	6	-	15
<i>WDR62</i>		1	-	-	1	3	4	12	2
<i>ZBTB21</i>		1	-	-	-	-	-	-	-
<i>ZNF574</i>		-	-	-	1	-	-	3	-
<i>ZNF696</i>		1	-	-	-	-	-	-	-
<i>PRKAR2B</i>	Yes	-	-	4	-	2	1	7	-
<i>IMMT</i>	Yes	11	10	2	13	-	1	-	10
<i>MIB1</i>	Yes	1	-	1	-	-	-	3	-
<i>KIF27</i>	Yes	-	-	-	1	-	-	4	1

<i>CKMT1A</i>		-	-	-	-	-	-	-	1	-
<i>PPP2R3B</i>		-	-	1	-	-	-	-	4	-
<i>PPP1CB</i>	Yes	1	1	2	1	1	2	1	-	-
<i>PPP1CC</i>	Yes	1	-	-	1	-	-	-	-	-
<i>RPL35</i>	Yes	2	1	1	1	-	3	-	4	
<i>PPP1CA</i>	Yes	2	1	-	-	-	-	1	-	
<i>SRSF2</i>		1	1	-	1	-	-	-	-	-
<i>SSNA1</i>	Yes	1	1	2	1	2	3	2	2	
<i>SERPINB3</i>		1	2	-	4	-	-	-	-	-
<i>TSPYL2</i>	Yes	1	-	1	2	1	-	-	-	-
<i>RUVBL2</i>	Yes	4	2	1	12	-	2	-	9	
<i>S100A14</i>		1	-	-	-	-	-	-	-	-
<i>RPS19</i>	Yes	-	1	2	3	-	1	-	1	
<i>RPS20</i>		1	-	1	2	-	-	-	-	-
<i>SAMD3</i>		-	-	-	-	-	-	-	-	-
<i>TEX9</i>	Yes	-	-	1	-	-	-	3	-	
<i>TUBB4A</i>		-	-	3	-	-	-	-	-	1
<i>TUBB4B</i>	Yes	3	3	1	1	-	3	-	1	
<i>TBCCD1</i>	Yes	-	-	-	-	-	-	1	-	
<i>TARDBP</i>		2	-	-	-	-	-	-	-	-
<i>TARBP1</i>		1	-	1	-	-	-	2	-	-
<i>RUVBL1</i>	Yes	6	-	1	10	-	1	-	8	
<i>TCP1</i>	Yes	1	-	2	10	-	2	-	8	
<i>TCTN2</i>	Yes	1	-	-	-	-	-	-	-	-
<i>TPM3</i>		-	-	2	2	1	-	-	-	-
<i>ACTR1A</i>	Yes	1	1	-	4	-	2	-	-	-
<i>YWHAB</i>	Yes	2	-	2	2	2	2	1	-	

<i>YWHAH</i>		1	-	-	-	-	-	-	1	1
<i>FAM13A</i>		-	-	-	-	-	-	-	-	-
<i>FAM83H</i>		2	-	-	-	-	-	-	7	1
<i>FBXW11</i>	Yes	4	-	4	-	1	2	4	1	
<i>GAS8</i>	Yes	1	-	-	-	-	2	-	-	
<i>ECM1</i>		1	-	-	2	-	-	-	-	-
<i>DEK</i>		1	1	-	3	-	-	-	-	1
<i>EDC3</i>		2	-	1	-	-	-	5	-	
<i>C19orf44</i>		-	-	-	-	-	-	-	-	-
<i>CDK5</i>		-	1	-	-	-	-	-	-	-
<i>IQGAP3</i>		-	1	-	1	-	-	-	-	-
<i>KIAA1549</i>		-	-	-	-	-	1	-	-	-
<i>KPNA2</i>	Yes	8	1	1	11	-	2	-	10	
<i>HSP90AA1</i>	Yes	5	2	4	11	-	7	-	9	
<i>AURKA</i>	Yes	2	-	2	2	1	10	6	1	
<i>B9D2</i>	Yes	1	-	-	-	-	-	-	-	
<i>SPOUT1</i>		2	1	2	3	1	1	-	2	
<i>COPZ1</i>		1	-	-	1	-	1	-	1	
<i>CKAP2</i>	Yes	2	-	-	1	-	-	-	-	
<i>NUMA1</i>	Yes	27	6	1	34	-	1	-	21	
<i>TOP2A</i>	Yes	20	7	10	39	-	4	-	27	
<i>SMC3</i>	Yes	20	2	1	23	-	3	-	22	
<i>NUP93</i>	Yes	17	1	-	11	-	-	-	12	
<i>WDR3</i>	Yes	15	1	-	17	-	-	-	3	
<i>KPNB1</i>	Yes	13	-	1	13	-	5	-	6	
<i>CHD4</i>	Yes	12	1	-	26	-	4	-	10	
<i>NUP98</i>	Yes	12	2	2	15	-	7	-	15	

SF3B3	Yes	11	4	4	20	-	1	-	15
NUP107	Yes	9	2	-	2	-	-	-	2
CDC5L	Yes	9	6	1	16	-	1	-	9
H2AFY	Yes	8	4	6	13	-	6	-	7
INCENP	Yes	7	-	3	10	-	5	-	11
RANGAP1	Yes	6	-	-	5	-	-	-	4
EBNA1BP2	Yes	6	1	2	10	-	4	-	8
KRI1	Yes	5	1	-	8	-	-	-	2
PPAN	Yes	5	1	1	7	3	-	-	5
SYNE2	Yes	5	2	-	33	1	2	-	6
MYO6	Yes	4	1	-	3	1	-	-	2
CCT2	Yes	4	-	1	10	-	7	-	10
PDCD6IP	Yes	3	-	-	8	1	1	-	1
NUP35	Yes	3	2	1	3	-	2	-	7
NOL8		3	-	-	11	3	1	-	-
UBA1	Yes	3	1	-	19	-	1	-	9
DCAF13	Yes	3	-	-	5	-	-	-	3
CHAF1A		3	-	-	1	-	-	-	-
RPL10A	Yes	3	-	-	5	-	2	-	4
RPL27	Yes	3	-	2	2	-	-	-	6
RPRD1A		3	-	-	2	2	-	-	1
SRSF7	Yes	3	1	2	4	-	2	-	5
KMT2A		3	-	-	-	-	-	-	-
RBM15		3	-	-	1	2	-	-	-
HSP90B1	Yes	3	16	-	19	-	6	-	9
FAM207A		3	-	-	1	-	-	-	1
RPL12	Yes	2	-	1	2	-	1	-	3

VDAC3	Yes	2	1	-	2	1	1	-	1
CSE1L	Yes	2	-	-	11	-	1	-	4
ZCCHC9		2	-	-	2	-	-	-	-
XPO1	Yes	2	1	-	7	-	2	-	5
RAN	Yes	2	3	2	3	-	-	-	4
RBM12B		2	-	-	-	-	-	-	-
TTBK2	Yes	2	1	-	-	-	3	8	2
RPS7	Yes	2	1	2	3	-	2	-	1
SARNP		2	2	-	-	2	-	-	-
CCT4	Yes	2	3	2	4	-	2	-	4
WIZ		2	-	-	3	1	-	-	-
TASOR		2	-	-	-	-	-	-	-
EEF2	Yes	2	-	3	13	-	10	-	6
DNMT3A		2	-	-	-	-	2	-	12
HDGFL2		2	-	-	-	-	-	-	-
SSB		2	1	-	5	-	-	-	4
AURKB	Yes	2	-	1	3	-	3	-	2
PDIA3	Yes	1	15	-	6	1	1	-	9
P4HB	Yes	1	-	-	7	-	2	-	4
PLRG1		1	1	-	3	1	-	-	1
CANX		1	4	-	-	-	-	-	2
CAPZB	Yes	1	3	-	2	-	2	-	1
ARMC9		1	-	-	-	-	-	-	-
CHD1		1	1	1	5	4	-	-	3
RING1		1	-	-	2	1	-	-	-
RPL18A		1	-	-	-	-	1	-	1
ZNF624		1	-	-	-	-	-	-	-

<i>TTLL4</i>	Yes	1	-	10	-	-	-	-	1	-
<i>TUBAL3</i>		1	-	1	1	1	-	-	1	-
<i>CCT3</i>	Yes	1	2	2	9	-	-	-	-	2
<i>YARS</i>		1	-	-	-	-	-	1	-	-
<i>TUBB2A</i>	Yes	1	3	-	3	-	-	5	-	1
<i>TUBA1A</i>	Yes	1	7	2	-	-	-	6	3	-
<i>UFM1</i>		1	-	-	1	-	-	-	-	-
<i>DUSP11</i>		1	-	1	-	-	-	-	-	-
<i>CRNKL1</i>	Yes	1	2	1	10	-	-	1	-	4
<i>MEAF6</i>	Yes	1	-	-	3	1	-	-	-	1
<i>KRT18</i>	Yes	1	10	-	18	-	-	2	-	22
<i>MAD2L1</i>	Yes	1	-	2	2	-	-	1	-	-
<i>NCS1</i>		-	-	-	-	2	-	-	1	-
<i>CCDC8</i>		-	-	-	-	-	-	-	-	-
<i>CCDC150</i>		-	-	-	-	-	-	-	-	-
<i>CPSF1</i>		-	-	1	-	-	-	-	-	-
<i>TRIM27</i>		6	1	9	1	2	1	11	3	
<i>TRAF5</i>	Yes	-	1	9	1	-	-	-	8	-
<i>IPO5</i>	Yes	-	-	-	3	4	1	-	-	3
<i>MLF1</i>	Yes	-	-	-	-	1	-	-	-	1
<i>HIST1H1E</i>		-	11	-	1	-	-	-	-	6
<i>XRCC5</i>		-	10	2	-	-	-	-	-	6
<i>SUPT16H</i>		-	9	-	-	-	-	2	-	9
<i>RSF1</i>		-	9	-	-	-	-	-	-	10
<i>SRRM2</i>		-	8	9	-	-	-	-	-	14
<i>CALR</i>		-	7	-	2	-	-	-	-	5
<i>TUBA4A</i>	Yes	-	5	2	2	2	-	5	1	

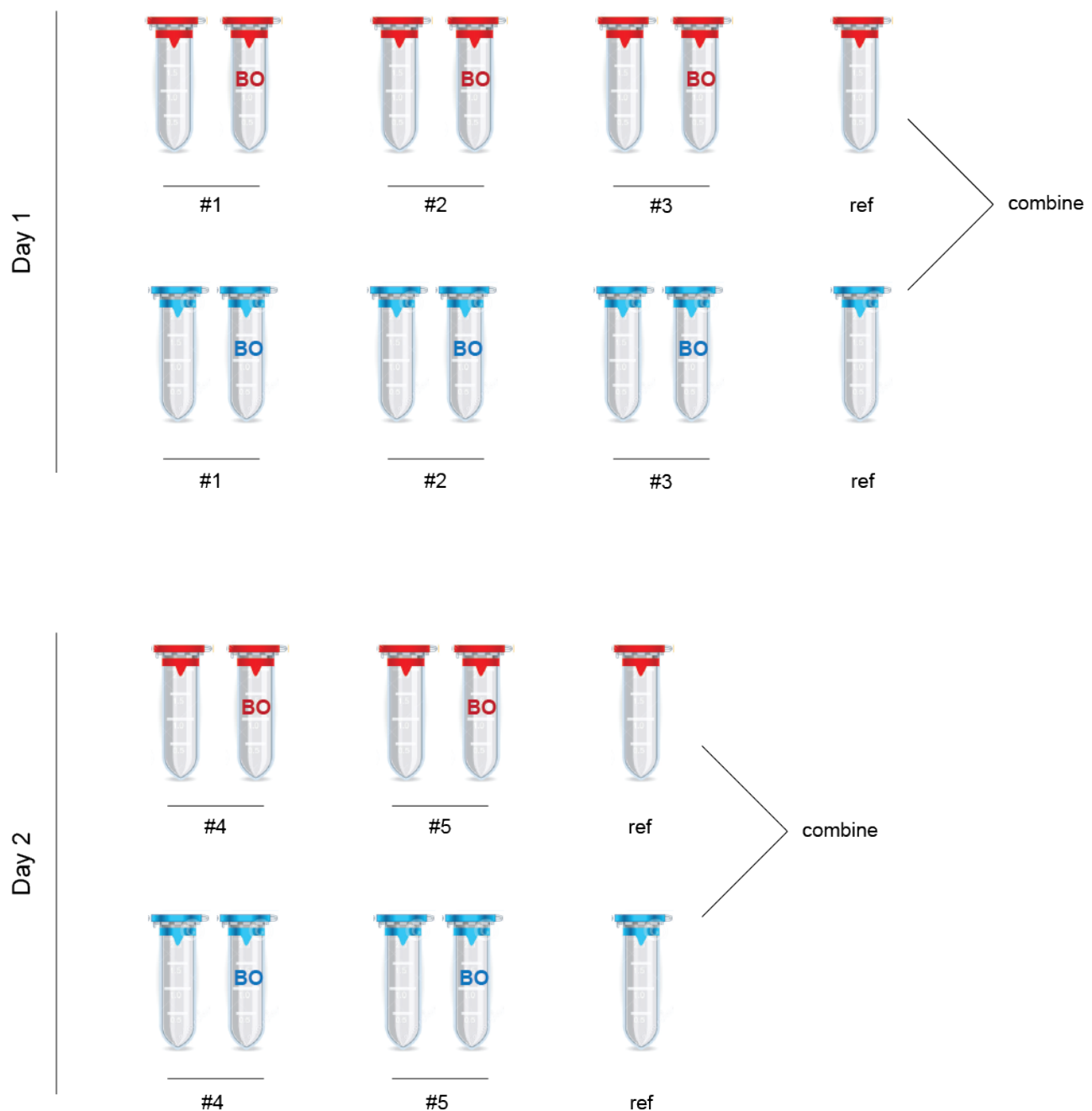
<i>SSRP1</i>		-	5	-	-	-	2	-	6
<i>EZR</i>		-	5	-	-	2	-	-	-
<i>HIST1H2BD</i>		-	4	-	-	-	-	-	-
<i>ATP1A1</i>		-	4	-	-	4	-	-	-
<i>DNAJC9</i>		-	4	2	-	-	-	-	-
<i>FSCN1</i>		-	4	-	2	-	-	-	4
<i>HSPB1</i>		-	4	1	-	-	-	-	-
<i>RPF1</i>		-	4	-	-	-	-	-	3
<i>GANAB</i>		-	4	-	4	-	1	-	4
<i>ESF1</i>		-	4	-	-	-	-	-	7
<i>CFAP97</i>		-	4	2	1	-	-	3	-
<i>PDIA4</i>		-	4	-	2	-	-	-	2
<i>ZNF512</i>		-	4	7	-	-	2	5	5
<i>CENPC</i>		-	4	-	-	-	1	-	2
<i>HIST1H2BO</i>		-	3	-	-	-	-	-	-
<i>TPM4</i>		-	3	-	-	-	-	1	1
<i>GNL2</i>		-	3	1	-	-	1	-	12
<i>NKAP</i>		-	3	-	-	-	-	-	-
<i>RPL13A</i>		-	3	-	-	4	-	-	3
<i>RBM19</i>		-	3	-	-	-	1	-	2
<i>PRKCSH</i>		-	3	-	1	1	-	-	-
<i>ECHS1</i>	Yes	-	3	-	2	2	-	-	-
<i>WDR46</i>		-	3	-	-	-	-	-	6
<i>ERP29</i>		-	3	-	-	-	-	-	-
<i>MYBBP1A</i>		-	3	-	-	-	-	-	4
<i>HDAC2</i>		-	3	3	5	-	-	-	3
<i>ZC3H18</i>		-	3	1	-	-	1	-	3

<i>NKTR</i>		-	3	-	-	-	-	-	-	-	-
<i>HYOU1</i>		-	3	-	-	-	-	-	-	-	3
<i>STAU1</i>		-	3	-	6	-	-	-	-	-	5
<i>RPN1</i>		-	3	1	-	-	-	-	-	-	3
<i>HIST1H2AD</i>		-	2	-	-	-	-	-	-	-	-
<i>HIST1H2AC</i>		-	2	-	1	-	-	-	-	-	-
<i>HIST2H2AB</i>		-	2	2	-	-	-	-	-	-	-
<i>KRT15</i>		-	2	-	-	-	-	1	1	-	-
<i>DDX39B</i>		-	2	-	-	-	-	2	-	-	8
<i>ERH</i>		-	2	1	-	-	-	1	-	-	-
<i>EEF1D</i>		-	2	-	4	-	-	-	-	-	4
<i>TRAP1</i>		-	2	-	-	-	-	-	-	-	-
<i>RPS27A</i>	Yes	-	2	-	10	-	-	-	-	-	2
<i>RPS21</i>		-	2	2	-	-	-	-	-	-	1
<i>PDE4DIP</i>	Yes	-	2	-	1	-	-	1	-	-	-
<i>RPL29</i>		-	2	-	-	1	-	-	-	-	-
<i>RCN1</i>		-	2	-	6	-	-	-	-	-	-
<i>YWHAG</i>		-	2	1	1	-	-	-	2	-	-
<i>CS</i>		-	2	-	4	-	-	-	-	-	-
<i>RAB14</i>		-	2	-	4	3	-	-	-	-	-
<i>NGDN</i>		-	2	1	-	-	-	1	-	-	2
<i>NCBP2</i>		-	2	-	1	2	-	-	-	-	-
<i>TMX1</i>		-	2	-	-	-	-	1	-	-	-
<i>RAB7A</i>		-	2	-	-	-	-	-	-	-	-
<i>RBM34</i>		-	2	-	-	-	-	2	-	-	4
<i>C5orf24</i>		-	2	-	-	-	-	-	-	-	1
<i>FABP5</i>		-	2	-	1	-	-	-	1	-	-

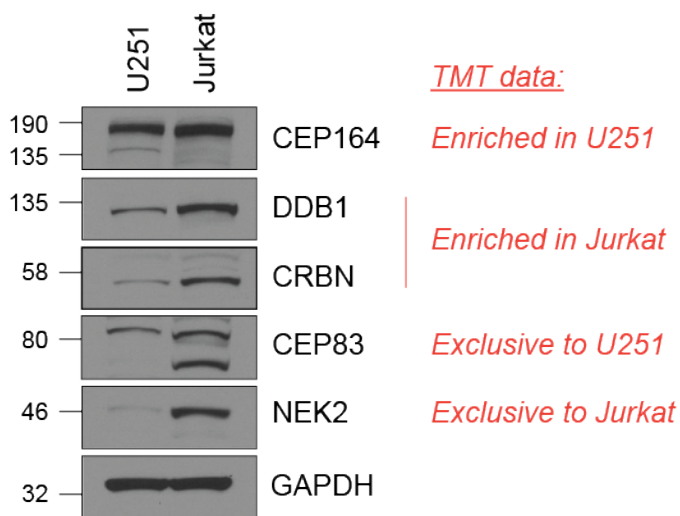
RACK1		-	2	-	-	-	-	-	1	-
KIF14	Yes	-	2	-	6	1	1	-	-	-
TMED9		-	2	-	1	-	-	-	-	-
PCNA		-	2	1	-	-	-	2	-	3
ZC3HAV1		-	2	-	10	-	-	-	-	-
WHSC1		-	2	-	-	-	-	-	-	-
MTA1		-	2	-	-	-	-	-	-	2
MYH7		-	2	-	-	-	-	-	-	-
RAB2A		-	2	-	4	-	-	-	-	-
PHF14		-	2	-	4	-	-	-	-	2
PSMD3	Yes	-	2	-	5	-	1	-	-	2
MRPS26		-	2	-	-	-	-	-	2	-
DNAJB8		-	2	-	-	-	-	-	-	-
SLC9A3R2		-	2	-	-	-	-	-	-	-
STIP1	Yes	-	2	-	4	-	3	-	-	-
ATAD2B		-	2	-	1	-	-	-	-	2
CALU		-	2	-	1	-	-	-	-	2
PARN		-	2	-	-	5	-	-	-	2
RBM25		-	2	-	-	2	-	-	-	-
ZNF280C		-	2	-	-	-	-	-	-	-
H2AFX		-	1	-	-	1	-	-	-	-
KRT6C		-	1	-	1	2	-	-	-	-
POTEF	Yes	-	1	1	-	-	-	-	-	-
KRT75		-	1	-	-	-	-	-	-	-
HNRNPH2		-	1	-	-	-	-	-	-	1
HMGA1		-	1	-	-	-	-	-	-	1
HMGA2		-	1	-	-	-	-	-	-	2

MYH3		-	1	-	-	-	-	-	-	-	-
BAZ2A		-	1	-	-	-	-	2	-	-	6
DYPSL2	Yes	-	1	-	1	-	-	-	-	-	2
NUCKS1		-	1	-	-	-	-	-	-	-	-
ZCCHC10		-	1	1	1	-	-	-	-	-	-
G6PD	Yes	-	1	-	8	-	-	-	-	-	-
CHCHD2P9		-	1	1	-	-	-	-	-	-	-
CENPB		-	1	1	-	-	-	-	1	-	-
CDCA8		-	1	1	-	-	-	3	-	-	3
TRIM24		-	1	-	5	-	-	-	-	-	4
DYNLL2	Yes	-	1	-	-	-	-	1	1	-	-
RBM4		-	1	-	3	-	-	-	-	-	4
NME2P1		-	1	-	-	2	-	-	-	-	-
HMGB1P1		-	1	-	-	-	-	-	-	-	1
ACAT1	Yes	-	1	-	5	-	-	-	-	-	-
NACA2		-	1	1	-	-	-	-	-	-	-
EIF3I		-	1	-	-	-	-	-	-	-	1
Uqcrc2	Yes	-	1	-	-	3	1	-	-	-	-

Appendix 7 – Experimental design for COMPACT-TMT in U251 (red) and Jurkat (blue) cells.
Each replicate (#1-5) represent different passage numbers. Samples were collected and
COMPACT performed over two consecutive days.



Appendix 8 – Expression levels of various TMT candidates in whole cell lysates of U251 and Jurkat cells, analysed via WB.



Appendix 9. COMPACT replicates performed in cells freshly isolated from mouse spleens. Top 100 for proteins found in both replicates are shown. Number of unique peptides are indicated for each experiment, and sorted from high to low according to colour (red – green).

Protein	Number of unique peptides	
	rep 1	rep 2
SPTA1	70	68
PCNT	54	50
CEP250	49	44
CNTRL	48	53
AKAP9	39	37
CROCC	36	28
TAF1	36	36
CEP350	31	31
CEP135	27	29
SPTB	25	27
NIN	25	30
FN1	24	24
MYH11	24	23
SPTAN1	23	29
COPA	22	25
AKNA	19	19
CEP128	19	20
SYNM	19	22
CDK5RAP2	18	22
COPB2	18	18
SPICE1	17	12
TAF2	17	20
TAF6	17	19
EMSY	16	16
LAMB2	16	13
TAF3	16	17
CKAP5	15	15
KDM5A	15	12
VCL	15	13
MACF1	14	15
ACTN4	14	17
CARD11	14	18
CNTROB	14	15
ODF2	14	15
TAF5	14	15
MKI67	13	12

CEP152	12	12
FILIP1L	12	10
TUBGCP3	12	13
LAMC1	12	12
PHF12	12	9
TAF7	12	10
MDM1	11	12
KRT19	11	12
CEP120	10	12
GSN	10	10
HCFC1	10	11
DDB1	9	11
SIN3B	9	10
ABLIM1	9	8
FLNB	9	7
HAUS5	9	7
LAMA2	9	9
LAMB1	9	7
OFD1	9	7
POC5	9	9
ADD1	8	10
ADD3	8	9
CEP57	8	8
CEP63	8	6
CEP78	8	8
COL6A4	8	8
LMNB2	8	4
MYO1C	8	7
MYO1G	8	8
PPP1R9B	8	8
NID2	8	6
SORBS2	8	6
SYNPO2	8	10
UGGT1	8	7
C2CD3	7	6
CEP162	7	5
CEP170	7	8
TUBGCP2	7	11
LAMA5	7	4
SLTM	7	5
SRRM2	7	2
SUN2	7	5

TMOD3	7	9
WDR90	7	10
DHX9	6	3
ANK1	6	4
CEP295	6	6
COCH	6	2
GNL3	6	8
LAMA4	6	2
LBR	6	3
LSP1	6	6
SON	6	8
TAF8	6	7
FERMT3	6	5
TUBA1B	5	5
RRP12	5	1
TOP2B	5	1
MSN	5	9
RPL6	5	4
CEP164	5	4
CEP44	5	5
CEP95	5	4
CLU	5	6
COL6A5	5	2